Technical Report No. 159

6137-6-T

A STUDY OF THE FERRITE PHASE-SHIFT AMPLIFIER

by

W. B. Ribbens

Approved by: 

B. F. Barton

for

COOLEY ELECTRONICS LABORATORY

Department of Electrical Engineering
The University of Michigan
Ann Arbor, Michigan

Contract No. DA-36-039-AMC-03733(E)
Department of the Army
Department of the Army Project No. 1P0 21101 A04201

Submitted in partial fulfillment of the requirements for
the degree of Doctor of Philosophy in
The University of Michigan

March 1965

ACKNOWLEDGMENTS

The author wishes to thank the members of his doctoral committee for their helpful comments and technical guidance. Special appreciation is due Professors D. M. Grimes, Chairman and B. F. Barton and Dr. P. J. Khan for their counsel in the final preparation of the paper.

Special gratitude is owed to Mrs. Lisa Shellman, Miss Ann Rentschler, and Mr. Gary Greenlee for preparing this manuscript for publication.

Finally, the author is appreciative of the support given this work by the U. S. Army Electronic Materiel Agency under Contracts DA 36-039 AMC-03733(E) and DA 28-043 AMC-00029(E).

TABLE OF CONTENTS

TABLE OF CONTENTS (Cont.)

LIST OF TABLES

LIST OF ILLUSTRATIONS

LIST OF ILLUSTRATIONS (Cont.)

LIST OF ILLUSTRATIONS (Cont.)

LIST OF SYMBOLS

Symbol	Meaning	Defined by or first used in
ω	angular frequency	Sect. 1.2
ω_1	signal frequency	Sect. 1.2
ω_2	local oscillator or pump frequency	Sect. 1.2
ω_{mn}	$m\,\omega_1 + n\,\omega_2$	Sect. 2.2
m, n	subscript integers	Sect. 2.2
$P_{m,n}$	average power entering reactive mixer at ω_{mn}	Eq. 2.1
ω_ℓ	$\omega_2 - \omega_1$ lower sideband frequency	Eq. 2.3
ω_u	$\omega_2 + \omega_1$ upper sideband frequency	Eq. 2.8
τ	voltage transmission coefficient	Eq. 2.13
G	conductive part of admittance	Eq. 2.13
B	susceptive part of admittance	Eq. 2.13
Y_o	characteristic admittance of transmission line	Eq. 2.13
ω_o	resonant frequency of tuned circuit	Fig. 2-1
$\Delta\omega_o$	$\omega_o - \omega$	Eq. 2.14
$\delta\phi$	incremental phase shift	Eq. 2.16
β_p	instantaneous bandwidth at local oscillator frequency	Eq. 2.17
Q_ℓ	loaded Q of resonant circuit	Eq. 2.19
G_t	transducer gain	Eq. 2.20
ζ	detector efficiency	Eq. 2.20
P_{sb}	total sideband power	Eq. 2.24
P_a	available source power	Eq. 2.26
V_p	amplitude of pump voltage	Eq. 2.21
P_p	pump power	Eq. 2.23

Symbol	Meaning	Defined by or first used in
i_s	amplitude of the signal current	Eq. 2.27
R_s	signal source resistance	Sect. 2.6
T_i	tunability	Eq. 2.27
$P_{u,\ell}$	upper and lower sideband power	Eq. 2.22
$\tau_{u,\ell}$	upper and lower sideband voltage transmission coefficient	Eqs. 2.33 & 2.35
β_i	input (signal frequency) bandwidth)	Eq. 2.36
$\overline{B}$	magnetic flux density (notation for vector)	Sect. 3.2
μ_o	permeability of free space	Sect. 3.2
$\overline{H}$	magnetic field intensity	Sect. 3.2
$\overline{m}$	magnetic moment per unit volume (i.e., magnetization)	Eq. 3.2
$\overline{J}$	true current density	Sect. 3.2
$\overline{D}$	electric flux density	Sect. 3.2
U_{aniso}	anisotropy energy	Eq. 3.1
α	damping constant in magnetic equation of motion	Eq. 3.5
$\overline{H}_o$	biasing magnetic field	Eq. 3.7
γ	gyromagnetic ratio	Eq. 3.2
$(\overline{\overline{X}})$	susceptibility tensor (notation for tensor)	Eq. 3.8
ω_{res}	ferromagnetic resonance frequency	Eq. 3.11
ω_r	$\alpha \gamma H_o$	Eq. 3.11
$\overline{H}_i$	magnetic field inside ferrite sample	Eq. 3.13
$\overline{N}$	demagnetizing tensor	Eq. 3.13
$M^{\pm}$	forward and backward circularly polarized magnetization	Eq. 3.17
$H^{\pm}$	forward and backward circularly polarized magnetic field	Eq. 3.18
M_o	saturation magnetization	Eq. 3.10

Symbol	Meaning	Defined by or first used in
K	anisotropy constant	Eq. 3.21
Φ	scalar magnetic potential	Eq. 3.24
$\overline{A}$	vector magnetic potential	Eq. 3.24
k	wave number	Eq. 3.26
K	diagonal component of susceptibility tensor	Eq. 3.36
ν	off diagonal component of susceptibility tensor	Eq. 3.45
$\Phi^{(2)}$	scalar potential correct to second order	Eq. 3.37
$A^{(2)}$	vector potential correct to second order	Eq. 3.42
$\overline{H}^{(2)}$	magnetic field correct to second order	Sect. 3.7.1
$\overline{M}^{(2)}$	magnetization correct to second order	Sect. 3.7.1
$\overline{M}_o$	zero order approximation to magnetization	Eq. 3.37
G	Green's function for scalar potential	Eq. 3.43
ρ_m	source for scalar potential	Sect. 3.7.1
$\omega_{mn\ell}$	resonant frequencies of sample modes	Sect. 3.7.4
$\overline{M}_n$	magnetization at frequency ω_n	Eq. 4.1
$\overline{H}_n$	magnetic field at frequency ω_n	Eq. 4.1
$\overline{\overline{\mu}}$	permeability tensor	Sect. 4.2
M_{in}	(i = x, y, z) magnetization components at frequency ω_n	Eq. 4.2
H_{in}	(i = xyz) magnetic field components at frequency ω_n	Eq. 4.2
$P_{\omega n}$	power leaving ferrite sample at ω_n	Sect. 4.5.2
ϕ_n	phase at frequency ω_n	Eq. 4.30
ω_p	γH_2	Sect. 4.5.3
ω_o	ferromagnetic resonance	Sect. 4.5.3 only
f_n	normalized field distribution at ω_n	Eq. 4.39
ΔH	ferromagnetic resonance linewidth	Eq. 4.47
v_c	volume of microwave cavity	Eq. 4.48
X_{ij}	susceptibility tensor components (i, j = 1, 2, 3)	Chapter 4

Symbol	Meaning	Defined by or first used in
$M_n^{\pm}$	circularly polarized magnetization at ω_n	Chapter 4
$H_n^{\pm}$	circularly polarized magnetic field at ω_n	Chapter 4
h	amplitude of signal field in the sample	Sect. 5.3
T	tunability with respect to signal magnetic field	Sect. 5.3
$f(\bar{r})$	signal field distribution (normalized)	Sect. 5.3
L	inductance of signal frequency circuit	Eq. 5.14
$\bar{\bar{\mu}}$	permeability tensor	Eq. 5.16
$\delta\mu$	incremental change in permeability tensor	Eq. 5.21
$\overline{E}_{1,2}$	r-f electric field in cavity for two values of biasing field in sample	Eq. 5.16
$\overline{H}_{1,2}$	r-f magnetic field in microwave cavity for 2 values of biasing field	Eq. 5.16
ω_1	complex resonant frequency of microwave cavity	Eq. 5.21
ω_o	real part of $\tilde{\omega}_1$	Eq. 5.31
$\delta\omega_o$	incremental change in ω_o	Eq. 5.31
a	sample radius	Sect. 5.5
f_o	$\omega_o/2\pi$	Sect. 5.5
v_s	sample volume	Eq. 5.46
H_e	externally applied biasing field	Eq. 5.51
δH_e	increment of H_e	Table 5-1
H	magnetic field distribution at pump frequency in the cavity	Eq. 5.40
A	$a \int_{v_s} \lvert H\rvert^2 dv \;/\; \int_{v_c} \lvert H\rvert^2 dv$	Eq. 5.46
H_c	coercive force	Fig. 5-10
H_s	applied magnetic field for saturation	Fig. 5-10
W	total free energy in magnetic sample	Sect. 5.7
K	anisotropy constant	Sect. 5.7

LIST OF SYMBOLS (Cont.)

Symbol	Meaning	Defined by or first used in
H_k	anisotropy field	Sect. 5.7
$L_{1,2}$	inductance of pair of coils wound on thin film sample	Sect. 5.7
A_m	cross-section of material in thin film sample	Eq. 5.66
A	total cross-section of thin film sample	Eq. 5.66
$k_{1,2}$	coil geometrical factors for coils would around thin film	Eq. 5.67
P_{th}	threshold power level	Sect. 6.1
γ_1	effective propagation coefficient	Eq. 6.6
μ_s	initial permeability	Eq. 6.12
$P_{th,m}$	optimum threshold	Eq. 6.12
β	complex propagation coefficient distributed ferrite loaded section	Sect. 6.3.2
$\overline{E}_{it}, \overline{H}_{it}$	(i = 1, 2) transverse electric and magnetic field for 2 bias fields	Sect. 6.3.2
$\beta_{1,2}$	β for 2 values of bias	Sect. 6.3.2
λ_m	guide wavelength inside ferrite	Eq. 6.22
$S_{m,g}$	cross-sectional areas of material and waveguide	Eq. 6.20
α	attenuation constant of ferrite loaded waveguide	Sect. 6.3.5
T	transmission coefficient	Eq. 6.34
Γ	reflection coefficient	Eq. 6.34
b	normalized susceptance	Eq. 6.35
ϕ	electrical length of ferrite loaded waveguide	Eq. 6.34
Y_L	load admittance	Sect. 7.2
ρ	reflection coefficient	Sect. 7.2
Δ_ρ	increment of ρ	Sect. 7.2
h_{crit}	critical pump field for spin wave excitation	Eq. 7.7
P_{crit}	pump power at which field is h_{crit}	Eq. 7.9

LIST OF SYMBOLS (Cont.)

Symbol	Meaning	Defined by or first used in
K (Ch 7 only)	pump threshold per unit bandwidth	Eq. 7.20
$\Delta\sqrt{w}$	incremental change in stored signal energy produced by Δh	Eq. 7.24
P_{avail}	available signal power	Eq. 7.28
N_i	thremal noise contributed by signal circuit	Eq. 7.42
F	noise figure of ferrite phase-shift amplifier	Eq. 7.44
F_{md}	noise figure for a double-sideband mixer	Eq. 7.45

LIST OF APPENDICES

ABSTRACT

The phase-shift amplifier is a member of the class of double-sideband reactive mixer circuits. Its properties have been studied throughly for the case in which a varactor serves as the reactive mixer element. For this case gain-bandwidths products of the order of 10^9 have been achieved with noise figures on the order of 2 db. The purpose of this paper is to study the phase-shift amplifier for the case in which a ferrite material serves as the reactive mixer.

Reactive mixing properties of ferrites are studied with respect to the fundamental material properties. The ferrite parametric amplifier, which is also a reactive mixer circuit, is discussed and the conditions for minimum pump power are found. The ferrite parameters pertinent to the phase-shift amplifier are isolated and studied.

Various distinct configurations for the ferrite phase-shift amplifier are presented and optimized with respect to material and design parameters. The factors which tend to limit gain-bandwidth product are reviewed and the maximum theoretical and experimental gain-bandwidth products are estimated. In addition, the noise phenomena fundamental to ferrites are surveyed and noise figure estimates are made. A revealing comparison between varactor and ferrite reactive mixers is developed which tends to explain why use of the former yields superior phase-shift amplifiers.

Although the results of the study indicate that the ferrite phase-shift amplifiers are not practical compared to a conventional varactor version, the thesis contains a variety of interesting investigations of important ferrite phenomena. For example, the boundary value problem of a small ferrite sample immersed in an r-f magnetic field is solved. This solution tends to explain the so-called magnetostatic resonances which have been observed in ferromagnetic resonance experiments. In addition, the ability of a ferrite material to tune a microwave cavity is studied both experimentally and theoretically for circumstances which have not previously been considered. Furthermore, an analysis of the Reggia-Spencer phase-shifter is conducted in which the ferrite properties most significant for the

operation of the device are isolated. The effect of tuning the phase shifter with reactive obstacles is studied theoretically by means of the appropriate signal flow graph. Thus, the ferrite phenomena fundamental to a variety of microwave devices are studied from somewhat unique standpoints.

CHAPTER 1

1. INTRODUCTION

The phase-shift amplifier, which was developed primarily by Adams (Ref. 1), has proven to be a significant contribution to amplifier technology. Gain-bandwidth products of the order of 1000 Mc and extremely low noise figures have been achieved for this amplifier which means that it has important application as a preamplifier in modern communication and radar systems. These important applications provide strong motivation for the detailed investigation of the phase-shift amplifier.

Adams has shown that the phase-shift amplifier is a member of the class of circuits called reactive mixer circuits. Any linear time independent circuit becomes a reactive mixer circuit when it is coupled to a nonlinear or linear time varying reactive element. A circuit element of this type is normally called a reactive mixer. The circuit component most familiar to electrical engineers which has reactive mixer properties is called a varactor. (The varactor is a special type of semiconductor diode whose junction capacitance is a sensitive function of the voltage across the junction.) The varactor was used by Adams in his study of reactive mixer circuits. However, a number of other components and materials exhibit reactive mixer properties such as certain ferromagnetic and ferroelectric materials. Ferrites are members of the former class of materials.

1.1 Statement of the Problem

Although the fundamental properties of phase-shift amplification were studied thoroughly by Adams, many of the conclusions and practical limitations which he found were based upon the properties of the varactor and are not applicable directly to circuits employing other reactive mixers. The purpose of this paper is to report an investigation of the properties of a phase-shift amplifier which employs a ferrite material as the reactive mixer. The limitations and special advantages of the ferrite reactive mixer for phase-shift amplification will be studied with respect to fundamental physical properties of the material.

At the outset, certain advantages of the use of ferrites can be anticipated. For

example, the principal source of noise in a varactor is shot noise which is not present in ferrites because they are electrical insulators. In addition, the power handling capacity of varactors is restricted by the small size of the junction in which reactive mixing occurs. On the other hand, no such restriction is evident for ferrites which can be prepared in samples of arbitrary size. Thus, it is expected that ferrites might give rise to phase-shift amplifiers with noise performance and power capacity superior to those of varactor amplifiers.

1.2 Topics of Investigation

It has been stated that the purpose of this paper is to report a study of the application of ferrites to phase-shift amplification. In this investigation the following topics will be explored:

(a) The physical properties of ferrite materials which make them useful for phase-shift amplification will be studied. For this study it is convenient to divide ferrites into two distinct classes depending upon whether they are magnetically saturated or unsaturated (the definition of magnetic saturation appears in Section 1.3.). This distinction is significant because the relationship between the pertinent electrical variables can be computed analytically for only the former case.

(b) The field distributions in a ferrite sample excited by an r-f source will be obtained by a solution to Maxwell's equations. An approximate boundary value problem, valid for small samples, will be obtained by manipulation of Maxwell's equations and will be solved exactly.

(c) The reactive mixing properties of ferrites will be studied under the assumptions:

(1) power is supplied at two frequencies ω_1 and ω_2 where $\omega_2 > \omega_1$,

(2) filters restrict the power flow to the four frequencies including: ω_1, ω_2, $\omega_2 \pm \omega_1$.

It is shown in Chapter 2 that these assumptions are significant for reactive mixer circuits.

(d) The limitations imposed by ferrites on phase-shift amplification will be studied with respect to the fundamental physical properties. A comparison between ferrites and varactors will be made on the basis of this study and the work reported by Adams. Such a comparison is significant because the varactor amplifiers have proved to be very successful.

(e) A number of practical configurations of the ferrite phase-shift amplifier will be studied experimentally and compared with theoretical predictions. Wherever possible, each configuration will be optimized with respect to material parameters.

(f) The noise figure and theoretical maximum gain-bandwidth product will be estimated for each practical configuration.

1.3 Review of the Literature

Adams (Ref. 1) has very thoroughly reviewed the literature which concerns the general properties of reactive mixer circuits from the earliest work (in about 1916) to the present. However, the bulk of the current literature (from 1954 to present) was primarily concerned with the varactor.

The first proposed application of ferrites as reactive mixers appeared in 1957 in a paper by Suhl (Ref. 22). This is primarily a theoretical paper proposing the use of a ferrite in a parametric amplifier which is a circuit closely related to the phase-shift amplifier. Suhl's paper is basically a survey of three principal modes of operation of the amplifier.

The first practical ferrite parametric amplifier was an experimental extension of Suhl's work by Denton (Ref. 23). The performance of this amplifier was somewhat marginal, being characterized significantly by an excessive noise figure.

Many variations of the configuration employed by Denton have been reported in the literature since the publication of his paper (Refs. 54-58) but these configurations are all

parametric amplifiers. To the author's best knowledge this paper reports the first application of ferrites to phase-shift amplification.

1.4 Thesis Organization

(a) Chapter 2 contains a brief survey of the important properties of reactive mixer circuits with special emphasis upon the phase-shift amplifier.

(b) Chapter 3 is a review of the physical properties of ferrite materials with emphasis on their reactive mixing properties.

(c) Chapter 4 is a study of reactive mixing in ferrites and contains a brief discussion of two circuits which are closely related to the ferrite phase-shift amplifier.

(d) Chapter 5 is a study of the physical properties of ferrites which apply directly to phase-shift amplification. In particular, the limitations imposed by these materials on this type of amplification is related to fundamental ferrite properties.

(e) Chapter 6 is a report of the experimental investigation of a number of practical configurations of the ferrite phase-shift amplifier. The experimental and theoretical limitations of each configuration are compared and discussed.

(f) Chapter 7 contains a study of the practical limitations of the ferrite amplifier, including a revealing comparison of ferrite and varactor reactive mixers. It also includes an estimate of the maximum theoretical gain-bandwidth product for various configurations and closes with the conclusions of this study.

CHAPTER 2

PROPERTIES OF REACTIVE MIXER CIRCUITS

2. 1 Introduction

The reactive mixing properties of ferrites make them useful in phase-shift amplification. Thus, a review of the fundamental properties of reactive mixers and reactive mixer circuits provides the proper background for the study of ferrite phase-shift amplifiers. The equations which describe the power flow through a reactive mixer are presented in this chapter. The relation of the phase-shift amplifier to the general reactive mixer is explored and contrasted to two other special classes of reactive mixer circuits. The pertinent gain and bandwidth relations are derived in Sections 2. 5 and 2. 6, respectively.

2. 2 A Survey of Reactive Mixer Properties

The term reactive element applies to a circuit element which is capable of storing energy. The ideal lumped circuit model for a reactive element is an ideal capacitor or inductor. A reactive mixer is a nonlinear or linear time varying, energy-storage element. Whenever two sinusoidal signals are coupled by such an element the phenomenon of frequency mixing will occur, i. e., if a linear time dependent reactance is excited by two sinusoidal signals ω_1, ω_2 then the output of this mixer will contain components at the frequencies $\omega_{mn} = m\omega_1 + n\omega_2$. This production of components $\omega_{m,n}$ is called reactive mixing. Any linear time independent circuit (e. g., filter) which is connected to the mixer will influence the relative distribution of power in this spectrum and may even suppress certain components. Adams has shown that filters which restrict the frequencies of power flow through the reactive element to a desired subset of the total set ω_{mn} can be successfully approximated. The properties of the circuit formed by coupling a reactive mixer to various filters depend markedly upon the set of frequencies at which real power flows.

The relationships which describe the real power flow through a reactive mixer were first derived by Manley and Rowe (Ref. 2):

$$\sum_{m=0}^{\infty} \sum_{n=0}^{\infty} \frac{m P_{mn}}{m\omega_1 + n\omega_2} = 0 \qquad (2.1)$$

$$\sum_{n=0}^{\infty} \sum_{m=0}^{\infty} \frac{n P_{nm}}{m\omega_1 + n\omega_2} = 0 \qquad (2.2)$$

where P_{mn} is the power entering the mixer at frequency $m\omega_1 + n\omega_2$. The above relations were written for a lossless capacitive mixer and give the inherent limitations governing power flow at one frequency or set of frequencies. A similar set of equations exists for an inductive mixer. Adams has shown that a large number of circuit properties can be controlled by suppressing various components of the set $\omega_{m,n}$. In this paper it is assumed that filters limit the power flow to four frequencies of the set $\omega_{m,n}$; i.e., ω_1, ω_2, $\omega_2 - \omega_1$, $\omega_2 + \omega_1$ where $\omega_2 > \omega_1$ and where sources are present at ω_1 and ω_2 only. It is assumed that all others are suppressed. Adams has shown that four frequencies are enough to provide several interesting circuit effects; and few enough that analysis is relatively simple. If $\omega_2 > \omega_1$, then ω_2 may be regarded as a local oscillator (often referred to as the pump) and ω_1 a reference signal. The signal at frequency $\omega_2 - \omega_1$ is normally called the lower sideband of the mixer and the signal at $\omega_2 + \omega_1$ is the upper sideband. Many interesting results are obtainable with circuits which suppress either of the sidebands.

Although Adams has shown that the phase-shift amplifier is a double-sideband reactive mixer (i.e., power flows at all four frequencies) and although the principal interest of this paper is the double-sideband circuit, it is instructive to review briefly some of the properties of the single-sideband circuits.

2.3 The Lower Sideband Reactive Mixer (Parametric Amplifier)

The circuit which utilizes the lower sideband and suppresses the upper sideband is conventionally called a parametric amplifier. The Manley-Rowe relations for this situation are

$$\frac{P_2}{\omega_2} + \frac{P_\ell}{\omega_\ell} = 0 = \frac{P_1}{\omega_1} - \frac{P_\ell}{\omega_\ell} \qquad (2.3)$$

where $\omega_\ell = \omega_2 - \omega_1$; i. e., the lower sideband. The conversion gain, defined as the ratio of lower sideband power to signal power, is given by:

$$G_{\ell_1} = -\frac{P_\ell}{P_1} = -\frac{\omega_\ell}{\omega_1} \tag{2.4}$$

If power is not supplied at ω_ℓ (i. e., in the normal circumstance) then

$$P_\ell \leq 0 \tag{2.5}$$

But

$$-\frac{\omega_\ell}{\omega_1} < 0 \tag{2.6}$$

so $P_1 < 0$. This relation shows that more power is leaving the circuit than is entering at ω_1. Notice that the signal frequency power leaving the circuit increases in proportion to the lower sideband power leaving the circuit. Thus, the reflection coefficient at the signal frequency is greater than unity. The circuit manifestation of this effect is a negative resistance which appears across the terminals of the signal circuit. Circuit analysis indeed shows this to be the case. If the lower sideband is terminated in a parallel resonant circuit ($P_\ell < 0$) then (assuming a linear time-varying capacitive mixer) at resonance the magnitude of the negative resistance is (Ref. 3):

$$\frac{C_\Delta^2 \omega_\ell \omega_1}{g_\ell} \tag{2.7}$$

Where C_Δ is the amplitude of the capacitance variation (which is proportional to pump power and g_ℓ is the total shunt susceptance of the lower sideband termination. If the pump power is sufficiently large, the magnitude of the negative conductance is the same as the conductance of the signal frequency circuit and all the signal power entering the circuit is reflected. This value of pump power is called the unity gain threshold, or sometimes simply the threshold. When the pump power exceeds the threshold the circuit acts as a power amplifier at the signal frequency. For sufficiently large pump power the magnitude of the negative resistance will match the transmission line supplying power at ω_1 and the circuit will oscillate.

The lower-sideband circuit has many other interesting properties which are discussed thoroughly in Adams (Ref. 1). For the purpose of this paper, the pertinent features of the lower-sideband reactive mixer have been adequately summarized.

2.4 The Upper Sideband Up-Converter

The circuit which utilizes the upper sideband and suppresses the lower sideband is characterized by the following Manley-Rowe relations (Ref. 1):

$$\frac{P_2}{\omega_2} + \frac{P_u}{\omega_u} = 0 = \frac{P_1}{\omega_1} + \frac{P_u}{\omega_u} \tag{2.8}$$

where $\omega_u = \omega_2 + \omega_1$; i.e., the upper sideband. Rearranging, the second relation predicts that the conversion gain $G_{u,1}$ from ω_1 to ω_u is proportional to the frequency ratio:

$$G_{u,1} = -\frac{P_u}{P_1} = \frac{\omega_u}{\omega_1} \tag{2.9}$$

which gain always exceeds unity. Note that if no power is supplied at ω_u, then $P_1 > 0$, so that the negative resistance effect characteristic of the lower sideband does not occur for the upper-sideband circuit. This circuit is stable for any pump power, provided power is not supplied at P_u.

By eliminating P_u/ω_u from the two relations and rearranging, one finds that

$$\frac{P_2}{P_1} = \frac{\omega_2}{\omega_1} \tag{2.10}$$

which may be interpreted to mean that the two sources contribute to the converted power in the ratio of their frequencies. Observe that frequency conversion in an upper-sideband up-converter is accompanied by power gain. This implies that this circuit will function as an amplifier at the signal frequency if the power in the upper sideband can be down converted to the signal frequency. Obviously, a reactive mixer cannot be used for the down-conversion because the down-conversion loss is equal to up-conversion gain. However it is a property of resistive mixers (e.g., diode) that down-conversion loss tends to be independent of frequency. Typical losses for down-conversion with a resistive mixer are as low as 6 db.

Thus, if the frequency ratio

$$\frac{\omega_u}{\omega_1} > 4 \tag{2.11}$$

then the upper-sideband converter conversion gain can exceed the down-conversion loss and the circuit can amplify the signal.

2.5 The Double-Sideband Reactive Mixer (Phase-Shift Amplifier)

The properties of the double-sideband circuit consist of combinations of the single-sideband circuits. For example, the utilization of the lower sideband increases the conversion gain between frequencies ω_1 and ω_u since it reflects negative resistance to the impedance at ω_1 which amplifies this signal before it is converted to ω_u. Further, if the power which flows at the lower sideband is sufficiently large compared to the power at the upper sideband then the circuit oscillates at the signal frequency for sufficiently large pump power.

It has been tacitly assumed in the preceding paragraph that the power in the sidebands can be independently controlled. If the frequency of the signal ω_1 is low, then the upper and lower sidebands fall in the passband of the filter used to separate the local oscillator ω_2 from ω_1. In this situation the sidebands cannot be controlled independently. In this case, where both sidebands are terminated in the same conductance (i.e., that of the local oscillator) it has been shown (Ref. 1) that the conductance reflected into the signal circuit is

$$\frac{C_\Delta^2 \omega_1}{g_2} (\omega_u - \omega_\ell) \tag{2.12}$$

This expression is always positive, since $\omega_u > \omega_\ell$, so that the circuit is stable for all values of pump power. However, this circuit cannot amplify the signal at ω_ℓ directly because it does not reflect a component of negative resistance. Amplification of the signal occurs with sufficient conversion gain between the signal and the two sidebands in a reactive mixer, accompanied by down-conversion to the signal frequency in a separate device. The loss which is fundamental to down-conversion must be less than the up-conversion gain for amplification. In this paper it is assumed that down-conversion is accomplished with a re-

sistive mixer (e.g., diode rectifier).

Adams has shown that the distinction between double-sideband amplification and lower-sideband amplification (i.e., parametric amplification) is somewhat subtle, since both can be accomplished with the same element (Ref. 4). Power gain in both results from conversion of the signal to a higher frequency by means of a reactive mixer. However, the term amplification implies power gain at the signal frequency, so conversion to a higher frequency must be accompanied by some form of down-conversion. Both conversions are accomplished in a single element in parametric amplification, whereas for double-sideband amplification, down-conversion must be accomplished with a second element. In addition, parametric amplification is basically a bandpass technique, whereas double-sideband amplification can be either bandpass or lowpass in character. Adams has shown that these types of amplification differ also in their gain-bandwidth product. Specifically, when the center frequency of the signal band is low, the double-sideband circuit offers greater gain for a given bandwidth, while at higher values of signal band center frequency parametric amplification is superior in this respect.

Adams has shown that in an optimum configuration, the sidebands constitute phase modulation of the carrier (Ref. 4). For this reason he has termed double-sideband amplification "phase-shift amplification." Thus the phase-shift amplifier is a double sideband reactive mixer. However, in practice, the term phase-shift amplifier is applied to any amplifier which produces gain by first converting to a higher frequency by means of a reactive mixer and then down-converting in a separate element. The down-conversion is normally accomplished by first converting the phase modulation to amplitude modulation and then detecting with an A-M detector. Any practical configuration of a phase-shift amplifier will be inherently a small-signal device. For this reason, phase modulation can be converted to amplitude modulation by inserting a carrier component phased in quadrature with the unmodulated carrier. The sidebands can then be coherently detected with a resistive diode. It will be assumed in this paper that the detection bandwidth is sufficiently large that it imposes no restrictions on the amplifier.

It is instructive to review briefly some of the properties of the phase-shift amplifier and to illustrate those circuit parameters which are influenced by the physical parameters of the ferrite, when this magnetic material is used as the reactive element. The

significant dependent variables appropriate to amplifier circuits are gain and bandwidth. For the purpose of investigating these quantities it is convenient to refer to Fig. 2-1 which is a prototype equivalent circuit for a phase-shift amplifier. Although this circuit is not necessarily

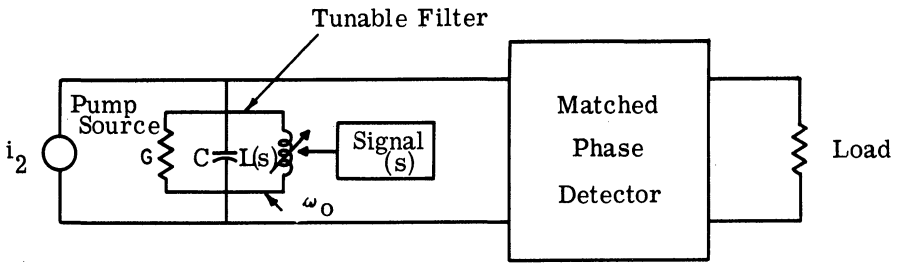

Fig. 2-1. Prototype equivalent circuit for a phase-shift amplifier. The parameter ω_o is the instantaneous resonant frequency of the tunable filter.

the optimum phase-shift amplifier, it is a convenient prototype model for studying the applicability of ferrites to phase-shift amplifiers. It will be shown later how this circuit can be optimized.

The ferrite reactive mixer in the circuit of Fig. 1 incorporates an inductor, the inductance(L)of which is proportional to some signal variable s (e.g., signal current). The tuned circuit is adjusted so that at zero signal the pump frequency and filter resonant frequency coincide. Under these conditions, the application of a signal s causes the resonant frequency of the tuned circuit to vary at the signal frequency. When the resonant frequency variation is small compared to the bandwidth of the tuned circuit, the effect is approximately that of phase modulation of the pump power transmitted to the detector.

The gain of the phase-shift amplifier depends upon the magnitude of the phase shift for a given signal amplitude. The magnitude of the incremental phase shift $\delta\phi$ produced by an incremental change in S can be determined from the voltage transmission coefficient τ:

$$\tau = \frac{2\,Y_o}{2\,Y_o + G + jB} \tag{2.13}$$

where Y_o is the characteristic admittance of the line, G the equivalent shunt conductance of the filter, and B the filter shunt susceptance. If the quiescent signal magnitude is such that

the resonant frequency is equal to the pump frequency, an increment δs produces a change $\Delta\omega_o$ in resonant frequency, and τ can be written:

$$\tau \cong \frac{2\,Y_o}{2\,Y_o + G + j\,2\,\Delta\omega_o C} \tag{2.14}$$

Expressing τ in the form

$$\tau = |\tau|\, e^{j\phi} \tag{2.15}$$

then the incremental phase shift $\delta\phi$ is given by:

$$\delta\phi \cong -\frac{2C\,\Delta\omega_o}{2Y_o + G} \tag{2.16}$$

The instantaneous bandwidth of the transmission coefficient $|\tau|$ is given by:

$$\beta_p = \frac{2\,Y_o + G}{C} \tag{2.17}$$

where β_p is twice the frequency difference $\Delta\omega_o$ for which $|\tau|^2$ is half its maximum value. The instantaneous bandwidth of the pump filter will be denoted by β_p throughout this paper and called pump bandwidth for convenience. This quantity can be substituted into Eq. 2.16.

$$\delta\phi \cong -\frac{2\,\Delta\omega_o}{\beta_p} \tag{2.18}$$

and

$$\delta\phi = -\frac{2\,Q_\ell\,\Delta\omega_o}{\omega_o} \tag{2.19}$$

where $Q_\ell = \omega_o/\beta_p$.

2.6 Transducer Gain and Tunability

The midband gain of the circuit can be found from $\delta\phi$, but before proceeding with this computation it is convenient to discuss the gain definition which is most significant for phase-shift amplifiers. This gain, called transducer gain, is defined as the ratio of signal

frequency power delivered to a matched load to the power available from the source. It is calculated for a down-conversion stage referred to as a "matched phase detector" (defined below), which introduces an efficiency factor ζ. This quantity is defined as the ratio of the signal power flowing in the load to the total sideband power which enters the matched phase detector and can reach a maximum of 50 percent. When this definition is used, the transducer gain is given by:

$$G_t = \frac{\zeta P_{sb}}{P_a} \tag{2.20}$$

where P_{sb} is the total sideband power and P_a is the available signal frequency power of the source.

The transducer gain can be related to the equivalent circuit parameters in the following way. The pump voltage which is transmitted to the phase detector can be written in the form:

$$V_2(t) = V_p \cos \left[\omega_2 t + \phi_2 + \delta\phi \cos (\omega_1 t + \phi_1) \right] \tag{2.21}$$

where V_p is the amplitude of the pump voltage, ϕ_2 is its phase, $\delta\phi$ is the amplitude of the phase shift produced by the signal, and ϕ is its phase. It is well known that in the small signal approximation the power in both the upper and lower sidebands is given by:

$$P_{u,\ell} = \frac{1}{4} P_p(\delta\phi)^2 \tag{2.22}$$

where P_p is the pump power which is delivered to the phase detector at zero signal and for a matched phase detector is given by

$$P_p = \frac{V_p^2}{2 Y_o} \tag{2.23}$$

The total sideband power is the sum of the upper and lower sideband power and is given by

$$P_{sb} = \frac{1}{2} P_p(\delta\phi)^2 \tag{2.24}$$

But it has been shown (Eq. 2. 19) that

$$\delta\phi = - \frac{Q_\ell \, \Delta\omega_o}{\omega_o} \tag{2.25}$$

Thus the transducer gain is given by:

$$G_t = \frac{\frac{1}{2} \zeta \, P_p}{P_a} \left(2 Q_\ell \, \frac{\Delta\omega_o}{\omega_o} \right)^2$$

$$= \frac{\frac{1}{2} \zeta \, P_p}{P_a} \left(2 Q_\ell \, \frac{1}{\omega_o} \, \frac{d\omega_o}{ds} \, \Delta s \right)^2 \tag{2.26}$$

where Δs is the amplitude of the signal variable. It is shown in Chapter 5 that for the ferrite phase-shift amplifier, s is most conveniently chosen as the signal frequency current Δi_s. If the signal source is represented by its Norton equivalent then

$$P_a = \frac{1}{2} R_s \, |\Delta i_s|^2$$

where R_s is the signal source resistance.

It is convenient to define a quantity which we call tunability T_i:

$$T_i = \frac{1}{\omega_o} \, \frac{d\omega_o}{d i_s} \tag{2.27}$$

When this quantity is substituted into the expression for transducer gain, the result is

$$G_t = \frac{2 \zeta \, P_p}{R_s} \, (Q_\ell \, T_i)^2$$

which is the most convenient form in the study of the ferrite phase-shift amplifier.

Tunability is an important parameter in this study because of its easily discernible relation to both amplifier gain and bandwidth and to the physical properties of the ferrite. Much of Chapter 5 is devoted to an investigation of the physics of ferrites with respect to tunability.

2.7 Bandwidth Considerations for a Phase-Shift Amplifier

Bandwidth is another important dependent variable in any amplifier circuit. The bandwidth of a phase-shift amplifier is limited by two basic effects: (1) the finite bandwidth of the parallel resonant circuit (see Fig. 2-1), and (2) the bandwidth of the signal transmission path. The latter is often limited by a large static reactance presented at the signal port of typical reactive mixers.

The pump filter bandwidth influences the transmission of sideband power to the matched phase detector, efficient sideband transmission being in fact the governing design consideration. The actual sideband power reaching the load is given by:

$$P_{sb\ load} = P_{sb,u} |\tau_u|^2 + P_{sb,\ell} |\tau_\ell|^2 \tag{2.28}$$

where $\tau_{u,\ell}$ are the transmission coefficients at upper and lower sidebands and $P_{sb,u}$, for example, is the upper sideband power generated in the reactance. Thus

$$P_{sb} = \frac{P_p(\Delta\phi)^2}{4} (|\tau_u|^2 + |\tau_\ell|^2) \tag{2.29}$$

The expression for τ was given previously, from which it is possible to compute:

$$|\tau|^2 = \frac{4\,Y_o^{\,2}}{\left|(2Y_o + G) + j\,\omega_o C\left(\frac{\omega}{\omega_o} - \frac{\omega_o}{\omega}\right)\right|^2} \tag{2.30}$$

$$|\tau|^2 \cong \frac{4\left(\frac{Y_o}{C}\right)^2}{\beta_p^{\,2} + \left(\omega - \frac{\omega_o^{\,2}}{\omega}\right)^2}$$

$$= \frac{4\,\frac{\omega^2 Y_o^{\,2}}{C^2}}{\omega^2 \beta_p^{\,2} + (\omega^2 - \omega_o^{\,2})^2} \tag{2.31}$$

where β_p is the pump bandwidth. But for the upper sideband $\omega_u = \omega_o + \omega_1$ and:

$$\omega^2 - \omega_o^2 = (\omega - \omega_o)(\omega + \omega_o)$$

$$= \omega_1 (2\omega_o + \omega_1) \tag{2.32}$$

Thus the transmission coefficient for the upper sideband is given by:

$$|\tau_u|^2 = \frac{4\left(\frac{\omega_u Y_o}{C}\right)^2}{\omega_u^2 \beta_p^2 + \omega_1^2 (2\omega_o + \omega_1)^2} \tag{2.33}$$

But if $\omega_o >> \omega_1$, then this is given approximately by:

$$|\tau_u|^2 = \frac{4\left(\frac{\omega_o Y_o}{C}\right)^2}{\omega_o^2 \beta_p^2 + 4\omega_1^2 \omega_o^2}$$

$$= \frac{4\left(\frac{Y_o}{\beta_{p_1} C}\right)^2}{1 + \left(\frac{\omega_1}{\beta_{p_1}}\right)^2} \tag{2.34}$$

where $\beta_{p_1} = \frac{1}{2}\beta_p$. A similar computation for τ_ℓ reveals:

$$|\tau_\ell|^2 = \frac{4\left(\frac{Y_o}{\beta_p C}\right)^2}{1 + \left(\frac{\omega_1}{\beta_{p_1}}\right)^2} \tag{2.35}$$

Assuming that the signal transmission has a lowpass character, the transducer gain is given by:

$$G_t(\omega_1) = \frac{G_{t_o}}{\left(1 + \frac{\omega_1^2}{\beta_i^2}\right)\left(1 + \frac{\omega_1^2}{\beta_{p_1}^2}\right)} \tag{2.36}$$

where β_1 is the input bandwidth. Here $G_{t_o} = G_t(0)$ and is identical with the previously computed function G_t. The half-power bandwidth ω_1 is given by the solution to:

$$(\omega_1^2 + \beta_i^2)\left(\omega_1^2 + \frac{\beta_p}{2}\right)^2 = 2\beta_i^2\left(\frac{\beta_p}{2}\right)^2 \qquad (2.37)$$

The actual solution to this equation is not as important as some of its properties. Observe that if $\beta_p/2 >> \beta_i$ the solution is $\omega_1 \cong \beta_i$. The circuit bandwidth is then limited by the bandwidth of the signal circuit or it can be said that the amplifier is input bandwidth limited. On the other hand if $\beta_i >> \beta_p/2$ then the solution is $\omega_1 \cong \beta_p/2$ and the amplifier is pump bandwidth limited. In the case that $\beta_i = \beta_p/2$ then $\omega_1 \cong \beta_i$ is the 6 db circuit bandwidth and the over-all circuit bandwidth is $\omega_1 = .64\,\beta_i$.

Another amplifier bandwidth limitation, which has not been previously discussed, might result from the detector circuit properties. However, the bandwidths of several currently available broadband detectors far exceed the over-all bandwidth of most phase-shift amplifiers. Thus, only for ultra-wideband circuits does the detector bandwidth tend to limit over-all amplifier bandwidth. This situation is not considered further in this thesis.

There are other important dependent variables of an amplifier circuit such as noise figure. These variables will also be related to the fundamental material properties so that the optimum configuration can be determined.

CHAPTER 3

BASIC PHYSICAL PROPERTIES OF FERRITE MATERIALS

3. 1 Introduction

The objective of this chapter is to illustrate the properties of ferrites which make them useful as reactive mixers and which suggest their use in phase-shift amplifiers. Ferrites are a class of magnetic materials which are good electrical insulators. Thus the chapter begins with a survey of the magnetic properties of magnetic materials. The survey includes the steady-state energy relations, a derivation of the dynamic equation of ferromagnetic materials and a discussion of ferromagnetic resonance. Many of the properties of ferromagnetic resonance are referred to in Chapter 6, including the peculiar multiple resonances which occur at frequencies near the main (expected) ferromagnetic resonance. An explanation of the latter phenomenon is facilitated by solution of a boundary value problem in Section 3. 7 which is an original contribution.

3. 2 A Survey of the Properties of Magnetic Materials

A magnetic material can be defined as any material in which $\frac{\overline{B}}{\mu_o} - \overline{H}$ is nonzero, where $\overline{B}$ is the magnetic flux density and $\overline{H}$ is the magnetic field intensity. The difference between these quantities is the magnetic moment density of the material and is called the magnetization ($\overline{M}$) of the material. This definition enables a separation of that part of the magnetic field which results from true and displacement currents, from that which results from the atomic currents of the material. The latter is the source of $\overline{M}$. For this definition of $\overline{M}$, Maxwell's equation for the circulation density of the magnetic field intensity is solenoidal regardless of the medium:

$$\nabla \times \overline{H} = \overline{J} + \frac{\partial \overline{D}}{\partial t}$$

where $\overline{J}$ is the true current density and $\frac{\partial \overline{D}}{\partial t}$ is the displacement current. In addition, the condition

$$\nabla \cdot \overline{B} = 0$$

determines the relation:

$$\nabla \cdot \overline{H} = -\nabla \cdot \overline{M}$$

Thus even in the absence of true and displacement currents, a nonzero magnetic field exists provided that:

$$\nabla \cdot \overline{M} \neq 0$$

The relation of $\overline{M}$ to $\overline{H}$ is particularly significant in studying the application of ferrites as reactive mixers.

3.3 Ferromagnetic Materials

Magnetic materials can be divided somewhat arbitrarily into three general classes depending upon the relative dependence of $\overline{M}$ upon $\overline{H}$. Of these three only the class known as ferromagnetics, for which $\overline{M}$ depends most strongly upon $\overline{H}$, will be considered in this paper. A nonzero magnetization exists in a ferromagnetic material even in the absence of applied magnetic field. This gives rise to a rather large magnetostatic energy which would appear not to satisfy thermodynamic equilibrium. Quantum theory offers an explanation to this apparent paradox in its characterization of the magnetization on an atomic scale. In quantum theory the ultimate source of magnetization is attributed to a quantity possessed by electrons called spin (Ref. 5). Although spin has no analog in macroscopic dynamics, many of its properties can be explained using a semiclassical model. The electron may be pictured as a body having small but nonzero charge spinning on an axis of symmetry and thus producing a magnetic field. Regardless of the validity of this model, it is an experimental fact that electrons do possess an intrinsic magnetic moment. In nonferromagnetic materials these magnetic moments are randomly oriented. However, in ferromagnetics the most favorable energy configuration is with the moments aligned parallel. Quantum theory explains this phenomenon in terms of a so-called exchange energy which is extremely large for two proximate electrons having their spins aligned anti-parallel. Since the exchange energy is part of the total free energy of a material, the latter is minimized for parallel alignment which produces a net magnetization.

No net magnetic field is observed external to large samples of certain materials in which the magnetic moments are aligned only within portions of the sample volume which are referred to as domains. Thus, a magnetic domain is a region in which the magnetization is aligned parallel. The existence of domains can be explained by noting that the exchange energy has a very short range effect (i. e., nearest neighbors) and that the magnetostatic energy increases with the size of a region in which the spins are aligned. The short range effect of exchange tends to keep spins aligned in a region or domain, while, because of the magnetostatic energy, alignment of adjacent domains antiparallel is the most favorable energy condition. Thus, the size of the domains and their relative orientation is determined by the condition that the total free energy is a minimum.

The relationship between the average sample magnetization and a magnetic field can be seen by considering the effect of an external magnetic field on the domain structure. When the magnetic field is applied, the domains tend to rotate into the direction of the field. As the field is increased the size of the domains having a component of magnetization in the direction of the field increase at the expense of those having components oppositely aligned. Finally, when the field reaches a certain size, all of the magnetization is aligned in the direction of the applied field and the domain structure no longer exist. The sample is then said to be saturated. This is the basic process responsible for the shape of the B vs. H curve of a ferromagnetic (Ref. 6). The observed hysteresis may be explained by noting that domains fail to return to their original orientation when the applied field is removed due to losses in the motion of domain boundaries.

Anisotropy energy also plays a significant role in ferromagnetic material. It receives this name because it is a function of the orientation of the magnetization relative to the crystalline axes. For example, Landau and Lifshitz (Ref. 5) have shown that for uniaxial crystals the anisotropy energy is

$$U_{aniso} = \tfrac{1}{2} \beta |M|^2 \sin^2 \theta \qquad (3.1)$$

where θ is the angle between the magnetization vector and the axis of symmetry of the crystal and β is a dimensionless constant. If $\beta > 0$, then U_{aniso} is minimized with $\overline{M}$ along the crystal symmetry axis sometimes called the easy axis. If $\beta < 0$, then U_{aniso} is minimized

for $\theta = \frac{\pi}{2}$ (i. e., M in the plane normal to the axis). Higher order corrections are needed to predict the actual direction in this case, but even to first order, the anisotropy energy is useful for explaining the finite size of a domain wall (i. e., the region between adjacent domains).

3. 4 A Dynamic Equation for Ferromagnetic Materials

So far, only the steady state relationship between $\overline{M}$ and $\overline{H}$ has been investigated. It is now of interest to examine the dynamic response of the sample magnetization to the applied field. A magnetic moment $\overline{m}$ in the presence of a uniform magnetic field $\overline{H}$ experiences a torque $\overline{m} \times \overline{H}$. In quantum theory, it was shown that $\overline{m}$ is related to some angular momentum $\overline{s}$ by the relation $\overline{m} = -\gamma \overline{s}$ where γ is the so-called gyromagnetic ratio ($\gamma = 2.8$ Mc/Oe). The quasiclassical equation of motion is then

$$\frac{d\overline{m}}{dt} = -\gamma \overline{m} \times \overline{H} \tag{3.2}$$

by analogy to the precessional motion of a gyroscope. If there are N spins/(unit volume) then the magnetization, which is the dipole moment per unit volume, is given by $\overline{M} = N\overline{m}$. Thus the dynamical equation for the magnetization is (Ref. 7):

$$\frac{d\overline{M}}{dt} = -\gamma \overline{M} \times \overline{H} \tag{3.3}$$

where $\overline{H}$ is the internal magnetic field. This expression is useful for characterizing the entire sample in the absence of domain boundaries (i. e., where all spins are aligned parallel). This same equation can be derived rigorously using quantum theory and very accurately describes dynamic properties of magnetic material when it has been modified to include the effect of losses. It is the form of this so-called equation of motion which suggests the use of a ferrite material as a reactive mixer and which will engage our attention for the bulk of this paper. However, it will be important first to modify the equation to account for losses.

3. 4. 1 Ferrites. In metallic ferromagnetics the losses can generally be attributed to eddy currents and the nonzero resistivity of the metal. However these materials will not find application in any of the r-f configurations dealt with in this paper because of

their extremely small skin depth. There are, however, a large number of insulating ferromagnetics in which the eddy currents may be totally neglected and whose skin depths are extremely large compared to sample dimensions of interest here. These materials are called ferrites in reference to their magnetic structure which is described as being ferrimagnetic. The distinction between ferromagnetic and ferrimagnetic structure is unimportant to the present discussion.

The losses in ferrites cannot be explained in terms of eddy currents because the conductivity of these materials is extremely low. The best explanation to date for losses in ferrites assumes the excitation of so-called spin waves. These are microscopic disturbances in the otherwise perfect alignment of spins, which propagate throughout the spin system much like lattice vibrations which propagate through the crystal lattice. In fact, it has been postulated that spin waves couple energy nonreciprocally to the lattice vibrations, thus offering a possible explanation for losses in ferrites.

3.4.2 Representation of Losses in the Equation of Motion. Quite apart from the physical origin of the losses in ferrites, it will be important to represent them in the equation of motion. There is considerable evidence that the magnitude of the magnetization is constant, i.e., $|M|^2 = \text{const.}$ or

$$\overline{M} \cdot \frac{d\overline{M}}{dt} = 0 . \tag{3.4}$$

For this reason it is natural to assume a loss term of the form $\overline{M} \times \dot{\overline{M}}$ (Ref. 8). This is included in the equation of motion as

$$\frac{d\overline{M}}{dt} = -\gamma \overline{M} \times \overline{H} + \frac{\alpha}{|M|} \overline{M} \times \dot{\overline{M}} \tag{3.5}$$

where α is dimensionless and is assumed constant. The equation in this form successfully describes most dynamic phenomena in ferrites.

3.5 Ferromagnetic Resonance

Perhaps the most striking of all dynamic magnetic phenomena is that of ferromagnetic resonance (Ref. 9). If the material is saturated by a dc magnetic field, r-f power supplied to the sample experiences a resonance absorption. In an infinite medium biased to saturation with a steady magnetic field H_0, ferromagnetic resonance can be predicted by the

steady-state solution to the equation of motion which is found by substituting

$$\overline{M}(t) = \overline{M}\, e^{i\omega t} \tag{3.6}$$

and

$$\overline{H} = \overline{H}_o + \overline{H}\, e^{i\omega t} \ . \tag{3.7}$$

The solution to this differential equation is

$$\overline{M} = (\bar{\bar{x}}) \cdot \overline{H} \tag{3.8}$$

where $(\bar{\bar{x}})$ is the so-called susceptibility tensor (Ref. 10). It has the following general symmetry:

$$\bar{\bar{x}} = \begin{vmatrix} x_{11} & -ix_{12} & 0 \\ ix_{12} & x_{11} & 0 \\ 0 & 0 & x_a \end{vmatrix} \tag{3.9}$$

The z axis direction has been taken in the direction of H_o and M_o.

$$x_{11} = \frac{M_o}{H_o}\left(\frac{\omega_{res}^2 + i\omega\omega_r}{\omega_{res}^2 - \omega^2 + 2\, i\omega\omega_r}\right)$$

$$x_{12} = \frac{M_o}{H_o}\ \frac{\omega\omega_H}{\omega_{res}^2 - \omega^2 + 2\, i\omega\omega_r} \tag{3.10}$$

$$x_a = \frac{M_o}{H_o}\ \frac{\omega_r}{i\omega + \omega_r}$$

where

$$\begin{aligned} \omega_{res} &= \omega_H^2 + \omega_r^2 \\ \omega_H &= \gamma H_o \\ \omega_r &= \alpha\gamma H_o \end{aligned} \tag{3.11}$$

where H_o is the applied biasing field in the sample. Note that there is no coupling between the component of applied field parallel to the biasing field and the transverse components.

Also notice that the component x_a is very small compared to x_{11} and x_{12} if the loss parameter α is small. It will be assumed that this term can be neglected in all ferrites of interest in this paper. Thus, only the components of magnetization normal to the biasing field will be significant. It is well known that the power absorbed by the sample is determined by the imaginary parts of x_{ii} and the real parts of x_{ij} $(i \neq j)$. These are a maximum for H_o such that $\omega_{res} = \omega$. If power is supplied to the sample, it will experience a resonance absorption as H is varied and will be maximum for $\omega = \omega_{res}$. This phenomenon is called ferromagnetic resonance. For low-loss ferrites (Ref. 11)

$$\omega_{res} \cong \omega_H = \gamma H_o . \tag{3.12}$$

If H_o is the field in the material, this relation is true for finite size samples as well as infinite samples. However, it is normally more convenient to express ferromagnetic resonance frequency in terms of the external applied field. For samples which are ellipsoids of revolution, a uniform magnetic field applied along the axis of symmetry will produce a uniform internal field which is somewhat smaller than the applied field due to the demagnetizing effect of the material. The internal field may be related to the applied field and the magnetization by the demagnetizing factors:

$$\overline{H}_i = \overline{H}_i - \overline{\overline{N}} \cdot \overline{M} . \tag{3.13}$$

The resonant frequency for this case is (Ref. 12)

$$\omega_o = \gamma\left\{\left[H_o + (N_x - N_y) M_o\right]\left[H_o + (N_y - N_z) M_o\right]\right\}^{1/2} \tag{3.14}$$

Only for the special case of the sphere where $N_x = N_y = N_z = \frac{1}{3}$ is the resonant frequency the same as for the infinite medium (i. e., $\omega_o = \gamma H_o$). If the sample is small compared to the electromagnetic wavelength of the r-f components of H, the internal r-f components can be found from the externally applied fields using the demagnetizing factors. In this case, the steady-state solution to the equation of motion is given by

$$\overline{M} = (\overline{\overline{x}})^e \cdot \overline{H}_e \tag{3.15}$$

where

$$(\bar{\bar{x}})^e = (\bar{\bar{x}})^{-1} + (\bar{\bar{N}})^{-1} \quad . \tag{3.16}$$

The symmetry of the susceptibility matrix suggests a simple linear combination which will diagonalize it. Defining the circularly polarized quantities

$$\begin{aligned} M^+ &= M_x + iM_y \\ M^- &= M_x - iM_y \end{aligned} \tag{3.17}$$

and

$$\begin{aligned} H^+ &= H_x + iH_y \\ H^- &= H_x - iH_y \end{aligned} \tag{3.18}$$

reduces the susceptibility tensor to 3 components

$$\begin{bmatrix} M^+ \\ M^- \\ M_z \end{bmatrix} = \begin{bmatrix} x^+ & 0 & 0 \\ 0 & x^- & 0 \\ 0 & 0 & x_a \end{bmatrix} \begin{bmatrix} H^+ \\ H^- \\ H_z \end{bmatrix} \tag{3.19}$$

where

$$\begin{aligned} x^{\pm'} &= \frac{M_o}{H_o} \; \frac{(\omega_{res}^2 - \omega^2)(\omega_{res}^2 \pm \omega\omega_H) + 2\omega^2 \omega_r^2}{(\omega_{res}^2 - \omega^2)^2 + 4\omega^2 \omega_r^2} \\ x^{\pm''} &= \frac{M_o}{H_o} \; \frac{\omega\omega_r(\omega_H \pm \omega)^2 + \omega_r^2}{(\omega_{res}^2 - \omega^2)^2 + 4\omega^2 \omega_r^2} \end{aligned} \tag{3.20}$$

where the single prime refers to the real part and the double prime refers to the imaginary part. Note that x^+ has a resonance shape similar to that for linearly polarized fields but that x^- experiences no resonance effect. Physically, this means that for only one sense of rotation of the circularly polarized fields, relative to the direction of the biasing field, will

the sample exhibit ferromagnetic resonance. The symmetry of the susceptibility tensor and its functional form are extremely important in many calculations in Chapter 5.

The expressions derived above are strictly valid for cubic crystals. In non-cubic crystals ω_{res} is a function of not only the magnitude of H_o but also its orientation relative to the crystalline axes (Ref. 13). This can be explained by representing the anisotropy energy in terms of an equivalent anisotropy field whose magnitude and direction are fixed relative to the crystalline axes. The total magnetic field which determines ferromagnetic resonance must include this field. This representation successfully explains the dependence of ω_{res} upon the orientation of the applied field.

In many experiments the sample is free to rotate under the influence of the applied field. It will do so until the anisotropy field is aligned with the applied field. In this case ferromagnetic resonance at a particular frequency will occur at a smaller value of external field than for a similar sample of cubic material. For a sphere the external field required for ferromagnetic resonance at ω is given by (Ref. 14):

$$H_{res} = \frac{\omega}{\gamma} - \frac{4}{3}\frac{K_1}{M_o} \tag{3.21}$$

This result is important in the calculations in Section 5. 5 and in the experimental investigations discussed in Sections 5. 5. 3 in which an actual sphere of ferromagnetic material is allowed to rotate until the easy axis is aligned with the biasing field.

3. 6 Domain Wall Motion

At this point, it is instructive to consider the dynamic properties of a sample below magnetic saturation. It has been shown that a magnetic field acts on a domain wall in such a way as to cause it to move. There are additional effects which can be modeled as effective mass and damping, so that the wall has a dynamic motion described approximately by $M_\omega \ddot{x} + \beta \dot{x} + \alpha x = M_o h$, where x is the location of the domain wall (Ref. 15). Assuming h is an r-f field then the steady-state solution can be found for x. The magnetization directed out of the wall is related to x by $M = \frac{2xM_o}{d}$, where d is the wall thickness. The r-f magnetization is related to h by

$$M = \frac{M_o}{H_o} \frac{\omega^2_{o_\omega}}{\omega^2_{o_\omega} - \omega^2 + i\omega\omega_{r_\omega}} \tag{3.22}$$

where

$$\omega_{o_\omega} = \frac{\alpha}{M_\omega}$$
$$\omega_{r_\omega} = \frac{\beta}{M_\omega} \tag{3.23}$$

Since energy is dissipated in moving the wall, a resonance phenomena occurs in ferrites even in the absence of an applied biasing field. However, the Q of this resonance is quite low and the resonant frequency is not changed appreciably by application of a biasing field.

3.7 Multiple Modes in Ferromagnetic Resonance

There is another peculiar aspect of ferromagnetic resonance which deserves attention. The usual experiment performed in studying ferromagnetic resonance consists of placing the ferrite in a high Q microwave cavity, exciting the cavity at resonance, and observing the reflected power as the magnetic field which biases the sample is varied. Ferromagnetic resonance is observed as a resonant absorption for a particular field. However, if the sample is located in a part of the cavity where the field is highly nonuniform, there are a number of other resonant absorptions of the same general strength which occur for biasing fields different from that for ferromagnetic resonance (Ref. 16). The locations of these absorption peaks are independent of the size of the sample up to a certain size but are strongly dependent upon sample shape. It has been postulated that these additional resonant peaks were actually higher order modes of oscillation of the sample magnetization than the uniform precession which corresponds to ferromagnetic resonance. The validity of this postulate can be established by the solution to Maxwell's equations for an experimental configuration in which the multiple resonances are observed. The solution to Maxwell's equations is basically the field distributions inside the sample for the experimental configuration. Thus, the field distributions for a ferrite sample at radio frequencies will be obtained. These fields can be found from the solution to a boundary-value problem.

3.7.1 Field Distributions Inside Ferrite Sample. Maxwell's equations for the region inside the ferrite surface are coupled, nonhomogeneous differential equations in the dependent variables, electric field $\overline{E}$ and magnetic field $\overline{H}$. The equations can be decoupled by a change of variables to a scalar ϕ and vector potential $\overline{A}$:

$$\overline{H} = \nabla\phi - \frac{\partial \overline{A}}{\partial t} \tag{3.24}$$

$$\overline{E} = -\frac{1}{\epsilon} \nabla \times \overline{A} \tag{3.25}$$

If these substitutions are made in Maxwell's equations, and if the Lorentz gauge condition is applied, then the potentials satisfy a pair of inhomogeneous wave equations:

$$\nabla^2\phi + k^2\phi = -\nabla \cdot \overline{M} \tag{3.26}$$

$$\nabla^2\overline{A} + k^2\overline{A} = -\mu_o\epsilon \frac{\partial \overline{M}}{\partial t} \tag{3.27}$$

where

$$k^2 = k_i^2 = \omega^2\mu_o\epsilon \quad \text{inside the sample}$$

$$= k_o^2 = \omega^2\mu_o\epsilon_o \quad \text{outside the sample}$$

where $\overline{M} = 0$ outside the sample and where μ and ϵ are the permeability and permittivity respectively.

Equations 3-26 and 3-27 with the proper boundary conditions are the boundary-value problems which we wish to solve. However, these equations are still coupled and are difficult to solve exactly. Fortunately an approximate boundary-value problem can be obtained from equations which can be solved exactly and which is valid for the small samples encountered in ferromagnetic resonance experiments. This approximate problem is framed in the following way. For a sample situated in free space, the potentials may be obtained formally in terms of the free-space Green's function, $\frac{e^{ikr}}{4\pi r}$, in the form

$$\phi = \frac{1}{4\pi} \int \nabla \cdot \overline{M} \frac{e^{ikr}}{r} \, dv' \tag{3.28}$$

$$\overline{A} = -\frac{1}{4\pi} \mu_o\epsilon \int \frac{\partial \overline{M}}{\partial t} \frac{e^{ikr}}{r} \, dv' \tag{3.29}$$

where

$$r = \sum_{i=1}^{3} (x_i - x_i')^2 \quad ^{\frac{1}{2}}$$

The primed variables are the coordinates of the source points and the unprimed variables are the coordinates of the field points. These potentials may be expanded formally in a power series of (ik)

$$\phi = -\frac{1}{4\pi} \sum_{n=0}^{\infty} \frac{(ik)^n}{n!} \int r^{n-1} (\nabla \cdot \overline{M})\, dv' \tag{3.30}$$

$$\overline{A} = -\frac{1}{4\pi} \sum_{n>0}^{\infty} \frac{(ik)^n}{n!} \int r^{n-1} \frac{\partial \overline{M}}{\partial t}\, dv' \tag{3.31}$$

$$\overline{A} = -\frac{1}{4\pi} \mu_o \epsilon \sum_{n>0}^{\infty} \frac{(ik)^n}{n!} \int r^{n-1} \frac{\partial \overline{M}}{\partial t}\, dv' \tag{3.31}$$

Then by substituting Eqs. 3-30 and 3-31 into 3-24 there results:

$$\begin{aligned} 4\pi \overline{H} = -\nabla \left[\int \frac{\nabla \cdot \overline{M}}{r}\, dv' + ik \int \nabla \cdot \overline{M}\, dv' + \ldots \right] \\ -(ik)^2 \left[\int \frac{\overline{M}}{r}\, dv' + ik \int \overline{M}\, dv' + \ldots \right] \end{aligned} \tag{3.32}$$

For all field points inside and on the sample, the magnitude of the n^{th} term in the first bracket is less than $[(ka)^n/n!]\, \left| \int (\nabla \cdot \overline{M}/r)\, dv' \right|$ where a is the largest sample dimension. If the sample is sufficiently small compared to a wavelength (i. e., $ka << 1$), then the contribution of higher-order terms is negligible. A similar situation exists for the terms of the second bracket. Its leading term is negligible relative to the leading term of the first bracket for sufficiently small ka.

3. 7. 2 The Walker Approximation. The lowest-order term in Eq. 3-32 is the so-called magnetostatic term. If

$$\Phi = \int (\nabla \cdot \overline{M}/4\pi r)\, dv' \tag{3.33}$$

then Φ is the magnetostatic potential. In most of the significant experiments on which the multiple resonances were observed, the samples were no bigger than a few mils. For these samples the approximation $ka << 1$ is satisfied so well that the fields can indeed be approximated by the magnetostatic term. The differential equation which the magnetostatic potential satisfied is

$$\nabla^2 \phi = -\nabla \cdot \overline{M} \ . \tag{3.34}$$

But the magnetization is related to the magnetic field by the susceptibility tensor:

$$\overline{M} = \overline{\overline{x}} \cdot \overline{H}$$

Thus

$$\nabla \cdot \overline{M} = \nabla \cdot \overline{\overline{x}} \cdot \nabla\phi \tag{3.35}$$

which due to the symmetry of $\overline{\overline{x}}$ reduces to

$$\nabla \cdot \overline{M} = K \nabla_t^2 \phi \tag{3.36}$$

where

$$\nabla_t^2 = \frac{\partial^2}{\partial x^2} + \frac{\partial^2}{\partial y^2}$$

and where K is the diagonal component of $\overline{\overline{x}}$. For the purpose of solving this boundary value problem, it will be assumed that the frequency is far enough from ferromagnetic resonance that K is real. We have shown then that the boundary value problem of the ferrite sample in a microwave cavity can, under the assumptions made, be successfully approximated by the problem $\nabla^2\phi = -K \nabla_t^2 \phi$. The boundary conditions are continuity of potential and the normal component of flux density. It is assumed that the cavity boundary is far enough from the sample that it may be neglected and that frequencies involved are far enough from ω_{res} that K is real. That this is a reasonable assumption can be established from the solution.

This boundary-value problem was solved by Walker (Ref. 18) for an arbitrary ellipsoid of revolution. He found that the potential consists of a set of normal expansion modes whose characteristic equation has nontrivial solutions for only a discrete set of frequencies. The latter are the resonant frequencies of these so-called magnetostatic modes.

It was later shown in Ref. 19 that these modes are independent of the nonreciprocal nature of the ferrite but depend only upon the dispersive nature of ferrite permeability. The solution for a spherical sample is a special case of Walker's general problem, but the characteristic equation has a singularity for the spherical shape which is difficult to treat analytically. For this and pedagogical reasons, the solution for a spherical sample is obtained in Appendix A

3.7.3 The Approximate Boundary-Value Problem. It can be seen by examination of Eq. 3-32 that the first-order correction to the magnetostatic approximation vanishes identically. The second-order approximation can be found by collecting the terms of Eq. 3-32 to second-order. If this is done and if $\Phi^{(2)}$ and $H^{(2)}$ represent respectively the scalar potential and magnetic field correct to second-order then:

$$\overline{H}^{(2)} = \nabla\Phi^{(2)} + \frac{k^2}{4\pi} \int \frac{\overline{M}_o}{r}\, dv' \tag{3.37}$$

where $\overline{M}_o$ is the magnetostatic approximation to the magnetization. The solution to the second-order problem requires knowledge of $\Phi^{(2)}$ and $\overline{M}_o$. It is possible to know $\Phi^{(2)}$ correctly only if M is known to second order. The magnetization is related to H through the susceptibility tensor, and because $\nabla \cdot \overline{B}$ must vanish a pair of self consistent equations (correct to second-order) can be solved simultaneously to determine $\Phi^{(2)}$:

$$\overline{M}^{(2)} = (\bar{\bar{X}})\, \nabla\Phi^{(2)} + \frac{k^2}{4\pi} \int \frac{\overline{M}_o}{r}\, dv' \tag{3.38}$$

and

$$\nabla^2 \Phi^{(2)} + k^2 \Phi^{(2)} = -\nabla \cdot \overline{M}^{(2)} \,. \tag{3.39}$$

Combining these equations produces an expression for $\Phi^{(2)}$:

$$(1+K)\, \nabla_t^{\,2}\, \Phi^{(2)} + \frac{\partial^2 \Phi^{(2)}}{\partial Z^2} + k_i^{\,2}\, \Phi^{(2)} = -\frac{k_i^{\,2}}{4\pi}\, \nabla \cdot (\bar{\bar{X}}) \int \frac{\overline{M}_o}{r}\, dv' \tag{3.40}$$

inside the sample and:

$$\nabla^2\, \Phi^{(2)} + k_o^{\,2}\, \Phi^{(2)} = 0 \qquad \text{(outside the sample)} \tag{3.41}$$

The boundary conditions at the sample are:

$$\Phi^{(2)}_{\text{inside}} = \Phi^{(2)}_{\text{outside}}$$

$$\left(\nabla \Phi^{(2)} + \frac{\partial \overline{A}^{(2)}}{\partial t} + \overline{M}^{(2)}\right)_{\text{inside}} \hat{n} = \left(\nabla \Phi^{(2)} + \frac{\partial \overline{A}^{(2)}}{\partial t}\right)_{\text{outside}} \hat{n}$$

Also $\Phi^{(2)}$ and $\overline{A}^{(2)}$ must be bounded for all space. This is the boundary value problem which we wish to solve.

The nonhomogeneous equation (Eq. 3-40) can be solved by use of the appropriate Green's function. The source of this equation $\rho = (-k_i^2/4\pi)\nabla \cdot [(X)\,\overline{A}_o]$ is derived from the magnetostatic approximation which will be presumed known. For the free-space situation $\overline{A}_o = \int \overline{M}_o\, r^{-1}\, dv'$ so the differential equation for $\overline{A}_o$ is:

$$\nabla^2 \overline{A}_o = -\overline{M}_o \tag{3.42}$$

This equation must be solved using the correct Green's function for the geometry in which $\overline{A}_o$ must satisfy the same homogeneous boundary conditions as $\overline{H}$. By Green's identity the solution to Eq. 3-40 will be

$$\Phi_i^{(2)} = \int_{\text{sample}} G\,\rho_m\, dv' - \int_{\text{sur. of sample}} \Phi^{(2)}\,\nabla_n G - G\,\nabla_n \Phi^{(2)}\, da'$$

where G is the Green's function and where $\rho_m = 4\rho(1+K)^{-1}$. The potential at the sample surface is known, i.e., $\Phi_i^{(2)}\big|_{\text{surf.}} = \Phi^{(2)}_{\text{out}}\big|_{\text{surf.}}$ but the normal gradient of $\Phi_i^{(2)}$ is not known there, so Green's function will be chosen to vanish on the surface. Thus the Green's function will satisfy:

$$\nabla_t^2 G + \frac{1}{1+K}\left(\nabla_Z^2 G + k_i^2 G\right) = -\delta(\bar{r} - \bar{r}') \tag{3.43}$$

$$G = 0 \text{ at sample surface .} \tag{3.44}$$

One of the boundary conditions has already been satisfied. The remaining condition of continuity of normal flux density is now introduced. Neglecting the permeability of free-space, which is a constant factor, this boundary condition may be written as follows:

$$\left(\frac{\partial \Phi_{out}^{(2)}}{\partial n} + k_o^2 \overline{A}_o \cdot \hat{n} \right) \Bigg|_{surf.} =$$

$$(1+K) \left(\frac{\partial \Phi_i^{(2)}}{\partial n} + k_i^2 \overline{A}_i \cdot \hat{n} \right) + i\nu \left(\frac{\partial}{\partial \tau} \Phi_i^{(2)} + k_i^2 \overline{A}_i \cdot \hat{\tau} \right) \Bigg|_{surf.} \qquad (3.45)$$

where n is the coordinate normal to the surface, τ is the coordinate tangential to the surface, and $\hat{n}$ and $\hat{\tau}$ are unit vectors in the respective coordinate directions. Equation 3.45 contains one undetermined constant. This constant is the ratio of the magnitudes of the scalar potentials outside to inside the sample. If ρ_m were an independent source (i.e., determined by external devices), then the above constant would be determined by Eq. 3.45. However, ρ_m depends on the coefficient of $\Phi^{(2)}$ so it is merely a source in the mathematical sense that is derived from the magnetostatic approximation. Therefore, there is an additional condition to be applied in this problem, namely, that the magnetostatic approximation must still be valid. In the limit of vanishing k the external potential must be equal to the internal magnetostatic potential at the sample surface. Thus the limit:

$$\lim_{k \to 0} \Phi_{out}^{(2)} \Big|_{\substack{\text{sample} \\ \text{surface}}} = \Phi_0^{(i)} \Big|_{\substack{\text{sample} \\ \text{surface}}} \qquad (3.46)$$

determines the constant in Eq. 3.45. When this value is substituted into Eq. 3.45, the latter becomes the characteristic equation of the sample modes. Equation 3.45 then will have roots for only discrete values of the parameters K and ν^* which depend on frequency and are not independent. The parameters K and ν may be expressed in terms of the frequency at which the sample magnetization is oscillating. Therefore roots of Eq. 3.45 will be allowed values of this frequency which may be identified as the resonant frequencies of sample modes.

For any given sample size, as k approaches zero, Eq. 3.45 approaches the characteristic equation of the magnetostatic modes, but letting $k \to 0$ for a fixed sample size is equivalent to letting the wavelength become arbitrarily large compared to the maximum sample dimension. The magnetostatic approximation is valid for this situation. Thus the effect of electromagnetic propagation on the resonant frequencies of the magnetostatic modes

*See Eq. 3.47.

may be demonstrated by independently varying the parameter k. In order to illustrate the details of this effect, a specific example will now be presented.

3.7.4 An Example. As an example, we will solve the approximate boundary value problem for the case of the circularly cylindrical ferrite rod between a pair of infinite parallel conducting plates with its axis normal to the plates (see Fig. 3-1). The boundary value problem to be solved is Eqs. 3.40 and 3.41 and the boundary conditions which are: the potential $\Phi^{(2)}$ and the normal component of flux density (Eq. 3.45) are continuous at the sample surface; the potentials must be bounded for all space and the normal component of flux density must vanish on the metal plates. However, it is assumed that the sample is saturated axially so the latter boundary condition reduces to the vanishing of the normal component of magnetic field (i.e., $\left[\nabla\Phi^{(2)} + \frac{\partial\bar{A}}{\partial t}\right] \cdot \hat{n} = 0$) at the metal plates. The susceptibility χ for this case is a tensor as shown in equation 3.47 where the conventional notation for the components is used (see Ref. 18). It is assumed that these quantities are independent of position in the sample. In general this assumption could not be made for any sample shape other than an ellipsoid of revolution, but by the method of appendix B it can be made for a cylinder.

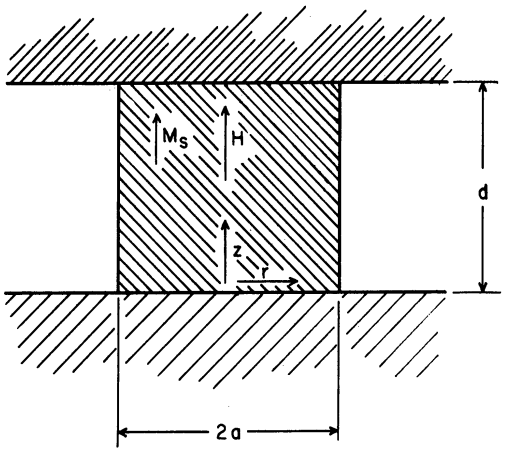

Fig. 3-1. Illustration of geometry of sample boundary value problem.

$$(\overline{\overline{X}}) = \begin{bmatrix} K & i\nu \\ -i\nu & K \end{bmatrix} \tag{3.47}$$

Because of the boundary conditions on the potential, the conditions on the Green's function for the scalar potential will be: G = 0 on the lateral surface (i. e., r = a) and $\nabla_n G = 0$ at the ends of the sample. In this case the solution to Eq. 3.40 becomes, by Green's identity:

$$\Phi_i^{(2)} = \int_{\text{sample}} G \rho_m \, dv' - \int_{\substack{\text{lateral} \\ \text{surface}}} \Phi_{out}^{(2)} \nabla_n G \, da' \,, \tag{3.48}$$

where $\rho_m = k_i^2 \nabla \cdot [(\mathbf{X}) \cdot \overline{A}_o] (1+K)^{-1}$.

The homogeneous boundary condition on the metal plates requires that the scalar potentials inside and outside the sample must vary as $\cos \beta_m Z$, where $\beta_m = \frac{m\pi}{d}$, and where d = length of the sample and also the spacing between the plates.

The external potential may be written down at once from Eq. 3.41:

$$\Phi_{out}^{(2)} = B K_n(\alpha_1 r) e^{\pm in\phi} \cos \beta_m Z \tag{3.49}$$

where $\alpha_1 = (\beta_m^2 - k_o^2)^{\frac{1}{2}}$, and K_n is the modified Bessel function of the second kind which must be chosen so $\phi^{(2)} \to 0$ as $r \to \infty$.

The Green's function for this case is:

$$G = - \frac{J_n(\alpha_2 r') C_n(\alpha_2 r) e^{\pm in(\phi-\phi')} \cos \beta_m Z \cos \beta_m Z'}{\alpha_2 \pi \, da \, C_n'(\alpha_2 a) J_n(\alpha_2 a)} \qquad r \geqq r'$$

$$G = - \frac{J_n(\alpha_2 r) C_n(\alpha_2 r') e^{\pm(\phi-\phi')} \cos \beta_m Z \cos \beta_m Z'}{\alpha_2 \pi \, da \, C_n'(\alpha_2 a) J_n(\alpha_2 a)} \qquad r \leqq r' \tag{3.50}$$

where $C_n(\alpha_2 r) = J_n(\alpha_2 r) + \Gamma_n N_n(\alpha_2 r)$ and where $C_n(\alpha_2 a) = 0$ determines Γ_n and where

$$\alpha_2 = \left(\frac{k_i^2 - \beta_m^2}{1 + K} \right)^{\frac{1}{2}}$$

and a = sample radius. Using this Green's function in the surface integral of Eq. 3.48, the latter becomes

$$\Phi^{(2)} = \int G \rho_m \, dv' + B \frac{K_n(\alpha_1 a) J_n(\alpha_2 r)}{J_n(\alpha_2 a)} e^{\pm in\phi} \cos \beta_m Z \ . \tag{3.51}$$

To determine ρ_m, the equation $\nabla^2 \overline{A}_o = - \overline{M}_o$ must be solved. This may be accomplished by means of another Green's function which satisfies

$$\nabla^2 G_o = -\delta(r - r') \, \delta(\phi - \phi') \, \delta(Z - Z') \ .$$

It should be recalled that $k^2 \overline{A}_o$ is the second-order contribution to the magnetic field due to the vector potential. This quantity will be used not only to obtain ρ_m, but to write the boundary condition of the normal flux density. Using Green's identity yields:

$$A_{o_i} = \int_{\text{all space}} G_o M_{o_i} \, dv' + \text{a surface integral} \tag{3.52}$$

for each component of $\overline{A}_o$. The surface integral will be taken along the plates and across a lateral surface at infinity. Since $\overline{M}_o$ contains only transverse components, $\overline{A}_o$ will contain only transverse components. The normal derivative of the transverse components of $\overline{A}_o$ must vanish at the plates, so that if $\nabla_n G_o = 0$ at the plate, then the surface integral is identically zero. This Green's function G_o then becomes:

$$G_o = \frac{K_n(\beta_m r') I_n(\beta_m r) e^{\pm in(\phi - \phi')} \cos \beta_m Z \cos \beta_m Z'}{\beta_m \pi \, da \left[I_n'(\beta_m a) K_n(\beta_m a) - I_n(\beta_m a) K_n'(\beta_m a) \right]} \qquad r \leqq r'$$

$$G_o = \frac{K_n(\beta_m r) I_n(\beta_m r') e^{\pm in(\phi - \phi')} \cos \beta_m Z \cos \beta_m Z'}{\beta_m \pi \, da \left[I_n'(\beta_m a) K_n(\beta_m a) - I_n(\beta_m a) K_n'(\beta_m a) \right]} \qquad r \geqq r \ . \tag{3.53}$$

Φ_o is the magnetostatic potential which was determined in a previous paper (Ref. 19):

$$\Phi_o = I_n\left(\frac{\beta_m r}{\sqrt{1+k}} \right) e^{\pm in\phi} \cos \beta_m Z \ . \tag{3.54}$$

Here a unity coefficient has been arbitrarily selected, without loss of generality. Using the expression found for the magnetostatic approximation to the potential and the susceptibility tensor, the magnetostatic approximation to the magnetization can be found:

$$\overline{M}_o = \left(K \frac{\partial \phi}{\partial x} - i\nu \frac{\partial \phi}{\partial y} \right) \hat{x} + \left(i\nu \frac{\partial \phi}{\partial x} + K \frac{\partial \phi}{\partial y} \right) \hat{y} . \tag{3.55}$$

However, the potential is known as a function of r, θ, and z rather than x, y, and z. Thus it is convenient to express the components of $\overline{M}$ in terms of these coordinates:

$$\begin{aligned} M_{ox} &= K\left(\frac{\partial r}{\partial x} \frac{\partial \phi}{\partial r} + \frac{\partial \theta}{\partial x} \frac{\partial \phi}{\partial \theta} \right) - i\nu \left(\frac{\partial r}{\partial y} \frac{\partial \phi}{\partial r} + \frac{\partial \theta}{\partial y} \frac{\partial \phi}{\partial \theta} \right) \\ M_{oy} &= i\nu \left(\frac{\partial r}{\partial x} \frac{\partial \phi}{\partial r} + \frac{\partial \theta}{\partial x} \frac{\partial \phi}{\partial \theta} \right) + K \left(\frac{\partial r}{\partial y} \frac{\partial \phi}{\partial r} + \frac{\partial \theta}{\partial y} \frac{\partial \phi}{\partial \theta} \right) \end{aligned} \tag{3.56}$$

It may be shown that:

$$\begin{aligned} \frac{\partial r}{\partial x} &= \cos\theta \\ \frac{\partial r}{\partial y} &= \sin\theta \\ \frac{\partial \theta}{\partial x} &= -\frac{\sin\theta}{r} \\ \frac{\partial \theta}{\partial y} &= \frac{\cos\theta}{r} \end{aligned} \tag{3.57}$$

Then:

$$\begin{aligned} M_{ox} &= K\left(\cos\theta \frac{\partial \phi}{\partial r} - \frac{\sin\theta}{r} \frac{\partial \phi}{\partial \theta} \right) - i\nu \left(\sin\theta \frac{\partial \phi}{\partial r} + \frac{\cos\theta}{r} \frac{\partial \phi}{\partial \theta} \right) \\ M_{oy} &= i\nu \left(\cos\theta \frac{\partial \phi}{\partial r} - \frac{\sin\theta}{r} \frac{\partial \phi}{\partial \theta} \right) + K \left(\sin\theta \frac{\partial \phi}{\partial r} + \frac{\cos\theta}{r} \frac{\partial \phi}{\partial \theta} \right) \end{aligned} \tag{3.58}$$

It is shown in Appendix C that if these quantities are substituted into the equation for the vector potential, then for the mode characterized by n_o and m_o (Ref. 19) of the magnetostatic potential the vector potential is:

$$A_{ox} = \frac{\pi \cos \beta_{m_o} Z}{f(m_o \pi \alpha)} \left[(K-\nu) A^{(r)}_{n_o+1} e^{i(n_o+1)\theta} + (K-\nu) B^{(r)}_{n_o-1} e^{i(n_o-1)\theta} \right] \tag{3.59}$$

$$A_{oy} = \frac{i\pi \cos\beta_{m_o} Z}{f(m_o\pi\alpha)} \left[(\nu\text{-}K)\, A^{(r)}_{n_o+1}\, e^{i(n_o+1)\theta} + (K\text{-}\nu)\, B^{(r)}_{n_o-1}\, e^{i(n_o-1)\theta} \right] \quad (3.60)$$

where A_{n_o+1} and B_{n_o-1} are defined in Appendix C.

The source for the integral equation for $\Phi^{(2)}$ can be computed in the following way:

$$\bar{\bar{x}} \cdot \bar{A}_o = (K A_{ox} - i\nu A_{oy})\,\hat{x} + (i\nu A_{ox} + K A_{oy})\,\hat{y}$$

$$\nabla \cdot \bar{\bar{x}} \cdot \bar{A}_o = \frac{\partial}{\partial x}(K A_{ox} - i\nu A_{oy}) + \frac{\partial}{\partial y}(i\nu A_{ox} + K A_{oy})$$

$$= \cos\theta \frac{\partial}{\partial r}(K A_{ox} - i\nu A_{oy}) - \frac{\sin\theta}{r}\frac{\partial}{\partial\theta}(K A_{ox} - i\nu A_{oy})$$

$$+ \sin\theta \frac{\partial}{\partial r}(i\nu A_{ox} + K A_{oy}) + \frac{\cos\theta}{r}\frac{\partial}{\partial\theta}(i\nu A_{ox} + K A_{oy}) \quad (3.61)$$

But this may be shown to be:

$$\nabla \cdot \bar{\bar{x}} \cdot \bar{A}_o = \frac{\pi \cos\beta_{m_o} z}{f(n_o\pi\alpha)}\, e^{in_o\theta} \left\{ (K\text{-}\nu)^2 \left[A^{(r)}_{n_o+1} + \frac{A^{(r)}_{n_o+1}(n_o+1)}{r} \right] \right.$$

$$\left. + (K+\nu)^2 \left[B'^{(r)}_{n_o-1} - \frac{(n_o-1)\, B^{(r)}_{n_o-1}}{r} \right] \right\} \quad (3.62)$$

Using this quantity the first term in Eq. 3.51 can be evaluated:

$$\int G_\rho\, dv' = \frac{k_i^2}{1+K} \int G \nabla \cdot \bar{\bar{x}} \cdot \bar{A}_o\, dv'$$

$$= \frac{k_i^2}{1+K} \frac{\cos\beta_{m_o} z\, e^{in_o\theta}}{f(m_o\pi\alpha)\, C'_{n_o}(\alpha_2 a)\, J_{n_o}(\alpha_2 a)\, \alpha_2 a} C_{n_o}(\alpha_2 r) \int_o^r J_n(\alpha_2 r') \left[(K\text{-}\nu)^2 \left(A'^{(r)}_{n_o+1} \right.\right.$$

$$\left.\left. + \left(\frac{n_o+1}{r}\right) A^{(r)}_{n_o+1} \right) + (K+\nu)^2 \left(B'^{(r)}_{n_o-1} - \frac{n_o-1}{r} B^{(r)}_{n_o-1} \right) \right] r'\, dr' \quad (3.63)$$

$$+ J_n \alpha_2 r \int_r^a C_n(\alpha_2 r') \left[(K\text{-}\nu)^2 \left(A'^{(r')}_{n_o+1} + \frac{n_o+1}{r} A^{(r)}_{n_o+1} \right) + (K+\nu)^2 \left(B'^{(r')}_{n_o-1} - \frac{n_o-1}{r} B^{(r)}_{n_o-1} \right) \right] r'\, dr'$$

If the above expression is defined as $\phi^{(2)}$ then it may be substituted in Eq. 3.45, and applying the condition (Eq. 3.41) the characteristic equation results. This was done in Appendix C, yielding the characteristic equation:

$$\frac{\alpha_1 K_n'(\alpha_1 a)}{K_n(\alpha_1 a)} - (1+K)\,\alpha_2 \frac{J_n'(\alpha_2 a)}{J_n(\alpha_2 a)} \pm \frac{n\nu}{a} = \frac{k_i^2}{I_n\left(\frac{\beta_m a}{\sqrt{1+K}}\right)} H(K,\nu) \qquad (3.64)$$

where H and the derivation of this equation appear in Appendix C.

The roots of the characteristic equation (Eq. 3.64) may be obtained graphically by defining $y = a(k_i^2 - \beta_m^2)^{\frac{1}{2}} (1+K)^{-\frac{1}{2}}$ as the independent variable and plotting both sides of Eq. 3.64 as a function of y for each n and m. The two resulting graphs for each n and m will intersect in an infinite number of points ($y_{nm\ell}$) which are the roots of Eq. 3.64. A similar technique was used (Ref. 19) to obtain the roots for the magnetostatic approximation by defining $X = \beta_m a\,(1+K)^{-\frac{1}{2}}$ and obtaining $X_{nm\ell}$. From the form of Eq. 3.64, it can be seen that it reduces to the characteristic equation of magnetostatic modes (Ref. 19) for $k_i = 0$. The fact that $y = iX$ for $k_i = 0$ is a consequence of the particular form in which the internal expansion modes were written.

From the sets of roots $y_{nm\ell}$ and $X_{nm\ell}$ the normal expansion modes and hence internal fields are specified for either the magnetostatic case or the second-order approximation. Thus a careful investigation of these roots will constitute a specification of the salient features of the effect of propagation on the magnetostatic approximation. There are five such features: (1) the roots specify a set of corresponding resonant frequencies $\omega_{nm\ell}$; (2) the effect of imaginary parameters on $\omega_{nm\ell}$ can be demonstrated; (3) the values of $y_{nm\ell}$ are shifted from $iX_{nm\ell}$ for $k_i > 0$ by an amount which depends on the sample shape; (4) values for $\omega_{nm\ell}$ correct to second order are size dependent whereas the magnetostatic values are size independent; (5) sample modes are possible in a frequency region not predicted by the magnetostatic approximation.

3.7.5 Resonant Frequencies. Each root of Eq. 3.64 ($y_{nm\ell}$) corresponds to a particular frequency ($\omega_{nm\ell}$) because each value $y_{nm\ell}$ corresponds to the values $k_{nm\ell}$ and $K_{nm\ell}$ and because both k and K are functions of frequency. Physically the value of K is determined from the frequency of oscillation of the assembly of magnetic moments which pro-

duce the magnetization of the sample. Therefore the normal expansion modes each correspond to an oscillation of the sample magnetization. Energy can be coupled into the sample from external microwave circuitry at each of these frequencies so that they may be considered sample resonances. In actual samples there will be losses so that a finite, measurable Q will exist at each sample resonance. These resonances have been observed experimentally and their characteristics noted (Ref. 16).

3.7.6 The Effect of Imaginary Parameters. The resonant frequencies will be real for all frequencies such that α_1 is real. However, when α_1 is imaginary the characteristic equation contains a ratio of Hankel functions which is in general complex. The roots in this case are complex and cannot correspond to resonant sample frequencies. For all $\omega < \omega_c = \beta_m(\mu_o\epsilon_o)^{-1/2}$ the parameter α_1 is real and resonant sample modes can exist. It is interesting to note that for α_1 imaginary the external potential is proportional to $H^{(1)}(\alpha_1 r)$ which in the present convention represents an outgoing wave. Thus the sample modes exist in a frequency region in which the external fields are evanescent.

It is also possible for α_2 to have imaginary values but the effect of this on the roots of Eq. 3.64 is much less severe. The internal potential is proportional to $J_n(\alpha_2 r)$ and this function enters the characteristic equation as $\alpha_2 J_n'(\alpha_2 a)/J_n(\alpha_2 a)$ which is a real ratio whether α_2 is real or imaginary. Therefore Eq. 3.64 has real roots independently of whether α_2 is real or imaginary.

3.7.7 Effect of Sample Shape on Roots. It has been shown that y=iX for k=0 and that the resonant frequencies derived from y reduce to those of the magnetostatic modes for k = 0. Physically this corresponds to an infinite wavelength which is physically incorrect for a time dependent field. However, it has been demonstrated that, for samples sufficiently small compared to a wavelength, k may be neglected relative to terms of the order of 1/a for a first-order approximation. Letting k = 0 in the second-order approximation is a somewhat artificial means of representing this situation. If k is replaced by ηk in Eq. 3.64 and η varied from zero to unity the effect of propagation on the roots of the characteristic equation can be demonstrated. It is found that for the roots corresponding to real α_2 the roots shift by a larger amount for large α than for small α, where α is the aspect ratio of the sample $(\frac{a}{d})$. This means that the magnetostatic approximation is better for a long thin cylinder than

for a flat thin disk provided the maximum size in either case is small compared to a wavelength.

The latter phenomenon may be explained by comparing the nature of the magnetostatic solution with the second-order solution. The axial components of the scalar potential of both consist of standing waves which is also the correct form for the exact solution. The approximation exists in the radial component and is better for small radii (thin cylinders) than large radii (flat disks) since ka is smaller for the former than for the latter. Thus the magnetostatic approximation is more correct for a thin cylinder than a flat disk. This situation, in which the validity of the magnetostatic approximation depends on sample shape, reflects the artificiality of the homogeneous boundary condition at the plates for the magnetostatic approximation (Ref. 19).

3.7.8 Size Dependence of Sample Modes. It was demonstrated in Ref. 19 that the resonant frequencies of the magnetostatic modes are independent of sample size but depend strongly on sample shape. This result occurs because the sample dimensions enter the characteristic equation for the magnetostatic modes only in the sample aspect ratio. However, it is not possible to specify Eq. 3.64 entirely in terms of this ratio. Rather it is necessary to know the actual radius and length of the sample to compute $y_{nm\ell}$. Therefore the resonant frequencies which are specified by $y_{nm\ell}$ depend on the actual sample size, a fact which is consistent with experiment (Ref. 16).

3.7.9 Resonance outside the Frequency Region of the Magnetostatic Modes. From the literature (Ref. 20) it has been shown that magnetostatic modes can be classified as volume modes or surface modes depending upon whether $1+K$ is positive or negative, respectively. It has also been shown (Ref. 18) that magnetostatic modes cannot exist in the frequency region $\omega < \gamma H_i$, where H_i is the internal bias magnetic field and γ is the gyromagnetic ratio. However, the approximate solution, correct to second order, shows that modes can exist in this region provided the sample size exceeds a certain minimum. This can be shown with reference to the definition of y and with the observation that $K > 0$ when $\omega < \gamma H_i$. Specifically,

$$y = a\left(\frac{k_i^2 - \beta_m^2}{1+K}\right)^{\frac{1}{2}}$$

so

$$(1+K)^{\frac{1}{2}} = \frac{a\left(k_i^2 - \beta_m^2\right)^{\frac{1}{2}}}{y} > 1 \qquad \text{for } \omega < \gamma H_i \tag{3.65}$$

Then

$$a > \frac{y_{nm\ell}}{\left(k_i^2 - \beta_m^2\right)^{\frac{1}{2}}} \qquad \text{for } \omega_{nm\ell} < \gamma H_i \tag{3.66}$$

However for samples of this size a $k_i > y_{nm\ell}(1-\beta_m^2/k_i^2)^{-1/2}$, which is not necessarily small compared to unity, and so the predictions based on the second-order solution are not valid. Nevertheless the exact solution involves the same Green's function for the scalar potential. Even though the latter is not sufficient by itself for writing the boundary conditions, it forms a part of the final characteristic equation and therefore determines, at least in part, the resonant frequencies of sample modes. The functional form of the exact potential is proportional to

$$J_n\left[a(k_i^2 - \beta_m^2)^{\frac{1}{2}}(1+K)^{-\frac{1}{2}}\right]$$

as it appears in the characteristic equation, and so the definition of y can be used for a graphical solution for the roots. Thus there is a set of values

$$y_{nm\ell} = a(k_i^2 - \beta_m^2)^{\frac{1}{2}}(1+K)^{-\frac{1}{2}}$$

which determines the sample resonant frequencies. For a sample resonance less than γH_i, it is necessary that $(1+K_{nm\ell}) > 1$, which once again implies a minimum sample size. This result is not surprising since for sufficiently large samples the sample resonances depend less critically upon the dispersive properties of the material. That is, for sufficiently large samples, resonant modes are observed even for non-dispersive scalar media.

If a_i is defined as the critical sample size where

$$a_i = y_{nm\ell}(k_i^2 - \beta_m^2)^{\frac{1}{2}}$$

then resonance below the region of magnetostatic modes is possible for all samples exceeding this size. This critical sample has a minimum for each root of the characteristic equation as a function of frequency. The location of the minimum is determined by the ratio of the saturation magnetization to the internal biasing field. If λ is that ratio then the frequency for the minimum sample size is

$$\omega_{min} = \gamma H_i \left[(1+\lambda) - (\lambda + \lambda^2)^{\frac{1}{2}}\right] .$$

Computation of the actual critical size requires determination of the roots of the exact characteristic equation. Nevertheless, it has been demonstrated heuristically that sample resonance below γH_i occurs for sufficiently large samples. This result has great significance for the noise properties of ferrite parametric amplifiers and is discussed further in Section 4. 5. 6.

3. 7. 10 Conclusions. It has been shown that the effect of electromagnetic propagation on the magnetostatic modes is the following:

(1) The resonant frequencies shift with the inclusion of propagation by an amount which depends on the sample shape.

(2) The resonant frequencies are size dependent.

(3) They can exist outside the frequency region of the magnetostatic modes.

These results are fundamental to the second-order approximation. However, for the particular example considered it was found that no sample resonances are possible above a cutoff frequency which depends on the spacing of the plates. The present investigation has extended Walker's lowest order approximation to include the second-order effect of propagation and has explained certain features of the multiple ferromagnetic resonances which are not explained by the magnetostatic approximation.

3. 8 Summary

In this chapter the physical properties of ferromagnetic materials were discussed. It was shown that the magnetic properties are determined by the magnetization ($\overline{M}$) and its relation to the magnetic field.

It was shown that ferrites are a special class of ferromagnetic materials. A survey of the pertinent energy relations in ferromagnetic media was presented, and the dynamic differential equation which relates $\overline{M}$ and $\overline{H}$ was derived. The steady-state solution to this equation was obtained under the condition that the sample was biased to saturation. This solution successfully explains the important phenomenon of ferromagnetic resonance which was described in some detail in the chapter. The approximate boundary value problem for small ferrite samples in r-f magnetic fields was solved for the purpose of explaining the multiple modes in ferromagnetic resonance. Certain properties of these modes and of ferromagnetic resonance are of extreme importance in deriving fundamental properties of ferrite phase-shift amplifiers and will be referred to extensively in subsequent chapters.

CHAPTER 4

REACTIVE MIXING PROPERTIES OF FERRITE

4. 1 Introduction

In the previous chapter, the steady-state solution of the equation of motion (i. e., excitation by a single sinusoidal source) was developed. In this chapter the mixing properties of ferrites, which are predicted by the equation of motion, are studied under the small signal approximation. It is assumed that filters restrict the power flow to only four frequencies. For this purpose the steady-state solutions of the equation of motion under the excitation of two sinusoidal sources at frequencies ω_1 and ω_2 are obtained. These solutions are written in a matrix equation which defines the so-called pumped susceptibility tensor. It is then shown that the power crossing the sample surface at each of the frequency components produced by mixing in the sample, as well as at the excitation frequencies, is determined by the components of this susceptibility tensor and the field distributions of the various components. These power relations and the susceptibility tensor components are then used in Sections 4. 5 and 4. 6 to investigate the properties of the lower- and upper-sideband up-converters, respectively, and to lay the groundwork for the double-sideband reactive mixer or phase-shift amplifier analysis.

4. 2 Steady-State Solution of the Equation of Motion for Double Excitation

In order to study the reactive mixing properties of ferrites, it is convenient to consider the excitation of the sample by two sources at different frequencies (i. e., ω_1 and ω_2, assume $\omega_2 > \omega_1$). Mixing occurs as predicted by the equation of motion. It is assumed that filters restrict the power flow to just the four frequencies ω_1, ω_2, $\omega_1 \pm \omega_2$, and lower sidebands produced. In the steady state the magnetic field and the magnetization have the general form:

$$\overline{M} = M_o z + \overline{M}_1 e^{i\omega_1 t} + \overline{M}_2 e^{i\omega_2 t} + \overline{M}_\ell e^{i\omega_\ell t} + \overline{M}_u e^{i\omega_u t} + \text{c. c.}$$

$$\overline{H} = H_o z + \overline{H}_1 e^{i\omega_1 t} + \overline{H}_2 e^{i\omega_2 t} + \overline{H}_\ell e^{i\omega_\ell t} + \overline{H}_u e^{i\omega_u t} + \text{c. c.} \qquad (4.1)$$

where c. c. denotes the complex conjugate, and the z-axis has been chosen in the direction of the biasing magnetic field.

If these expansions are substituted in the equation of motion and terms of equal frequency collected, the following set of equations are then obtained:

$$i\omega_u M_{xu} = -\gamma \left[M_{yu} H_o + M_{y1} H_{z2} - M_o H_{yu} - M_{zp} H_{y1} - M_{y2} H_{z1} - M_{z1} H_{y2}\right] + \frac{\alpha}{M_o}(-i\omega_u M_o M_{yu} - i\omega_1 M_{z2} M_{yi} - i\omega_2 M_{z1} M_{y2})$$

$$i\omega_u M_{yu} = -\gamma \left[M_o H_{xu} + M_{z2} H_{xu} + M_{z1} H_{x2} - M_{xu} H_o - M_{x2} H_{z1} - M_{x1} H_{z2}\right] + \frac{\alpha}{M_o}(i\omega_u M_o M_{xu} + i\omega_1 M_{z2} M_{x1} + i\omega_2 M_{z1} M_{x2})$$

$$i\omega_\ell M_{x\ell} = -\gamma \left[M_{y\ell} H_o + M_{y1}^* H_{2z} + M_{y2} H_{z1}^* - M_o H_{y\ell} - M_{z2} H_{y1}^* - M_{z1}^* H_{y2}\right] + \frac{\alpha}{M_o}(-i\omega_\ell M_o M_{y\ell} - i\omega_1 M_{z2} M_{y1}^* - i\omega_2 M_{z1}^* M_{yz}$$

$$i\omega_\ell M_{y\ell} = -\gamma \left[M_o H_{x\ell} + M_{z2} H_{x1}^* + M_{z1} H_{x2} - M_{x\ell} H_o - M_{x2} H_{z1}^* - M_{x1}^* H_{z2}\right] + \frac{\alpha}{M_o}(i\omega_\ell M_o M_{x\ell} + i\omega_2 M_{z1}^* M_{x2} + i\omega_1 M_{z2} M_{x1}^*)$$

$$i\omega_1 M_{x1} = -\gamma \left[M_{y1} H_o + M_{yu} H_{z2}^* + M_{y2}^* H_{zu} + M_{y\ell}^* H_{z2} + M_{y2} H_{z\ell}^* - M_o H_{y1} - M_{zu} H_{yz}^* - M_{z2} H_{yu} - M_{z2} H_{y\ell}^* - M_{z\ell}^* H_{y2}\right] - \frac{\alpha}{M_o}(i\omega_1 M_o M_{y1} + i\omega_2 M_{y2}^* + i\omega_\ell M_{z2} M_{y\ell}^* + i\omega_2 M_{z\ell}^* M_{y2} + i\omega_u M_{z2}^* M_{yu})$$

$$
\begin{aligned}
i\omega_1 M_{y1} = -\gamma \Big[& M_o H_{x1} + M_{zu} H_{x2}^* + M_{z2}^* H_{xu} + M_{z\ell}^* H_{x2} + M_{z2} H_{x\ell}^* \\
& - M_{x1} H_o - M_{x2}^* H_{zu} - M_{xu} H_{z2}^* - M_{x\ell}^* H_{z2} - M_{x2} H_{z\ell}^* \Big] + \frac{\alpha}{M_o} (i\omega_1 M_o M_{x1} \\
& + i\omega_2 M_{z\ell}^* M_{x2} + i\omega_2 M_{zu} M_{x2}^* + i\omega_\ell M_{z2} M_{x\ell}^* + i\omega_u M_{z2}^* M_{xu}) \\
i\omega_2 M_{x2} = -\gamma \Big[& M_{y2} H_o + M_{y1}^* H_{zu} + M_{yu} H_{z1}^* + M_{y\ell} H_{z1} + M_{y1} H_{z\ell} \\
& - M_o H_{y2} - M_{z1}^* - M_{zu} H_{y1}^* - M_{z\ell} H_{y1} - M_{z1} H_{y\ell} \Big] \\
& - \frac{\alpha}{M_o} (i\omega_2 M_o M_{y2} + i\omega_u M_{z1}^* M_{yu} + i\omega_1 M_{zu} M_{y1}^* \\
& + i\omega_\ell M_{z1} M_{y\ell} + i\omega_1 M_{z\ell} M_{y1}) \\
i\omega_2 M_{y2} = -\gamma \Big[& M_o H_{x2} + M_{zu} H_{x1}^* M_{z1}^* H_{xu} + M_{z\ell} H_{x1} + M_{z1} H_{x\ell} \\
& - M_{x2} H_o - M_{xu} H_{z1}^* - M_{x1}^* H_{zu} - M_{x\ell} H_{z1} - M_{x1} H_{z\ell} \Big] \\
& + \frac{\alpha}{M_o} (i\omega_2 M_o M_{x2} + i\omega_u M_{z1}^* M_{xu} + i\omega_1 M_{zu} M_{x1}^* \\
& + i\omega_\ell M_{z1} M_{x\ell} + i\omega_1 M_{z\ell} M_{x1}) \qquad (4.2)
\end{aligned}
$$

It has been assumed in these equations that $|M| \cong M_o$ and that $\frac{\partial M_z}{\partial t} \cong 0$. It is useful at this point to justify these assumptions on the basis of the small signal assumption. The material is saturated magnetically, so that in the absence of r-f excitation the magnetization is aligned along H_o and $|\overline{M}| = M_o$ exactly. The application of r-f fields causes the magnetization to precess around the direction of H_o forming an angle ϕ with that direction. The transverse component $\overline{M}_t$ is related to $\overline{M}$ by the relation

$$|M_t| = |\overline{M}| \sin\phi = M_o \sin\phi \qquad (4.3)$$

since $|\overline{M}|$ is assumed constant. In the small signal assumption ϕ is very small and in fact to a very good approximation

$$|M_t| = M_o \phi \qquad (4.4)$$

But the longitudinal component

$$M_z \cong M_o \left(1 - \frac{\phi^2}{2}\right) \tag{4.5}$$

which to first order in ϕ is $M_z = M_o$ (i. e., it is constant). Therefore, the z-directed components of magnetization at the four frequencies can be approximated by zero in the small signal analysis. A considerable simplification results if this approximation is substituted in the above equations.

4.3 The Pumped Susceptibility Tensor

The equations may be written in a matrix equation of the form

$$\overline{H} = \overline{\overline{T}} \cdot \overline{M} \tag{4.6}$$

which when inverted is the steady state solution to the equation of motion:

$$\overline{M} = (\overline{\overline{x}}) \cdot \overline{H} \tag{4.7}$$

It is most convenient to regard the transverse components of magnetization and magnetic field at the signal and sideband frequencies as variables, and the pump frequency components as the parameters which couple them. This is done, not of necessity, but simply to minimize the number of elements in $(\overline{\overline{x}})$ for each of computation. Any component can be interpreted as the source, which permits a convenient designation for any particular configuration.

4.4 The Power-Flow Relations

The definitions for voltage and current have somewhat less significance in microwave circuits than in low-frequency circuits. However, the concepts of power and power flow have the same physical significance as in low frequency circuits. For example, the Manley-Rowe (Ref. 2) equations, which have great utility at microwave frequencies, relate real power flow and exchange. Our objective here is to relate power flow to the magnetization and magnetic field in the sample of ferrite. It is then possible to use the results in studying the particular way in which the ferrite acts as a reactive mixer.

Consider a sample of ferrite biased to saturation along an axis which is being excited by two r-f sources and which is producing the upper and lower sidebands internally

as a result of mixing. Since we are interested in power, and all power measurements take place outside the sample, it is natural to begin with the quadratic relation which measures the power flow across a closed surface external to the sample. That quadratic relation is the following:

$$P_{s\omega} = \frac{1}{2} \operatorname{Re} \int_{\text{surf}} (\overline{E} \times \overline{H}^*) \cdot d\overline{s} = \frac{1}{2} \operatorname{Re} \int_{\text{volume}} \nabla \cdot (\overline{E} \times \overline{H}^*)\, dv \tag{4.8}$$

where $P_{s\omega}$ is the net power flow out of the surface at frequency ω when $\overline{\overline{E}}$ and $\overline{\overline{H}}$ are the total fields on that surface at frequency ω. For a closed-surface integration over the sample surface, then the volume integration extends over the entire volume of the sample. The integrand on the right-hand side of the equation can be expanded using Maxwell's equations:

$$\begin{aligned} \nabla \cdot \overline{E} \times \overline{H}^* &= \overline{H} \cdot \nabla \times \overline{E} + \overline{E} \cdot \nabla \times \overline{H}^* \\ &= \overline{H}^* \cdot (-j\omega \overline{\overline{\mu}}) \cdot \overline{H} + \overline{E}^* \cdot (-j\omega \overline{\overline{\epsilon}}) \cdot \overline{E} \end{aligned} \tag{4.9}$$

For most ferrite materials at x-band $\overline{\overline{\epsilon}}$ is approximately a real scalar for all frequencies of interest in this report. Substituting the above in the expression for $P_{s\omega}$ produces;

$$P_{s\omega} = \frac{1}{2} \operatorname{Re}\ -j\omega \int_{V_s} \overline{H}_\omega{}^* \cdot (\overline{\overline{\mu}} \cdot \overline{H})_\omega\, dv \tag{4.10}$$

where the subscript ω refers to those components which vary at frequency ω. But

$$\overline{\overline{\mu}} = \mu_o(\overline{\overline{1}} + \overline{\overline{x}}) \tag{4.11}$$

and since $\overline{\overline{H}}_\omega \cdot \overline{H}_\omega{}^*$ is entirely real, the expression for $P_{s\omega}$ reduces to:

$$P_{s\omega} = \frac{\mu_o \omega}{2} \operatorname{Im} \int_{V_s} \overline{H}_\omega{}^* \cdot (\overline{\overline{X}} \cdot \overline{H})_\omega\, dv \tag{4.12}$$

Thus, it is clear that once the pumped susceptibility and field distributions are known, the net power leaving the sample at any frequency can be found.

In the absence of pumping (i. e., excitation at a single frequency only) Eq. 4. 12 reduces to that for the power absorbed in a sample. As an example of this, consider excitation of the sample at frequency ω_1, assuming that the field components are transverse to

the direction of the biasing field. Due to the symmetry of the susceptibility tensor, $P_{s\omega}$ reduces to a simple expression:

$$P_{s\omega} = \frac{\mu_o \omega}{2} \operatorname{Im} \int_{V_s} X_{11} |H|^2 \, dv + i \int X_{12} \overline{H}_1^* \times H_1 \cdot z \, dv \qquad (4.13)$$

Assuming the fields are linearly polarized then $H^* \times H = 0$ and, assuming that the sample is a sphere of low loss material, then $\omega_{res} \cong \omega_H = \gamma H_o$. Then

$$P_{s\omega} = - \frac{\mu_o \omega}{2} \frac{\alpha \omega_m \omega_H^2 \omega}{(\omega_H^2 - \omega^2)^2 + 4\alpha^2 \omega_H^2 \omega^2} \int_{V_s} |H|^2 \, dv \qquad (4.14)$$

If this function is plotted vs. ω_H for a fixed excitation frequency, then the shape of the curve shows some similarity to that observed in ferromagnetic resonance experiments for spheres (Ref. 21). Actually, H in the material is not independent of the orientation of the biasing field relative to the crystalline axes due to anisotropy, so the dependence of $P_{s\omega}$ on ω_H is somewhat more complicated than indicated above.

4.5 The Lower-Sideband Ferrite Reactive Mixer

The use of ferrites in a lower-sideband reactive mixer, which is commonly called a parametric amplifier, was first proposed by Suhl (Ref. 22). His proposal was prompted by the discovery of the so-called magnetostatic modes and the observation that the equation of motion for ferrite predicts the proper coupling between fields at different frequencies. The high-Q magnetostatic modes suggested a ready means of filtering the lower sideband and suppressing the upper sideband. If the sample is placed in a microwave cavity then in addition to the resonant magnetostatic modes there is a set of cavity modes whose resonant frequencies are perturbed somewhat from the empty cavity values. Suhl proposed three basic types of possible amplifier operation, distinguished according to the type of resonance which was used to filter the lower sideband and signal. The so-called magnetostatic type of operation uses two magnetostatic modes; the electromagnetic operation uses two cavity modes which the sample tends to couple; and the semistatic operation uses one magnetostatic mode and one cavity mode. The distinction between these basic types of operation is artificial since neither the so-called electromagnetic modes nor the magnetostatic modes

are really independent energy storage resonances. The distinction between the two mode types is really based upon the crudeness of the approximate analysis of the fields inside the cavity.

For each of these semi-distinct types of operation Suhl computed the threshold pump field intensity, which is defined as that field for which the characteristic roots of the equation motion cross into the right half plane. It is interesting that the Suhl threshold is also that pump power for which the gain of the circuit is unity. In principle, this computation is useful but, in practice, it has the drawback that detailed calculations of the actual threshold are impossible to make due to lack of exact knowledge of the field distributions. In addition, he overlooked the effect of pumping on the susceptibility tensor, which tends to make his threshold calculations in error on the low side. The purpose of this section is to consider the parametric amplifier in the more modern theory in which it is known to be a special case of reactive mixer.

The pumped susceptibility tensor is found for the lower-sideband configuration and using it the threshold is computed without making any assumptions about the field distributions. It is assumed, in the following analysis, that resonant modes are available for separating the lower sideband but no assumption will be made concerning their field distributions in developing the general threshold relation. The sample is assumed to be located in a microwave cavity which is resonant at the pump frequency to facilitate pumping.

4. 5. 1 The Lower-Sideband Pumped Susceptibility Tensor. For the lower sideband circuit the set of equations of motion is reduced to the following four:

$$
\begin{aligned}
i\omega_1 M_{x1} &= -\gamma \left[M_{y1} H_o + M_{y\ell}^{*} H_{z2} + M_{y2} H_{z\ell}^{*} - M_o H_{y1} \right] - i\alpha\omega_1 M_{y1} \\
i\omega_1 M_{y1} &= -\gamma \left[M_o H_{x1} - M_{x1} H_o - M_{x\ell} H_{z2} - M_{x2} H_{z\ell}^{*} \right] + i\alpha\omega_1 M_{x1} \\
i\omega_\ell M_{x\ell}^{*} &= -\gamma \left[M_{y\ell}^{*} H_o + M_{y1} H_{z2}^{*} + M_{y2}^{*} H_{z1} - M_o H_{y\ell}^{*} \right] + i\alpha\omega_\ell M_{y\ell}^{*} \\
i\omega_\ell M_{y\ell}^{*} &= -\gamma \left[M_o H_{x\ell}^{*} - M_{x\ell}^{*} H_o - M_{x2}^{*} H_{z1} - M_{x1} H_{z2}^{*} \right] - i\alpha\omega_\ell M_{x\ell}^{*}
\end{aligned}
\qquad (4.15)
$$

It is instructive to speculate about the relative orientation of the two source field distributions for maximum coupling before solving this set of equations for M(H). Observe that if

no power is supplied at the lower sideband, then, in the small-signal approximation, $H_{z\ell} = 0$. Thus, the only component of coupling in the first equation is $M_{y\ell}{}^* H_{z2}$, that is, the coupling comes entirely from the longitudinal component of the pump. For maximum pumping efficiency the pump field intensity should be z-directed (i. e., parallel to the biasing field). The most successful ferrite parametric amplifier built to date uses this parallel pumping scheme (Ref. 23). If $H_{2t} = 0$, then $M_{t2} = 0$, and by a similar argument it may be shown that the most efficient use of signal power occurs if the signal field is tranverse to the pump field. Using these orientations for the field distribution, the equations of motion may be written in matrix form:

$$\begin{bmatrix} H_{x1} \\ H_{y1} \\ H_{\ell x}{}^* \\ H_{\ell y}{}^* \end{bmatrix} = \begin{bmatrix} \omega_o + i\alpha\omega_1 & -i\omega_1 & \gamma H_{z2} & 0 \\ i\omega_1 & \omega_o + i\alpha\omega_1 & 0 & \gamma H_{z2} \\ \gamma H_{z2}{}^* & 0 & \omega_o - i\alpha\omega_\ell & i\omega_\ell \\ 0 & \gamma H_{z2}{}^* & -i\omega_\ell & \omega_o - i\alpha\omega_\ell \end{bmatrix} \cdot \begin{bmatrix} M_{x1} \\ M_{y1} \\ M_{x\ell}{}^* \\ M_{y\ell}{}^* \end{bmatrix} \qquad (4.16)$$

The steady-state solution to the equations of motion is found by inverting this matrix. The inverted matrix, which we call the pumped susceptibility tensor, was found to first order in H_{z2} and appears in Appendix D. It has the general symmetry

$$\begin{aligned} x_{11} &= x_{22} & x_{33} &= x_{44} \\ x_{12} &= -x_{21} & x_{34} &= -x_{43} \\ x_{13} &= x_{24} & x_{31} &= x_{42} \\ x_{14} &= -x_{23} & x_{32} &= -x_{41} \end{aligned} \qquad (4.17)$$

Notice that the terms x_{13}, x_{14}, x_{31}, x_{41}, etc., are proportional to the pump field intensity. These terms represent the coupling between the signal and lower sideband fields.

4. 5. 2 Power Flow at the Signal Frequency. The net power leaving the sample at the signal frequency can be found:

$$P_{\omega 1} = \frac{\omega_1 \mu_o}{2} \operatorname{Im} \int_{V_s} \overline{H}_1^* \cdot (\overline{\overline{X}} \cdot \overline{H})_1 \, dv$$

$$= \omega_1 \mu_o \operatorname{Im} \Big[\int (H_{1x}^* X_{11} H_{1x} + H_{1x}^* X_{12} H_{1y} + H_{1x}^* H_{x\ell} X_{13}^* + H_{1x}^* X_{1x} H_{\ell y}^*$$

$$+ H_{1y}^* X_{21} H_{1x} + H_{1y}^* X_{22} H_{1y} + H_{1y}^* X_{23} H_{\ell x}^* + H_{1y}^* X_{24} H_{\ell y}^*) \, dv \Big] \qquad (4.19)$$

but using the symmetry relations this becomes:

$$P_{\omega 1} = \frac{\omega_1 \mu_o}{2} \operatorname{Im} \Big[\int X_{11} |H|^2 \, dv + \int X_{12} \overline{H}_1^* \times \overline{H}_v \cdot z \, dv$$

$$+ \int X_{13} \overline{H}_1^* \cdot \overline{H}_\ell^* \, dv + \int X_{14} \overline{H}_1^* \times \overline{H}_\ell^* \cdot z \, dv \Big] \qquad (4.20)$$

The field distributions were assumed to be linearly polarized so $\overline{H}_1^* \times \overline{H}_1 = 0$. If the sample is an ellipsoid of revolution, then the biasing field will be uniform inside the material and the tensor elements will be independent of position in the sample. Using this fact and the form of $\operatorname{Im} x_{11}$ found in Appendix D, and assuming ω_1 far from ferromagnetic resonance, the expression for the power may be written:

$$P_{\omega 1} = \frac{\omega_1 \mu_o}{2} \Bigg[- \frac{\alpha(\omega_o^2 + \omega_1^2)}{(\omega_o^2 - \omega_1^2)} \int_{V_s} |H_1|^2 \, dv + \operatorname{Im} X_{13} \int \overline{H}_1^* \cdot \overline{H}_\ell^* \, dv$$

$$+ \operatorname{Im} X_{14} \int \overline{H}_1^* \times \overline{H}_\ell \cdot z \, dv \Bigg] \qquad (4.21)$$

The first term in this expression is negative and represents the signal power dissipated in the sample. In terms of the equivalent circuit (see Fig. 4-1) it represents the power dissipated in the input circuit conductance. In this equivalent circuit the resonant magnetostatic modes are represented by parallel resonant circuits and the coupling between them by a sinusoidally varying capacitor at the pump frequency ω_2. The other terms in Eq. 4.21 represent the power reflected into the input from the lower sideband. It is well known that this is a positive power; however it is instructive to examine the exact form in which this occurs in ferrites, and to compute the unity gain threshold power for which $P_{\omega 1}=0$.

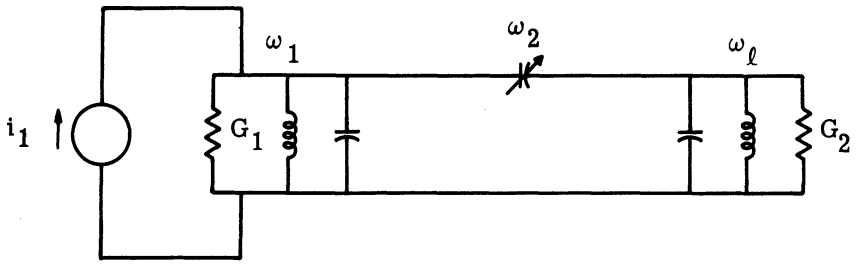

Fig. 4-1. Equivalent circuit of lower-sideband reactive mixer or parametric amplifier. The frequencies ω_1 and ω_ℓ are the resonant frequencies of the correspondingly labelled circuit. G_1 includes the source, and the load and stray conductances of the input circuit.

4.5.3 Power Flow at the Lower Sideband. Adams has shown that the impedance reflected into the signal circuit contains a negative real part only if real power is dissipated at the lower sideband circuit (Ref. 24). For this reason it is necessary to examine the power flow at the lower sideband. The amount leaving the sample is given by:

$$P_{\omega\ell} = \frac{\mu_o \omega_\ell}{2}\left[\text{Im}\int \bar{H}_\ell^* \cdot \bar{M}_\ell \, d\upsilon\right] = -\frac{\mu_o \omega_\ell}{2}\left[\text{Im}\int \bar{H}_\ell \cdot \bar{M}_\ell^* \, d\upsilon\right] \qquad (4.22)$$

The latter form is most useful because of the particular nature of the pumped susceptibility tensor for the lower sideband (i.e., M_1 couples to M^*). Using the symmetry relations among the tensor components, and the assumption that the fields are linearly polarized, the expression for the lower sideband power may be written:

$$P_{\omega\ell} = -\frac{\mu_o \omega_\ell}{2}\left[\frac{\alpha\omega_\ell(\omega_o^2 + \omega_\ell^2)}{(\omega_o^2 - \omega_\ell^2)^2}\int |H_\ell|^2 \, d\upsilon + \text{Im}\int X_{31} H_\ell H_1 \, d\upsilon + \text{Im}\, X_{32}\int H_\ell \times H_1 \cdot z \, d\upsilon\right] \qquad (4.23)$$

If no power is supplied at the lower sideband then $P_{\omega\ell} \geq 0$ because the only source of power at ω_ℓ is the mixing in the sample. The first term is negative and represents the sideband power dissipated in the sample. The sum of the other two terms must be positive from the condition $P_{\omega\ell} \geq 0$. If the lower sideband frequency is far from ferromagnetic resonance

$$X_{31} \cong \frac{\omega_p(\omega_o^2 - \omega_1\omega_\ell)}{(\omega_o^2 - \omega_1^2)(\omega_o^2 - \omega_\ell^2)} \quad \text{and} \quad X_{32} \cong \frac{\alpha\omega_1\omega_o(\omega_\ell - \omega_1)}{(\omega_o^2 - \omega_1^2)(\omega_o^2 - \omega_\ell^2)} \tag{4.24}$$

where $\omega_p = \gamma H_{z2} = \gamma h_p$. Continuing under this assumption:

$$\frac{\omega_p(\omega_o^2 - \omega_1\omega_\ell)}{(\omega_o^2 - \omega_1^2)(\omega_o^2 - \omega_\ell^2)} \operatorname{Im} \int_{v_s} \overline{H}_\ell \cdot \overline{H}_1 \, dv - \left(\frac{\omega_p\omega_o(\omega_\ell - \omega_1)}{(\omega_o^2 - \omega_1^2)(\omega_o^2 - \omega_\ell^2)} \right) \times$$

$$\left(\operatorname{Re} \int_{v_s} \overline{H}_\ell \times \overline{H}_1 \cdot z \, dv \right) \geq + \frac{\alpha\omega_\ell(\omega_o^2 + \omega_\ell^2)}{(\omega_o^2 - \omega_\ell^2)^2} \int |H_\ell|^2 \, dv > 0 \tag{4.25}$$

This inequality can be used to show that the power reflected into the signal circuit is positive. In Appendix D it was shown that $x_{13} = x_{31}$ and $x_{32} = x_{14}$. Using these relations in Eq. 4.21, the power reflected into the signal circuit may be written:

$$\begin{aligned}
&\operatorname{Im} X_{13} \int \overline{H}_1^* \cdot \overline{H}_\ell^* \, dv + \operatorname{Im} X_{14} \int \overline{H}_1^* \times \overline{H}_\ell^* \cdot z \, dv = \\
&- \frac{\omega_p(\omega_o^2 - \omega_1\omega_\ell)}{(\omega_o^2 - \omega_1^2)(\omega_o^2 - \omega_\ell^2)} \operatorname{Im} \int \overline{H}_1^* \cdot \overline{H}_\ell^* \, dv \\
&- \frac{\omega_p\omega_o(\omega_\ell - \omega_1)}{(\omega_o^2 - \omega_1^2)(\omega_o^2 - \omega_\ell^2)} \operatorname{Re} \int \overline{H}_1^* \times \overline{H}_\ell^* \cdot z \, dv \\
&= \frac{\omega_p(\omega_o^2 - \omega_1\omega_\ell)}{(\omega_o^2 - \omega_1^2)(\omega_o^2 - \omega_\ell^2)} \operatorname{Im} \int \overline{H}_1 \cdot \overline{H}_\ell \, dv \\
&+ \frac{\omega_p\omega_o(\omega_\ell - \omega_1)}{(\omega_o^2 - \omega_1^2)(\omega_o^2 - \omega_\ell^2)} \operatorname{Re} \int \overline{H}_1 \times \overline{H}_\ell \cdot z \, dv
\end{aligned} \tag{4.26}$$

But this quantity is larger than or equal to:

$$\frac{\alpha\omega_\ell(\omega_o^2 + \omega_\ell^2)}{(\omega_o^2 - \omega_\ell^2)^2} \int |H_\ell|^2 \, dv > 0 \tag{4.27}$$

as proved in Eq. 4.27 independent of ω_1, ω_2, ω_o. Therefore, for sufficiently large ω_p $(=\gamma h_p)$, $P_{\omega 1} > 0$, corresponding to the condition that more signal power leaves than enters the sample. This is equivalent to a power gain at the signal frequency.

4.5.4 The Threshold Pump Power for Parametric Amplification. The threshold pump power can be found by eliminating the amplitudes of the signal and lower-sideband field distributions from the two expressions

$$P_{\omega 1} = 0$$

$$P_{\omega \ell} > 0 \ . \tag{4.28}$$

This process yields the threshold completely independent of any assumptions about the field distributions, though the actual pump power does depend upon the field distributions. Before making such a calculation, it will be necessary to discuss what is meant by the amplitude and phase of a pair of complex field distributions. The field distribution can be written as a complex function of the coordinates in the form of $|H(\bar{r})|\, e^{i\phi(\bar{r})}$. The phase $\phi(\bar{r})$ will always contain a component which is independent of position in the sample (i. e., $\phi(r) = \phi_o + f(\bar{r})$). This component represents the time phase of the field distribution in the same sense as the time phase for the lumped parameter equivalent circuit. For example, the fields in an ellipsoid of revolution are of the form $F(\xi,\eta)\, e^{in\theta}$ where θ is the angle measured about the axis of symmetry and F is real (Chapter 3). The phase of this function depends upon the choice of the coordinate axes. Thus the quantity which will be called the time phase of the field distribution will be that part which is independent of the choice of spatial coordinate axes. The amplitude of the fields can be defined rather arbitrarily but a reasonably good choice is as follows.

$$a^2 = \int_{V_S} |H_i|^2 \, dv \tag{4.29}$$

where a is to be considered the amplitude of the fields. Then the field distribution can be written

$$H_i(\bar{r}) = a\, e^{i\phi_i} h_i(\bar{r}) \qquad \text{and} \qquad H_\ell(\bar{r}) = b\, e^{i\phi_\ell} h_\ell(\bar{r}) \tag{4.30}$$

There is another property of the phase which is fundamental to parametric amplifiers, i. e., the signal power reflected to the input circuit is proportional to (Ref. 25)

$$\mathrm{Im}\left(e^{j(\phi_2 - \phi_1 - \phi_\ell)} \right) . \tag{4.31}$$

The midband gain of the circuit corresponds to the maximum of this function which occurs at

$$\phi_2 - \phi_1 - \phi_\ell = \left(\frac{\pi}{2} + 2n\pi\right) . \tag{4.32}$$

It has been assumed in Eq. 4. 26 that $\phi_2 = 2n\pi$ thus

$$-(\phi_1 + \phi_\ell) = \frac{\pi}{2} + 2(n-k)\,\pi \tag{4.33}$$

at midband. Using this relationship in Eq. 4. 26, it may be written

$$\frac{\omega_p}{(\omega_o^2 - \omega_1^2)(\omega_o^2 - \omega_\ell^2)} \left[(\omega_o^2 - \omega_1 \omega_\ell)\, \mathrm{Im} \int ab e^{j\frac{\pi}{2}} \bar{h}_1^* \bar{h}_\ell \, d\upsilon \right.$$

$$\left. + \omega_o(\omega_2 - \omega_1)\, \mathrm{Re} \int ab e^{j\frac{\pi}{2}} \bar{h}_1^* \times \bar{h}_\ell^* \cdot z \, d\upsilon \right] = \frac{ab\,\omega_p\, H}{(\omega_o^2 - \omega_1^2)(\omega_o^2 - \omega_\ell^2)}$$

$$H = (\omega_o^2 - \omega_1\omega_2)\, \mathrm{Re} \int_{v_s} \bar{h}_1^* \cdot \bar{h}_\ell^* \, d\upsilon + \omega_o(\omega_2 - \omega_1)\, \mathrm{Im} \int_{v_s} \bar{h}_1^* \times \bar{h}_\ell^* \cdot z \, d\upsilon \tag{4.34}$$

but for the threshold condition this quantity must equal

$$\frac{\alpha\, a^2\, \omega_1(\omega_o^2 + \omega_1^2)}{(\omega_o^2 - \omega_1^2)^2} \int_{v_s} (\bar{h}_1 \cdot \bar{h}_1^*) \, d\upsilon \tag{4.35}$$

It is convenient for the computation of the threshold to assume $P_{\omega\ell} = 0$, which is equivalent to the assumption that all of the lower sideband power is dissipated in the sample, or that the sample itself provides the lower-sideband termination. Using this equality Eq. 4. 26 becomes:

$$\frac{ab\,\omega_p}{(\omega_o^2-\omega_1^2)(\omega_o^2-\omega_\ell^2)}\left[(\omega_o^2-\omega_1\omega_\ell)\,\mathrm{Re}\int_{V_s}\bar{h}_1\cdot\bar{h}_\ell\,d\upsilon+\omega_o(\omega_2-\omega_1)\,\mathrm{Im}\int_{V_s}\bar{h}_1\times\bar{h}_\ell\,z\,d\upsilon\right]$$

$$=\frac{\alpha\,b^2\,\omega_\ell(\omega_o^2+\omega_\ell^2)}{(\omega_o^2-\omega_\ell^2)^2}\int_{V_s}\bar{h}_\ell\cdot\bar{h}_\ell^{*}\,d\upsilon \tag{4.36}$$

If a and b are eliminated between Eqs. 4.34 and 4.36 then the threshold pump field intensity can be found:

$$(\gamma h_p)^2=\frac{\alpha^2\,\omega_1\omega_2(\omega_o^2+\omega_\ell^2)(\omega_o^2+\omega_1^2)\int_{V_s}\bar{h}_1\cdot\bar{h}_1^{*}\,d\upsilon\int_{V_s}\bar{h}_\ell\cdot\bar{h}_\ell^{*}\,d\upsilon}{F_1F_2} \tag{4.37}$$

$$F_1=(\omega_o^2-\omega_1\omega_2)\,\mathrm{Re}\int_{V_s}\bar{h}_1\cdot\bar{h}_\ell\,d\upsilon+\omega_o(\omega_2-\omega_1)\,\mathrm{Im}\int_{V_s}\bar{h}_1\times\bar{h}_\ell\cdot z\,d\upsilon$$

$$F_2=(\omega_o^2-\omega_1\omega_2)\,\mathrm{Re}\int_{V_s}\bar{h}_1^{*}\cdot\bar{h}_\ell^{*}+\omega_o(\omega_2-\omega_1)\,\mathrm{Im}\int_{V_s}\bar{h}_1^{*}\times\bar{h}_\ell^{*}\cdot z\,d\upsilon$$

Observe that the threshold is infinite if the field distributions at ω_1 and ω_ℓ are orthogonal over the sample, or equivalently the coupling between these fields is zero. In samples which are ellipsoids of revolution, the field distribution is always of the form

$$\bar{h}(r)=\bar{h}\,f(\eta\,\xi)\,e^{in\theta} \tag{4.38}$$

where θ is the aximuthal coordinate and $f(\eta\,\xi)$ are real functions of the other coordinates. For such samples the only nonzero values for the integrals in F_1 and F_2 will occur for $n_1=-n_\ell$. For any other combination n_1 and n_ℓ $h_p\to\infty$. For this case both integrals will be entirely real and only the first term in F_1 and F_2 will be nonzero. The threshold in this case can be written:

$$(\gamma h_p)^2=\frac{\alpha^2\,\omega_1\omega_2(\omega_o^2+\omega_1^2)(\omega_o^2+\omega_\ell^2)\int_{V_s}f_1^2(\eta\,\xi)\,d\upsilon\int_{V_s}f_\ell^2(\eta\,\xi)\,d\upsilon}{(\omega_o^2-\omega_1\omega_2)^2\left[\int_{V_s}f_1(\eta\,\xi)\,f_\ell(\eta\,\xi)\,d\upsilon\right]^2} \tag{4.39}$$

where for finite h_p $n_1=-n_\ell$.

4. 5. 5 The Field Distributions for Minimum Threshold. It is characteristic of existing ferrite parametric amplifiers that their thresholds are very large. For this reason it would be of considerable interest to find the pair of field distributions which minimize h_p^2. The approach to be followed in computing this minimum is to assume a field distribution f_1 for the ω_1 field, find the distribution f_ℓ which minimizes h_p, and then find the combination which minimizes that form. For this purpose the quantity F is defined:

$$F = \frac{\int_{V_S} f_1^2(\eta\,\xi)\,d\upsilon \int_{V_S} f_\ell^2(\eta\,\xi)\,d\upsilon}{\left[\int_{V_S} f_1(\eta\,\xi)\,f_\ell(\eta\,\xi)\,d\upsilon\right]^2} \tag{4.40}$$

Minimizing F minimizes h_p. Thus the procedure is to find f_ℓ for which F is stationary and then to show that this is a minimum for F.

The f_ℓ for stationary F is found by substituting $f_\ell = f_{\ell_o} + b\delta f$, thereby defining F(b). The f_ℓ for which F(b) is stationary is f_{ℓ_o} and the condition for stationarity is F'(0) = 0 (Ref. 26). Differentiating

$$F(b) = \frac{\int_{V_S} f_1^2\,d\upsilon \int_{V_S} (f_{\ell o} + b\delta f)^2}{\left(\int f_1(f_{\ell o} + b\delta f)\,d\upsilon\right)^2} \tag{4.41}$$

with respect to b, evaluating at b = 0, and setting F'(0) = 0 yields

$$F(0)\left[\int f_1\,\delta f\,d\upsilon \int f_1 f_{\ell o}\,d\upsilon + \int f_1 f_{\ell o}\,d\upsilon \int f_1\,\delta f\,d\upsilon\right]$$
$$= 2\int f_1^2\,d\upsilon \int f_{\ell o}\,\delta f\,d\upsilon \tag{4.42}$$

Then, using F(0), this equality can be written

$$\int \delta f \left[\frac{f_1}{\int f_1 f_{\ell_o}\,d\upsilon} - \frac{f_{\ell_o}}{\int f_{\ell_o}^2\,d\upsilon}\right] d\upsilon = 0 \tag{4.43}$$

The solution to this equation is $f_1 = f_{\ell_o}$. One then finds that F(0) = 1, independent of f_1. It

remains to be shown that this stationary value is a minimum. For this purpose it is convenient to form the expression F - F(0) = F - 1 and show that F - 1 $\geq$ 0, which establishes that F(0) is a minimum.

$$F-1 = \frac{\int f_1^2 \, d\upsilon \int f_\ell^2 \, d\upsilon - \left(\int f_1 f_\ell \, d\upsilon \right)^2}{\int f_1 f_\ell \, d\upsilon \,^2} \tag{4.44}$$

To show that this quantity is never negative, consider the expression:

$$\frac{1}{2} \int_V \int_V \left[f_1(r_1) \, f_\ell(r_2) - f_\ell(r_1) \, f_1(r_2) \right]^2 \, d\upsilon_1 \, d\upsilon_2 \geq 0$$

$$= \frac{1}{2} \int\int \left[f_1^2(r_1) \, f_\ell^2(r_2) + f_\ell^2(r_1) \, f_1^2(r_2) - \left(f_1(r_1) \, f_\ell(r_1) + f_1(r_2) \, f_\ell(r_2) \right) \right] d\upsilon_1 \, d\upsilon_2$$

$$= \int f_1^2(r_1) \, d\upsilon_1 \int f_\ell^2(r_1) \, d\upsilon_2 - \int f_1(r_1) \, f_\ell(r_1) \, d\upsilon_1 \int f_1(r_2) \, f_\ell(r_2) \, d\upsilon_2 \tag{4.45}$$

but one cannot distinguish r_1 from r_2 in definite integrals so:

$$= \int f_1^2(r) \, d\upsilon \int f_\ell^2(r) \, d\upsilon - \left(\int f_1 f_\ell \, d\upsilon \right)^2 \geq 0 \tag{4.46}$$

This is the so-called Cauchy inequality. Thus F - 1 > 0, so F(0) is indeed a minimum which means that h_p is a minimum for $f_1 = f_{\ell o}$.

It has already been shown that $n_1 = -n_\ell$, thus $h_1 = h_{\ell o}{}^*$. The minimum threshold occurs when the signal and lower-sideband field distributions are complex conjugates. It might appear at first thought that field distributions which are complex conjugates have the same frequency. However, the physical significance of conjugate field distributions is that they are identical spatial distributions which precess in opposite directions around the biasing field. It is a peculiar property of ferrites that identical field distributions which precess oppositely have different resonant frequencies. This was demonstrated by Walker for the magnetostatic approximation (Ref. 18) and further in Chapter 3 for the second-order approximation. Thus, the so-called degenerate operation (i. e., $\omega_1 = \omega_\ell$) does not correspond to minimum threshold. On the other hand the frequencies of such modes will be close to one another. Denton (Ref. 23) observed that the pump threshold was smallest for mode pairs whose frequencies were closest. Although there is some doubt concerning which magneto-

static modes he actually used, it is advanced here that the mode pairs for which he observed smallest threshold were in reality modes whose field distributions were complex conjugates.

4.5.6 Estimate of Minimum Threshold. It is possible to estimate the minimum pump threshold power from $h_{p\,min}$

$$\gamma h_{p\,min} = \alpha \sqrt{\frac{\omega_1\omega_2(\omega_o^2 + \omega_1^2)(\omega_o^2 + \omega_\ell^2)}{(\omega_o^2 - \omega_1\omega_\ell)^2}} \lesssim \alpha\sqrt{\omega_1\omega_2} \qquad (4.47)$$

$$h_p \sim \Delta H \sqrt{\frac{\omega_1\omega_2}{\omega_o^2}}$$

But ω_1 and ω_2 will be of the order of ω_o. Thus, $h_{p\,min} \cong \Delta H$ where ΔH is the linewidth of ferromagnetic resonance which is typically of the order of one oersted. For a low-loss cavity the loaded Q at resonance might be of the order of 1000 at $f_o = 10^4$ Mc. From the formula for Q one can relate the pump power to the stored energy.

$$QP_s = \omega_o U|_{res} \cong \omega_o \mu_o h_p^2 v_c \qquad (4.48)$$

At this resonant frequency the cavity will be of the order of 10^{-5} m^3. Using these values, one obtains $P_s = 3\,m\omega$ as a fairly crude estimate of the pump power necessary for unity gain.

The particular ferromagnetic parametric amplifier that has proved to be most efficient is the one developed by Denton. The important aspect of this amplifier is that it operates on a continuous basis with a much lower pump power than achieved by previously developed amplifiers. A small sphere (0.045-inch diameter) of single crystal Y ttrium Iron Garnet is mounted in a half-wave X-band cavity which is resonant at 9196 Mc. The ferrite is mounted in a region of maximum pump magnetic field and is biased with a dc field parallel to the pump field. When the pump power was set at 500 mw, a gain of 20 db with a bandwidth of 100 kc at 4560 Mc was observed. Unfortunately, the amplifier noise figure is about 14 db and is nearly independent of the sample temperature (Ref. 53). Denton has shown that this noise is produced by spin waves which are pumped into oscillation by the large pump power. It appears to be fundamental to this type of amplifier. However, it has been shown by Suhl (Ref. 47) that spin waves tend to be excited only at frequencies above γH_i

where H_i is the internal biasing magnetic field. It was shown in Section 3.7.9 that sample resonance below γH_i is possible for sufficiently large samples. It is possible that a low-noise ferrite parametric amplifier could be built using these low-frequency sample resonances.

It will be shown later in this paper that many of the difficulties of this amplifier are fundamental to ferrites and cannot be significantly improved. On the other hand, there are many distinct contrasts between this amplifier and the ferrite phase-shift amplifier which tend to imply the superiority of the latter.

4.6 The Upper-Sideband Up-Converter

It was shown earlier that the upper-sideband converter does not reflect power into the signal circuit. Contrasting its equivalent circuit with that of the lower-sideband device shows that no negative resistance effect is possible with an upper-sideband converter. However, the Manley-Rowe relations predict that the power in the upper sideband comes primarily from the pump (Ref. 29). Therefore, a rather small amount of power at the signal frequency can control an arbitrarily large upper-sideband power provided the upper-sideband frequency is sufficiently large compared to the signal frequency. The circuit can be used as an amplifier if the signal power can be recovered from the upper sideband.

In this chapter, the use of ferrites in upper-sideband reactive mixers is studied merely to illustrate the particular way in which this circuit differs from the lower-sideband mixer and to contrast it with the double-sideband mixer. The pumped susceptibility tensor for the upper-sideband mixer will be found. Then it will be shown that dissipation of power in the upper sideband does not cause signal frequency power to be reflected into the input, as is the case for lower-sideband dissipation. The particular way in which this relates to the tensor symmetry and field symmetry is of interest in this comparison. Then the effect of losses on the conversion gain will be computed to show the way in which intrinsic ferrite losses reduce the conversion gain from the ideal as predicted by the Manley-Rowe relations.

4.6.1 The Upper-Sideband Pumped Susceptibility Tensor. There are four important steady state equations of motion for the upper sideband mixer. The optimum pump-field orientation is longitudinal (i.e., along the biasing field) for the upper-sideband converter just the same as for the lower-sideband mixer. The following relations are valid for

longitudinal pumping: $\overline{H}_2 = \overline{H}_{z2}\,\hat{z}$ and $\overline{M}_p = 0$. In this case the equations of motion reduce to:

$$\begin{aligned}
i\omega_u M_{xu} &= -\gamma\left[M_{yu} H_o + M_{y1} H_{z2} - M_o H_{yu}\right] - i\alpha\omega_u M_{yu} \\
i\omega_u M_{yu} &= -\gamma\left[M_o H_{xu} - M_{xu} H_o - M_{x1} H_{z2}\right] - i\alpha\omega_u M_{xu} \\
i\omega_1 M_{x1} &= -\gamma\left[M_{y1} H_o + M_{yu} H_{xp}^* - M_o H_{y1}\right] - i\alpha\omega_1 M_{y1} \\
i\omega_1 M_{y1} &= -\gamma\left[M_o H_{x1} - M_{x1} H_o - M_{xu} H_{zp}^*\right] - i\alpha\omega_1 M_{x1}
\end{aligned} \tag{4.49}$$

These can be written in tensor form:

$$\gamma M_o \begin{bmatrix} H_{x1} \\ H_{y1} \\ H_{xu} \\ H_{yu} \end{bmatrix} = \begin{bmatrix} \gamma H_o + i\alpha\omega_1 & -i\omega_1 & \gamma H_{z2}^* & 0 \\ i\omega_1 & (\gamma H_o + i\alpha\omega_1) & 0 & \gamma H_{z2}^* \\ \gamma H_{z2} & 0 & (\gamma H_o + i\alpha\omega_u) & -i\omega_u \\ 0 & \gamma H_{z2} & i\omega_u & \gamma H_o + i\alpha\omega_u \end{bmatrix} \begin{bmatrix} M_{x1} \\ M_{y1} \\ M_{xu} \\ M_{yu} \end{bmatrix} \tag{4.50}$$

Note in particular that the fields H_1 couple to M_u rather than M_u^* as in the case of the lower-sideband mixer. This fact will be important later in illustrating the difference in the roles of the two sidebands.

Once again the pumped susceptibility can be found by inverting this matrix. This is done in Appendix E where the following symmetry is noted:

$$\begin{aligned}
x_{11} &= x_{22} & x_{33} &= x_{44} \\
x_{12} &= -x_{21} & x_{34} &= -x_{43} \\
x_{13} &= x_{24} & x_{31} &= x_{42} \\
x_{14} &= -x_{23} & x_{32} &= -x_{41}
\end{aligned} \tag{4.51}$$

4.6.2 The Power at the Upper Sideband. Using this symmetry, and assuming linearly polarized field distributions, one can determine the power leaving the sample at the upper sideband:

$$P_{\omega_u} = \frac{\omega_u \mu_o}{2} \left[\text{Im} \int_{v_s} X_{33} \overline{H}_u \cdot \overline{H}_u^* \, dv + \text{Im} \int_{v_s} X_{31} \overline{H}_u^* \cdot \overline{H}_1 \, dv \right.$$

$$\left. + \text{Im} \int X_{32} \overline{H}_u^* \times \overline{H}_1 \cdot z \, dv \right] \tag{4.52}$$

4.6.3 The Power at the Signal Frequency. Similarly, the power leaving the sample at the signal frequency is given by:

$$P_{\omega_1} = \frac{\omega_1 \mu_o}{2} \text{Im} \left[\int X_{11} \overline{H}_1 \cdot \overline{H}_1^* \, dv + \int X_{13} \overline{H}_1^* \cdot \overline{H}_u \, dv \right.$$

$$\left. + \int X_{14} \overline{H}_1^* \times \overline{H}_u \cdot z \, dv \right] \tag{4.53}$$

It is convenient to assume a sample shape such that x_{ij} are independent of position in the sample. It is shown in Appendix E that

$$\text{Im } X_{33} < 0 \tag{4.54}$$

$$\text{Im } X_{33} = X_{33}'' = - \frac{\alpha \omega_u (\omega_o^2 + \omega_u^2)}{(\omega_o^2 - \omega_u^2)^2} \tag{4.55}$$

However, if no power is supplied to the sample at the upper sideband then

$$P_{\omega_u} \geq 0 \tag{4.56}$$

for which

$$- \frac{\alpha \omega_u (\omega_o^2 + \omega_u^2)}{(\omega_o^2 - \omega_u^2)^2} \int \overline{H}_u \cdot \overline{H}_u^* \, dv + \text{Im } X_{31} \int \overline{H}_u^* \cdot \overline{H}_1 \, dv$$

$$+ \text{Im } X_{32} \int \overline{H}_u^* \times \overline{H}_1 \cdot z \, dv \geq 0 \tag{4.57}$$

Thus,

$$\text{Im } X_{31} \int \overline{H}_u^* \cdot \overline{H}_1 \, d\upsilon + \text{Im } X_{32} \int \overline{H}_u^* \times \overline{H}_1 \cdot z \, d\upsilon \geq$$

$$\frac{\alpha \omega_u (\omega_o^2 + \omega_u^2)}{(\omega_o^2 - \omega_u^2)^2} \int \overline{H}_u \cdot \overline{H}_u^* \, d\upsilon > 0 \tag{4.58}$$

If it is assumed that the pump field is real then $\omega_p^* = \omega_p$ and $x_{31} = x_{13}$, $x_{14} = x_{32}$. Note that this imposes no fundamental restriction on any of the following calculations since the pump signal and upper sideband have a unique phase relationship at any operating point. Using this assumption, and the values found for the tensor elements in expression 4.58 yields expression 4.59.

$$\text{Im} \left[- \frac{\omega_p (\omega_o^2 + \omega_u \omega_1) + i\alpha \omega_o (\omega_u + \omega_1)}{(\omega_o^2 - \omega_u^2)(\omega_o^2 - \omega_1^2)} \int \overline{H}_u^* \cdot \overline{H}_1 \, d\upsilon \right.$$

$$\left. + \omega_p \frac{2\alpha \omega_u \omega_1 - i\omega_o (\omega_u + \omega_1)}{(\omega_o^2 - \omega_1^2)(\omega_o^2 - \omega_u^2)} \int \overline{H}_u^* \times \overline{H}_1 \cdot z \, d\upsilon \right] > 0 \tag{4.59}$$

But for low-loss ferrites $\alpha << 1$, so expression 4.59 can be approximated by:

$$- \frac{\omega_p}{(\omega_o^2 - \omega_u^2)(\omega_o^2 - \omega_1^2)} \left[(\omega_o^2 + \omega_u \omega_1) \, \text{Im} \int \overline{H}_u^* \cdot \overline{H}_1 \, d\upsilon \right.$$

$$\left. + \omega_o (\omega_u + \omega_1) \, \text{Re} \int \overline{H}_u^* \times \overline{H}_1 \cdot z \, d\upsilon \right] > 0 \tag{4.60}$$

But

$$\text{Im} \int \overline{H}_u^* \cdot \overline{H}_1 \, d\upsilon = -\text{Im} \int \overline{H}_1^* \cdot \overline{H}_u \, d\upsilon \tag{4.61}$$

and

$$\text{Re} \int \overline{H}_u^* \times \overline{H}_1 \cdot z \, d\upsilon = -\text{Re} \int \overline{H}_1^* \times \overline{H}_u \cdot z \, d\upsilon \tag{4.62}$$

Then:

$$- \frac{\omega_p}{(\omega_o^2 - \omega_u^2)(\omega_o^2 - \omega_1^2)} \left[(\omega_o^2 + \omega_u\omega_1) \operatorname{Im} \int \overline{H}_1^* \cdot \overline{H}_u \, dv \right.$$

$$\left. + \omega_o(\omega_u + \omega_1) \operatorname{Re} \int \overline{H}_1^* \times \overline{H}_u \cdot z \, dv \right] < 0 \qquad (4.63)$$

Using this same set of approximations for the expression for signal power yields

$$P_{\omega_1} = \frac{\omega_1\mu_o}{2} \left\{ - \frac{\alpha\omega_1(\omega_o^2 + \omega_1^2)}{\omega_o^2 - \omega_1^2} \int \overline{H}_1^* \cdot \overline{H}_1 \, dv \right.$$

$$- \frac{\omega_p}{(\omega_o^2 - \omega_u^2)(\omega_o^2 - \omega_1^2)} \left[(\omega_o^2 + \omega_u\omega_1) \operatorname{Im} \int \overline{H}_1^* \cdot \overline{H}_u \, dv \right.$$

$$\left. \left. + \omega_o(\omega_u + \omega_1) \operatorname{Re} \int \overline{H}_1^* \times \overline{H}_u \cdot z \, dv \right] \right\} \qquad (4.64)$$

The first term in Eq. 4.64 is obviously negative; the second and third terms are shown to be negative by Eq. 4.63. Thus,

$$P_{\omega_1} < 0 \qquad (4.65)$$

for all values of H_p. This statement is equivalent to the observation from the equivalent circuit that a positive resistance is reflected into the signal circuit by the upper-sideband mixer. Notice that the sense of the inequality (4.63) was the result of the fact that the signal component H_1 coupled to M_u, rather than to M_u^*.

4.6.4 The Up-Conversion Gain. The upper-sideband mixer does not reflect negative resistance at the signal frequency as does the lower-sideband mixer. However, the Manley-Rowe relations predict a conversion gain from the signal to the upper sideband for a lossless mixer. For this reason it will be of interest to compute the signal and upper-sideband power in the absence of loss, and then consider the effect of losses on conversion gain.

For a lossless ferrite the parameter $\alpha = 0$ and $\operatorname{Im} x_{33} = \operatorname{Im} x_{11} = 0$. From Eqs. 4.52 and 4.53, we find:

$$\frac{P_{\omega_u}}{P_{\omega_1}} = \frac{\omega_u}{\omega_1} \frac{X'_{31}\,\mathrm{Im}\int \bar{H}_u^* \cdot \bar{H}_1\,d\upsilon + X''_{14}\,\mathrm{Re}\int \bar{H}_u^* \times \bar{H}_1 \cdot z\,d\upsilon}{X'_{13}\,\mathrm{Im}\int \bar{H}_1^* \cdot \bar{H}_u\,d\upsilon + X''_{32}\,\mathrm{Re}\int \bar{H}_1^* \times \bar{H}_u \cdot z\,d\upsilon} \tag{4.66}$$

where it has been assumed that H_p is real. But $X'_{31} = -X'_{13}$ and for the lossless case $X''_{14} = X''_{32} = 0$. Thus, for a lossless ferrite reactive mixer we have:

$$\frac{P_{\omega_u}}{P_{\omega_1}} = -\frac{\omega_u}{\omega_1} \tag{4.67}$$

which is the appropriate statement of the Manley-Rowe relations for upper-sideband reactive mixers (Ref. 28).

4.6.5 The Effect of Sample Losses on Conversion Gain. For lossy ferrites the conversion gain is given by:

$$\frac{P_{\omega_u}}{P_{\omega_1}} = -\frac{\omega_u}{\omega_1} \frac{X_{31}\,\mathrm{Im}\int \bar{H}_u^* \cdot \bar{H}_1\,d\upsilon + X''_{14}\,\mathrm{Re}\int \bar{H}_u^* \times \bar{H}_1 \cdot z\,d\upsilon + X''_{33}\int |H_u|^2\,d\upsilon}{X_{31}\,\mathrm{Im}\int \bar{H}_u^* \cdot \bar{H}_1\,d\upsilon + X''_{32}\,\mathrm{Re}\int \bar{H}_u^* \times \bar{H}_1 \cdot z\,d\upsilon - X''_{11}\int |H_1|^2\,d\upsilon} \tag{4.68}$$

It has already been shown that:

$$X'_{31}\,\mathrm{Im}\int \bar{H}_u^* \cdot \bar{H}_1\,d\upsilon + X''_{14}\,\mathrm{Re}\int \bar{H}_u^* \times \bar{H}_1 \cdot z\,d\upsilon > -X'_{33}\int |H_u|^2\,d\upsilon \tag{4.69}$$

and since X''_{11} and X''_{33} are both negative the numerator is smaller than for lossless ferrites and the denominator is larger. Thus

$$\frac{P_{\omega_u}}{P_{\omega_1}} \leq -\frac{\omega_u}{\omega_1} \tag{4.70}$$

which fact is already known about upper-sideband reactive mixers (Ref. 28). That is, the effect of losses is to lower the conversion gain of upper-sideband reactive mixers from that predicted by the Manley-Rowe relation.

The upper-sideband up-converter can be used as an amplifier at the signal frequency provided the power in the upper sideband can be down-converted. However, down-

conversion cannot be accomplished with a reactive mixer because the down-conversion loss is the same as the up-conversion gain and no net gain would result at the signal frequency. On the other hand, if the local oscillator power is added to the upper sideband, then an ordinary resistive diode can accomplish the down-conversion. The down-conversion loss for this case will be greater than 6 db, so up-conversion gain must be relatively large for net signal frequency gain.

Certain observations can be made about the coupling in ferrites which is responsible for up-conversion gain. For certain field distributions the integrals

$$\int \overline{H}_u{}^* \cdot \overline{H}_1 \, dv$$

and

$$\int \overline{H}_u{}^* \times \overline{H}_1 \, dv$$

can be zero, and there is then no coupling and of course no up-conversion gain. However, for the case in which the field distributions are nonorthogonal, the conversion gain is less than that predicted by the Manley-Rowe relations primarily due to losses rather than coupling.

4.7 Summary

In this chapter the reactive mixing properties of a sample excited by two r-f sources were investigated. The steady-state solution to the equation of motion for this excitation was determined and represented in a matrix equation which defines the pumped susceptibility tensor. It was shown that power flow and power conversion are determined by the components of this tensor and by the field distribution in the sample at the frequencies where real power flows. This general theory was applied to two specific cases in which the power flow was restricted by filters to only three frequencies. In the first case the three frequencies included the two r-f sources and the lower sideband, while in the second they included the sources and the upper sideband. The lower-sideband reactive mixer is the familiar parametric amplifier configuration for which the unity gain threshold pump power was derived. The field distributions for minimum threshold were obtained by a variational technique and an estimate of this minimum threshold power was found. The conversion gain,

and the effect of losses upon this gain, were found for the upper sideband circuit. The significance of the study of these two reactive mixers is the groundwork which it lays for the double-sideband reactive mixer, i. e., the phase-shift amplifier.

CHAPTER 5

THE FERRITE PHASE-SHIFT AMPLIFIER

5. 1 Introduction

It has been demonstrated that a signal can be amplified with an upper-sideband up-converter whose upper-sideband power is converted back to signal frequency power. To obtain gain, it is necessary only that the up-conversion gain be greater than down-conversion loss. A natural extension of this idea is the use of the double-sideband up-converter as an amplifier. In this case, the power in both sidebands is converted to signal frequency power. This technique of up-converting to both sidebands and then down-converting was discussed in Chapter 2 and given the name phase-shift amplification. The purpose of the remainder of this paper is to consider the application of ferrites to this type of amplification. In this chapter, the limitations imposed upon the circuit by the ferrite properties will be investigated.

It was shown in Section 2. 5 that phase-shift amplifiers can be divided into two distinct classes depending upon the passband of the signal. If the center frequency of the signal band is high, the sidebands can be separated from the pump by means of filters and the circuit properties can be predicted from the properties of the single-sideband circuits. However, when the center frequency of the signal band is low, the sidebands are too close to the pump to be separated effectively from it, so that both sidebands tend to be loaded by the conductance of the pump filter. Adams has used the term dependent loading to describe this circumstance. The discussion of the remainder of the paper will be restricted to such amplifiers.

In this chapter, the limitations imposed upon phase-shift amplification by the physical properties of ferrites are discussed. In Section 5. 2, the pumped susceptibility tensor is derived in a way which determines the orientation of the field quantities for maximum gain. It is then shown that the optimum field orientation implies a simplified analysis of the

amplifier in which the ferrite properties are represented by the quantity which is called tunability. The tunability for three distinct configurations are considered: 1) magnetically saturated bulk ferrite; 2) magnetically unsaturated ferrite material; 3) thin-film ferromagnetic samples. Fundamental limits on tunability for these three configurations are determined, and the maximum expected tunabilities are determined for each and compared.

5. 2 The Double-Sideband Pumped Susceptibility Tensor

Although the ferrite phase-shift amplifier is properly represented by a pumped susceptibility tensor together with the components of magnetization and magnetic field at the four frequencies, analysis of the amplifier tends to involve unwieldy calculations due to the large number of components. However, coupling between a pair of fields in ferrites depends upon their relative orientation, so that there is some orientation for which that coupling is a maximum. For these specific orientations, the fields can be expressed in terms of their magnitudes and orientations relative to some reference, such as the direction of the biasing magnetic field. A considerable reduction results in the complexity of the analysis. In particular, if it is assumed that the fields are oriented for maximum coupling, then the amplifier can be represented by the field amplitudes and distributions only, which significantly simplifies the amplifier analysis. The field orientation for maximum coupling can be found from the pumped susceptibility tensor. Thus, the determination of this tensor is the first step in the analysis of the ferrite phase-shift amplifier.

The pumped susceptibility tensor is found by inverting the matrix of the equation (5. 1):

$$i\omega_u M_{x_u} = -\gamma \left[M_{y_u} H_o + M_{y_1} H_{z_2} - M_o H_{y_u} + M_{y_2} H_{z_1} \right] - i\alpha \omega_u M_{y_u}$$

$$i\omega_u M_{y_u} = -\gamma \left[M_o H_{x_u} - M_{x_u} H_o - M_{x_2} H_{z_1} - M_{x_1} H_{z_2} \right] + i\alpha \omega_u M_{x_u}$$

$$i\omega_\ell M_{x_\ell} = -\gamma \left[M_{y_\ell} H_o + M^*_{y_1} H_{z_2} + M_{y_2} H^*_{z_1} - M_o H_{y_\ell} \right] - i\alpha \omega_\ell M_{y_\ell}$$

$$i\omega_\ell M_{y_\ell} = -\gamma \left[M_o H_{x_\ell} - M_{x_\ell} H_o - M_{x_2} H^*_{z_1} - M^*_{x_1} H_{z_2} \right] + i\alpha \omega_\ell M_{x_\ell}$$

$$
\begin{aligned}
i\omega_2 M_{x_2} &= -\gamma\left[M_{y_2} H_o + M_{y_\ell} H_{z_1} + M_{y_u} H_{z_1} - M_o H_{y_2}\right] - i\alpha\omega_2 M_{y_2} \\
i\omega_2 M_{y_2} &= -\gamma\left[M_o H_{x_2} - M_{x_2} H_o - M_{x_\ell} H_{z_1} - M_{x_u} H^*_{z_1}\right] + i\alpha\omega_2 M_{x_2} \\
i\omega_1 M_{x_1} &= -\gamma\left[M_{y_1} H_o + M^*_{y_\ell} H_{z_2} + M_{y_u} H^*_{z_2} - M_o H_{y_1}\right] - i\alpha\omega_1 M_{y_1} \\
i\omega_1 M_{y_1} &= -\gamma\left[M_o H_{x_1} - M_{x_1} H_o - M^*_{x_\ell} H_{z_2} - M_{x_u} H^*_{z_2}\right] + i\alpha\omega_1 M_{x_1}
\end{aligned}
\qquad (5.1)
$$

5.2.1 The Pumped Tensor for Circularly Polarized Fields. The magnetization components at the upper- and lower-sideband frequencies are a measure of the conversion gain. An examination of these components reveals that coupling takes place between longitudinal components of magnetic field and transverse components of magnetization. It is useful to consider the set of components which tend to maximize the magnetization at the upper and lower sidebands. It is then possible to determine the relative orientations of the signal and pump fields which produce the maximum sideband power. Though this can be accomplished by inverting the matrix of the set of equations (5.1), the work involved is rather formidable. Fortunately, no essential information is lost if it is assumed that the transverse field components are circularly polarized. In fact, circularly polarized fields were used in many of the experiments which were performed in this study on the double-sideband reactive mixer. For such fields, the equations of motion are reduced to four in number:

$$
\begin{aligned}
\omega_u M_u^{\pm} &= \mp\gamma H_o M_u^{\pm} \pm \gamma M_o H_u^{\pm} \pm \gamma H_{z_1} M_2^{\pm} \pm \gamma H_{z_2} M_1^{\pm} \pm i\alpha\omega_u M_u^{\pm} \\
\omega_\ell M_\ell^{\pm} &= \mp\gamma H_o M_\ell^{\pm} \pm \gamma M_o H_\ell^{\pm} \pm \gamma H_{z_2} (M_1^{\pm})^* \pm \gamma H^*_{z_1} (M_2^{\pm}) \pm i\alpha\omega_\ell M_\ell^{\pm} \\
\omega_2 M_2^{\pm} &= \mp\gamma H_o M_2^{\pm} \pm \gamma M_o H_2^{\pm} \pm \gamma H_{z_1} M_\ell^{\pm} \pm \gamma H^*_{z_1} M_u^{\pm} \pm i\alpha\omega_2 M_2^{\pm} \\
\omega_1 M_1^{\pm} &= \mp\gamma H_o M_1^{\pm} \pm \gamma M_o H_1^{\pm} \pm \gamma H_{z_2} (M_\ell^{\pm})^* \pm \gamma H^*_{z_2} M_u^{\pm} \pm i\alpha\omega_1 M_1^{\pm}
\end{aligned}
\qquad (5.2)
$$

In principle, the inverse of the matrix of these equations could be found. It could properly be called the circularly polarized, pumped susceptibility tensor. However, the above matrix

is not square and no mathematical technique is known for inverting a nonsquare matrix. On the other hand, because coupling tends to take place between axial field components and transverse magnetization components there are two extreme cases which can be considered for which the matrix of the above equations is square. The matrix will be inverted for these two special cases and from these it can be determined which field orientations tend to give rise to maximum power conversion. The two special cases are:

(1) the signal field H_1 axial and the pump field H_2 totally transverse and circularly polarized;

(2) the pump field axial and the signal field totally transverse and circularly polarized. (It will be shown later that, because of its nonresonant characteristic, the left hand polarization H^- is not of interest.)

5.2.2 The Pumped Tensor for Case (1). The pumped susceptibility $\bar{\bar{x}}^+$ can be found for Case 1 above by inverting the matrix of the following set of equations:

$$\begin{aligned}
(\omega_u - \gamma H_o - i\alpha\omega_u) M_u^+ &= -\gamma M_o H_u^+ + \gamma H_{z_1} M_2^+ \\
(\omega_\ell - \gamma H_o - i\alpha\omega_\ell) M_\ell^+ &= -\gamma M_o H_\ell^+ + \gamma H_{z_1}^* M_2^+ \\
(\omega_2 - \gamma H_o - i\alpha\omega_2) M_2^+ &= -\gamma M_o H_2^+ + \gamma H_{z_1} M_\ell^+ + \gamma H_{z_1}^* M_u^+
\end{aligned} \tag{5.3}$$

or in matrix form

$$-\gamma M_o \begin{bmatrix} H_\ell^+ \\ H_2^+ \\ H_u^+ \end{bmatrix} = \begin{bmatrix} \omega_\ell(1-i\alpha) - \gamma H_o & \gamma H_{z_1}^* & 0 \\ \gamma H_{z_1} & \omega_2(1-i\alpha) - \gamma H_o & \gamma H_{z_1}^* \\ 0 & 0 & \omega_u(1-i\alpha) - \gamma H_o \end{bmatrix} \begin{bmatrix} M_\ell^+ \\ M_2^+ \\ M_u^+ \end{bmatrix} \tag{5.4}$$

For a small-signal analysis, the tensor need only be evaluated to first order in γH_1. Thus, the determinant D is given by:

$$D = \left[\omega_\ell(1-i\alpha) - \gamma H_o\right]\left[\omega_2(1-i\alpha) - \gamma H_o\right]\left[\omega_u(1-i\alpha) - \gamma H_o\right] \tag{5.5}$$

Using Eq. 5. 5, we can find the susceptibility components:

$$x_{11} = \frac{\gamma M_o}{\gamma H_o - \omega_\ell(1- i\alpha)} \qquad x_{12} = \frac{\gamma^2 M_o H^*_{z_1}}{\left[\gamma H_o - \omega_\ell(1- i\alpha)\right]\left[\gamma H_o - \omega_2(1- i\alpha)\right]} \qquad x_{13} = 0$$

$$x_{21} = \frac{\gamma^2 M_o H_{z_1}}{\left[\gamma H_o - \omega_\ell(1- i\alpha)\right]\left[\gamma H_o - \omega_2(1- i\alpha)\right]} \qquad x_{22} = \frac{\gamma M_o}{\gamma H_o - \omega_2(1- i\alpha)}$$

$$x_{23} = \frac{\gamma^2 M_o H^*_{z_1}}{\left[\gamma H_o - \omega_2(1- i\alpha)\right]\left[\gamma H_o - \omega_u(1- i\alpha)\right]} \tag{5.6}$$

$$x_{31} = 0 \qquad x_{32} = \frac{\gamma^2 M_o H_{z_1}}{\left[\gamma H_o - \omega_2(1- i\alpha)\right]\left[\gamma H_o - \omega_u(1- i\alpha)\right]} \qquad x_{33} = \frac{\gamma M_o}{\gamma H_o - \omega_u(1- i\alpha)}$$

The magnetization at the upper sideband frequency can be found from these tensor elements:

$$M_u^+ = -\frac{\gamma M_o H_u^+}{\gamma H_o - \omega_u(1- i\alpha)} - \frac{\gamma^2 M_o H_{z_1} H_2^+}{\left[\gamma H_o - \omega_2(1- i\alpha)\right]\left[\gamma H_o - \omega_o(1- i\alpha)\right]} \tag{5.7}$$

The upper-sideband power will tend to be largest when the second term is largest and for this reason we will compare it with the corresponding term for Case 2.

5. 2. 3 The Pumped Tensor for Case (2). For Case 2, the set of equations to be inverted is given by (5. 8):

$$\begin{aligned}
(\omega_u - \gamma H_o - i\alpha\omega_u) M_u^+ &= -\gamma M_o H_u^+ + \gamma H_{z_2} M_1^+ \\
(\omega_\ell - \gamma H_o - i\alpha\omega_\ell) M_\ell^+ &= -\gamma M_o H_\ell^+ + \gamma H_{z_2} (M_1^+)^* \\
(\omega_1 - \gamma H_o - i\alpha\omega_1) M_1^+ &= -\gamma M_o H_1^+ + \gamma H_{z_2} (M_\ell^+)^* + \gamma H^*_{z_2} (M_u^+)
\end{aligned} \tag{5.8}$$

Note that H_1^+ tends to couple to $(M_\ell^+)^*$ (which, incidentally, is not necessarily equal to M_ℓ^- unless $M_x = M_x^*$ etc.). For this reason, it will be convenient to replace the second of equations 5.8 with its complex conjugate. The resulting matrix to be inverted is:

$$-\gamma M_o \begin{bmatrix} (H_\ell^+)^* \\ H_1^+ \\ H_u^+ \end{bmatrix} = \begin{bmatrix} \omega_\ell - \gamma H_o + i\alpha\omega_\ell & \gamma H_{z_2}^* & 0 \\ \gamma H_{z_2} & \omega_1(1-i\alpha) - \gamma H_o & \gamma H_{z_2}^* \\ 0 & \gamma H_{z_2} & \omega_u(1-i\alpha) - \gamma H_o \end{bmatrix} \begin{bmatrix} (M_\ell^+)^* \\ M_1^+ \\ M_u^+ \end{bmatrix} \tag{5.9}$$

The determinant D is:

$$D = \left[\omega_\ell(1+i\alpha) - \gamma H_o\right]\left[\omega_1(1-i\alpha) - \gamma H_o\right]\left[\omega_u(1-i\alpha) - \gamma H_o\right] \tag{5.10}$$

The components of the pumped susceptibility tensor are:

$$x_{11} = \frac{\gamma M_o}{\gamma H_o - \omega_\ell(1+i\alpha)} \qquad x_{12} = \frac{\gamma^2 M_o H_{z_2}}{\left[\gamma H_o - \omega_\ell(1+i\alpha)\right]\left[\gamma H_o - \omega_1(1-i\alpha)\right]} \qquad x_{13} = 0$$

$$x_{21} = \frac{\gamma^2 M_o H_{z_2}}{\left[\gamma H_o - \omega_\ell(1+i\alpha)\right]\left[\gamma H_o - \omega_1(1-i\alpha)\right]} \qquad x_{12} = \frac{\gamma M_o}{\gamma H_o - \omega_1(1-i\alpha)}$$

$$x_{23} = \frac{\gamma^2 M_o H_{z_2}}{\left[\gamma H_o - \omega_1(1-i\alpha)\right]\left[\gamma H_o - \omega_u(1-i\alpha)\right]} \tag{5.11}$$

$$x_{31} = 0 \qquad x_{32} = \frac{\gamma^2 M_o H_{z_2}}{\left[\gamma H_o - \omega_1(1-i\alpha)\right]\left[\gamma H_o - \omega_u(1-i\alpha)\right]} \qquad x_{33} = \frac{\gamma M_o}{\gamma H_o - \omega_u(1-i\alpha)}$$

The magnetization component at the upper sideband is given by:

$$M_u^+ = -\frac{\gamma M_o H_u^+}{\gamma H_o - \omega_u(1-i\alpha)} - \frac{\gamma^2 M_o H_{z_2} H_1^+}{\gamma H_o - \omega_1(1-i\alpha)\quad \gamma H_o - \omega_u(1-i\alpha)} \tag{5.12}$$

5.2.4 The Optimum Field Orientation. The most meaningful comparison between the two cases is the comparison of the second term on the right of Eqs. 5.7 and 5.12 under the condition that the field intensities $|H_1|$ and $|H_2|$ are the same. It would appear by comparison of the two terms under this condition that by properly selecting H_o (i.e., ferromagnetic resonance) either term could be made the larger. However, there is a physical restriction to the lower limit at which ferromagnetic resonance occurs. It is not ordinarily observed much below 1 Gc (Ref. 29). For this reason it is not possible to make $\gamma H_o - \omega_1$ arbitrarily small in all cases. In particular, if the signal pass band has a low pass characteristic (e.g., dc up to 100 Mc), then the frequency difference $\gamma H_o - \omega_1$ may be quite large. On the other hand, the pump frequency is ordinarily selected in the microwave spectrum where ferromagnetic resonance is a pronounced phenomenon and where $\gamma H_o - \omega_2$ can be made quite small. From this it can be concluded that for those circuits in which the signal spectrum is lowpass, Case 1 is optimum when ferromagnetic resonance is near to the pump frequency. In summary, then, it has been shown that the optimum sideband conversion takes place between H_{z_1} and M_{p_2}. Any transverse component of signal and longitudinal component of pump will contribute negligibly to sideband power, yet will increase the stored energy and dissipated power at their frequencies and must be considered undesirable. Thus, the optimum field orientation consists of axial signal field components and transverse pump components. It should be recalled that the physical significance of this orientation is that it maximizes coupling between the fields at the two frequencies.

In addition, this orientation is significant because it suggests a means of synthesizing the prototype model for the phase-shift amplifier which was presented in Chapter 2 (see Fig. 2-1). That prototype is repeated for convenience in Fig. 5-1. Because it is parallel to the biasing field the signal field can be regarded as a time-varying component of that field. But the instantaneous biasing field determines the permeability at the pump frequency, so the effect of the signal field is to cause the permeability to vary at the signal

frequency. If the sample is part of an energy storage element, and if the latter is part of a tuned circuit as shown in the figure, then the resonant frequency of that circuit varies at the signal frequency. Synthesis of the prototype model of the phase-shift amplifier is accomplished by placing this time-varying resonant circuit between the pump source and a phase detector.

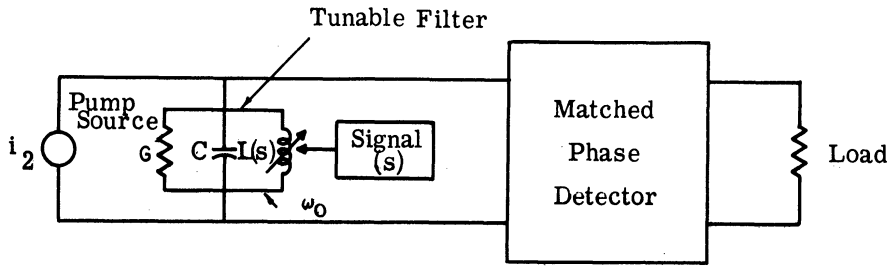

Fig. 5-1. Prototype ferrite phase-shift amplifier.

Adams has shown that the gain bandwidth product for a phase-shift amplifier tends to be an increasing function of pump frequency (Ref. 30). For this reason, and because ferrites tend to be nonlinear at microwave frequencies, it will be assumed that the pump frequency is in the microwave spectrum. A microwave cavity provides a convenient resonant circuit. Thus the prototype model for a ferrite phase-shift amplifier consists of a microwave cavity which contains the ferrite sample and which is placed between a source and a matched phase detector. The sample is biased normal to the direction of the pump magnetic field and the signal field is applied parallel to the biasing field.

5.3 Amplifier Analysis Based Upon Tunability

It was shown in Chapter 2 that the transducer gain for the prototype circuit of Fig. 5-1 is given by:

$$G_t = \frac{2\zeta P_p}{R_s} (2Q_\ell T_i)^2 \qquad (5.13)$$

where the tunability T_i was defined

$$T_i = \frac{1}{\omega_o} \frac{d\omega_o}{di_s}$$

As stated in the introduction, this quantity depends markedly upon the material parameters. The purpose of this chapter is to illustrate this dependence. However, for this purpose it is convenient to define a slightly different tunability:

$$T = \frac{1}{\omega_o} \frac{d\omega_o}{dh}$$

where h is the magnetic field* in the sample at some specified point (e. g., sample center). If this field is produced by the signal frequency current, then T is related simply to T_i:

$$T_i = \frac{dh}{di_s} T$$

This definition has the advantage that it tends to separate that part of the tunability T_i which is determined by the material parameters (i. e., T) from that which is determined by the signal frequency circuit (i. e., $\frac{dh}{di_s}$). However, it should be emphasized that, although it is convenient to study these quantities separately, optimization of G_t requires optimization of T_i.

Since the signal frequency circuit is linear, we can write

$$\frac{dh}{di_s} = \frac{h}{i_s}$$

and this quantity can be determined with respect to the signal frequency field distribution. For this purpose, we define the signal magnetic field $\overline{H}(\overline{r})$ by the relation:

$$\overline{H}(\overline{r}) = h\,\overline{f}(\overline{r})$$

where $\overline{f}(\overline{r}) = 1$ at the specified point where the tunability is measured. But if the signal-frequency current produces $\overline{H}$ it must flow through an inductance L (see Fig. 5-2) and from the magnetic energy relation we know:

---

*Magnetic field at the signal frequency.

$$\frac{1}{2} L i_s^2 = \frac{h^2}{2} \int_{\text{space}} \mu |f(\bar{r})|^2 \, du$$

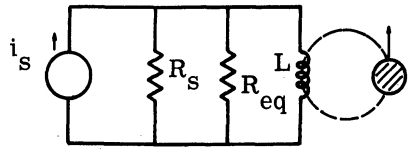

Fig. 5-2. Equivalent signal frequency circuit illustrating coupling between the signal field and the sample R_{eq} is the equivalent shunt conductance of the signal coil.

from which it can be deduced that:

$$\frac{h}{i_s} = \frac{L}{\int \mu |f|^2 \, du} \tag{5.14}$$

Using the definition of T and the above relation the transducer gain can be written in the form:

$$G_t = \frac{2 \zeta P_p L}{R_s \int \mu |f|^2 \, du} (Q_\ell \, T)^2$$

Thus, the observation that the optimum field orientation enables a convenient synthesis of the prototype ferrite phase-shift amplifier has reduced the analysis of the amplifier from a complicated set of calculations involving the pumped susceptibility tensor for the double-sideband reactive mixer to the above expression for transducer gain.

Although G_t is a simple function of T, it is a complicated function of the material type and configuration. Of all the parameters in G_t, only ζ and P_p are independent of the material. On the other hand, if the material losses are small relative to the cavity losses, then Q_ℓ tends to be independent of material. The parameter which depends most strongly on material is T' where

$$T' = \frac{T}{\left(\int \mu |f|^2 \, dv\right)^{\frac{1}{2}}}$$

Optimization of G_t necessarily involves optimization of T' with respect to sample shape, size, orientation and material type. The optimization of a variety of amplifier configurations is considered in the next chapter. However, before this can be accomplished the dependence of T upon the sample parameters must be known. The remainder of this chapter is devoted to a study of this dependence.

5.4 Dependence of Tunability upon Sample Parameters

The tunability T for the prototype ferrite phase-shift amplifier has been defined:

$$T = \frac{1}{\omega_o} \frac{d\omega_o}{dh} = \frac{1}{\omega_o} \frac{d\omega_o}{dH_o}$$

where ω_o is the cavity resonant frequency and H_o is the biasing field.* Aside from its simplicity this definition is advantageous because it is independent of whether or not the sample is magnetically saturated. This means that the phase-shift amplifier, unlike the single-sideband mixer circuits, can be mathematically studied for unsaturated samples. To be practically useful for studying phase-shift amplifiers, the tunability must be related to material parameters. The following section, in which this relationship is derived, is an extension of the ordinary cavity perturbation technique. The extension is convenient since the perturbation technique can be used to compute the frequency perturbation of the cavity resonant frequency from its empty-cavity value (Ref. 31). This is more information than is needed, since only the variation in loaded-cavity resonant frequency due to variation in the biasing field need be known to compute tunability. The precision to which the field distributions must be known for a good approximation to $\frac{\partial \omega_o}{\partial H}$ is not nearly as severe in the latter case. Perhaps more importantly, the validity of the approximation proves to be independent of the sample size in the latter case.

The tunability is computed in the following way. The steady biasing field H_{o_1} is applied to the sample for which the sample permeability is $\bar{\bar{\mu}}_1$ and the cavity is resonant at

*Note signal field parallel to biasing field.

ω_1. The fields in the cavity at this resonant frequency are $\overline{E}_1$ and $\overline{H}_1$. If the biasing field is changed to H_{o_2} then the permeability is changed to $\overline{\overline{\mu}}_2$, the fields change to $\overline{E}_2$ and $\overline{H}_2$ and the resonant frequency to ω_2. At all times these fields must satisfy Maxwell's equations:

$$\begin{aligned} \nabla \times \overline{E}_1 &= -i\omega_1 \overline{\overline{\mu}}_1 \cdot \overline{H}_1 \\ \nabla \times \overline{H}_1 &= i\omega_1 \overline{\overline{\epsilon}}_1 \cdot \overline{E}_1 \\ \nabla \times \overline{E}_2 &= -i\omega_2 \overline{\overline{\mu}}_2 \cdot \overline{H}_2 \\ \nabla \times \overline{H}_2 &= i\omega_1 \overline{\overline{\epsilon}}_2 \cdot \overline{E}_1 \end{aligned} \tag{5.16}$$

For most ferrites the conductivity is extremely small and the permittivity may be regarded as a scalar ϵ which is independent of H_o. Consider the quadratic relation:

$$\begin{aligned} \nabla \cdot (\overline{E}_1^* \times \overline{H}_2 + \overline{E}_2 \times \overline{H}_1^*) &= \overline{H}_2 \cdot \nabla \times \overline{E}_1^* + \overline{E}_1^* \cdot \nabla \times \overline{H}_2 \\ &\quad + \overline{H}_1^* \cdot \nabla \times \overline{E}_2 + \overline{E}_2 \cdot \nabla \times \overline{H}_1 \end{aligned} \tag{5.17}$$

But from Maxwell's equations this can be written

$$\begin{aligned} \nabla \cdot (\overline{E}_1^* \times \overline{H}_2 + \overline{E}_2 \times \overline{H}_1^*) &= i\omega_1 \overline{H}_2 \cdot (\overline{\overline{\mu}}_1 \cdot \overline{H}_1^*) - i\omega_2 H_1^* \cdot (\overline{\overline{\mu}}_2 \cdot \overline{H}_2) \\ &\quad - i(\omega_1 - \omega_2)\, \epsilon\, \overline{E}_1^* \cdot \overline{E}_2 \end{aligned} \tag{5.18}$$

Then both sides of the equation can be integrated over the cavity volume and Gauss' law applied:

$$\int_V \nabla \cdot (\overline{E}_1^* \times \overline{H}_2 + \overline{E}_2 \times \overline{H}_1^*)\, dv = \int_S (\overline{E}_1^* \times \overline{H}_2 + \overline{E}_2 \times \overline{H}_1^*) \cdot n\, ds$$

$$= i \int_{V_c} \left[\omega_1 \overline{H}_2 \cdot (\overline{\overline{\mu}}_1 \cdot \overline{H}_1)^* - \omega_2 H_1^* \cdot (\overline{\overline{\mu}}_2 \cdot \overline{H}_2) - (\omega_1 - \omega_2)\, \epsilon\, \overline{E}_1^* \cdot E_2 \right] dv \tag{5.19}$$

But the boundary conditions at the cavity wall are

$$\overline{E} \times n = 0 \qquad \text{so} \qquad \overline{E}_1 \times \overline{H}_2 \cdot n = 0$$

where n is a unit normal vector at the cavity wall. Thus we obtain:

$$\omega_1 \int_{V_c} \overline{H}_2 \cdot (\bar{\bar{\mu}}_1 \cdot \overline{H}_1)^* \, dv - \omega_2 \int_{V_c} \overline{H}_1^* \cdot (\bar{\bar{\mu}}_2 \cdot \overline{H}_2) \, dv - (\omega_1 - \omega_2) \epsilon \int_{V_c} \overline{E}_1^* \cdot \overline{E}_2 \, dv = 0 \tag{5.20}$$

Since we are only interested in $\frac{\partial \omega_o}{\partial H}$, it will be convenient to let

$$\overline{H}_{o_2} = \overline{H}_{o_1} + \delta H_o$$

then

$$\bar{\bar{\mu}}_2 = \bar{\bar{\mu}}_1 + \delta \bar{\bar{\mu}}$$

$$\omega_2 = \omega_1 + \delta \omega$$

$$\overline{E}_2 = \overline{E}_1 + \delta \overline{E}_1$$

$$\overline{H}_2 = \overline{H}_1 + \delta \overline{H} \quad .$$

If these quantities are substituted in (5.20) there results:

$$\int_{V_c} dv \quad \omega_1(\overline{H}_1 + \delta\overline{H}) \cdot (\bar{\bar{\mu}}_1 \cdot \overline{H}_1)^* - (\omega_1 + \delta\omega) H_1^* \cdot (\bar{\bar{\mu}}_1 + \delta\bar{\bar{\mu}}) \cdot (\overline{H}_1 + \delta\overline{H})$$

$$+ \delta\omega \epsilon \overline{E}_1^* \cdot (\overline{E}_1 + \delta\overline{E}) \quad = 0 \tag{5.21}$$

This can be rewritten, correct to first order, as:

$$-\delta\omega \int_{V_c} \epsilon \overline{E}_1^* \cdot \overline{E}_1 + \overline{H}_1^* \cdot \bar{\bar{\mu}}_1 \cdot \overline{H}_1 \, dv = \omega_1 \int_{V_c} \overline{H}_1 \cdot (\bar{\bar{\mu}}_1 \cdot \overline{H}_1)^* - \overline{H}_1^* \cdot (\bar{\bar{\mu}}_1 \cdot \overline{H}_1) \, dv$$

$$+ \omega_1 \int_{V_c} \overline{H}_1^* \cdot \delta\bar{\bar{\mu}}_1 \cdot \overline{H}_1 + \delta\overline{H} \cdot (\bar{\bar{\mu}}_1 \cdot \overline{H}_1)^* - \overline{H}_1^* \cdot (\bar{\bar{\mu}}_1 \cdot \delta\overline{H}) \, dv \tag{5.22}$$

Upon close examination of (5.22), it is clear that this can be reduced. Notice that:

$$H_1 \cdot (\bar{\bar{\mu}}_1 \cdot \overline{H}_1)^* = H_1^* \cdot (\bar{\bar{\mu}}_1 \cdot H_1)^*$$

so

$$\overline{H}_1 \cdot (\bar{\bar{\mu}}_1 \cdot \overline{H}_1)^* - H_1^* \cdot (\bar{\mu}_1 \cdot \overline{H}_1) = 2 \, i \, \mathrm{Im} \, \overline{H}_1 \cdot (\bar{\bar{\mu}}_1 \cdot \overline{H}_1)^* \tag{5.23}$$

This can be reduced even further using the symmetry of tensor permeability. For any non-zero biasing field the tensor permeability will have the general form:

$$\bar{\bar{\mu}} = \begin{bmatrix} \mu_{11} & -i\,\mu_{12} & 0 \\ i\,\mu_{12} & \mu_{11} & 0 \\ 0 & 0 & \mu_z \end{bmatrix}$$

LeCraw and Spencer have shown that a ferrite must have this symmetry regardless of whether or not it is magnetically saturated (Ref. 32). Then using tensor notation, $\bar{H}_1 \cdot (\bar{\bar{\mu}} \cdot \bar{H}_1)^*$ can be evaluated:

$$\begin{bmatrix} H_{1x} \\ H_{1y} \\ H_{1z} \end{bmatrix} \cdot \begin{bmatrix} \mu_{11}^* & i\,\mu_{12}^* & 0 \\ -i\,\mu_{12}^* & \mu_{11}^* & 0 \\ 0 & 0 & \mu_z^* \end{bmatrix} \cdot \begin{bmatrix} H_{1x}^* \\ H_{1y}^* \\ H_{1z}^* \end{bmatrix} \tag{5.24}$$

$$= \begin{bmatrix} H_{1x} \\ H_{1y} \\ H_{1z} \end{bmatrix} \cdot \begin{bmatrix} \mu_{11}^* H_{1x}^* + i\,\mu_{12}^* H_{1y}^* \\ -i\,\mu_{12}^* H_{1x}^* + \mu_{11}^* H_{1y}^* \\ \mu_z H_{1z}^* \end{bmatrix}$$

$$= \mu_{11}^* H_{1x} H_{1x}^* + i\,\mu_{12}^* H_{1x} H_{1y}^* - i\,\mu_{12}^* H_{1y} H_{1x}^* + \mu_{11}^* H_{1y}^* H_{1y} + \mu_z H_{1z} H_{1z}^*$$

$$= \mu_{11}^* \bar{H}_{1t} \cdot \bar{H}_{1t}^* + i\,\mu_{12}^* \bar{H}_1 \times \bar{H}_1^* \cdot \hat{z} + \mu_z^* H_{1z} H_{1z}^*$$

Two special cases of polarization will occur in most normal applications, these being linear polarization for which $\bar{H}_1 \times \bar{H}_1^* = 0$, and circular polarization for which $\mu_{12} = 0$. Thus (5.24) reduces even further to

$$\mu_{11}^* \bar{H}_{1t} \cdot \bar{H}_{1t}^* + \mu_z^* H_{1z} H_{1z}^*$$

For most ferrites at frequencies of interest $\mathrm{Im}\ \mu_z \cong 0$ so

$$\mathrm{Im}\ \mu_{11} \bar{H}_{1t} \cdot \bar{H}_{1t}^* + \mu_z H_{1z} H_{1z}^* = \mu_{11}'' |H_{1t}|^2 \tag{5.25}$$

We next examine more closely the last term in Eq. 5.22, i.e., $\delta H \cdot (\bar{\bar{\mu}}_1 \cdot \bar{H}_1)^* - H_1^* \cdot (\bar{\bar{\mu}}_1 \cdot \delta\bar{H})$

$$\delta\bar{H} \cdot (\bar{\bar{\mu}}_1 \cdot \bar{H}_1)^* = \begin{bmatrix} \delta H_x \\ \delta H_y \\ \delta H_z \end{bmatrix} \cdot \begin{bmatrix} \mu_{11}^* & i\mu_{12}^* & 0 \\ -i\mu_{12}^* & \mu_{11}^* & 0 \\ 0 & 0 & \mu_z^* \end{bmatrix} \cdot \begin{bmatrix} H_{1x}^* \\ H_{1y}^* \\ H_{1z}^* \end{bmatrix}$$

$$= \begin{bmatrix} \delta H_x \\ \delta H_y \\ \delta H_z \end{bmatrix} \cdot \begin{bmatrix} \mu_{11}^* H_{1x}^* + i\mu_{12}^* H_{1y}^* \\ -i\mu_{12}^* H_{1x}^* + \mu_{11} H_{1y}^* \\ \mu_z H_{1z}^* \end{bmatrix}$$

$$= \mu_{11}^* \delta\bar{H}_t \cdot \bar{H}_{1t}^* + i\mu_{12}^* \delta\bar{H} \times \bar{H}_1^* \cdot \hat{z} + \mu_z \delta H_z H_{1z}^* \tag{5.26}$$

$$H_1^* \cdot (\bar{\bar{\mu}}_1 \cdot \delta\bar{H}) = \begin{bmatrix} H_{1x}^* \\ H_{1y}^* \\ H_{1z}^* \end{bmatrix} \cdot \begin{bmatrix} \mu_{11} & -i\mu_{12} & 0 \\ i\mu_{12} & \mu_{11} & 0 \\ 0 & 0 & \mu_z \end{bmatrix} \cdot \begin{bmatrix} \delta H_x \\ \delta H_y \\ \delta H_z \end{bmatrix}$$

$$= \begin{bmatrix} H_{1x}^* \\ H_{1y}^* \\ H_{1z}^* \end{bmatrix} \cdot \begin{bmatrix} \mu_{11}\delta H_x - i\mu_{12}\delta H_y \\ i\mu_{12}\delta H_x + \mu_{11}\delta H_y \\ \mu_z \delta H_z \end{bmatrix} \tag{5.27}$$

$$= \mu_{11} \bar{\bar{H}}_1^* \cdot \delta\bar{\bar{H}} + i\mu_{12} \delta\bar{H} \times \bar{\bar{H}}_1^* \cdot \hat{z} + \mu_z \delta H_z H_{1z}^* \tag{5.28}$$

Thus

$$\delta H \cdot (\bar{\bar{\mu}}_1 \cdot \bar{H}_1)^* - H_1^* \cdot (\bar{\bar{\mu}} \cdot \delta\bar{H}) = 2i\mu_{11}'' \delta H_t \cdot H_t^*$$

$$+ 2i\mu_{12}'' \delta\bar{H} \times \bar{H}_1^* \cdot z \tag{5.29}$$

For all frequencies differing from ferromagnetic resonance by more than $\gamma\Delta H$ in low loss ferrites, μ_{11}'' and μ_{12}'' are small quantities. Thus to a good approximation, except very near ferromagnetic resonance, the above term can be neglected. These reductions can be substituted in Eq. 5.22:

$$-\delta\omega\left[\int_{V_c} \epsilon\,\overline{E}_1\cdot\overline{E}_1^{\,*} + \mu_{11}\,\overline{H}_{1t}\cdot\overline{H}_{1t}^{\,*} + \mu_z\,H_{1z}\,H_{1z}^{\,*}\;dv\right] = \omega_1\int_{V_c}\overline{H}_1^{\,*}\cdot(\delta\overline{\overline{\mu}}_1\cdot\overline{H}_1)\,dv \tag{5.30}$$

But for the tunability we are only interested in the change in resonant frequency, i.e., in the real part of ω_1 (since $\omega_1 = \omega_o + i\frac{\beta}{2}$). Taking the real part of Eq. 5.30

$$\delta\omega_o\left[\int_{V_c} \epsilon\,\overline{E}_1\cdot\overline{E}_1^{\,*} + \mu_{11}'\,\overline{H}_{1t}\cdot\overline{H}_{1t}^{\,*} + \mu_z'\,H_{1z}\,H_{1z}^{\,*}\;dv\right]$$

$$-\frac{\delta\beta}{2}\int_{V_c}\mu_{11}''\,\overline{H}_{1t}\cdot\overline{H}_{1t}^{\,*}\,dv = \mathrm{Re}\,\omega_1\int_{V_c}\overline{H}_1^{\,*}\cdot(\delta\overline{\overline{\mu}}_1\cdot\overline{H}_1)\,dv \tag{5.31}$$

The second term on the left side of Eq. 5.31 is small compared to the first term for low-loss ferrites, and may be completely ignored. It is consistent with our small-signal assumption (i.e., $M_z \cong 0$) that only transverse components of $\delta\overline{\overline{\mu}}$ are non-zero. Thus the right side of Eq. 5.31 may be written:

$$\mathrm{Re}\left[\omega_1\int_{V_c}(\delta\mu_{11}\,\overline{H}_{1t}\cdot\overline{H}_{1t}^{\,*} + i\,\delta\mu_{12}\,\overline{H}_{1t}\times\overline{H}_{1t}^{\,*}\cdot z)\,dv\right] \tag{5.32}$$

and once again, for either linear or circular polarization,

$$\delta\mu_{12}(\overline{H}_{1t}^{\,*}\times\overline{H}_{1t}) = 0\ .$$

Then Eq. 5.32 can be written:

$$\omega_o\int_{V_s}\delta\mu_{11}'(\overline{H}_{1t}\cdot\overline{H}_{1t}^{\,*})\,dv + \frac{\beta}{2}\int_{V_s}\delta\mu_{11}''(\overline{H}_{1t}\cdot\overline{H}_{1t}^{\,*})\,dv$$

$$\cong \omega_o\int_{V_s}\delta\mu_{11}'\,\overline{H}_{1t}\cdot\overline{H}_{1t}^{\,*}\,dv \tag{5.33}$$

where the integration is taken only over the sample since $\delta\bar{\bar{\mu}} = 0$ outside the sample. Then solving for $\delta\omega_o$

$$\delta\omega_o = - \frac{\omega_o \int_{V_s} \delta\mu_{11}' (\bar{H}_{1t} \cdot \bar{H}_{1t}^*)\, dv}{\int_{V_c} \epsilon \bar{E}_1 \cdot \bar{E}_1^* + \mu_{11}' \bar{H}_{1t} \cdot \bar{H}_{1t}^* + \mu_z' H_{1z} H_{1z}^*\, dv} \tag{5.34}$$

The initial assumption for this problem was that ω_1 is a complex frequency of cavity resonance. Thus fields $\bar{E}_1$ and $\bar{H}_1$ are the fields at resonance which implies that the electric energy stored is the same as the magnetic energy stored. That is:

$$\int_{V_c} \epsilon \bar{E}_1 \cdot \bar{E}_1^*\, dv = \int_{V_c} \mu_{11}' \bar{H}_{1t} \cdot \bar{H}_{1t}^* + \mu_z' H_{1z} H_{1z}^*\, dv$$

Then Eq. 5.34 can be written in terms of the permeability and magnetic fields only.

$$\frac{\delta\omega_o}{\omega_o} = - \frac{1}{2} \frac{\int_{V_s} \delta\mu_{11}' \bar{H}_{1t} \cdot \bar{H}_{1t}^*\, dv}{\int_{V_c} \mu_{11}' \bar{H}_{1t} \cdot \bar{H}_{1t}^* + \mu_z' H_{1z} H_{1z}^*\, dv} \tag{5.35}$$

It was originally postulated for this problem that $\delta\bar{\bar{\mu}}$ is produced by δH_o

$$\delta\bar{\bar{\mu}} = \frac{\partial\bar{\bar{\mu}}}{\partial H_o} \delta H_o = \mu_o \frac{\partial\bar{\bar{x}}}{\partial H_o} \delta H_o$$

Using this relation, the tunability can be found from Eq. 5.35.

$$T = \frac{1}{\omega_o} \frac{\partial\omega_o}{\partial H_o} = - \frac{1}{2} \frac{\int_{V_s} \frac{\partial\mu_{11}'}{\partial H_o} (\bar{H}_{1t} \cdot \bar{H}_{1t}^*)\, dv}{\int_{V_c} \mu_{11}' \bar{H}_{1t} \cdot \bar{H}_{1t}^* + \mu_z' H_{1z} H_{1z}^*\, dv} \tag{5.36}$$

Notice that the tunability will be largest for those field distributions with no axial (i. e., along H_o) component. For such field distributions Eq. 5.36 becomes:

$$T = -\frac{1}{2}\frac{\int_{V_s} \frac{\partial x_{11}'}{\partial H_o} |H_{1t}|^2 \, dv}{\int_{V_c} |H_{1t}|^2 \, dv + \int_{V_s} x_{11}' |H_{1t}|^2 \, dv} \tag{5.37}$$

It should be noted that the derivation of (5.31) is independent of the type of polarization assumed. If circular polarization is assumed then $x_{11}' \rightarrow (x^{\pm})'$ in (5.31) where the ± refers to the forward and backward precessing fields in the sample with respect to H_o. In this case $|H_{1t}|^2$ is the absolute value of the total transverse field; i.e.,

$$|H_{1t}|^2 = |H_x|^2 + |H_y|^2$$

The expression (5.37) can be used to find the tunability for an arbitrary sample in a cavity, as long as losses can safely be ignored. This latter condition is approximately satisfied for low-loss ferrites at frequencies away from ferromagnetic resonance. For ferrites below saturation, it would be necessary to measure $\frac{\partial x_{11}'}{\partial H_o}$ to compute tunability. However, for ferrites above saturation the Polder susceptibility describes the magnetic state of the sample quite closely (Ref. 33). Even for this case, it is difficult to compute T unless x_{11}' and $\frac{\partial x_{11}'}{\partial H_o}$ are uniform throughout the sample. Such is the case for ellipsoids of revolution which are biased along the axis of symmetry. Because it is relatively easy to obtain low-loss samples in ellipsoidal shapes, and because spheres were used in experiments, specialized expressions for tunability applicable to these geometries will prove useful.

5.5 The Tunability for Magnetically Saturated Samples

The tunability will be studied for a small sphere of low-loss ferrite at frequencies far enough from ferromagnetic resonance that $x'' << x'$. The restriction to a small sphere is not necessary for the validity of Eq. 5.37. Rather, it affords a simplification in the expression which renders T more easily calculable. It will be shown later that the insight gained from the study of Eq. 5.37 will enable us to predict a maximum tunability for any configuration. For a spherical sample biased to saturation, $\frac{\partial x_{11}'}{\partial H_o}$ and x_{11}' are independent of position and can be factored out of the integrals in Eq. 5.37. For the small sample approximation then:

$$\int_{V_c} |H_{1t}|^2 \, dv >> \int_{V_s} |H_{1t}|^2 \, dv$$

Thus, Eq. 5.31 can be written

$$T = -\frac{1}{2} \frac{\partial x_{11}'}{\partial H_o} \frac{\int_{V_s} |H_{1t}|^2 \, dv}{\int_{V_c} |H_{1t}|^2 \, dv} \tag{5.38}$$

It has already been remarked that Eq. 5.37 (and, of course, Eq. 5.38) is independent of the polarization of the fields. Because circularly polarized fields were used in experimental determinations of T, such polarization will be assumed in the following computations for which x_{11}' must be replaced by $(x^{\pm})'$. The right-hand polarized component will be assumed since it leads to the largest T. Away from ferromagnetic resonance,

$$x^{+\prime} = \frac{\gamma M_o(\gamma H_o - f)}{(\gamma H_o - f)^2 + \alpha^2 f^2}$$

(Ref. 33). Substituting this in Eq. 5.38, thus:

$$\frac{1}{f_o} \frac{df_o}{dH_o}\bigg|_{f=f_o} = \frac{\gamma^2 M_o\left[(\gamma H_o - f_o)^2 - \alpha^2 f_o^2\right]}{\left[(\gamma H_o - f_o)^2 + \alpha^2 f_o^2\right]^2} \frac{\int_{V_s} |H|^2 \, dv}{\int_{V_c} |H|^2 \, dv}$$

$$= \frac{a\left[(\gamma H_o - f_o)^2 - \alpha^2 f_o^2\right]}{\left[(\gamma H_o - f_o)^2 + \alpha^2 f_o^2\right]^2} \tag{5.40}$$

It was shown that Eq. 5.40 is independent of first order variations in the r-f magnetic field distribution. Thus for small changes in H_o, "a" will be approximately independent of H_o. It will be convenient in subsequent calculations to disregard any variations in "a", but it should be remembered that the validity of any expression is restricted by this assumption. It will be important at a later point to notice that, for small enough samples, "a" is roughly proportional to the ratio of sample to cavity volumes.

5. 5. 1 Properties of the Tuning Curve. Equation 5. 40 can be solved by rearranging and integrating. However, the integration is rather complicated and the solution is the inverse of the desired function in transcendental form. Fortunately, it is possible to sketch the solution to this equation for various values of the parameter a. For very small values of H_0 the cavity frequency is near its unperturbed value and the slope df/dH_0 is nearly zero. As the magnetic field is increased, the frequency difference between ferromagnetic resonance and cavity resonance is decreased, and the slope df_0/dH_0 is increased. Two fairly distinct tuning profiles [i. e., $f_0(H_0)$] can result depending upon the relative size of a. For very small "a", the cavity resonant frequency is perturbed up to some maximum frequency, and df_0/dH_0 reaches a maximum when ferromagnetic resonance and cavity resonance are very close together. This situation is depicted in Fig. 5-3 by the dashed curve and is the normal circumstance in ferromagnetic resonance experiments. However, if "a" is relatively large, then as ferromagnetic resonance is brought near cavity resonance the slope df_0/dH_0 increases to a maximum of γ. For this case it is impossible for ferromagnetic resonance and cavity resonance to coincide. This latter situation is depicted in the solid curve of Fig. 5-3, and will be discussed both analytically and experimentally in the next few paragraphs because it is this circumstance which is most useful for building phase-shift amplifiers.

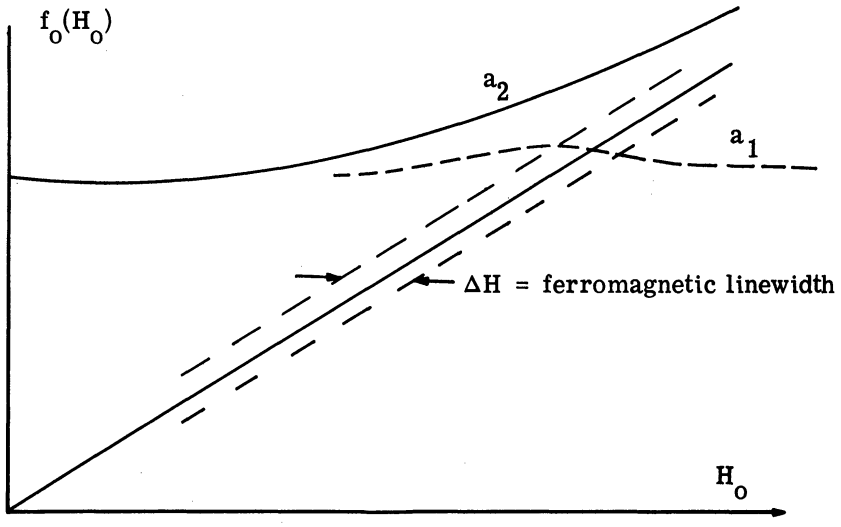

Fig. 5-3. Cavity resonant frequency vs. applied magnetic field for two different sample sizes. The parameter a_2 is related to the larger sample while a_1 is related to the smaller, so that $a_2 >> a_1$.

Several interesting properties of the curve labeled a_1 can be observed. The curve has a horizontal tangent where

$$f_o(1 \pm \alpha) = \gamma H_o$$

and as $H_o \to \infty$. When cavity and ferromagnetic resonances are equal, the slope is negative. In addition, if f_o is a microwave signal then the slope df_o/dH_o is very small near $H_o = 0$. Thus for very small H_o the cavity resonance is only slightly perturbed, but as H_o is increased $f_o - \gamma H_o$ decreases and the slope increases, reaching a maximum value. A further increase in H_o causes the slope to decrease to a minimum value and then back to zero as $H_o \to \infty$. The general shape of $f_o(H_o)$ is shown in the figure.

5. 5. 2 Solution of the Tuning Curve Equation. Of even greater interest is the curve labelled a_2, for which it has been assumed that "a" is sufficiently large that $|H_o - f_o/\gamma|$ is several times larger than the ferromagnetic linewidth. In this case, Eq. 5. 40 reduces to:

$$\frac{df_o}{dH_o} \cong \frac{a}{(\gamma H_o - f_o)^2} \tag{5. 41}$$

It is convenient to solve this equation for the dependent variable y where $y = \gamma H_o - f_o$. Equation 5. 41, written in terms of the new variable, has the form:

$$y^2 \frac{dy}{dH_o} = -(a - \gamma y^2) \tag{5. 42}$$

This equation is difficult to solve directly for $y(H_o)$. However, the inverse function $H_o(y)$ can be found by straightforward integration:

$$-(H_o - H_{o_i}) = \int_{y_o}^{y} \frac{y^2\, dy}{a - \gamma y^2} \tag{5. 43}$$

where for convenience H_{o_i}, the initial value for H_o, is chosen as zero. The solution can be written at once using integration tables:

$$-H_o = \frac{y - y_o}{-\gamma} + \frac{a}{2\gamma\sqrt{a\gamma}} \log \left[\left(\frac{a + y\sqrt{a\gamma}}{a - y\sqrt{a\gamma}} \right) \left(\frac{a - y_o\sqrt{a\gamma}}{a + y_o\sqrt{a\gamma}} \right) \right] \tag{5. 44}$$

Several interesting properties of the solution are evident upon close inspection. The unperturbed resonant frequency of the cavity is quite large, so $y_o << -\sqrt{(a/\gamma)}$ and:

$$-H_o = \frac{y - y_o}{-\gamma} + \frac{a}{2\gamma\sqrt{a\gamma}} \log\left(\frac{y_o + \sqrt{\frac{a}{\gamma}}}{y_o - \sqrt{\frac{a}{\gamma}}}\right) \tag{5.45}$$

For a real solution, $y \geq \sqrt{(a/\gamma)}$, or $y \leq -\sqrt{(a/\gamma)}$. A graph of the solution to this differential equation is given in Fig. 5-4, assuming $y_o << -\sqrt{(a/\gamma)}$. Observe that this solution approaches $\sqrt{(a/\gamma)}$ exponentially for large H_o. Thus, the curve $f_o(H_o)$ approaches the curve γH_o exponentially for large H_o, and that the frequency difference between cavity resonance and ferromagnetic resonance approaches a constant value which depends upon a/γ and therefore upon

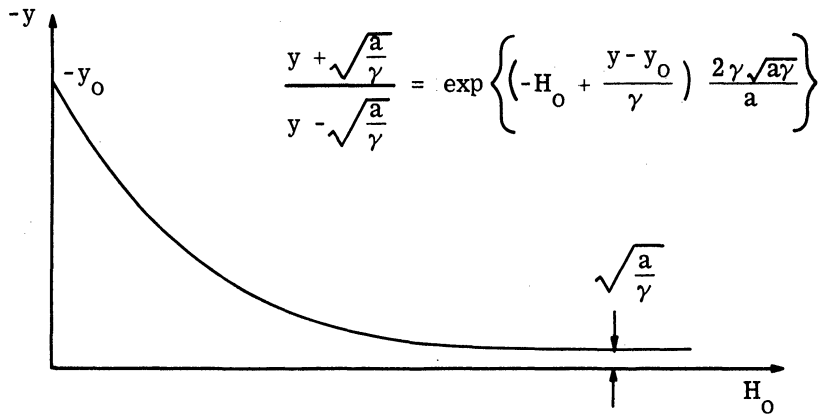

Fig. 5-4. Graph of the solution $y(H_o)$.

the ratio of sample size to cavity size. It is worthwhile to check the validity of the assumption which was made in deriving the simplified form of Eq. 5.40. That assumption was that $\gamma H_o - f_o >> \alpha f_o = \gamma\Delta H$ where ΔH is the ferromagnetic linewidth. But it has just been shown that $y \leq -\sqrt{(\alpha/\gamma)}$ which means $\gamma f_o - H_o > \sqrt{(\alpha/\gamma)}$. But:

$$a = \gamma^2 M_o \frac{v_s}{v_c} \tag{5.46}$$

Thus, if $\frac{\gamma M_o v_s f_o}{v_c} \gtrsim 10\,\gamma\Delta H$, the assumption is valid. This dictates that

$$\frac{v_s}{v_c} \gtrsim \frac{100(\gamma\Delta H)^2}{\gamma M_o f_o} \tag{5.47}$$

which for YIG is approximately

$$\frac{v_s}{v_c} \gtrsim 10^{-5} \tag{5.48}$$

That is, this approximate theory is valid if $v_s \gtrsim 10^{-5} v_c$.

Another, and even more important, fact is that $\frac{df_o}{dH_o}$ has a maximum value. This can be shown by finding the maximum value from Eq. 5.41 which leads to

5.41 which leads to

$$\frac{d^2 f_o}{dH_o^2} = 0 = -\frac{2a\left(\gamma - \frac{df_o}{dH_o}\right)}{(\gamma H_o - f)^3} \tag{5.49}$$

Clearly, $\left.\frac{df_o}{dH}\right|_{max} = \gamma$, independent of the size of a. This result is extremely significant for phase-shift amplifiers, since it predicts that the tunability for any cavity which is tuned by a sample near ferromagnetic resonance has the maximum value:

$$T_{max} = \frac{\gamma}{f_o} \tag{5.50}$$

It is important to note that this result is not fundamental to ferrite-tuned cavities but results only when the ferrite is operating near ferromagnetic resonance. This result may be attributed to the fact that the nonlinear properties occur in the frequency region in which the ferrite is also most dispersive. In a succeeding section, it will be shown that tunability of unsaturated samples near zero bias can actually be larger than γ/f_o. However, it is first of interest to give experimental evidence in support of the prediction $T_{max} = \gamma/f_o$.

5.5.3 Experimental Verification of Maximum Tunability. An experiment was performed which tends to support the validity of Eq. 5.40 and the approximations which lead to Eq. 5.41. A Sphere (diameter . 100") of highly polished YIG was mounted in the center of a circularly cylindrical cavity. The cavity was excited in the TM_{110} circularly polarized mode,

and the entire structure was placed between the pole faces of a large, regulated electromagnet. A pump field transverse to the biasing field was used. Resonant frequency vs. applied magnetic field was measured (see Fig. 5-5). The resonant frequency was measured with a high-Q reaction-type wavemeter. The magnetic field at the sample location (H_e) was determined, based on a measurement of the field at a convenient location outside the cavity. The cavity was then removed and the field at the sample location was then calibrated with respect to these measurements by measurements of fields with the cavity removed. This procedure determines H_e quite precisely because the cavity is nonmagnetic, and the sample is small.

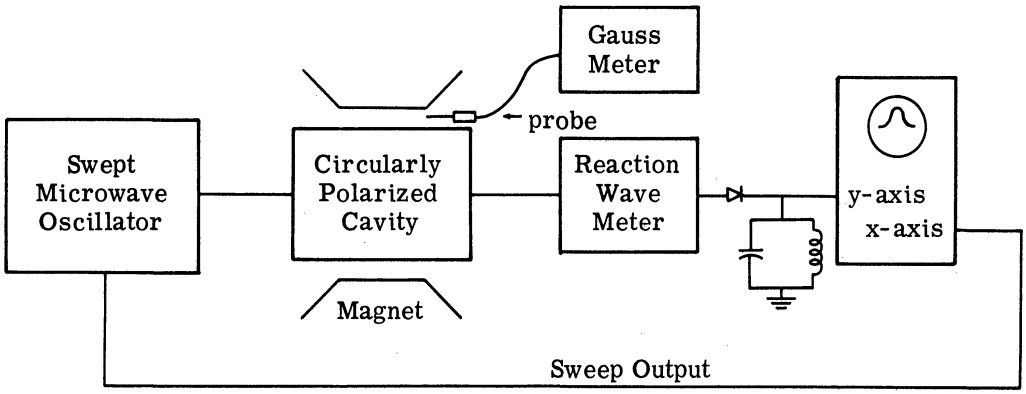

Fig. 5-5. Block diagram of circuit used to measure magnetic field relationship at resonant frequency. The external magnetic field at the sample location can be found from its value at the magnet pole faces.

The sample was loosely mounted, so that upon application of the field it could be rotated until the easy axis was aligned with the biasing field. From Section 3. 5. 1 it is known that ferromagnetic resonance is given, in this case, by:

$$f_{res} = \gamma\left(H_e + \frac{4}{3}\frac{K}{\gamma M_o}\right) \tag{5.51}$$

H_e is the externally applied field, and for YIG $\frac{4}{3}\frac{K}{\gamma M_o} \cong 57$ Oe. The effect of anisotropy has been accounted for in the computations by placing

$$H_o = (H_e + 57 \text{ Oe}) \tag{5.52}$$

According to the assumptions, expression 5. 41 can be written in the form:

$$\frac{df_o}{dH_o} = \frac{Af_o}{(\gamma H_o - f_o)^2} \tag{5.53}$$

For the sample used in this experiment $\frac{v_s}{v_c} \cong 2 \times 10^{-3}$, so that the condition (5.48) is satisfied and the above equation is valid. The coefficient A was empirically evaluated at one point and $\frac{df_o}{dH_o}$ computed at seven other data points. The accompanying data in Table 5-1 and the graph illustrate the excellent correlation between theoretical and measured $\frac{df_o}{dH_o}$ (see Fig. 5-6).

f_o = cavity resonant frequency

H_e = external magnetic field

δH_e = incremental change in H_e

Table 5-1. Tuning Rate Data

$f_o(G_c)$	H_e(KOe)	δH_e(Oe)	$\frac{df_o}{dH_o}$ Mc/Oe
9.225	2.580	0	0.05
9.230	2.955	105	0.12
9.241	3.031	181	0.20
9.260	3.132	282	0.40
9.285	3.184	334	1.28
9.308	3.202	352	1.78
9.340	3.220	370	2.22
9.380	3.238	388	2.55
9.426	3.256	406	2.60
9.470	3.274	424	2.70
9.519	3.292	442	2.75
9.570	3.310	460	2.80
9.622	3.328	478	2.80

A is evaluated at the first point:

$$\frac{df_o}{dH_o} = \frac{A f_o}{(\gamma H_o - f)^2} = 0.05$$

$$= \frac{A(9.225 \times 10^3)}{115 \times 10^4} \tag{5.54}$$

$$A = 6.3$$

Using this value for A the theoretical and experimental values for $\frac{df_o}{dH_o}$ are shown in Fig. 5-6.

The rather good correlation between theoretical and experimental results tends to verify that the maximum tuning rate is that of ferromagnetic resonance (i. e., 2. 8 Mc/Oe).

Another rough check on the validity of this equation can be made by estimating A.

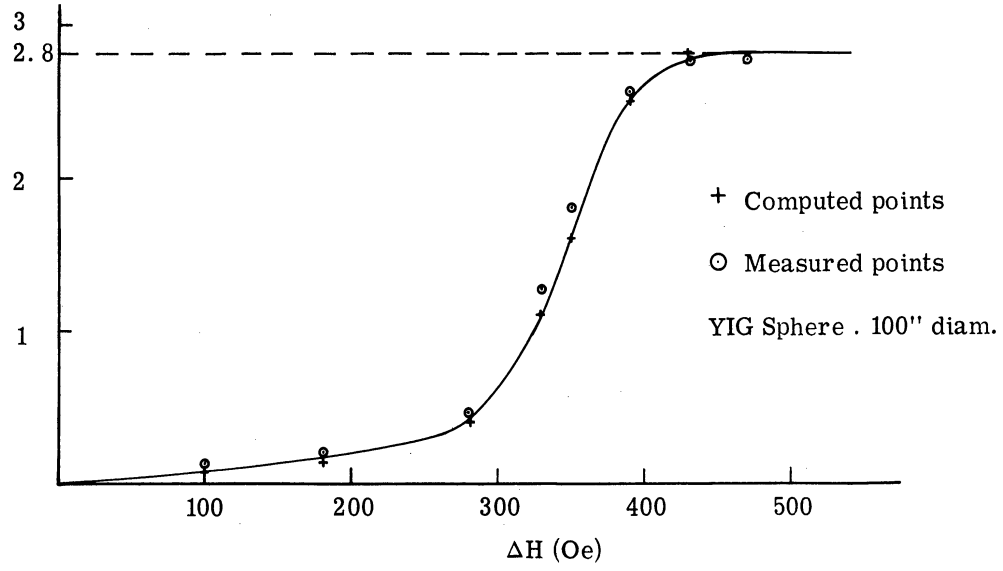

Fig. 5-6. Graph of tuning rate df_o/dH_o of circularly polarized cavity with . 100" diameter sphere of YIG. δH is the variation in biasing field from the arbitrary starting point H_e = 2. 85 KOe.

$$A = \frac{\gamma^2 M_o}{2} \frac{\int_{v_s} |H_{1t}|^2 \, dv}{\int_{v_c} |H_{1t}|^2 \, dv} \cong \frac{\gamma^2 M_o v_s}{2 v_c} \tag{5.55}$$

where

$r = 2.8$

$4\pi M_o = 1700$ Gauss

$v_s/v_c \cong 2 \times 10^{-3}$

for which A = 3.4. This value compares favorably with the empirical constant 6.3. Thus, in this experiment the tunability has been found to be a function of sample size and to have a value not greater than γ/f_o.

5.5.4 An Alternative Viewpoint to Maximum Tunability. Another interesting explanation for the observed maximum tunability near ferromagnetic resonance can be seen from the equivalent circuit for this configuration which is presented in Fig. 5-7. In this figure the cavity has been represented at one of its resonant modes ω_c, and the sample has

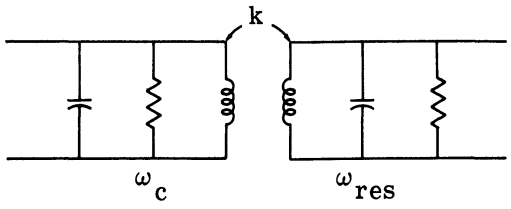

Fig. 5-7. Equivalent circuit of ferrite loaded cavity where ω_c is the cavity resonant frequency and ω_{res} is the ferromagnetic resonsnt frequency.

been represented as a resonant circuit which is inductively coupled to the cavity. The coupling coefficient k is determined by the sample volume and by its location in the cavity. This circuit is equivalent, with respect to the cavity input, to the circuit shown in Fig. 5-8.

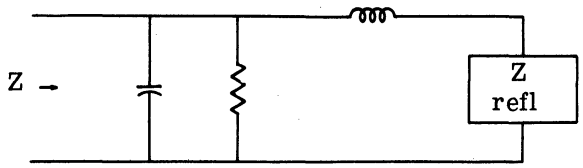

Fig. 5-8. Equivalent circuit for Fig. 5-7 with respect to the input terminals. $Z_{refl.}$ is the impedance reflected to the primary of the transformer.

For the case just considered, ferromagnetic resonance is sufficiently far from cavity resonance that the reflected impedance Z_{refl} is almost entirely reactive (i.e., $Z_{refl} \cong 1/j\omega_c$). Variations in the bias field produce variations in the magnitude of the reflected reactance and serve to vary the cavity resonant frequency ω_c. It was shown for this case that the rate

at which ω_c varies per unit change in signal field is the gyromagnetic ratio (i. e., 2.8 Mc/Oe). However when ferromagnetic resonance is near ω_c the perturbation approximation of the previous case is not valid and a somewhat different technique must be used to compute the tunability.

When ferromagnetic resonance is near the empty-cavity resonance, then the equivalent circuit consists of two strongly coupled tuned circuits of nearly equal resonant frequency. It is well known that the magnitude of the driving point impedance for this circuit is similar to that shown in Fig. 5-9. The concept of tunability is applicable at both ω_1 and ω_2. This parameter is proportional to:

$$T_{1,2} \sim \frac{d\omega_{1,2}}{dH}$$

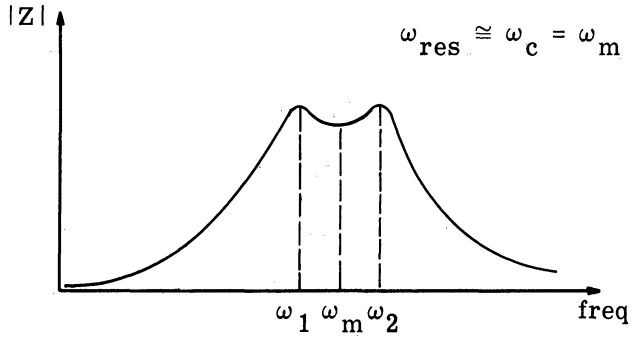

Fig. 5-9. Magnitude of the driving point impedance for two strongly coupled resonant circuits.

It is well known (e. g., Ref. 51) that these frequencies (i. e., ω_1 and ω_2) are related to the uncoupled resonant frequencies:

$$\omega_{1,2} = \omega_{res} \pm \frac{k\,\omega_m}{2}$$

where $\omega_m = \omega_c \cong \omega_{res}$ and k is the coupling coefficient. The tunabilities which can be defined for this circumstance are:

$$T_{1,2} = \frac{1}{\omega_{1,2}} \frac{d\omega_{1,2}}{dH}$$

$$= \frac{1}{\omega_{1,2}} \frac{d\omega_{res}}{dH}$$

$$= \frac{2\pi\gamma}{\omega_{1,2}} = \frac{\gamma}{f_o} \qquad (5.56)$$

Thus it has been shown that the tunability, for the configuration in which a magnetically saturated ferrite sample is used to tune a microwave cavity, is fundamentally limited to $\frac{\gamma}{f_o}$

5.6 Tunability of Magnetically Unsaturated Samples

As stated previously, an analysis based upon tunability is applicable to both saturated and unsaturated samples. The principal difference between these cases is that no simple functional relation $f_o(H_o)$ can be found for the latter. However, a number of experimental measurements have been performed to determine $\mu(H_o)$ for various ferrites for values of H_o below magnetic saturation and such information is available in graphical form in the literature. Examination of these curves reveals that ferrite materials are the most nonlinear near ferromagnetic resonance and near zero bias field (Ref. 34). The dependence of x' upon H_o at f = 6.2 kMc for high density Mn Mg ferrite of low coercive force has been given in an article by Weiss (Ref. 35) (Here we use the simplified notation x' for x'_{11})

$$\left.\frac{\partial x'}{\partial H}\right|_{H_o \to 0} \cong .07$$

$$\left. x' \right|_{H_o \to 0} \cong .81 \qquad (5.57)$$

The properties which make a ferrite useful in a phase-shift amplifier can be seen qualitatively by examining a typical B-H loop of these materials as shown in Fig. 5-10. It is difficult to define a field at which it is fully saturated, because saturation in ferrites occurs very gradually. However, a convenient measure of saturation is the field at which $B = .9\, B_{max}$. This field can be labelled H_s. An estimate of the maximum slope $\frac{\partial \mu}{\partial H}$ in

terms of these quantities is, referring to Fig. 5-10,

$$\left.\frac{\partial \mu}{\partial H}\right|_{max} \cong \frac{\mu_{max} - \mu_o}{H_c - H_s} \tag{5.58}$$

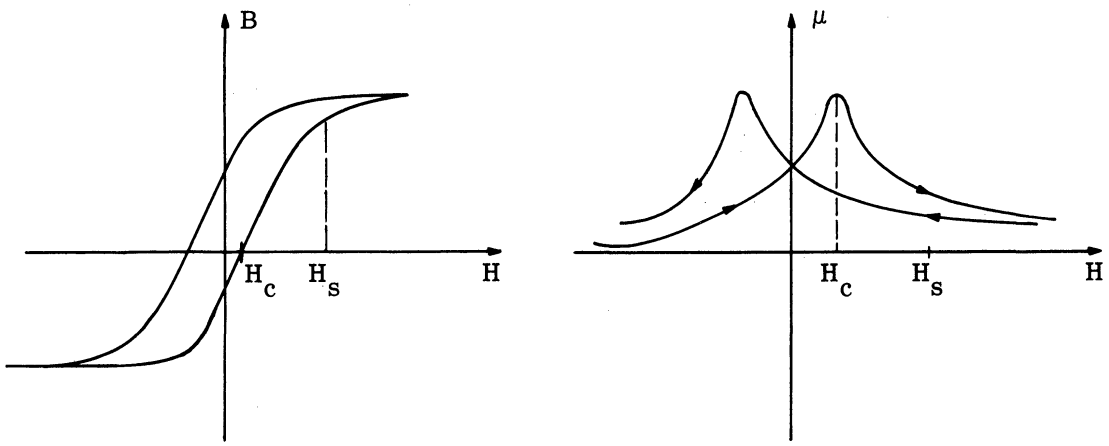

Fig. 5-10. B-H loop and permeability for typical ferrite.

Materials which tend to saturate for small magnetic fields generally tend to be most useful in ferrite phase-shift amplifiers. Such materials are generally referred to as square-loop materials and it is known that H_c is some significant fraction of H_s. Thus, magnetic material with a low saturation will generally be optimum for phase-shift amplification. The material reported by Weiss has these desirable properties and is perhaps the best material for our purpose which has been reported in the literature.

If it is assumed that $\frac{\partial x'}{\partial H_o}$ is approximately independent of position in the sample, tunability can be estimated from Eq. 5.38. For purposes of comparison with the saturated samples, the tuning rate can be found from the tunability. This number will tend to be the largest for the condition

$$\frac{\int_{V_s} |H|^2 \, dv}{\int_{V_c} |H|^2 \, dv} = 1 \tag{5.59}$$

for which the tuning rate is given by:

$$\left.\frac{df_o}{dH_o}\right|_{H_o=0} = -\frac{f_o}{2}\left.\frac{\partial x'}{\partial H_o}\right|_{H_o=0}$$

$$\cong 350 \text{ Mc/Oe} \qquad (5.60)$$

The result (Eq. 5.60) appears significant when compared with the tunability of the ferromagnetic resonance configuration and suggests that the unsaturated sample which completely fills the cavity tends to be optimum. However, it was shown that the transducer gain varies inversely with sample volume, while the unsaturated sample must fill the cavity if the large tuning rate is to be obtained. This tends to offset some of the apparent advantage enjoyed by the larger tunability. For this reason a more meaningful comparison between these two configurations can be made on the basis of the parameter T' which has already been defined:

$$T' = \frac{T}{\left(\int \mu\, f^2(r)\, dv\right)^{\frac{1}{2}}} \qquad (5.61)$$

It is of interest to compare the maximum value of T' for the material reported by Weiss and for the configuration at ferromagnetic resonance. The signal field which tends to maximize T' is that for which the integral

$$\int_{v_c - v_s} \mu\, |f(r)|^2\, dv$$

is a minimum. This integral is minimized for the condition

$$f(r) = 1 \text{ inside the sample}$$

$$= 0 \text{ outside the sample}$$

and the minimum value for this condition is $\mu_s v_s$. But since it has already been demonstrated that T depends upon v_s for both configurations, there is a v_s for each for which T' is maximized. Figure 5-11 illustrated $T(v_s)$ for both configurations. From these curves it is clear that, for ferromagnetic resonance configuration, T' is maximum for $v_s = v_{sm}$ and that while for the other configuration, T' is maximum for $v_s = v_c$.

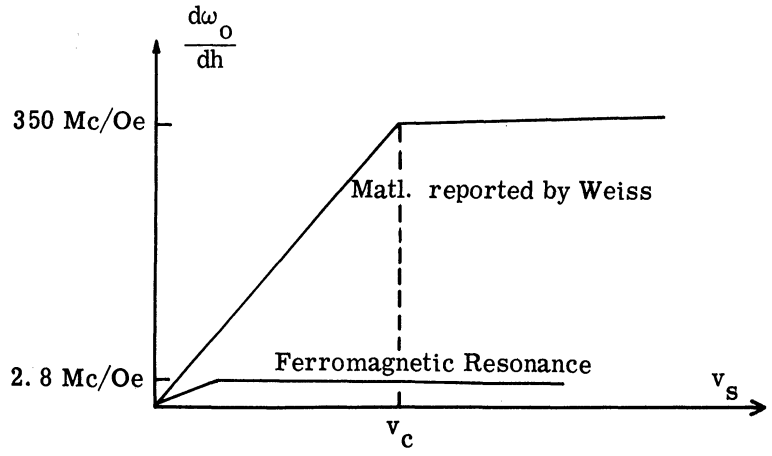

Fig. 5-11. Tunability vs. sample volume. Curves have no physical significance to the right of v_c and are not to scale.

Though computation of v_{sm} is very difficult, an order of magnitude estimate is possible, leading to only an order of magnitude estimate of T'. However, this provides an adequate comparison since the estimate of T for the unsaturated case was based upon an estimate of $\frac{\partial x'}{\partial H_o}$ which is good to only an order of magnitude. It has been shown that, if $v_s > 10^{-5} v_c$, then the curve labelled a_2 in Fig. 5-3 is the appropriate tuning curve. For v_s smaller than this value, a_1 is appropriate. Thus $v_{sm} = 10^{-5} v_c$ is an order of magnitude estimate, where v_c is the empty cavity volume.

A similar estimate of maximum T' can be made for an unsaturated sample in an optimum configuration, i. e., with the sample completely filling the cavity. Since the dimensions of the ferrite filled cavity are reduced from the empty cavity values by the factor $(\mu\epsilon)^{-\frac{1}{2}}$,

$$v_s = (\mu\epsilon)^{-\frac{3}{2}} v_c$$

For the material reported by Weiss $\mu \cong 1$ and $\epsilon \cong 16$ for which

$$v_s \cong \frac{v_c}{70}$$

where v_c is the volume of an empty cavity.

The sample permeabilities at the signal frequency tend to be quite different for the two cases. The ferromagnetic resonance configuration is magnetically saturated so $\mu_s \cong 1$ for this case. However, for the Mn Mg material reported by Weiss $\mu_s \cong 70$.

Using these estimates the T' for the two cases are given approximately by:

$$T' = \frac{2.8}{f_o \sqrt{10^{-5} v_c}}$$

$$\cong \frac{10^3}{f_o \sqrt{v_c}} \qquad \text{for the ferromagnetic resonance configuration}$$

and

$$T' = \frac{350}{f_o \sqrt{\frac{\mu_s v_c}{70}}}$$

$$\cong \frac{350}{f_o \sqrt{v_c}} \qquad \text{for the unsaturated case using the material reported by Weiss.} \qquad (5.62)$$

Since these estimates are only good to an order of magnitude, it is impossible to conclude that either is superior, even though the T value for the unsaturated material exceeds that near ferromagnetic resonance by more than two orders of magnitude. An experimental investigation of these two cases reported in the next chapter shows which of these configurations tends to be optimum for phase-shift amplification.

It has been shown that the threshold for a ferrite phase-shift amplifier is proportional to the integral

$$\int \mu |f|^2 \, dv$$

where f(r) is the signal field distribution. From this it was shown that the minimum threshold tends to be proportional to sample volume assuming the signal field is large in the sample and small outside. In this case, a small-sized sample is clearly optimum which suggests that thin magnetic films might be successfully employed in phase-shift amplifiers. For this reason, it is natural to study the tunability of thin films.

5.7 Tunability of Thin-Film Samples

The tunability of bulk ferrite samples is determined by the dependence of the permeability at some r-f frequency upon the magnetic field at some lower frequency. Recall that optimum coupling occurs in ferrites when these two fields are physically orthogonal. Thus it is natural, in investigating tunability of thin films, to consider the dependence of r-f permeability in a thin film upon a low-frequency magnetic field which is orthogonal to the permeability components. This relationship has been investigated on the basis of the free energy in the sample and is reported in the literature (Ref. 36).

For frequencies below about one hundred megacycles thin films can be characterized by the so called quasi-static theory. For a single domain with magnetic fields h_1 and h_2 applied simultaneously, the free energy of the sample is given by (Ref. 36)

$$W = K \sin^2 \phi - h_1 \frac{M}{\mu_o} \cos\phi \cos\psi - h_2 \frac{M}{\mu_o} \sin\phi \cos\psi + \frac{M^2}{\mu_o^3} \sin^2\psi$$

where M is the magnetization, K is the anisotropy constant, and both ϕ and ψ are defined in Fig. 5-12.

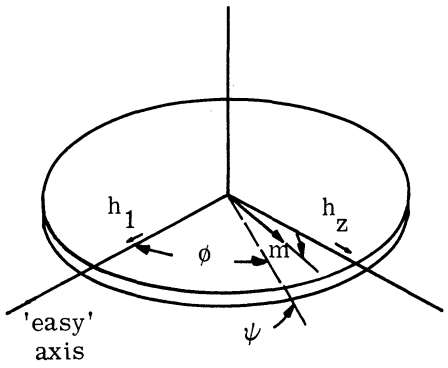

Fig. 5-12. The schematic representation of a thin film (single domain) illustrating the coordinate system and the applied magnetic fields.

Clearly this function is minimized with respect to ψ at $\psi = 0$, and it can be minimized with respect to ϕ by placing $\frac{\partial W}{\partial \phi} = 0$. The result of this latter calculation gives:

$$\sin\phi = \frac{h_2}{H_k}\left(1 + \frac{h_1}{H_k}\cos\phi\right)^{-1} \tag{5.63}$$

where $H_k = \frac{2\mu_o K}{M}$ is the so-called anisotropy field.

This function is extremely useful for representing the response of the thin film to applied fields:

$$\begin{aligned} B_1 &= \mu_o (h_1 + M\cos\phi) \\ B_2 &= \mu_o (h_2 + M\sin\phi) \end{aligned} \tag{5.64}$$

The nonlinear coupling between h_1 and h_2 is potentially useful for phase-shift amplification because the stored energy in the field h_2 can be controlled by the field h_1.

A convenient prototype for illustrating this phenomenon is shown in Fig. 5-13 (Ref. 37).

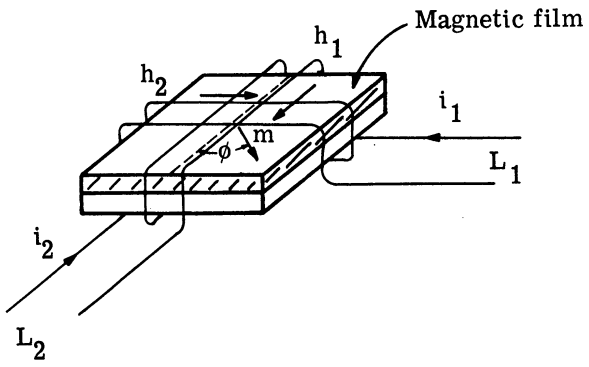

Fig. 5-13. Schematic illustration of the use of a thin film magnetic sample for phase-shift amplification.

In the small-signal approximation $\sin\phi \cong \phi$ and the coil inductance L_2 will be approximately independent of h_2, though it is a very sensitive function of h_1. The proper use of an element with this property in a phase-shift amplifier is shown in Fig. 5-14.

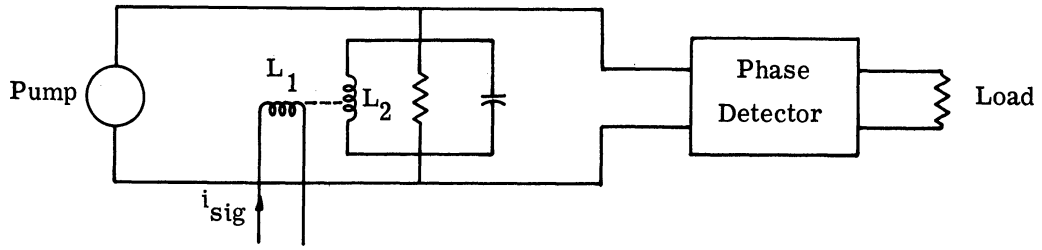

Fig. 5-14. Illustration of the use of the thin film prototype in a phase-shift amplifier.

The inductance L_2 is incorporated in a resonant circuit at the pump frequency; the inductance L_1 is used to produce variations in L_2 and can properly be called the signal circuit inductance. The performance of this circuit can be predicted successfully if the tunability of L_2 is known. The most useful tunability is defined by:

$$T = \frac{1}{\omega_o} \frac{\delta \omega_o}{\delta i_1} = -\frac{1}{2} \frac{1}{L_2} \frac{\delta L_2}{\delta i_1} \tag{5.65}$$

The inductance L_2 can be approximated by the low-frequency model up to UHF frequencies, due to the extremely small size of such a single-domain thin-film sample. Using this approximation, the inductance L_2 is given by:

$$L_2 = \frac{\lambda_2}{i_2}$$

$$\cong L_o \left[1 + \frac{M A_m}{A H_k} \left(\frac{1}{1 + \frac{h_1}{H_k}} \right) \right] \tag{5.66}$$

where $L_o = \mu_o N k_2$ is the inductance of the air-core coil L_2, A_m and A are, respectively, the cross-sectional area of the material and coil, and k_1 and k_2 are given by:

$$h_1 = k_1 i_1$$

$$h_2 = k_2 i_2$$

The tunability is given by

$$T = \frac{\dfrac{k_1 M A_m}{2AH_k^2\left(1+\dfrac{h_1}{H_k}\right)^2}}{1+\dfrac{A_m M}{A H_k}\left(\dfrac{1}{1+\dfrac{h_1}{H_k}}\right)} \tag{5.67}$$

which is maximum at $i_1 = 0$ (i. e., $h_1 = 0$). Thus at $i_1 = 0$ the tunability is given by:

$$T = \frac{\dfrac{M A_m k_1}{2A H_k^2}}{1+\dfrac{M A_m}{A H_k}} \tag{5.68}$$

This quantity tends to be optimized for the smallest possible H_k and the largest A_m/A. However, H_k is determined by the material composition and by the technique used to deposit the film. Typically, H_k is not less than about 1 or 2 Oersteds. The cross-sectional area of the film, relative to the total cross section of film and substrate, is determined largely by practical considerations of strength, but generally the tunability is optimized for the smallest possible substrate.

Although it is not strictly a ferrite the material which has received greatest study lately as a thin film and which has a low H_k ($\approx$ 2 Oe) is permalloy of the approximate composition Ni - 80 percent, Fe - 20 percent. It is vacuum-deposited in thin films on thin glass substrates of the order of .006" thick. A typical film will be in the order of 2000 to 10000 Å thick and of the order of 1 cm wide. Further, for a sample cut to dimensions perhaps 1/4" by 1/4", the thin film will tend to be a single magnetic domain. Such a sample was used to prepare an inductor in the form of the prototype model. The inductance L_2 was measured vs. the current i_1 for a coil L_1 consisting of 40 turns. The results of this measurement, made at 8 Mc, are shown in Fig. 5-15 (Ref. 37).

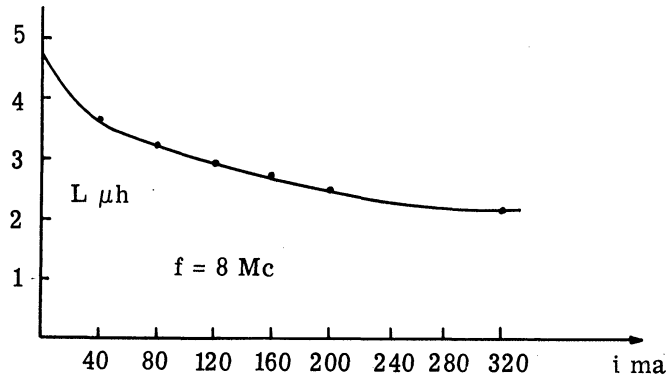

Fig. 5-15. Plot of the variable inductance L_2 vs. applied current i_1 in L_1 (40 turns) in sample prepared according to the prototype model - Fig. 5-10.

The tunability of this circuit near $i_1 = 0$ can be estimated from the slope of the curve $L_2(i)$. For an L_1 consisting of 40 turns of wire wound close to the sample, the tunability is approximately:

$$T \cong \frac{1}{120}/Oe \tag{5.69}$$

The theoretical limits for tunability can be seen from a somewhat more sophisticated model of the inductor than the static approximation. Smith (Ref. 36) has shown that thin films experience ferromagnetic resonance in much the same way as bulk ferrites. For this reason it can be shown (Ref. 52) that the small-signal equivalent circuit of the transverse winding (i. e., L_2) of the thin-film configuration is as shown in Fig. 5-16:

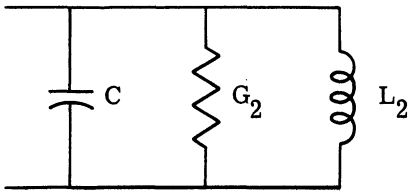

Fig. 5-16. Small-signal equivalent circuit for the transverse winding labelled L_2 in Fig. 5-13.

The values of C, G and L_2 have been determined in Ref. 52:

$$C = \frac{(1+\alpha)^2}{\gamma^2\, 4\pi\, M\, k_2\, \lambda_{2m}}$$

$$G = \frac{\alpha}{\gamma\, k_2\, \lambda_{2m}}$$

$$L_2 = \frac{k_2\, \lambda_{2m}}{H_k + H_1} \tag{5.70}$$

where $k_2 = H_2/i_2$, and λ_{2m} is the maximum saturation flux linkage due to M. The resonant frequency is given by:

$$\omega_{res} = \gamma \sqrt{4\pi\, M(H_k + H_1)} \tag{5.71}$$

where for permalloy films $4\pi M \cong 10^4$ Gauss. Using this formula, the tunability is given by:

$$T = -\frac{1}{\omega_{res}} \frac{d\omega_{res}}{dH_1}$$

$$= \frac{1}{2(H_k + H_1)} \tag{5.72}$$

independent of γ and M. This is the theoretical maximum tunability for any given resonant frequency. For example, the tunability at 400 Mc is about .25/Oe. Notice that this is a relatively large tunability compared to that observed for bulk ferrites and compared to the value observed by Pohm.

In addition to the large tunability for this configuration there are also, unfortunately, large sample losses for which the circuit Q tends to be very low. Pohm has shown that the Q due to material losses is given by:

$$Q = \frac{\omega_r (1+\alpha)^2}{4\pi\, M \gamma\, \alpha} \tag{5.73}$$

For permalloy films $\alpha \cong .015$, so that at 400 Mc:

$$Q \cong 1$$

Thus, although the tunability of this configuration is relatively large, its low Q tends to eliminate the possibility of using this configuration in a phase-shift amplifier. On the other hand, if the pump frequency is well below ferromagnetic resonance, then the material losses are less important and a higher circuit Q is possible. For example, Pohm observed Q = 14 at 30 Mc for this configuration. In addition if the material loss parameter α can be reduced by an order of magnitude, then the Q at 400 Mc will be increased to roughly 10. Certain of the techniques which were used to develop narrow linewidth bulk ferrites could, in principle, be used to significantly improve the thin film Q. It will be shown in the next chapter that a Q of 10 enables the construction of a phase-shift amplifier with a reasonable gain-bandwidth product.

It has already been shown that various bulk ferrites can be meaningfully compared on the basis of T'. However, the comparison of bulk ferrites to thin films must account for the difference in optimum pump frequency. For this reason it is convenient to compare the product $f_p\ T'_{max}$ where f_p is the appropriate pump frequency. Table 5-2 has been constructed for this purpose. It reveals the importance of the thin-film configuration for phase-shift amplifiers. It will be shown in the next chapter that phase-shift amplifiers of reasonable gain-bandwidth product can be built if the material Q can be improved by an order of magnitude. Q's comparable with those of bulk ferrite samples should be possible for single crystal films grown on polished substrate. If this improvement in film Q proves possible, the thin film will definitely be the optimum configuration for ferrite phase-shift amplifiers.

Table 5-2 Comparison of Tunabilities

Configuration	T_{max}	f_m (Mc)	$v_{s,min}$ (in^3)	μ_s	T'_{max}	$f_m T'_{max}$ ($Mc/Oe\sqrt{in^3}$)
Bulk unsaturated sample (Weiss)	0.035/Oe	$\approx 10^4$	0.2	≈ 70	$0.07/Oe\sqrt{in^3}$	700
Bulk sample near resonance (opt. size)	2.8×10^{-4}/Oe	$\approx 10^4$	2×10^{-66}	1	$0.14/Oe\sqrt{in^3}$	1400
Thin film (observed by Pohm)	1/ (120 Oe)	50	10^{-6}	1	$8/Oe\sqrt{in^3}$	400
Thin film at resonance	0.25/Oe	400	10^{-6}	1	$240/Oe\sqrt{in^3}$	$\approx 10^5$

5.8 Summary

In this chapter the ferrite phase-shift amplifier was considered. It was shown that there is a field orientation at which maximum coupling and, correspondingly, maximum phase-shift amplifier gain occurs. For signal passbands centered at very low frequencies, it was shown that the signal field should be oriented parallel to the biasing field and the pump field should be transverse to that field. For this orientation a particularly convenient prototype amplifier configuration can be synthesized, which is conveniently represented by the parameter which we called tunability. It was further shown that the transducer gain tends to be proportional to the parameter T' which is defined:

$$T' = \frac{T}{\left(\int \mu \, |f^2(r)| \, dv \right)^{\frac{1}{2}}}$$

where T is the tunability, f(r) the signal field distribution, and μ the permeability component at the signal frequency. The remainder of the chapter was devoted to a study of the dependence of tunability upon material parameters.

The dependence of T upon the sample shape was investigated for a number of basic prototype configurations. Tunability depends upon material shape, size, and permeability, and tends to be proportional to the slope $\frac{\partial \mu}{\partial H_o}$, where H_o is the biasing field and μ is

the appropriate permeability at the pump frequency. It was shown that, for bulk ferrite samples, this quantity tends to be largest near ferromagnetic resonance and near zero biasing field. It was shown that tunability near ferromagnetic resonance is limited to γ/f_o, where γ is the gyromagnetic ratio (γ = 2. 8 Mc/Oe) and f_o is the pump frequency. This limitation can be attributed to the fact that ferrites are most dispersive near ferromagnetic resonance, and is fundamental to operation near that operating condition. On the other hand, no fundamental restriction can be determined for the ferrites near zero bias because no analytic expression for $\mu(h)$ is known. However, it was shown that the optimum material for operation near zero bias is that with a square B-H curve for which $\frac{\partial \mu}{\partial H}$ is large. The largest reported value for this slope in the literature was given by Weiss: $\frac{\partial \mu}{\partial H} \cong .07/\text{Oe}$. Using this value it was shown that the tunability at x-band is limited to about

$$T_{max} \cong \frac{350}{f_o}/\text{Oe}$$

In spite of the disparity between the tunabilities for zero bias and for ferromagnetic resonance, it was shown that on the basis of the parameter T' neither is superior by an order of magnitude.

Perhaps the most promising configuration is the thin-film permalloy variable inductor, whose tunability T' is nearly two orders of magnitude larger than that for the best bulk ferrites. The most significant limitation on the thin-film configuration is the extremely low Q at useful pump frequencies. However it is expected that the Q of the thin film inductors will be improved by techniques which led to improved Q in bulk ferrites. The development of such an inductor will considerably enhance the potential of ferrite phase-shift amplifiers.

This chapter has reported an investigation of the limitations which are imposed upon ferrite phase-shift amplifiers by material. In the next chapter the limitations of several circuit configurations on amplifier performance are considered.

CHAPTER 6

PRACTICAL CONFIGURATIONS FOR THE FERRITE PHASE-SHIFT AMPLIFIER

6. 1 Introduction

This chapter is devoted to a study of the circuit properties and limitations of ferrite phase-shift amplifiers based upon the physical properties of available materials. The dependent variables appropriate to such circuits are transducer gain, bandwidth and pump power. However, because the transducer gain is proportional to pump power, a more significant dependent variable is defined which we call threshold. The threshold is that pump power for which the transducer gain is unity. Thus:

$$G_t = \frac{P}{P_{th}}$$

where G_t is the transducer gain and P_{th} the threshold. The threshold depends strictly upon circuit configuration and material parameters and for that reason is directly comparable between various configurations. It is additionally useful for deriving optimum configurations and for developing design curves for them. This is done in the present chapter for several configurations, taking full account of the limitations which have been found for the tunabilities in the previous chapter. A comparison is made between the various configurations on the basis of their optimum performance. A discussion of certain practical considerations such as noise figure, etc. is deferred until the final chapter. In Sections 6. 2 and 6. 3 configurations using magnetically unsaturated bulk ferrite samples are considered. In Sections 6. 4, 6. 5, and 6. 6 configurations using bulk ferrite samples biased near ferromagnetic resonance are discussed. In Section 6. 7 the thin-film, variable-inductor configuration is considered.

In Section 5. 3 the transducer gain for a ferrite phase-shift amplifier was found:

$$G_t = \frac{2\zeta P_p (Q_\ell T)^2 L}{R_s \int_{\text{space}} \mu |f(\bar{r})|^2 \, dv} \tag{6. 1}$$

where:

ζ = detection efficiency

P_p = pump power

Q_ℓ = loaded Q of the pump frequency filter (Fig. 5- 1)

T = tunability of the pump frequency filter

L = inductance of the signal frequency coil

R_s = signal frequency source resistance

$f(\bar{r})$ = signal frequency magnetic field distribution

For reasons which will become clear, it is useful to rewrite Eq. 6. 1 in terms of a slightly different set of independent variables. For example, it can be seen with reference to Fig. 5-2 that the input bandwidth can be written:

$$\beta_i = \frac{R_s}{L}$$

provided the Q of the signal-frequency coil is sufficiently large. The significance of making this substitution into Eq. 6. 1 will be clear when it is demonstrated that the ferrite phase-shift amplifiers tend to be input-bandwidth limited. In addition, it can be seen from the definitions for Q_ℓ and T that a further substitution can be made in Eq. 6. 1:

$$Q_\ell T = \frac{\omega_o}{\beta_p} \frac{1}{\omega_o} \frac{d\omega_o}{dh}$$

where ω_o = filter resonant frequency and β_p = pump bandwidth (Section 2. 1). Thus:

$$Q_\ell T = \frac{1}{\beta_p} \frac{d\omega_o}{dh}$$

If these substitutions are made in Eq. 6. 1, the threshold power for a ferrite phase-shift amplifier can be written:

$$P_{th} = \frac{\beta_i \beta_p^2 \int \mu |f(\bar{r})|^2 \, dv}{2 \zeta \left(\frac{d\omega_o}{dh} \right)^2} \tag{6.2}$$

This expression is extremely important to the study of the practical amplifier configurations discussed in this chapter. It will become clear in this study that, because the ferrite amplifier tends to be input-bandwidth limited, the threshold per unit input bandwidth (i. e., P_{th}/β_i) is an important parameter for comparing the various configurations.

In many of the configurations discussed in this chapter it will be seen that the signal is not coupled efficiently into the sample. This circumstance is manifested by a large value for the integral:

$$\int \mu |f(\bar{r})|^2 \, dv$$

The effect of this poor coupling is a large threshold for the configuration. Note that this integral is influenced by the design of the signal-frequency circuit, and is nearly independent of the sample electrical properties. The optimum design of the signal circuit is that for which

$$\begin{aligned} f(\bar{r}) &= 1 \quad \text{inside the sample} \\ &= 0 \quad \text{outside the sample} \end{aligned} \tag{6.3}$$

For this optimum design, the integral reduces to:

$$\int \mu |f(\bar{r})|^2 \, dv = \mu_s v_s \tag{6.4}$$

In the optimization of the various configurations discussed in this chapter, it is desirable to consider optimization with respect to the design of this circuit. For this reason the substitution Eq. 6. 4 will be used in computing each optimum threshold. On the other hand, it should be noted that the field distribution Eq. 6. 3 might be incompatible with certain configurations.

6. 2 The Reggia Tunable Filter Configuration

The first configuration to be considered uses the tunable, bandpass filter proposed by Reggia (Ref. 39). Physically, the filter consists of a rectangular, ferrite slab which is placed in a waveguide and whose faces normal to the waveguide axis are silvered (see Fig. 6- 1). The transmission characteristic of this structure is that of a bandpass filter with an insertion loss of approximately 1 db and a bandwidth of approximately 100 Mc (see Fig. 6. 2). The silvered faces present reactive shunts to the dominant mode and tend to tune each other out at frequency f_1 of Fig. 6. 2. The frequency (f_1) at which this occurs is the filter resonant frequency, and depends upon the electrical length of the material. However, the electrical length depends upon material parameters which can be varied by means of an applied magnetic field H_o. The equivalent circuit for the filter is as shown in Fig. 6. 2, in which the variable resonant frequency is modelled by a variable inductance. It is clear, through reference to Fig. 2- 1 that this filter is applicable to a phase-shift amplifier circuit. A block diagram of the amplifier is shown in Fig. 6-3.

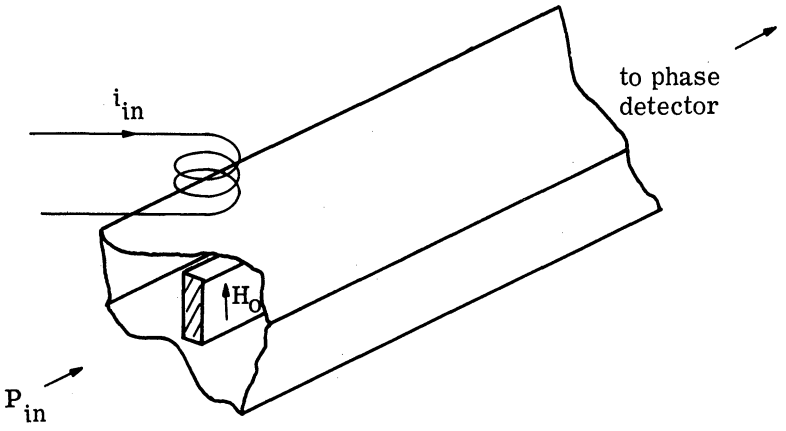

Fig. 6- 1. Reggia tunable bandpass filter for use as phase-shift amplifier.

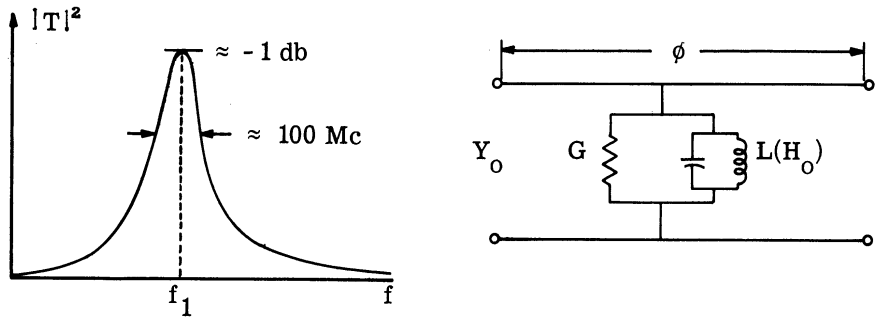

Fig. 6-2. Transmission characteristics and equivalent circuit for Reggia tunable filter.

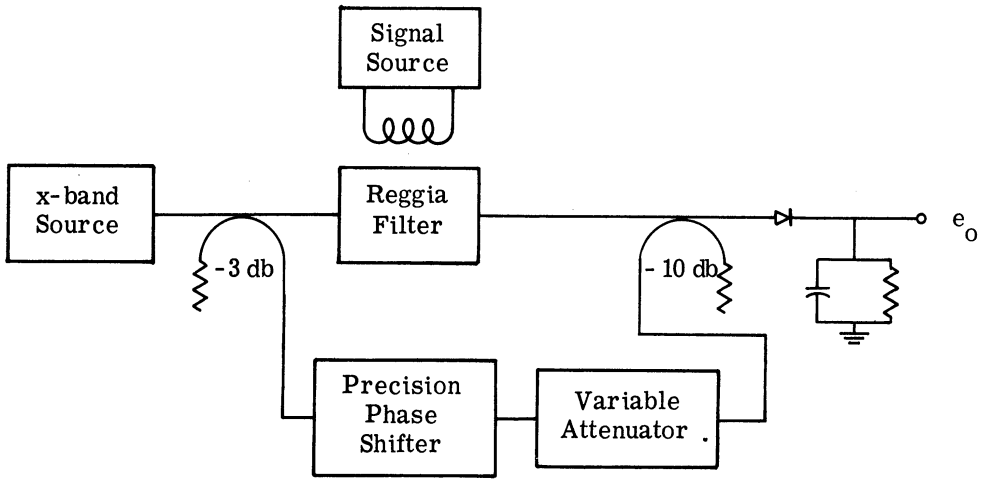

Fig. 6-3. Block diagram of ferrite phase-shift amplifier which uses Reggia tunable filter.

One of the primary purposes of this chapter is to find the optimum design for each configuration which includes, of course, finding the optimum with respect to material parameters. For this reason it is logical to determine the dependence of the threshold upon material parameters. The study of the dependence of P_{th} on the choice of material and upon the sample shape and size cannot be restricted to a single variable in Eq. 6. 1. Rather each must be studied individually and careful attention must be paid to possible interdependence between them. It is convenient to refer to Fig. 6-4 for the definitions of the appropriate dimensional variables.

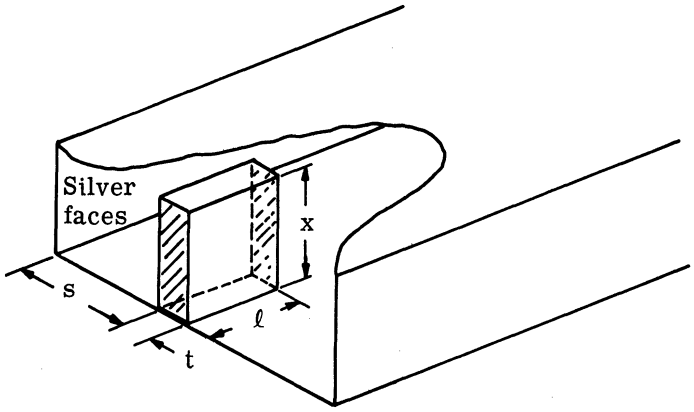

Fig. 6-4. Illustration of sample dimensional parameters for Reggia tunable filter.

6. 2. 1 Dependence of Filter Properties on Sample Parameters. The variations of the resonant frequency f_o and pump bandwidth β_p, with respect to variations in sample dimension, can be measured directly by means of a swept microwave oscillator and a high-Q, reaction-type wavemeter. The results of these measurements for low-density Mg Mn ferrite are shown in Figs. 6-5 and 6-6, respectively.

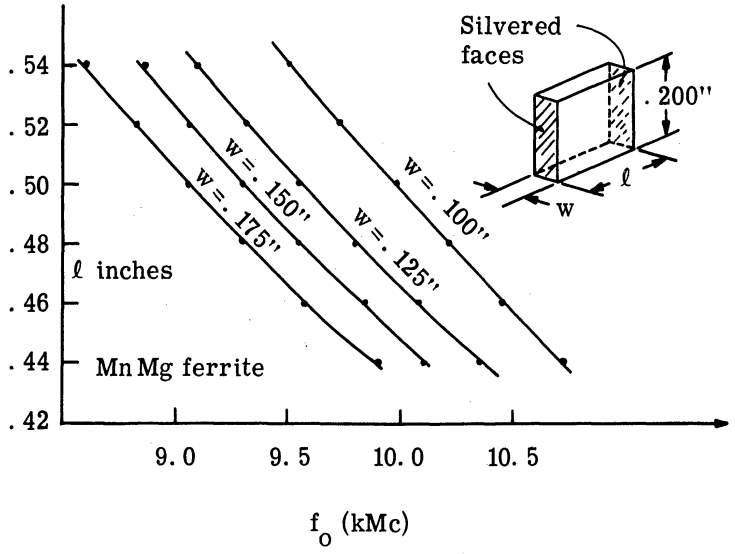

Fig. 6-5. Dependence of the center frequency of the Reggia filter upon length and width (see Ref. 39).

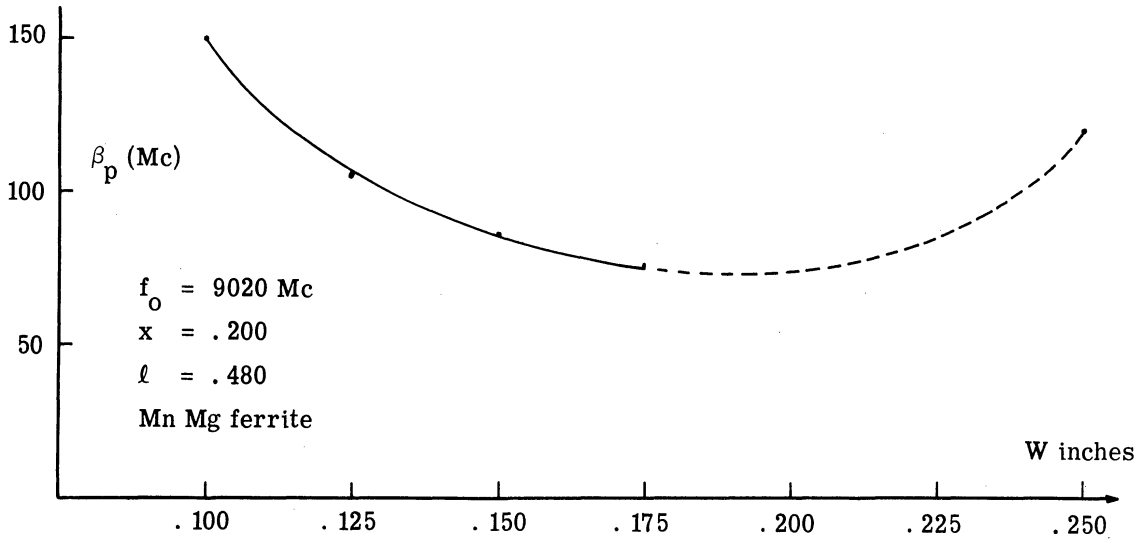

Fig. 6-6. Dependence of filter bandwidth (matched load) upon sample width for fixed length and height.

The measurements were made in a reduced-height waveguide having a height of 0. 200". Note that the resonant frequency f_o varies inversely with ℓ. This tends to support the explanation that the resonant frequency is that for which the reactive shunts tend to tune each other out. The dependence of the filter bandwidth upon width, at a fixed length, is shown in Fig. 6-6.

These measurements were made with a swept microwave oscillator, a high-Q ($\approx$ 5000) reaction-type wavemeter and a precision variable attenuator. The attenuator and frequency meter were adjusted to locate the frequencies at which the transmission of the filter to a matched detector is down 3 db. The precision of the measurements are of the order of the wavemeter bandwidth (i. e., $\approx$ 2 Mc). In each case, the samples were cut to a tolerance of 0. 001" and were prepared with silver faces using Hanovia silver paste. An explanation for the shape of the curve in Fig. 6-6 can be found by noting that β_p is determined by losses which occur at two distinct places in this configuration, i. e., in the material and in the finite conductance of the silver coatings. For very thin samples the losses in the material, which are proportional to sample volume, are negligible relative to the losses in the silver faces. As the sample thickness increases from a very small value, the width of the silver faces also increases and the equivalent shunt conductance increases. This is the reason

that β_p decreases with increasing w in the region 0. 100" $<$ w $\lesssim$ 0. 175". However, for w $\gtrsim$ 0. 200" the losses in the sample tend to dominate. They tend to increase with increasing thickness, with the result that β_p increases.

Additional measurements reveal other interesting properties of β_p. It was observed that, for materials other than the Mn Mg reported in Fig. 6-6, $\beta_p(w)$ differs from the curve in Fig. 6-6 only for larger w. This can be explained also by noting that sample losses depend upon the nature of material. Thus $\beta_p(w)$ will be the same for all materials provided w is small enough that the losses in the silver faces tend to dominate.

From a series of measurements it was found that β_p is minimum in the region 0. 200 $\lesssim$ w $\lesssim$ 0. 225, depending upon material type and the quality of the silver coating. If a good quality silver paint is used, the minimum bandwidth is approximately 60 Mc and the insertion loss is of the order of 1 to 3 db.

The tuning rate of the filter, $d\omega_o/dh$, is rather difficult to define because of the nonuniformity of the signal field in the sample. * Perhaps the most useful point in the sample at which to measure h is its geometrical center. At this point in the sample the field has its smallest value. This field can be computed from the magnitude of a uniform applied external field by means of a table of approximate demagnetizing factors published by the U. S. Department of Commerce (Ref. 40). Measurement of $d\omega_o/dh$ at the center has the additional advantage that the value observed when the sample is placed in a uniform external field is larger than $d\omega_o/dh_a$, where h_a is the applied uniform field. For this reason, the former value can be used to compute the upper bound for $d\omega_o/dh$, which is useful for estimating optimum P_{th}.

There is another difficulty in measuring $d\omega_o/dh$, which results from the difficulty of determining $\delta\omega_o$ for the Reggia filter when $\delta\omega_o << \beta_p$. This is the normal circumstance for this configuration. However, $\delta\omega_o$ produces a phase shift of $\delta\phi$ which can be measured very precisely by means of the bridge circuit shown in Fig. 6-7.

---

*Recall that h = amplitude of signal field in the sample (denoted by H_o in Fig. 6-1), thus $\delta h = \delta H_o$.

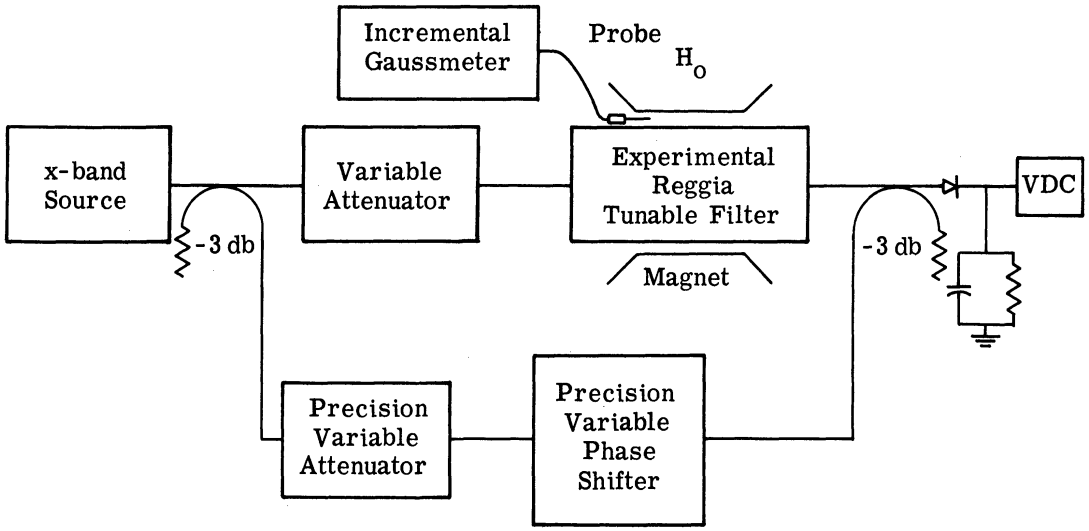

Fig. 6-7. Bridge circuit used to measure incremental phase shift produced by δH_o.

The measurement procedure is as follows:

1) The bridge is balanced for zero VDC at $f_{source} = f_o$.
2) The applied field H_o is changed by δH_o and δH_o is recorded.
3) The precision phase-shifter and attenuator are adjusted to rebalance bridge.
4) $\delta\phi$ is read from phase-shifter and recorded.
5) δH_o inside sample is computed from H_o by means of approximate demagnetizing factor.

The desired quantity $d\omega_o/dh$ center is given by:

$$\frac{d\omega_o}{dh_{center}} = \beta_p \frac{d\phi}{dh_{center}} \qquad (6.5)$$

This quantity was measured vs. sample width for a variety of common ferrites; the results are plotted in Fig. 6-8.

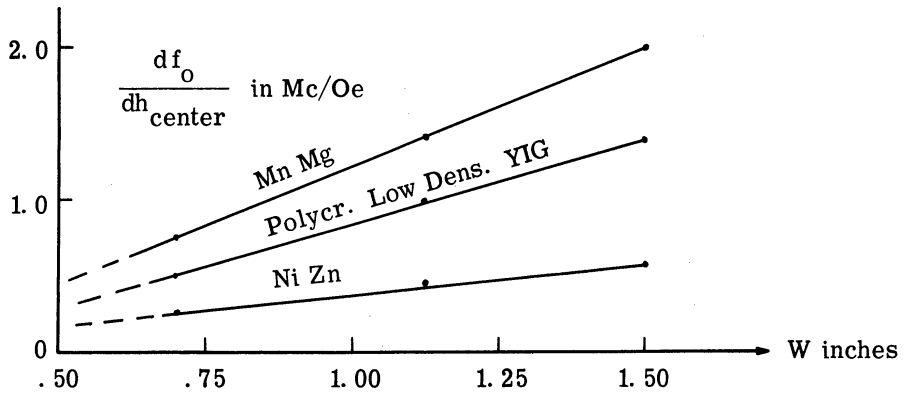

Fig. 6-8. Plot of tuning rate vs. width w for 3 common ferrites.

A similar measurement was made of $d\omega_o/dh$ vs. sample length; the results are shown in Fig. 6-9.

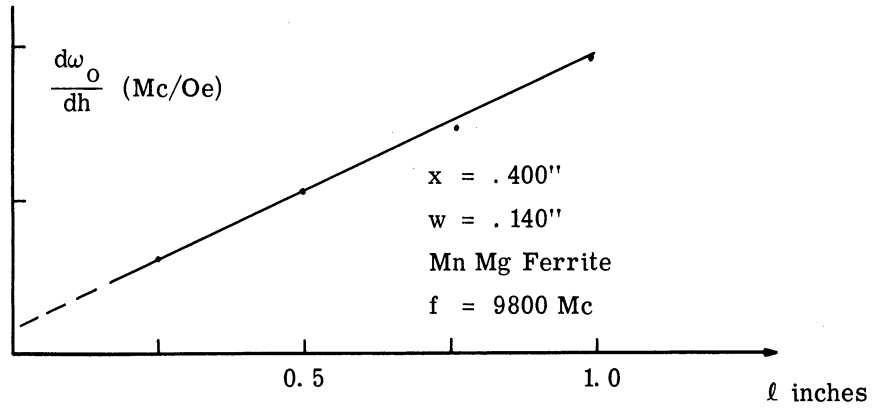

Fig. 6-9. Dependence of tuning rate upon sample length for Mn Mg ferrite at 9800 Mc.

This measurement was made using the bridge circuit of Fig. 6-7 and the previously described measurement procedure. Observe that the tuning rate tends to be proportional to length.

An explanation of the data reported in Fig. 6-9 can be found from our explanation of the phenomenon of resonance in the Reggia tunable filter. The filter is resonant at the frequency at which the susceptance of one shunt reflected to the location of the second short

tends to resonate with the latter. That is, the two obstacles tend to tune each other out at some frequency. The resonant electrical length for this effect ϕ is given by:

$$\phi = \gamma_1 \ell \tag{6.6}$$

where γ_1 is the effective propagation coefficient for the section of the waveguide. But it has already been shown that:

$$\frac{d\omega_o}{dh} = \beta_p \frac{d\phi}{dh}$$

$$= \beta_p \ell \frac{d\gamma_1}{dh} \tag{6.7}$$

For samples which are sufficiently thin, the bandwidth is determined by the sample width and is independent of length. The propagation constant depends upon material and is nearly independent of length. Thus, our explanation of the resonance phenomenon for the Reggia filter has correctly predicted that the tuning is proportional to sample length. According to the theory developed in the previous chapter, Mn Mg material has the largest $d\omega_o/dh$ because it has the largest $\partial x/\partial h$. Measurement of this material shows that $\frac{\partial x}{\partial h} \cong 0.004/\text{Oe}$. However, it has been reported by Weiss (Ref. 35) that a Mn Mg ferrite which has a low coercive force has been developed for which:

$$\frac{\partial x}{\partial h} = .07/\text{Oe}$$

Assuming the explanation of the dependence of $d\omega_o/dh$ upon material parameters is correct, the tuning rate for this material is 15 times as large as the measured value for the low-density Mn Mg ferrite. This material was not available for the measurements reported in Fig. 6-8 so no check on this prediction has been made. However, the calculation of the optimum ferrite phase-shift amplifier assumes that this value is correct; should this configuration prove to be promising, experimental verification would be warranted.

6.2.2 Optimum Threshold. Using the information which we have gained about the dependence of the factors of P_{th} upon the sample parameters, it should be possible to find the optimum design by finding the minimum value for the quantity

$$\frac{P_{th}}{\beta_i} = \frac{\beta_p^2 \int \mu |f(\bar{r})|^2 \, dv}{2\zeta \left(\frac{d\omega_o}{dh}\right)^2}$$

$$\frac{P_{th}}{\beta_i} \geq \frac{\beta_p^2 \mu_o v_s}{2\zeta \left(\frac{d\omega_o}{dh}\right)^2} \tag{6.8}$$

The circuit is optimized by the same set of conditions which minimize the right-hand side of the inequality. The proper material for this minimum was shown to be the Mn Mg ferrite reported by Weiss (Ref. 35) because $\frac{d\omega_o}{dh}$ is largest for that material. It has been shown that $\frac{d\omega_o}{dh}$ is approximately proportional to sample length and, of course, v_s is proportional to length. Assuming, then, that β_p is independent of length, the threshold is minimized by the longest possible sample length. However, the length is determined by the desired pump frequency and sample width. Thus, there is an optimum sample width for which P_{th} is minimized. Although the exact form of $\beta_p(w)$ is not known, it is possible to approximate β_p near its minimum by the relation:

$$\beta_p \sim \frac{b+w^2}{w} \tag{6.9}$$

Then, because both v_s and $\frac{d\omega_o}{dh}$ are proportional to w, the threshold is proportional to:

$$P_{th} \sim \frac{(b+w^2)^2}{w^3} \tag{6.10}$$

which is minimized by the condition:

$$w = \sqrt{b} \tag{6.11}$$

But this is the same width which minimizes β_p. Thus, the optimum width is that for which the pump bandwidth is minimized. In summary, it has been found that the optimum phase-shift amplifier uses the Mn Mg ferrite reported by Weiss of the dimensions:

x = height of waveguide

ℓ = greatest length for desired f_o

w = width which minimizes β_p.

The optimum threshold for the Reggia tunable filter configuration is found by substituting these values into the expression

$$\frac{P_{th\,m}}{\beta_i} = \frac{\beta_p^{\,2}\,\mu_s\,v_s}{2\,\zeta\left(\frac{d\omega_o}{dh}\right)^2} \tag{6.12}$$

But for minimum β_p, w is approximately 0.200", at which $\beta_p \cong 50$ Mc and ℓ for resonance at 9050 Mc = 0.500". The initial permeability μ_s for the low density Mn Mg material reported by Weiss is:

$$\mu_s \cong 100$$

Then, assuming the maximum detection efficiency (i.e., $\zeta = \frac{1}{2}$) the threshold is given by:

$$\frac{P_{th\,m}}{\beta_i} = 220 \text{ watts/Mc} \tag{6.13}$$

The same calculation was made for the low-coercive-force Mn Mg material reported by Weiss. The result is approximately

$$\frac{P_{th\,m}}{\beta_i} \cong 1 \text{ watt/Mc}$$

It was shown in the preceding chapter that if either the pump or signal circuit bandwidth is much larger than the other, then the smaller tends to limit the overall circuit bandwidth. The phase-shift amplifier which uses the Reggia tunable filter is clearly input-bandwidth limited for all pump powers below the kilowatt range. In addition, the actual threshold per unit bandwidth is greater than $P_{th,\,m}/\beta_i$ because

$$\int \mu\,|f(\bar{r})|^2\,dv \gg \mu_o\,v_s \tag{6.14}$$

for any physically realizable configuration. Nevertheless $P_{th,\,m}$ is a useful number for estimating the performance which can be expected from ferrite phase-shift amplifiers of this type.

6. 2. 3 An Experimental Model. As a comparison with this optimum circuit, an experimental phase-shift amplifier was constructed consisting of a ferrite block in a reduced-height waveguide. The signal-frequency coil was wound around a ferrite core and mounted coaxial with the sample outside the waveguide as shown in Fig. 6-1. The sample was a rectangular block of low-density Mn Mg ferrite of dimensions:

ℓ = 0. 400"

x = 0. 200" = height of waveguide also

w = 0. 175"

f_o = 9350 Mc

β_p = 120 Mc

The measured threshold input bandwidth relation was:

$$P_{th} = 30 \text{ watts/KC } \beta_i(\text{KC})$$

for which

$$\frac{P_{th}}{\beta_i} = 150\ \frac{P_{th\ m}\ (\text{Mn Mg})}{\beta_i} \qquad (6.\ 15)$$

Although this circuit is not optimum with respect to sample dimensions, this is not the principal reason for the large disparity between P_{th} and $P_{th,\,m}$. The latter comes largely from the fact that the magnetic circuit of the signal frequency circuit is not optimum and that a large magnetic energy must be stored at the signal frequency to produce sufficient signal field in the sample. This large energy is responsible for reducing the input circuit bandwidth. A redesign of the signal circuit is necessary before the actual threshold per unit bandwidth is of the order of $P_{th,\,m}/\beta_i$. However, even if such a design could be developed, and $P_{th,\,m}$ could be approached, the resulting phase-shift amplifier would require such large pump powers for reasonable bandwidth that this configuration must be considered impractical.

6.3 Distributed Ferrite Phase-Shift Amplifier

It was shown in Chapter 2 that the optimum double sideband up-converter is a phase modulator, the double sideband amplifier being given the name phase-shift amplifier for this reason. This is also the reason that the essential function of ferrites in phase-shift amplifiers is to effect phase modulation. Thus it is natural to search for the ferrite configuration which tends to produce the largest phase shift for a given applied field. Perhaps the most prominent of these configurations is the one developed by Reggia and Spencer (Ref. 41). It is a distributed circuit in which the propagation coefficient is varied by means of an applied field and is an interesting contrast to the configuration of the preceding section.

Although it can be argued properly that the Reggia filter of the previous section is, in reality, a distributed circuit, it is clear that the effect of the ferrite block can be represented by a lumped resonant circuit at some reference plane. However, no such lumped-parameter equivalent circuit is possible for the Reggia-Spencer phase-shifter. The prototype model is shown in Fig. 6-10 and consists of a section of waveguide which contains a cylindrical ferrite rod located coaxial with the waveguide. The ends are tapered to facilitate impedance matching. A coil is wound around the guide in such a way that it can produce an axial magnetic field along the rod. The phase shift across the section is varied by means of this applied field due to its control over the material parameters.

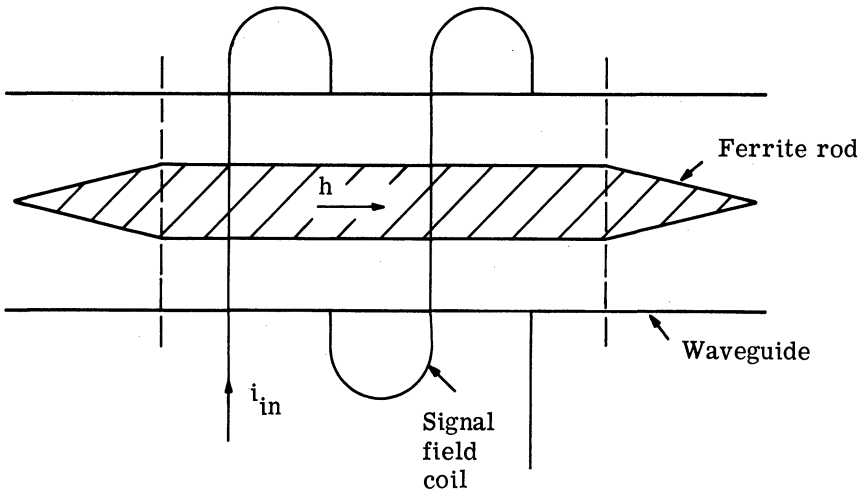

Fig. 6-10. Prototype model of distributed phase modulator useful for phase-shift amplification.

6. 3. 1 Threshold Relation for the Reggia-Spencer Configuration. If pump power is propagated through this section to a matched phase detector, and if the signal power is supplied to the coil, then the configuration is a phase-shift amplifier. However, because the structure is nonresonant, the concept of tunability and the threshold relation derived in Section 6. 1 are not applicable for the amplifier's description. On the other hand, it is meaningful to compute the quantity $\frac{d\phi}{dh}$ (where ϕ = electrical length of the section) which can properly be called the phase sensitivity of the section. The phase sensitivity is important for the determination of a convenient threshold formula for this configuration. For this purpose it can be shown that the transducer gain is given by:

$$G_t = \frac{2\zeta \left(\frac{d\phi}{dh}\right)^2 P_p}{\beta_i \int \mu |f(\bar{r})|^2 \, dv} \tag{6. 16}$$

where all of the symbols have their usual meaning. From this the threshold can be determined:

$$P_{th} = \frac{\beta_i \int \mu |f(\bar{r})|^2 \, dv}{2\zeta \left(\frac{d\phi}{dh}\right)^2} \tag{6. 17}$$

Thus the significance of the phase sensitivity parameter has been established.

Optimization of the threshold with respect to material parameters requires a knowledge of the dependence of the phase sensitivity upon these parameters. However, because of the nonuniformity of the Reggia-Spencer structure along its axis, it is difficult to determine the functional relation between phase sensitivity and material parameters. On the other hand, this functional relation can be found for sections of infinite uniform structure whose cross section is the same as the Reggia-Spencer cross section at the center. If the ends of our prototype model are suitably tapered, then its phase sensitivity is approximately the same as for an equal length of the infinite uniform structure. For this reason it is desirable to compute $\frac{d\phi}{dh}$ for the infinite structure.

6. 3. 2 Determining Phase Sensitivity. The phase sensitivity for the infinite structure can be found from the relation:

$$\frac{d\phi}{dh} = \ell \frac{d\beta}{dh}$$

where β is the complex propagation constant which can easily be found in the following way. Let $\overline{E}_1$ and $\overline{H}_1$ be the fields in the uniform waveguide for the value of the applied field h_1.* Similarly, let $\bar{\bar{\mu}}_1$ and β_1 be the permeability and propagation constant for that field. Further, quantities $\overline{E}_2$, $\overline{H}_2$, $\bar{\bar{\mu}}_2$ and β_2 can be associated with an applied field h_2. It is useful to start with the following quadratic relation which contains β_1 and β_2 explicitly (where $\frac{\partial E_i}{\partial z} = \beta_i E_i$ etc.):

$$\nabla_t \cdot (\overline{E}_{2t} \times \overline{H}_{1t}^* + \overline{E}_{1t}^* \times \overline{H}_{2t}) - i(\beta_2 - \beta_1) \quad \overline{E}_{2t} \times \overline{H}_{1t}^* + \overline{E}_{1t}^* \times \overline{H}_{2t}$$

$$+ i\omega \quad \overline{H}_1^* \cdot (\bar{\bar{\mu}}_2 \cdot \overline{H}_2) - \overline{H}_2 \cdot (\bar{\bar{\mu}}_1 \cdot \overline{H}_1)^* \quad = 0 \qquad (6.18)$$

Here the subscript t refers to the components transverse to the waveguide axis. The parameters β_2 and β_1 can be expressed in known quantities if this quadratic relation is integrated over a normal cross section. Using Gauss' two-dimensional theorem, this integration can be written:

$$\int_L \overline{E}_{2t} \times \overline{H}_{1t}^* + \overline{E}_{1t}^* \times \overline{H}_{2t} \cdot n_o \, dL - i(\beta_2 - \beta_1) \int_{S_g} (\overline{E}_{2t} \times \overline{H}_{1t}^* + \overline{E}_{1t}^* \times \overline{H}_{2t}) \cdot n \, ds$$

$$+ i\omega \int_{S_m} \overline{H}_{1t}^* \cdot (\bar{\bar{\mu}}_2 \cdot \overline{H}_{1t}) - \overline{H}_{2t} \cdot (\bar{\bar{\mu}}_1 \cdot \overline{H}_{1t})^* \, ds = 0 \qquad (6.19)$$

where S_g is the waveguide cross section and S_m is the cross section of the material. L is the curve formed by the intersection of S_g with a plane cross section of the waveguide. The first term is zero due to the boundary conditions at the waveguide wall. Since for our applications only small changes in the applied field will occur, it is of interest to consider the above equation for the condition $h_2 = h_1 + \delta h$. In this case $\bar{\bar{\mu}}_2 = \bar{\bar{\mu}}_1 + \delta\bar{\bar{\mu}}$, $\beta_2 = \beta_1 + \delta\beta$, $\overline{E}_2 = \overline{E}_1 + \delta\overline{E}$, $\overline{H}_2 = \overline{H}_1 + \delta\overline{H}$ for which the above equation can be written, correct to first order, in the form

---

*At the signal frequency.

$$2\,i\,\delta\,\beta\,\mathrm{Re}\int_{S_g}\bar{E}_{1t}\times\bar{H}_{1t}^{*}\cdot n\,dS = i\,\omega\int_{S_m}\bar{H}_{1t}^{*}\cdot\mu_2\cdot\bar{H}_2-\bar{H}_{2t}\cdot(\mu_1\cdot\bar{H}_1)^{*}\,ds$$

$$\delta\beta = \frac{\omega}{2}\,\frac{\int_{S_m}\bar{H}_{1t}^{*}\cdot(\bar{\bar{\mu}}_2\cdot\bar{H}_{2t})-\bar{H}_{2t}\cdot(\bar{\bar{\mu}}_1\cdot\bar{H}_1)^{*}\,ds}{\mathrm{Re}\int_{S_g}(\bar{E}_{1t}\times\bar{H}_{1t}^{*}\cdot n)\,ds} \tag{6.20}$$

The special case of interest here is $h_1 = 0$, for which the permeability is a scalar and is nearly real for low-loss ferrites. The above expression then reduces to:

$$\delta\beta = \frac{\omega}{2}\,\frac{\mu_o}{Z_o}\,\frac{\int_{S_m}\delta x'\,|H_{1t}|^2\,ds}{\int_{S_g}|H_{1t}|^2\,ds}$$

where Z_o is the wave impedance of the fields E_{1t}, H_{1t}, and x' is the real part of the diagonal component of the susceptibility tensor. * The change in the propagation constant is real, which means that varying the applied magnetic field introduces a phase shift across a length ℓ of $\delta\phi = \ell\,\delta\beta$. The phase sensitivity $\frac{d\phi}{dh}$ is given by the relation:

$$\frac{d\phi}{dh} = \frac{\ell\,\omega\,\mu_o}{2\,Z_o}\,\frac{\int_{S_m}\frac{\partial x'}{\partial h}\,|H_{1t}|^2\,ds}{\int_{S_g}|H_{1t}|^2\,ds} \tag{6.21}$$

which, when far above cutoff for the mode E_1, H_1 reduces to:

$$\frac{d\phi}{dh} \cong \frac{2\pi\ell}{2\lambda_m}\,\frac{\int_{S_m}\frac{\partial x'}{\partial h}\,|H_{1t}|^2\,ds}{\int_{S_g}|H_{1t}|^2\,ds} \tag{6.22}$$

---

*Here we use the simplified notation for this component.

Assuming the signal field δh is uniform throughout the sample, and that the sample is located where the fields are largest, then the above reduces even further to:

$$\frac{d\phi}{dh} \cong \frac{\pi \ell}{\lambda_m} \frac{\partial x'}{\partial h} \tag{6.23}$$

where it was assumed that the fields are confined largely to the material. Observe that the phase sensitivity depends upon the diagonal component of susceptibility but is independent of the off-diagonal component to first order. That is, the phase-shift property is independent of the nonreciprocal nature of ferrites. This same effect was observed independently by Weiss (Ref. 35) in a phenomenological theory of the operation of the Reggia-Spencer phase-shifter.

The phase shift per unit length is the parameter which best characterizes a particular material and sample design. This quantity is largest under the condition for which Eq. 6.23 is valid. Using the largest published value for $\frac{\partial x'}{\partial h}$ (Mn Mg ferrite reported by Weiss) the maximum phase sensitivity per unit length is given by:

$$\frac{1}{\ell} \frac{d\phi}{dh}\Big|_{max} = \frac{\pi}{\lambda} \frac{\partial x'}{\partial h}\Big|_{max}$$

$$\cong \frac{0.31}{\lambda_m} \tag{6.24}$$

where λ_m is the wavelength in the material. For most Mn Mg ferrites, $\epsilon = 16$ and $\mu = 1$, so $\lambda_m = \frac{\lambda f_s}{\sqrt{\mu\epsilon}} = 0.75$ cm $= 0.3$ in. Thus

$$\frac{1}{\ell} \frac{d\phi}{dh}\Big|_{max} = 1.1 \text{ rad/Oe}$$

$$= 60^{\circ}/\text{Oe} \tag{6.25}$$

This value compares well with the largest observed value (20°/inch Oe) (Ref. 41).

6.3.3 Dependence of Phase Sensitivity on Sample Parameters. The measurements of Reggia and Spencer tend to support Eq. 6.22 and the validity of the assumption leading to Eq. 6.23. The quantity which we have called phase sensitivity

$$\frac{d\phi}{dh}$$

is approximately proportional to length for rods of a fixed diameter and of a given material. The phase sensitivity near h = 0 is plotted in Fig. 6-11 from the data of Reggia and Spencer.

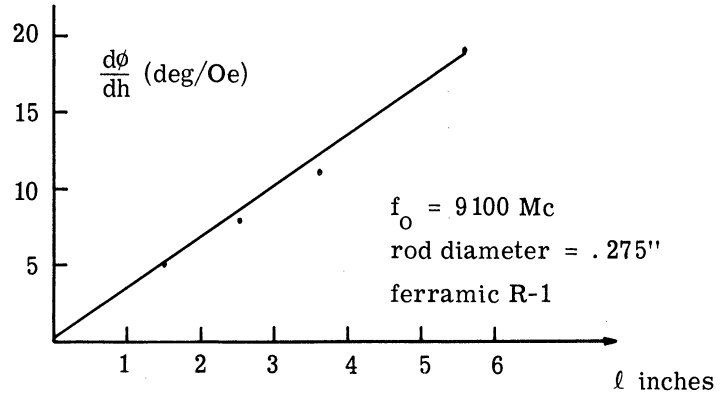

Fig. 6-11. Phase sensitivity vs. sample length.

Equation 6.22 predicts that the phase sensitivity also depends upon the cross-sectional area of the rod relative to the cross-sectional area of the waveguide. If the field H_1 were uniformly distributed across Sg, then formula 6.22 would reduce to:

$$\frac{d\phi}{dh} = \frac{\pi \ell}{\lambda_m} \frac{S_m}{S_g} \frac{\partial x'}{\partial h}$$

However, Reggia and Spencer have shown that the fields tend to be concentrated in the ferrite, so that the actual ratio of the integrals exceeds S_m/S_g. Figure 6-12 illustrates the dependence of phase sensitivity upon the ratio of the areas, S_m/S_g. Notice that the curve levels out for $S_m/S_g \gtrsim 0.20$. This can be explained by observing that the fields are not uniformly distributed throughout the waveguide cross section but tend to be largest in the material. This tendency increases as S_m/S_g increases until at some value of this ratio:

$$\frac{\int_{S_m} |H_1|^2 \, dv}{\int_{S_g} |H_1|^2 \, dv} = 1$$

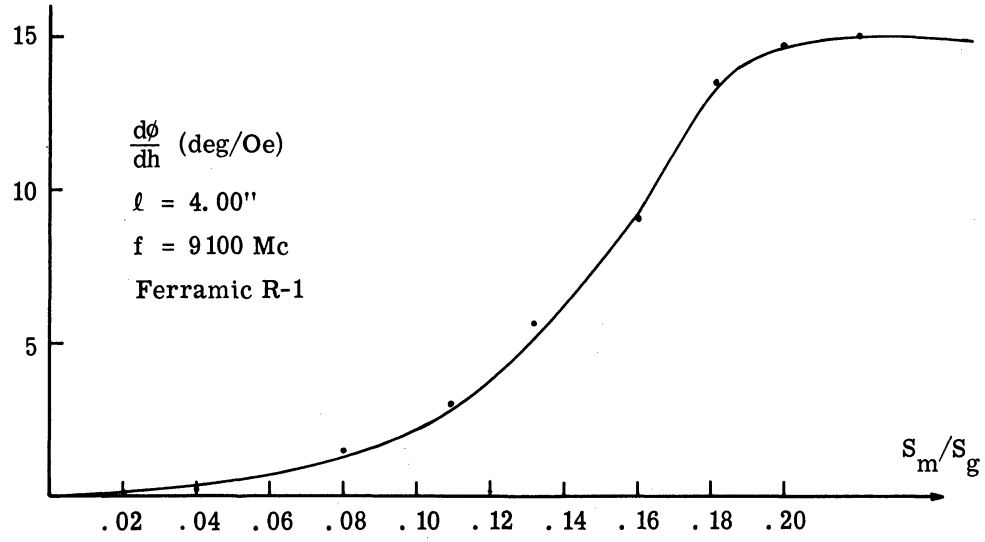

Fig. 6-12. Phase sensitivity vs. the ratio of the cross-sectional areas of material and waveguide.

In the experiments of Reggia and Spencer this effect occurs for $S_m/S_g = 0.20$. An experimental Reggia and Spencer phase-shifter was build and tested which consists of a rod whose cross-sectional area $S_m = 0.18\, S_g$. Thus the approximate relation (6.23) is valid for this experimental circuit.

In addition to the dependence upon length and cross-sectional area, and phase sensitivity of a Reggia-Spencer phase-shifter depends upon frequency. According to Eq. 6.23 $\frac{d\phi}{dh}$ is proportional to frequency. This result tends to be supported experimentally by Reggia and Spencer.

6.3.4 Experimental Measurement of Phase Sensitivity. The validity of the expression (6.23) for phase sensitivity was tested for the experimental Reggia-Spencer phase-shifter. This device consists of an 8" ferrite rod of 0.275" diameter which is placed along the axis of a section of waveguide. A coil was wound around the waveguide so as to produce

an axially-directed, applied magnetic field h. The rod is tapered at both ends for impedance-matching purposes, which tends to make the section resemble electrically a section of the infinitely-long prototype model. The rod material was manganese-magnesium ferrite for which $\left.\frac{\partial x'}{\partial h}\right|_{h=0} \cong 0.004/\text{Oe}$. The permittivity of the material is high (≈ 16) and the permeability is nearly unity, so the wavelength in the material will be of the order of $\lambda_m \cong \frac{\lambda_{space}}{4}$, which at 10 kMc is about 0.75 cm. Using these values, the phase-shift sensitivity was computed:

$$\frac{d\phi}{dh} = \left(\frac{20\pi}{0.75}\right) \quad 0.004/\text{Oe}$$

$$\cong 0.4 \text{ rad/Oe} \tag{6.27}$$

The measured value was 0.25 rad/Oe, in close agreement with our prediction, considering the rather crude approximations which were made.

6.3.5 Optimum Threshold for the Reggia-Spencer Configuration. It is possible to use the information which has just been gained about the dependence of phase sensitivity upon material parameters to estimate the optimum threshold $P_{th,\,m}$

$$\frac{P_{th,\,m}}{\beta_i} = \frac{\mu_s v_s}{2\,\zeta \left(\frac{d\phi}{dh}\right)^2} \tag{6.28}$$

In this expression the integral

$$\int \mu \, |f(\bar{r})|^2 \, dv$$

has been replaced by its minimum value, which is appropriate for determining the optimum threshold.

The threshold can be optimized with respect to sample dimensions by noting that

$$v_s = S_m \ell$$

The numerator of (6.28) is smallest for the smallest S_m but the denominator is minimized for the largest $\frac{d\phi}{dh}$ which also depends upon S_m. Examination of Fig. 6-13 reveals that the threshold is minimized for $S_m/S_g = 0.2$.

Since the threshold also tends to be inversely proportional to length, it might appear that the optimum threshold occurs for infinite length. However, there is another effect which influences this conclusion which has been neglected to this point. The sideband power produced by the phase modulator is attenuated by the losses in the material. For a sample of length ℓ the attenuation is $\ell^{-2\alpha\ell}$ where α is the attenuation constant of the guide. For this reason the threshold power is proportional to $e^{2\alpha\ell}\ \ell^{-1}$. This function is minimized for length:

$$\ell_m = \frac{1}{2\alpha}$$

$$= \frac{4.3}{I_\ell}$$

where I_ℓ is the insertion loss per unit length. The optimum length for this configuration is ℓ_m, and the optimum cross-sectional area is 0.20 S_g. The insertion loss of the experimental phase-shifter is about 0.2 db, for which the optimum length is about 20 in. Using these values, the threshold for the optimum configuration is given by:

$$\frac{P_{th,m}}{\beta_i} = \frac{e^1 \mu_s (0.2\ S_g)\ \ell}{\left(\frac{d\phi}{dh}\right)^2} \tag{6.29}$$

For the Mn Mg ferrite reported by Weiss $\left.\frac{d\phi}{dh}\right|_{\ell=20''} \cong 20$ rad/Oe, and $\mu \cong 100$, yielding

$$\frac{P_{th,m}}{\beta_i} = 1.5 \text{ watts/Mc} \tag{6.30}$$

For the Mn Mg ferrite used in the experimental amplifier $\left.\frac{d\phi}{dh}\right|_{20''} \cong 1$ rad/Oe, and $\mu_s \cong 50$, yielding

$$\frac{P_{th}}{\beta_i} = 670 \text{ watts/Mc} \tag{6.31}$$

6.3.6 Experimental Reggia-Spencer Amplifier. An experimental amplifier was constructed using the previously constructed experimental Reggia-Spencer phase-shifter. The threshold power was 200 mw and the input bandwidth was 0.4 kc. Thus:

an axially-directed, applied magnetic field h. The rod is tapered at both ends for impedance-matching purposes, which tends to make the section resemble electrically a section of the infinitely-long prototype model. The rod material was manganese-magnesium ferrite for which $\left.\frac{\partial x'}{\partial h}\right|_{h=0} \cong 0.004/\text{Oe}$. The permittivity of the material is high (≈ 16) and the permeability is nearly unity, so the wavelength in the material will be of the order of $\lambda_m \cong \frac{\lambda_{space}}{4}$, which at 10 kMc is about 0.75 cm. Using these values, the phase-shift sensitivity was computed:

$$\frac{d\phi}{dh} = \left(\frac{20\pi}{0.75}\right) \quad 0.004/\text{Oe}$$

$$\cong 0.4 \text{ rad/Oe} \tag{6.27}$$

The measured value was 0.25 rad/Oe, in close agreement with our prediction, considering the rather crude approximations which were made.

6.3.5 Optimum Threshold for the Reggia-Spencer Configuration. It is possible to use the information which has just been gained about the dependence of phase sensitivity upon material parameters to estimate the optimum threshold $P_{th,m}$

$$\frac{P_{th,m}}{\beta_i} = \frac{\mu_s v_s}{2\zeta\left(\frac{d\phi}{dh}\right)^2} \tag{6.28}$$

In this expression the integral

$$\int \mu \, |f(\bar{r})|^2 \, dv$$

has been replaced by its minimum value, which is appropriate for determining the optimum threshold.

The threshold can be optimized with respect to sample dimensions by noting that

$$v_s = S_m \ell$$

The numerator of (6.28) is smallest for the smallest S_m but the denominator is minimized for the largest $\frac{d\phi}{dh}$ which also depends upon S_m. Examination of Fig. 6-13 reveals that the threshold is minimized for $S_m/S_g = 0.2$.

Since the threshold also tends to be inversely proportional to length, it might appear that the optimum threshold occurs for infinite length. However, there is another effect which influences this conclusion which has been neglected to this point. The sideband power produced by the phase modulator is attenuated by the losses in the material. For a sample of length ℓ the attenuation is $\ell^{-2\alpha\ell}$ where α is the attenuation constant of the guide. For this reason the threshold power is proportional to $e^{2\alpha\ell}\ \ell^{-1}$. This function is minimized for length:

$$\ell_m = \frac{1}{2\alpha}$$

$$= \frac{4.3}{I_\ell}$$

where I_ℓ is the insertion loss per unit length. The optimum length for this configuration is ℓ_m, and the optimum cross-sectional area is $0.20\ S_g$. The insertion loss of the experimental phase-shifter is about 0.2 db, for which the optimum length is about 20 in. Using these values, the threshold for the optimum configuration is given by:

$$\frac{P_{th,m}}{\beta_i} = \frac{e^1 \mu_s (0.2\ S_g)\ \ell}{\left(\frac{d\phi}{dh}\right)^2} \tag{6.29}$$

For the Mn Mg ferrite reported by Weiss $\left.\frac{d\phi}{dh}\right|_{\ell=20''} \cong 20$ rad/Oe, and $\mu \cong 100$, yielding

$$\frac{P_{th,m}}{\beta_i} = 1.5 \text{ watts/Mc} \tag{6.30}$$

For the Mn Mg ferrite used in the experimental amplifier $\left.\frac{d\phi}{dh}\right|_{20''} \cong 1$ rad/Oe, and $\mu_s \cong 50$, yielding

$$\frac{P_{th}}{\beta_i} = 670 \text{ watts/Mc} \tag{6.31}$$

6.3.6 Experimental Reggia-Spencer Amplifier. An experimental amplifier was constructed using the previously constructed experimental Reggia-Spencer phase-shifter. The threshold power was 200 mw and the input bandwidth was 0.4 kc. Thus:

$$\frac{P_{th}}{\beta_i} = 2.5 \text{ watts/kc} \tag{6.32}$$

It is interesting to note that even though the sample geometry is not very close to optimum, the threshold per unit bandwidth is only about 4 times as large as its minimum computed value. This configuration approaches the optimum much more closely than the previous configurations primarily because the signal-frequency energy tends to be coupled more completely into the sample.

6.3.7 Comparison of Configurations of Sections 6.2 and 6.3. Another interesting comparison between this and the previous configuration is that the threshold of the former is about 3 orders of magnitude smaller than the latter. For an explanation of this result, it is convenient to compare the phase sensitivity for each. For the Reggia-Spencer circuit

$$\frac{d\phi}{dh} = 0.62/\text{Oe}$$

For the Reggia tunable filter we measured

$$\frac{d\phi}{dh} = \frac{1}{\beta_p}\frac{d\omega_o}{dh}$$

$$= 0.04/\text{Oe}$$

Perhaps an even more revealing comparison can be made on the basis of phase sensitivity per unit length:

$$\begin{aligned} &(1)\ \frac{1}{\ell}\frac{d\phi}{dh} = 0.03 \text{ for the Reggia-Spencer circuit} \\ &(2)\ \frac{1}{\ell}\frac{d\phi}{dh} = 0.08 \text{ for the Reggia tunable filter} \end{aligned} \tag{6.33}$$

This comparison suggests that the large threshold computed for the Reggia configuration of Section 6.2 is the result of its non-optimum sample length. It should be recalled that the sample length was chosen $\ell = 0.500''$ for the desired center frequency. However, it is clear that this is not the optimum length for the configuration.

6.3.8 The Tuned Reggia-Spencer Configuration. In this section it will be shown that the sensitivity of this circuit can be improved by reducing the excess pump bandwidth. The pump bandwidth can be reduced by placing reactances at either end of the Reggia-Spencer phase-shifter, thus making a tuned circuit. Note that this resonant structure is completely equivalent to the configuration discussed in Section 6.2. An equivalent circuit for the resulting structure is shown in Fig. 6-13, where $\phi(h)$ is the electrical length of the section which is a function of the applied field h. It will be convenient for analysis purposes to assume $B_1 = B_2$. Relatively little useful information is lost in this assumption. The effect of these obstacles on sensitivity, $\frac{d\phi}{dh}$, and on the pump bandwidth will be computed next.

Perhaps the most convenient analysis tool for microwave circuits is the signal-flow-graph technique. The signal-flow-graph is a method of writing a set of equations whereby the variables are represented by points and the interrelations by directed lines, enabling a direct picture of signal flow. The flow graph technique of circuit analysis is a somewhat

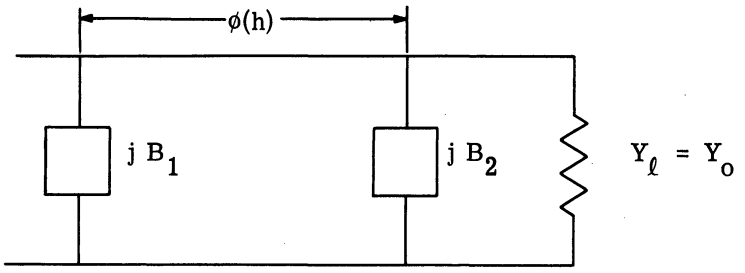

Fig. 6-13. Equivalent circuit for the tuned Reggia-Spencer phase-shifter.

more natural concept for distributed circuits than for lumped circuits because one's thinking in the former case is adapted to incident and reflected voltages rather than stationary voltages and currents. The points in a flow graph for a microwave circuit represent incident or reflected fields (or voltages) and the directed lines represent transfer functions between the adjacent reference planes at which these fields or voltages are measured. When microwave network equations are written in scattering matrix form, the corresponding flow graph is particularly useful because in this case the flow graph of a system of cascaded networks is

constructed simply by joining together the flow graphs of the individual networks. The algebra of flow graphs leading to solutions by direct inspection has been developed by S. J. Mason (Ref. 42). The solution is available directly by application of the non-intersecting loop rules developed by C. S. Lorens (Ref. 43).

The flow graph for the above equivalent circuit is shown in Fig. 6-14, where a_i and b_i are the amplitudes of the forward and backward traveling wave at location i, and where $\Gamma = -\frac{y}{2+y}$ with $y = \frac{Y}{Y_o}$. In all of our applications, the section is assumed to be terminated in a matched load for which $\Gamma_\ell = 0$. The transmission T from a_1 to b_4 is the quantity sought. From the standard flow graph solution, T is given by:

$$T = \frac{(1+\Gamma)^2 e^{-j\phi}}{1-\Gamma^2 e^{-2j\phi}} \tag{6.34}$$

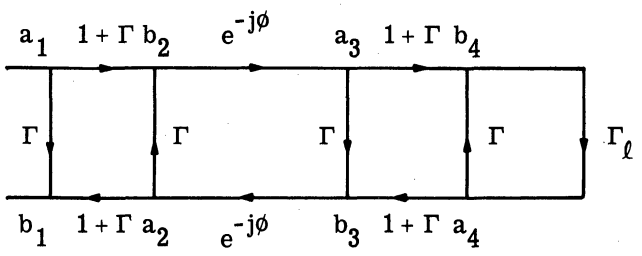

Fig. 6-14. Flow graph for tuned Reggia-Spencer phase-shifter.

where for $\frac{Y}{Y_o} = j\frac{B}{Y_o} = jb$, is given by:

$$\Gamma = -\frac{jb}{2+jb} \tag{6.35}$$

Then solving for T in terms of b:

$$T = \frac{e^{-j\phi}}{[1-(b^2/4)+jb] + (b^2/4)\csc 2\phi - j(b^2/4)\sin 2\phi} \tag{6.36}$$

This expression can conveniently be written in the form:

$$T = |T| e^{-j(\phi+\theta)} \tag{6.37}$$

where:

$$|T|^2 = \Big(1 + (b^2/2)(\cos 2\phi - 1) + (b^2/16)(\cos 2\phi - 1)^2 + b^2 [1 - (b/2)\sin 2\phi + (b^2/16)\sin^2 2\phi] \Big)^{-1}$$

$$= [1 + (b^2/2)(\cos 2\phi + 1) - (b^3/2)\sin 2\phi + (b^4/8)(1 - \cos 2\phi]^{-1} \qquad (6.38)$$

$$\tan\theta = \frac{b\left(1 - \frac{b}{4}\sin 2\phi\right)}{1 + (b^2/4)(\cos 2\phi - 1)} \qquad (6.39)$$

Substituting the identities:

$$1 + \cos 2\phi = 2\cos^2\phi$$

$$1 - \cos 2\phi = 2\sin^2\phi$$

Equation 6.38 can be written in the form:

$$|T|^2 = \frac{1}{1 + b^2\sin^2\phi\left(\frac{b}{2} - \cot\phi\right)^2}$$

or

$$= \frac{1}{1 + b^2\left(\frac{b}{2}\sin\phi - \cos\phi\right)^2} \leqq 1 \qquad (6.40)$$

If B is capacitive, both b and ϕ are linear functions of frequency and $|T|^2$ is a transcendental function of frequency as shown in Fig. 6-15.

The transmission vs. frequency is that of a series of bandpass filters whose center frequencies occur where $b(\frac{b}{2}\sin\phi - \cos\phi) = 0$. Any of these bandpass filters can be selected for the pump filter. If this tuned structure is to be used as a phase-shifter amplifier, the pump should be supplied at the center frequency of the pass band. It will be shown presently that maximum phase modulation results if this frequency condition is met. For high frequencies

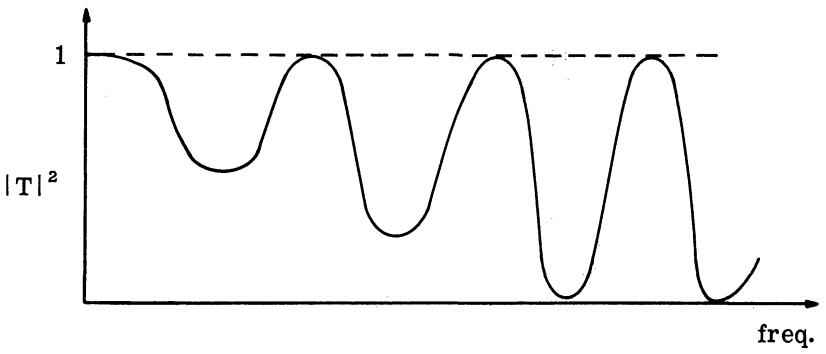

Fig. 6-15. Graph of $|T|^2$ vs. f assuming b and ϕ are both linear functions of frequency.

the center frequencies of adjacent pass bands will be spaced so that $\phi_{i,o} - \phi_{i+1,0} = \pi$ where $\phi_{i,o}$ is the electrical length at the center frequency ω_{io}. The bandwidth of each pass band can be found by solving the equation:

$$\frac{b}{2}^2 (b \sin\phi - 2\cos\phi)^2 = 1$$

$$\frac{b}{2} (b \sin\phi - 2\cos\phi) = \pm 1 \qquad (6.41)$$

for ω. A graphical solution illustrates the bandwidth associated with each (see Fig. 6-16).

$$G(\phi, b) = \frac{1}{(b \sin\phi - 2\cos\phi)} \qquad (6.42)$$

The poles of $G(\phi, b)$ are the center frequencies ω_{io}. The intersections of $G(\phi, b)$ and $\pm\frac{b}{2}$ define the band edges. Note that the bandwidths are narrower for higher center frequency. The actual bandwidth at the higher frequencies can be found more conveniently by examining the graphical solution to the reciprocal of the previous expression (see Fig. 6-17).

$$\frac{1}{G(\phi, b)} = \pm\frac{2}{b}$$

$$= b \sin\phi - 2\cos\phi \qquad (6.43)$$

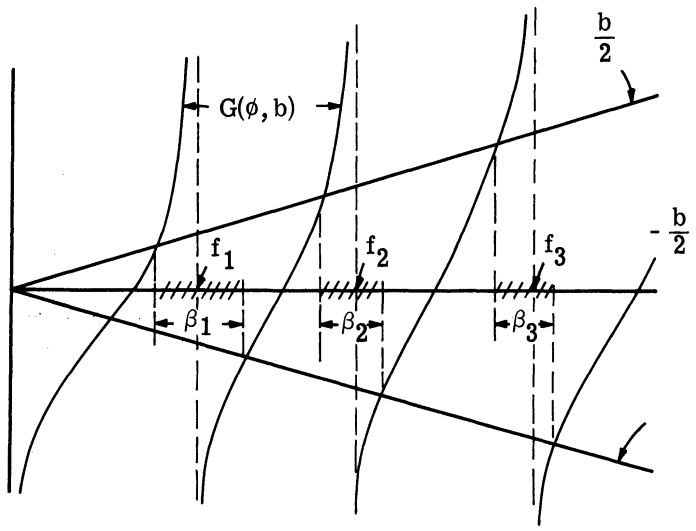

Fig. 6-16. Graphical representation of solution for bandwidth of the pass band of T.

For high enough pump frequency at a given shunt capacitance, $b >> 2$ and $(b \sin\phi - 2\cos\phi) = b \sin\phi$. But near the center frequency ω_{oi} $\phi = \phi_{oi} + \Delta\phi$.

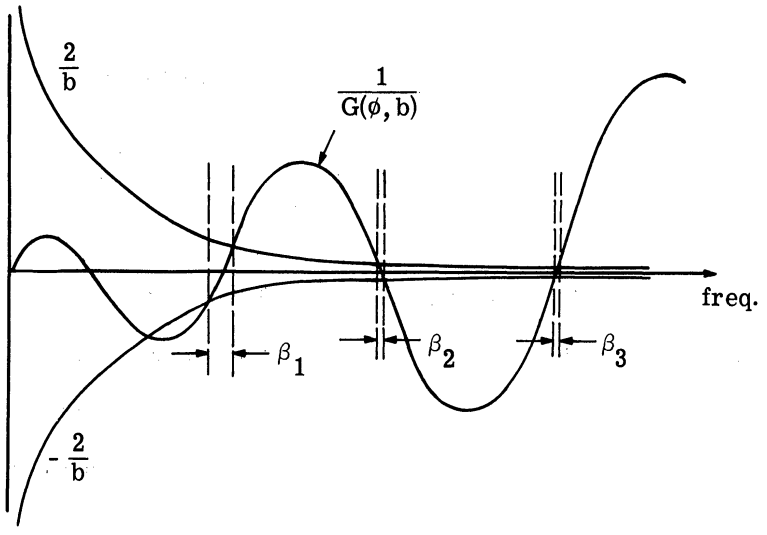

Fig. 6-17. Reciprocal graphical representation of functions in Fig. 6-16.

But

$$\phi = \frac{\phi_o \omega}{\omega_o}$$

so

$$\Delta\phi_i = \frac{\phi_o \Delta\omega_i}{\omega_{oi}} \quad \text{where } \Delta\omega_i = \omega_{oi} - \omega \tag{6.44}$$

Also near the center frequency ω_{oi}

$$\sin\phi_k = \sin(k\pi + \Delta\phi_k) = \sin\Delta\phi_k$$

$$\cong \Delta\phi_k \tag{6.45}$$

The approximate bandwidth condition is:

$$b_k \sin\Delta\phi_k = \pm\frac{2}{b_k}$$

For which

$$\frac{\phi_o \Delta\omega_k}{\omega_o} = \left.\frac{2}{b_k}\right|_{\omega_{ok}} \tag{6.46}$$

and

$$\beta_k = 2\Delta\omega_k = \left.\frac{4\omega_{ok}}{\phi_{ok} b^2}\right|_{\omega_{ok}} \tag{6.47}$$

Thus the bandwidth can be reduced by increasing the b or by selecting a longer sample for which ϕ_{ok} is larger. It will be shown next that reducing the excess pump bandwidth increases the total phase sensitivity.

The phase sensitivity for the reactively loaded Reggia-Spencer section is $\frac{d}{dh}(\phi + \theta)$ where:

$$\tan\theta = \frac{b - \frac{b^2}{4}\sin 2\phi}{1 + (b^2/4)(\cos 2\phi - 1)} \tag{6.48}$$

By a simple differentiation it can be shown that

$$\frac{d\theta}{dh} = -\frac{b^2}{4}\left[\frac{\frac{b^2}{4}(1-\cos 2\phi) - b\sin 2\phi + \cos 2\phi}{1 + \frac{b^2}{4}(b\sin\phi - 2\cos\phi)^2}\right]\frac{\partial\phi}{\partial h} \tag{6.49}$$

Then regrouping the terms slightly and factoring gives

$$\frac{\partial\theta}{\partial h} = -\frac{b^2}{2}\left[\frac{\frac{1-\cos 2\phi}{4}\left(b^2 - \frac{4b\sin 2\phi}{1-\cos 2\phi} + \frac{4(\cos 2\phi + 1)}{1-\cos 2\phi}\right) - 1}{1 + \frac{b^2}{4}(b\sin\phi - 2\cos\phi)^2}\right]\frac{\partial\phi}{\partial h} \tag{6.50}$$

but the factors have already been found for the quantity in brackets; i. e. ,

$$b^2 - \frac{4b\sin 2\phi}{1-\cos 2\phi} + \frac{4(\cos 2\phi + 1)}{1-\cos 2\phi} = (b - 2\cot\phi)^2 \tag{6.51}$$

also

$$\frac{1-\cos 2\phi}{4} = \frac{\sin^2\phi}{2} \tag{6.52}$$

Substituting these functions in the above expression gives:

$$\frac{\partial\theta}{\partial h} = \frac{b^2}{2}\left(\frac{1 - \frac{1}{2}(b\sin\phi - 2\cos\phi)^2}{1 + \frac{b^2}{4}(b\sin\phi - 2\cos\phi)^2}\right)\frac{\partial\phi}{\partial h} \tag{6.53}$$

Note that

$$1 - \frac{1}{2}(b\sin\phi - 2\cos\phi)^2 \leq 1$$

and

$$1 + \frac{b^2}{4}(b\sin\phi - 2\cos\phi)^2 \geq 1 \tag{6.54}$$

thus

$$\frac{\partial \theta}{\partial h} \leq \frac{b^2}{2} \frac{\partial \phi}{\partial h} \tag{6.55}$$

where the equality holds at each center frequency at which $(b \sin\phi - 2 \cos\phi) = 0$. Thus the phase sensitivity is improved most at each of the center frequencies where:

$$\frac{\partial \theta}{\partial h} = \frac{b^2}{2} \frac{\partial \phi}{\partial h} \tag{6.56}$$

Notice also that:

$$\lim_{b \to 0} \frac{\frac{\partial \theta}{\partial h}}{\frac{\partial \phi}{\partial h}} = 0$$

That is

$$\frac{\partial (\phi + \theta)}{\partial h}\Big|_{b=0} = \frac{\partial \phi}{\partial h} \tag{6.57}$$

$$\lim_{b \to \infty} \frac{\frac{\partial \theta}{\partial h}}{\frac{\partial \phi}{\partial h}} = -1 \text{ except at the center frequencies .}$$

That is, $\lim_{b \to \infty} \frac{\partial (\phi + \theta)}{\partial h} = 0$ which must clearly be the case since $b \to \infty$ is the case of a shorted waveguide section for which varying h can have no effect on the phase of the transmitted signal.

At each center frequency the total sensitivity will be improved by the factor $1 + \frac{b^2}{2}$ or:

$$\frac{\partial (\phi + \theta)}{\partial h} = \left(1 + \frac{b^2}{2}\right) \frac{\partial \phi}{\partial h} \tag{6.58}$$

If this increased sensitivity is substituted in the expression for optimum threshold there results:

$$P_{th,m} = \frac{\beta_i \mu_s v_s}{2 \zeta \left(1 + \frac{b^2}{2}\right)^2 \left(\frac{d\phi}{dh}\right)^2} \tag{6.59}$$

But it has already been shown that b^2 is inversely proportional to pump bandwidth, so it can be concluded that reducing the pump bandwidth by tuning this structure improves the threshold. In this way it has been shown that a tuned r-f structure is optimum for ferrite phase-shift amplification.

It is illustrative to compute the optimum threshold for this configuration under the condition that the pump bandwidth is the same as that used in the calculation of the optimum for the Reggia tunable-filter configuration. From Eq. 6.45, the bandwidth can be related to b^2. For the experimental Reggia-Spencer phase-shifter, $\beta = 50$ Mc corresponds to $b^2 = 8$. Thus

$$\left(1 + \frac{b^2}{2}\right)^2 = 25$$

and the optimum threshold is given by:

$$\frac{P_{th,m}}{\beta_i} = \frac{\mu_s v_s}{25\left(\frac{d\phi}{dh}\right)^2} \tag{6.60}$$

which, upon substitution of the appropriate optimum values yields

$$\frac{P_{th,m}}{\beta_i} = 60 \text{ mw/Mc} \tag{6.61}$$

The threshold of the experimental configuration in this circumstance is:

$$\frac{P_{th,m}}{\beta_i} = 100 \text{ w/Mc} \tag{6.62}$$

The disparity between these two thresholds can be attributed to the inefficient coupling of the signal into the sample and to the relative insensitivity of the material in the experimental model.

A comparison between the optimum threshold per unit bandwidth of this configuration and that discussed in Section 6.2 is meaningful because of the basic similarity of the models. The superiority of the present case can be attributed to its near optimum length.

6.4 Use of Samples Operating Near Ferromagnetic Resonance

It has already been demonstrated that ferrite permeability tends to depend strongly upon the applied magnetic field, optimizations occurring near zero applied field and near ferromagnetic resonance. The two configurations considered so far have met the former condition; it is of interest now to consider taking advantage of the latter. Perhaps the simplest configuration in which ferromagnetic resonance can be excited as shown in Fig. 6-18 and is the same as that used for the tunability measurements reported in the previous chapter.

A circularly cylindrical microwave cavity is excited from a waveguide by means of a Bethehole coupler. The hole is properly located so that circularly polarized fields are excited. Though it is not necessary for the fields to be circularly polarized, it was convenient to use a cavity prepared for the measurements of the previous chapter.

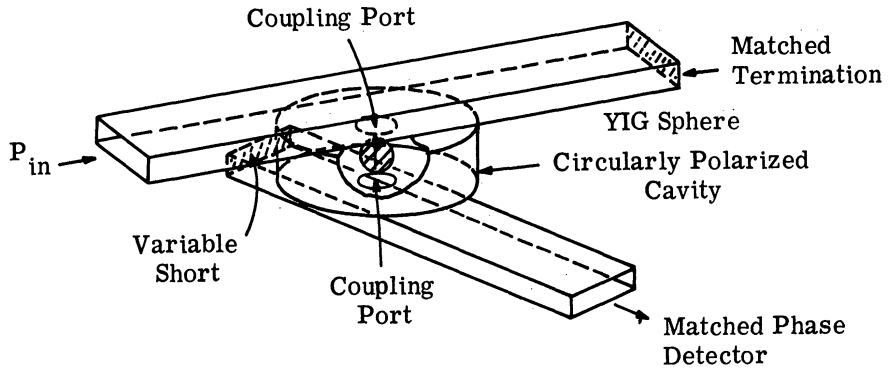

Fig. 6-18. Illustration of the experimental ferromagnetic resonance phase-shift amplifier.

It was shown in the previous chapter that the cavity tunability for such a structure operating near ferromagnetic resonance reaches a maximum value of $\frac{\gamma}{\omega_o}$, provided the fields have the optimum orientation (i. e., pump field transverse to the biasing field and signal field parallel to the biasing field) and provided the sample is sufficiently large relative to the cavity. It is of interest to compute the threshold power for this configuration and compare its optimum with that of the configurations discussed previously in this chapter.

6.4.1 Threshold Relation. The threshold pump power P_{th} is given by

$$P_{th} = \frac{\beta_i \beta_p^2 \int \mu |f(\bar{r})|^2 dv}{2 \zeta \gamma^2} > \frac{\beta_i \beta_p^2 \mu_o v_s}{2 \zeta \gamma^2} \tag{6.63}$$

The optimum threshold is given by the right-hand side of the inequality as usual.

The pump bandwidth of this circuit is determined more by the cavity design than by the material because the sample is very small and because the maximum tuning occurs far enough from ferromagnetic resonance that the ferrite losses tend to be small. For a properly machined cavity with plated surfaces, the unloaded Q can be as high as about 10^4. However, the actual cavity will be loaded rather heavily in order to couple most of the sideband power into the load. The loaded Q of the cavity which was used in the experiments of the last chapter was about 1000 at x-band, for which $\beta_p \cong 10$ Mc.

6.4.2 The Optimum Threshold. The optimum threshold for this bandwidth can be computed by observing that the sample is saturated, for which:

$$\mu_s = \mu_o$$

and:

$$\int \mu_s |f(r)|^2 dv\Big|_{min} = \mu_o v_s$$

where we will assume that the sample volume is the minimum for which $T = \frac{\gamma}{f_o}$ as found in the preceding chapter:

$$v_s \cong 10^{-5} v_c$$

For the cavity used in the experiments of Chapter 5, $v_c \cong 1.2 \times 10^{-6}$ m^3. Under these conditions the minimum threshold is given by:

$$\frac{P_{th,m}}{\beta_i} = 0.1 \text{ mw/Mc} \tag{6.64}$$

Although the sample size is not optimum, it is useful to compute the minimum threshold for the .100" sphere of YIG which was used in the measurements of Section 5.5.3.

For this sample the optimum threshold is given by:

$$\frac{P_{th,m}}{\beta_i} = 1 \text{ mw/Mc} \quad \text{for .100" YIG sphere} \tag{6.65}$$

An experimental amplifier circuit was constructed using the 100" diameter sphere of YIG as described above, located in a resonant circularly polarized x-band cavity ($Q \cong 1000$). The signal coil consists of 30 turns wound in the form of a flat circular coil of radius 0.6 cm. The measured input bandwidth of this circuit is 100 kc with a pump threshold of 1 watt and a pump bandwidth of 10 Mc. Thus the threshold per unit input bandwidth is given by:

$$P_{th} = 10 \text{ watts/Mc } \beta_i(\text{Mc}) \tag{6.66}$$

6.4.3 Comparison of Optimum and Experimental Thresholds. The disparity between the optimum threshold and the observed experimental threshold can be attributed to the inefficiency with which signal energy is coupled to the sample. To expand this explanation, consider the relation

$$\int \mu \, |f(\bar{r})|^2 \, dv = A \, \mu_o \, v_s \tag{6.67}$$

If the signal energy were perfectly coupled to the sample, A would be unity. This circumstance was assumed for the calculation of the optimum threshold. To account for the large difference between the experimental threshold and the optimum threshold A would have to be 10^4.

To test the assertion that the disparity of the threshold results from inefficient coupling the active signal field distribution for the experimental amplifier must be determined and used to compute A. The orientation and spacing of the sample and signal field coil of the experimental amplifier are shown in Fig. 6-19. The sample is located on the axis of the coil at a distance $x \cong a$. The assumption that f(r) is uniform throughout the sample is reasonable provided the sample is small compared to coil dimensions or is located at a large distance from the sample. It is shown in Appendix F that:

$$A \cong 9 \times 10^3 \tag{6.68}$$

Observe that this figure 9×10^3 compares favorably with the observed value 10^4 and our assertion is proved.

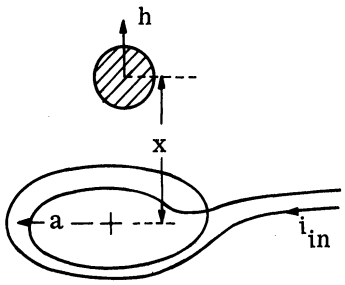

Fig. 6-19. Illustration of location of sample relative to signal coil in configuration of Fig. 6-19.

The calculation above has suggested that a more efficient means must be found for introducing the signal field into the sample without storing large amounts of signal energy, compared to the simple arrangement of Fig. 6-19. One possible configuration which satisfies this criterion employs a toroidal sample. The signal field for this shape tends to be confined to the sample. In this case most of the signal field which is produced is useful for tuning the cavity. However, there are severe practical difficulties which limit the use of such a sample shape. The most important of these is the difficulty of introduction of the pump field into the sample. Nevertheless, the possibility of a suitable design exists, so that the problem remains of developing a ferrite phase-shift amplifier which approaches the optimum.

6.5 Use of Ferromagnetic Resonance to Provide Pump Filter

Since ferrite samples possess an intrinsic resonance, it is not essential to place the sample in a cavity to separate the various sidebands. That is, ferromagnetic resonance provides a convenient filter for separating the upper and lower sidebands from other unwanted components. One possible filter is illustrated in Fig. 6-20. Three mutually perpendicular coils L_1, L_2, and L_3 are wound about the sample. Coupling between any pair of coils (e.g., L_1 and L_2) is zero unless a magnetic field is applied along the intersection of the plane of these two coils. This field biases the sample to ferromagnetic resonance. When

biased in this way, the nonreciprocal nature of the material will couple these otherwise uncoupled coils. Thus, the transmission from L_1 to L_2 is tuned at ferromagnetic resonance when a field H_o is applied of proper direction and strength. This circuit can be used as a nonreciprocal filter for signals transmitted between a source connected to L_1 and a load connected to L_2. The field of the third coil h_3 is parallel to H_o and causes variations in that field which tend to vary the frequency of ferromagnetic resonance. The tunability for this circuit is the same as the maximum tunability of the cavity described in the previous section (i. e., $\frac{\gamma}{\omega_o}$). Clearly this circuit can be used as a phase-shift amplifier if the pump is connected to L_1, the phase detector to L_2, and the signal to L_3.

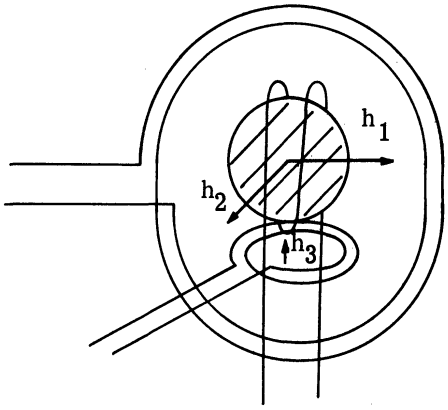

Fig. 6-20. Illustration of ferromagnetic resonance amplifier requiring no resonant cavity.

This circuit is similar in many respects to that described in the previous section in which the ferrite is used to tune a cavity. The tunability of this circuit is the same as the maximum tunability of the cavity (i. e., $T = \frac{\gamma}{\omega_o}$), and the minimum pump threshold is still given by:

$$P_{th,\,m} = \frac{\beta_i \beta_p{}^2 \mu_o v_s}{2\gamma^2} \tag{6.60}$$

Perhaps the most significant difference between the two circuits is the fact that the coupled-coil circuit operates exactly at ferromagnetic resonance, while the cavity tuning circuit

operates off ferromagnetic resonance. As a consequence of this, the material linewidth completely determines bandwidth in the former circuit and for this reason β_p can be no less than $\gamma\Delta H$. In the latter circuit, by contrast, the bandwidth can be controlled by controlling the cavity parameters.

6.6 Use of Magnetostatic Modes to Accomplish Pump Filtering

A circuit of the type described above can be designed having a pump bandwidth smaller than $\gamma\Delta H$. In particular, certain of the magnetostatic modes can be used to couple the r-f signals in the same way as ferromagnetic resonance. They have the advantage, however, of having a narrower linewidth. In some cases their linewidth is as little as one-third of the pump bandwidth; potentially, then, P_{th} can be reduced by a factor of 9 below the value obtained using ferromagnetic resonance. Such a tremendous improvement in input bandwidth can be important in circuits which tend to be input-bandwidth limited.

Although there are advantages to using magnetostatic modes in a phase-shift amplifier, there is also a difficulty in using them due to the problems of coupling energy into them. They tend to be excited most easily at their resonant frequency in the presence of highly nonuniform r-f fields. This idea can be exploited through the use of a transmission type filter such as that shown in Fig. 6-21. The ferrite sample is placed in a small hole which has been cut in the wall of guide No. 2, and a magnetic field is applied such that the

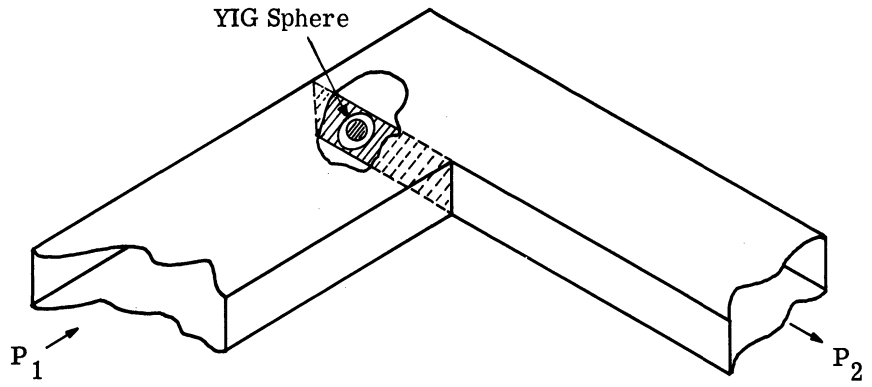

Fig. 6-21. Illustration of magnetostatic phase-shift amplifier.

sample can support magnetostatic modes. If power P_1 is supplied in guide No. 1, then the fields will be very nonuniform in the vicinity of the sample and for a frequency near the resonance of a magnetostatic mode the latter will be excited and energy will be coupled into guide No. 2. A bandpass transmission characteristic will exist from guide No. 1 to guide No. 2. As the biasing field is varied, the resonant frequencies of the magnetostatic modes vary at a maximum rate of 2.8 Mc/Oe. If a signal coil is now mounted so that the field which it produces is parallel to the biasing field, this structure can be used to make a phase-shift amplifier having a bandwidth smaller than $\gamma\Delta H$ and a sensitivity proportionately larger than that obtained for ferromagnetic resonance.

6.7 The Thin-Film Phase-Shift Amplifier

It was shown in the previous chapter that thin-film variable inductors are useful for the construction of phase-shift amplifiers. It was further shown that the equivalent circuit for the transverse winding of the prototype configuration is a resonant circuit whose resonant frequency is controlled by the current in the other winding. The proper use of the inductor in a phase-shift amplifier is shown in Fig. 5-14.

6.7.1 Threshold Relation for the Thin-Film Configuration. The threshold for this configuration is written most conveniently in the form:

$$P_{th} = \frac{R_s}{2\zeta (Q_\ell T_i)^2} \tag{6.70}$$

where

$$T_i = -\frac{1}{2L_2}\frac{dL_2}{di_1} \tag{6.71}$$

For the configuration of Fig. 5-13, T_i has a value of approximately 0.25/ma at ferromagnetic resonance. Recall that although this tunability is relatively large, the Q at resonance is approximately unity. It was previously suggested that, using certain techniques which yield a high-Q bulk ferrite, an improvement in thin-film Q by an order of magnitude should be possible. Assuming this can be accomplished (i.e., $Q \approx 10$) a pump bandwidth of approximately 40 Mc would be obtainable at a resonant frequency of 400 Mc. For the configuration reported

by Pohm, the inductance of the coil labelled L_1 is about 4 μh. Assuming the signal is supplied by a source with a 50 Ω output impedance the input bandwidth is given by

$$\beta_i = \frac{R_s}{2\pi L_1} \tag{6.72}$$

$$\cong 2 \text{ Mc}$$

and the threshold per unit bandwidth is

$$\frac{P_{th}}{\beta_i} \cong 0.01 \text{ mw/Mc} \tag{6.73}$$

6.7.2 Experimental Model. For the actual configuration reported by Pohm the tunability is approximately 1/120 ma and the Q = 10, yielding:

$$\frac{P_{th}}{\beta_i} \cong 7 \text{ mw/Mc} \tag{6.74}$$

It should be emphasized that, although these configurations are not necessarily optimum, they have relatively small thresholds compared to those of the bulk ferrite configurations. The investigation of the thin-film configurations is somewhat incomplete due to the difficulty of obtaining suitable samples. However, the above threshold relations are sufficiently encouraging that further investigation of this configuration is justified.

6.8 Comparison of Thresholds for Configuration in Chapter 6

A comparison of the various amplifier configurations considered in this chapter can be made on the basis of the threshold per unit input bandwidth. For this purpose Table 6-1 has been constructed.

Table 6-1 Comparison of Thresholds

Amplifier Configuration	$\frac{P_{th,m}}{\beta_i}$ Theoretical watts/Mc	$\frac{P_{th,m}}{\beta_i}$ Experimental watts/Mc
Reggia Tunable Filter		
Mn Mg Laboratory	200	3×10^4
Mn Mg from Weiss	≈ 1	
Reggia-Spencer		
Mn Mg Laboratory	670	2.5×10^3
Mn Mg from Weiss	1.5	
tuned	.06	100
Ferromagnetic Resonance		
a. .100" sample in microwave cavity	10^{-3}	10
b. optimum circuit with respect to sample size	10^{-5}	No Experimental model
Thin Film	.01	≈ 7

6.9 Conclusions

It is clear from this table that the ferromagnetic resonance configuration is the optimum bulk material amplifier. However, the thin-film amplifier has a much lower experimental threshold and is potentially the best overall configuration. The development of thin films for UHF and higher frequencies will permit magnetic phase-shift amplifiers of video bandwidth to be built.

CHAPTER 7

PRACTICAL LIMITATIONS ON THE FERRITE PHASE-SHIFT AMPLIFIER

7. 1 Introduction

The implication of the threshold calculations of the previous chapter is that arbitrary gain bandwidths are possible for each circuit provided only that sufficient pump power is available. However, there are several practical limitations which influence this possibility. A number of factors such as saturation and noise generation tend to limit the pump power which can usefully be applied. The purpose of this chapter is to estimate the maximum useful pump power, and from this to estimate maximum gain-bandwidth products.

In addition to the maximum gain-bandwidth estimate, various practical effects influencing amplifier performance are explored. In Section 7. 2 the advantage of a one-port phase modulator, rather than the two-port device assumed previously, is described. The noise phenomena in ferrite phase-shift amplifiers are discussed in Section 7. 5. Section 7. 4 contains a revealing comparison between ferrites and varactors which tends to explain why the latter have proved to be so much more successful in amplifier configurations than the former. The final section (7. 6) includes a summary of the work reported in this paper and a list of the important conclusions.

7. 2 Advantage of the Use of the Circulator

It has been assumed in previous discussions of the phase-shift amplifier that the phase modulator is inserted between the source and the load, so that the power transmitted to the load is phase-modulated. The disadvantage of this circuit is that some of the sideband power is reflected to the source where it is dissipated in the source impedance and is, therefore, not useful for amplification of the signal. Since the practical circuits which we are considering operate with a microwave pump frequency, a circulator can be used to make a one-port phase-shift amplifier. The circulator can separate the sideband power which is reflected from the phase modulator from the pump power, so that all of it can be delivered to the

phase detector. A transformer can be used to match the phase modulator to the transmission line supplying the power.

The performance of a phase-shift amplifier which uses a circulator is best characterized by the sensitivity of its reflection coefficient to the signal magnetic field. The latter can be found from the phase-shift sensitivity, which has already been computed. It was pointed out in the introduction that in the optimum quiescent condition the pump frequency is the same as the center frequency of the filter. The phase characteristic under this condition has also been exhibited:

$$\Delta\phi = \frac{\omega \Delta C}{2Y_o + G} \tag{7.1}$$

where G is the admittance of the pump filter at center frequency.

A circulator permits the microwave circuit shown in Fig. 7-1:

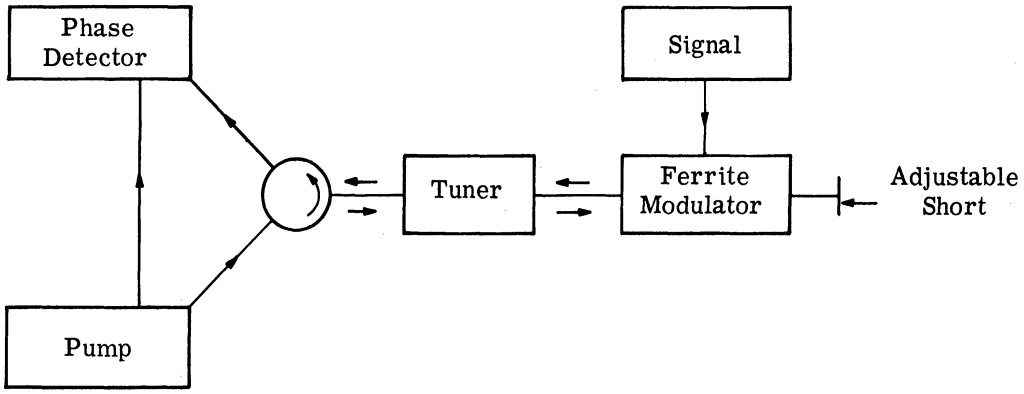

Fig. 7-1. Microwave circuit for the ferrite phase-shift amplifier using a circulator.

Adams has shown that the real part of the admittance looking into the phase modulator should match the transmission line (Ref. 48). If this conductance is different from Y_o, then a slide screw tuner can be used which functions as an ideal transformer so that the admittance looking into the tuner from the circulator is Y_o. The transformer ratio for this condition is

$$n = \sqrt{\frac{Y_o}{G}}$$

The reflection coefficient of the transformed load is given by:

$$\rho = \frac{Y_o - Y_L}{Y_o + Y_L}$$

$$= \rho_o + \Delta\rho$$

where $\rho_o = 0$ for the optimum phase-shift amplifier, and

$$\Delta\rho = \frac{j\,\omega_o \Delta C \frac{Y_o}{G}}{2\,Y_o + j\,\omega_o \Delta C \frac{Y_o}{G}}$$

$$\cong j\,\frac{\omega_o \Delta C}{2G}$$

But

$$\Delta\phi = \frac{\omega_o \Delta C}{2Y_o + G} \tag{7.3}$$

$$\Delta\rho = j\Delta\phi\left(\frac{Y_o}{G} + \frac{1}{2}\right) \tag{7.4}$$

The sideband power delivered to the matched phase detector $P_{s_{br}}$ by the one-port device is given by:

$$P_{s_{br}} = \frac{1}{2}(\Delta\rho)^2 P_p$$

$$= \frac{1}{2}\left(\frac{Y_o}{G} + \frac{1}{2}\right)^2 (\Delta\phi)^2 P_p$$

$$= \left(\frac{Y_o}{G} + \frac{1}{2}\right)^2 P_{s_{bt}} \tag{7.5}$$

where $P_{s_{bt}}$ is the power delivered to the phase detector by the two-port device, as shown in Fig. 2-1. Notice that if $Y_o \cong G$, which is commonly the case in the circuits which were

measured, then:

$$P_{s_{br}} \cong 2P_{s_{bt}} \tag{7.6}$$

That is, approximately twice as much sideband power is delivered to the load by the one-port device as by the two-port device. In general, the gain for the one-port phase-shift amplifier will tend to be 3 db greater than for the two-port amplifier, all other conditions being the same. This improved gain can be explained by considering that all of the sideband power produced in the one-port circuit is delivered to the load, whereas in the two-port circuit approximately half the sideband power is returned to the source where it is dissipated in the source impedance. Thus, whenever possible the phase-shift amplifier should be built as a one-port device for the additional 3-db gain over the two-port device.

7.3 Nonlinear Effects

The analysis in the preceding chapters was based upon the small-signal approximation. This approximation can be examined further to determine whether reliable predictions can be made concerning high-power operation of ferrites. The small-signal approximation reduces the equation of motion to its linearized form, which is useful for explaining ferromagnetic resonance and other ferrite r-f phenomena. However, in each of these, this small-signal theory becomes less and less valid as the r-f power is increased. One example of this effect is the phenomenon of ferromagnetic resonance saturation. The power absorbed at ferromagnetic resonance is roughly proportional to $\frac{M_z}{H_o}$ which is given by M_o/H_o in the small-signal approximation. According to theory, this level should decrease due to the decrease in M_z as the r-f power level is increased. This effect, called saturation, does indeed occur, though at a power level two or three orders of magnitude smaller than predicted by simple theory (Ref. 46).

An explanation of this effect was offered by Suhl (Ref. 47), who found that energy can be taken irreversibly from the uniform precessional motion of the magnetization, which is characteristic of ferromagnetic resonance, and transferred to the crystal lattice of the sample. Fundamental to this process is the excitation of spin waves, which are wave-like modes of energy propagation in the magnetic lattice of the material analogous to crystal lattice vibrations. Suhl showed that spin waves can be parametrically pumped by the uniformly

precessing magnetization, which occurs at or near ferromagnetic resonance, when the precessional amplitude exceeds a certain level. He found that the spin waves, parametrically excited at the lowest r-f power level, are those which propagate along the direction of the biasing magnetic field (i. e., z direction). The computed power level for excitation of these spin waves agrees very well with the observed power level at which saturation occurs. This fact, together with the fact that these z-directed spin waves can cause a reduction in M_z, explains the effect of r-f saturation very satisfactorily.

7. 3. 1 Power-Limiting Effect of Spin Waves. There is another aspect of r-f saturation which is very undesirable for ferrite amplifiers. The fact that spin waves are parametrically excited by the r-f source means that they extract energy from it. The power so extracted is not useful for pumping the sample. The spin waves act to produce a power-limiting effect, and in fact ferrites are actually used in some circuits to build power limiters. Denton (Ref. 23) showed in his ferrite parametric amplifier that an increase in pump power above the spin-wave level predicted by Suhl produced a negligible change in circuit gain.

7. 3. 2 Spin Wave Threshold. The ferrite phase-shift amplifier which uses a sample biased near ferromagnetic resonance is subject to the same type of pump power limitation as Denton's parametric amplifier. Any increase in pump power above the critical Suhl level (or saturation level) will not produce a proportionate increase in transducer gain. The critical pump field intensity at which saturation occurs at ferromagnetic resonance was shown by Suhl to be:

$$h_{crit} = \frac{\Delta H}{2}\sqrt{\frac{2\Delta H}{M}} \tag{7.7}$$

which is of the order of 0. 1 Oe for low-loss ferrites. The pump power necessary to produce this field intensity can be found from the cavity Q and size:

$$P_s = \frac{\omega_o U}{Q} \tag{7.8}$$

where U is the stored energy at resonance and Q is that of the unloaded cavity. Assuming

the pump field is uniformly distributed throughout the cavity

$$U = \frac{1}{2} \mu_o h^2 v_c$$

But:

$$Q = \frac{\omega_o}{\beta_p}$$

So:

$$P_{s\ crit} = \frac{\beta_p \mu_o h^2_{crit} v_c}{2} \tag{7.9}$$

For the circularly polarized cavity used in these experiments:

$$v_c \cong 10^{-4}\ m^3$$

and:

$$\beta_p \cong 10\ Mc \tag{7.10}$$

Substituting these values in $P_{s\ crit}$ gives:

$$P_{s\ crit} \cong 100\ mw \tag{7.11}$$

If this value of pump power is compared with the threshold relation (Eq. 6.66) a maximum input bandwidth can be found which is of the order of 10 kc. The corresponding maximum theoretical value for this is found from Eq. 6.64 to be 100 Mc.

On the other hand, Suhl has shown that away from ferromagnetic resonance the critical pump field for saturation is given by:

$$h_{crit} \cong \frac{\omega - \omega_{res}}{\gamma} \sqrt{\frac{2\Delta H}{M_s}} \cong \frac{\omega - \omega_{res}}{\gamma \Delta H} h_{crit}\Big|_{\omega_{res}} \tag{7.12}$$

Clearly it is an advantage to operate away from ferromagnetic resonance to avoid saturation. However, operation must be sufficiently close to ω_{res} to attain maximum tunability. In the

experiments performed with the . 100" sphere of YIG, maximum tunability was reached at

$$\frac{\omega - \omega_{res}}{\gamma \Delta H} \cong 6$$

for which:

$$h_{crit} \cong 0.6 \text{ Oe} \tag{7.13}$$

Using this value of critical field intensity, the saturation power level can be computed from:

$$\frac{P_{crit}}{P_{crit\ res}} = \frac{h_{crit}^2}{h_{crit}^2}\bigg|_{\omega_{res}} \cong 36 \tag{7.14}$$

or

$$P_{crit} \cong 3.6 \text{ watts} \tag{7.15}$$

for which $\beta_{i\ max} \cong 0.36$ Mc (Eq. 6.64). Thus, operation away from ferromagnetic resonance is advantageous for pumping efficiency, although the pump frequency must be close enough to resonance that the cavity tunability is maximum. The value of $\omega - \omega_{res}$ for which T_{max} is achieved depends roughly on the sample size:

$$(\omega - \omega_{res})^2 = \frac{v_s}{v_c} \gamma M \omega \tag{7.16}$$

For a given P_{crit} the approximate sample size will be given by

$$P_{crit} = \frac{v_s}{v_c} \frac{\gamma M \omega}{(\gamma \Delta H)^2} P_{crit} \cong \frac{0.1 v_s M \omega}{\gamma v_c (\Delta H)^2} \tag{7.17}$$

At this point an additional advantage can be seen in using the magnetostatic modes whose resonant frequencies tend to be displaced from ferromagnetic resonance. Certain of the modes are sufficiently remote from ferromagnetic resonance that the saturation power is of the order of a few watts. The advantage offered by unsaturated samples is perhaps even clearer in this respect.

It can be concluded from the above discussion that there is a definite advantage in using the ferrite to tune a cavity as opposed to using ferromagnetic resonance as the pump filter. That is, the pump frequency can be remote from ferromagnetic resonance and yet maximum tunability can be achieved. It was shown that pump saturation for this case occurs at a much higher pump power than at ferromagnetic resonance.

7.3.3 Pump Saturation Effect in Magnetically Unsaturated Samples. The magnetically unsaturated samples clearly avoid the difficulty of the spin-wave pump saturation effect. However, there are certain nonlinear effects in unsaturated materials which are undesirable for phase-shift amplifiers. The most unfortunate of these is hysteresis, which has been totally ignored in the discussion thus far. The phenomenon of hysteresis is responsible for losses in magnetic materials, but the exact mechanism is not fully understood.

Another very undesirable nonlinear effect in unsaturated ferrites results from the highly nonlinear permeability. This effect is particularly pronounced at high power levels and has the effect of gain saturation with respect to pump power. This effect is illustrated in Fig. 7-2 where hysteresis is ignored. The r-f or pump permeability is the slope of this curve, which tends to decrease for $H \gtrsim H_1$. It is the variation of this slope with respect

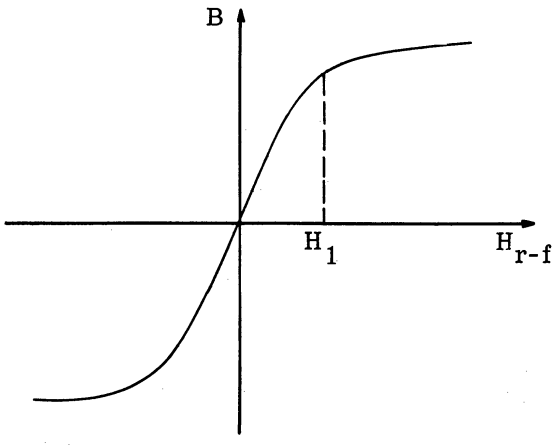

Fig. 7-2. Flux density vs. applied field for a material with negligible hysteresis.

to another applied field which enables this material to function properly in phase-shift amplifiers. However, since the slope becomes much less sensitive to the applied field as H exceeds H_1, the material tends to look more and more linear as H exceeds H_1 in the r-f cycle. Recall that the transducer gain is proportional to pump power as long as $H << H_1$. Thus when the pump power exceeds $P(H_1)$ (i. e., the pump power at which the pump magnetic field $= H_1$) the gain per unit pump power (i. e., G_t/P_p) is a decreasing function of P_p. Thus the same property which tends to make ferrites useful in nonlinear reactance circuits (i. e., low H_c and low saturation field) tends to limit the pump power at which gain saturation occurs. There is a rather sharp break in the curve B vs. H for most materials so that H_1 is rather well defined. For example, H_1 for Mn Mg ferrite reported by Weiss (Ref. 35) is of the order of 1 or 2 Oersteds. The pump power for this field can be estimated in the same manner as for the saturated case:

$$P(H_1) = \frac{\beta_p^2 \mu_o H_1^2 v_c}{2} \tag{7. 18}$$

Assuming the cavity used for this estimate is the same as that used for the estimate for the ferromagnetic resonance configuration is can be shown that:

$$P\big|_{H=1 \text{ Oersted}} \cong 10 \text{ watts} \tag{7. 19}$$

Thus, the maximum useful pump power for the unsaturated configuration is approximately 10 watts, yielding a maximum theoretical input bandwidth of 6 Mc.

7. 3. 4 Nonlinear Effects in Thin Films. The nonlinear effects in thin films tend to be the same as those in saturated bulk ferrites provided the thin film is small enough that it has a single magnetic domain. This circumstance is quite normal for thin-film phase-shift amplifier configurations. Thus, the nonlinear effects which result from the excitation of spin waves tend to limit the useful pump power for this configuration near ferromagnetic resonance. However, since the thin-film variable inductor can be operated successfully remote from ferromagnetic resonance, spin wave saturation does not necessarily limit the useful pump power for this configuration. However, not enough is known of nonlinearities in thin films at the present time to predict the useful limit on pump power. For that matter,

since the thin film configuration is not necessarily input-bandwidth limited, the actual pump power limitation may never seriously restrict the amplifier.

7. 3. 5 Maximum Gain-Bandwidth Estimate. The significance of the pump saturation effect is that it tends to limit the ultimate gain-bandwidth product. It has been shown that the pump threshold for any configuration is proportional to the input bandwidth, and that the pump power for each configuration is limited by the so-called nonlinear effects. In addition, it was shown that most ferrite phase-shift amplifiers tend to be input-bandwidth limited. Assuming this to be the case the gain-bandwidth product is given by:

$$\begin{aligned} \beta G_t &= \beta_i G_t \\ &= \frac{\beta_i P_{max}}{P_{th}} \\ &= \frac{\beta_i P_{max}}{K \beta_i} \end{aligned} \tag{7.20}$$

Thus the maximum gain-bandwidth product is:

$$\beta G_{t_{max}} = \frac{P_{max}}{K_{min}} \tag{7.21}$$

Using this relation, the values for P_{max} determined in this section, and K from the previous chapter, the maximum gain-bandwidth product is estimated for a variety of configurations and reported in Table 7-1.

Table 7-1 Maximum Gain Bandwidth

Configuration	$\beta G_{t_{max}}$ Theoretical	$\beta G_{t_{max}}$ Experimental
Reggia Tunable filter		
a. Mn Mg ferrite of Weiss	10 Mc	No experiment
b. Mn Mg ferrite	50 kc	0.33 kc
Reggia-Spencer (untuned)		
a. Mn Mg ferrite of Weiss	7 Mc	No experiment
b. Mn Mg	7 kc	4 kc
Ferromagnetic Resonance		
a. 0.100" YIG sample	100 Mc	1 Mc
b. Optimum sample size	10 Gc	No experiment
Thin film	unknown	10 Mc

7.4 Comparison of Ferrites and Varactors

A comparison would be useful between ferrites and varactors for application in phase-shift amplifiers since amplifiers using the latter have proved so successful. It has been shown that tunability is an important parameter for characterizing the reactive mixer in a phase-shift amplifier. On the other hand, the tunabilities which have proved most convenient for discussing the various reactive mixers are not directly comparable. For example, the ferrite tunability is defined:

$$T = \frac{1}{\omega_o} \frac{d\omega_o}{dh} \tag{7.22}$$

and is measured in units of $(\text{Oersteds})^{-1}$ while the varactor tunability is conveniently defined

$$T = \frac{1}{\omega_o} \frac{d\omega_o}{dv} \tag{7.23}$$

and is measured in $(\text{volts})^{-1}$. A direct comparison of these parameters is clearly meaningless. A universal parameter, which can easily be related to these tunabilities and which can be used to predict the performance of a phase-shift amplifier, must be found.

The ferrite amplifiers studied have tended to be input-bandwidth limited, whereas the varactor amplifiers tend to have extremely large input bandwidths. It is useful, therefore, to define a tunability with respect to a parameter which is easily related to the input bandwidth. The quantity which relates the input bandwidth to tunability is the amount of signal energy which must be stored to produce that tunability. Thus, we are led to define a quantity termed energy tunability T_E:

$$T_E = \frac{1}{\omega_o} \frac{\delta\omega_o}{\delta\sqrt{W}} \tag{7.24}$$

where ω_o is the center frequency of the pump filter and W is the stored signal energy required to produce $\delta\omega_o$. In the ideal case the input circuit of a phase-shift amplifier is entirely reactive. This reactance is due in part to the reactive mixer and in part to the surrounding structure (e.g., mounts, etc.). In the interest of uniqueness, the latter contribution to the reactance of the input circuit will be ignored.

For greatest utility, energy tunability should enable a computation of the transducer gain. That this is indeed the case can be seen through reference to the equivalent circuit of an arbitrary phase-shift amplifier (Fig. 7-3). If the phase modulator contains a reactive mixer whose energy tunability in a particular configuration is given by:

$$T_E = \frac{1}{\omega_o} \frac{\Delta\omega_o}{\Delta\sqrt{W}} \tag{7.25}$$

then the phase sensitivity of the phase modulator is given by

$$\frac{\Delta\phi}{\Delta\sqrt{W}} = Q_\ell \, T_E \tag{7.26}$$

This circuit will deliver sideband power P_{sb} to a matched phase detector

$$P_{sb} = \frac{1}{2}\left(\frac{\Delta\phi}{\Delta\sqrt{W}}\right)^2 W P_p \tag{7.27}$$

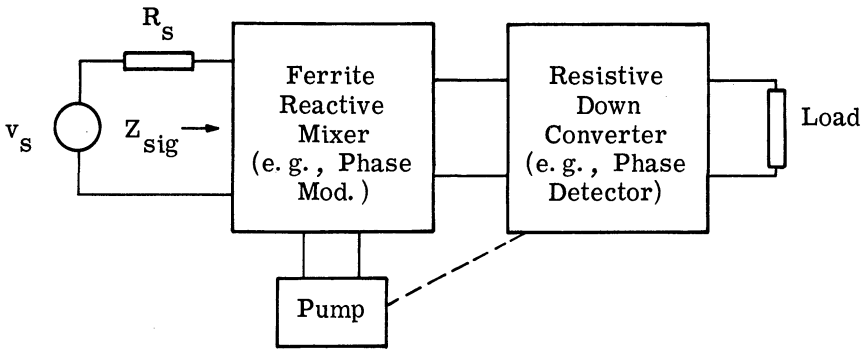

Fig. 7-3. Equivalent circuit of general ferrite phase-shift amplifier.

If the detection efficiency is ζ, the midband transducer gain G_t is:

$$G_t = \frac{P_\ell}{P_{avail}} = \frac{\zeta}{2}\left(\frac{\Delta\phi}{\Delta\sqrt{W}}\right)^2 \frac{W P_p}{P_{avail}} \tag{7.28}$$

where P_{avail} is the available signal-frequency source power. The relationship between P_{avail} and the stored signal energy is found from elementary circuit considerations.

The ideal signal-circuit impedance for a phase-shift amplifier is almost purely reactive, being inductive in the case of the ferrite amplifier (L) and capacitive in the case of the varactor amplifier. For the ferrite amplifier, the stored signal energy is given by:

$$W_h = \frac{1}{2} L i^2 \tag{7.29}$$

which at midband becomes:

$$W_h = \frac{1}{2} L\left(\frac{V_s}{R_s}\right)^2$$

$$= \frac{2L}{R_s} \frac{V_s^2}{4R_s}$$

$$= \frac{2L}{R_s} P_{avail}$$

$$= \frac{2 P_{avail}}{\beta_i} \tag{7.30}$$

For varactor amplifiers the stored energy is given by:

$$W_e = \frac{1}{2} C v^2$$

which at midband is:

$$W_e = \frac{1}{2} R_s C \frac{V_s^2}{R_s}$$

$$= 2 R_s C \frac{V_s^2}{4R_s}$$

$$= \frac{2 P_{avail}}{\beta_i} \qquad (7.31)$$

Thus a single expression relates the stored signal energy to the available source power of all phase-shift amplifiers having reactive input impedances.

Using the above relation, the transducer gain is given conveniently by:

$$G_t = \zeta \left(\frac{\Delta\phi}{\Delta \sqrt{W}} \right)^2 \frac{P_p}{\beta_i}$$

$$= \frac{\zeta (Q_\ell T_E)^2 P_p}{\beta_i} \qquad (7.32)$$

Thus, the input-bandwidth threshold pump power and transducer gain are uniquely specified by T_E, for a given Q_ℓ.

The maximum energy tunability of ferrites can now be compared with that of a commercially available varactor. It was shown previously that the stored signal energy for ferrite reactive mixers is given by:

$$W_h = \frac{1}{2} h^2 \int \mu [f(r)]^2 \, d\upsilon$$

$$\geqq \frac{1}{2} \mu_s h^2 \upsilon_s \qquad (7.33)$$

where f(r) was defined earlier in the chapter. The maximum energy tunability is determined by the smallest energy for which the field in the sample is h. This energy must at

least equal the energy stored in the sample (i. e., $W_h = \frac{1}{2} \mu_s h^2 v_s$). Note that, using this limiting value, the actual energy tunability is over-estimated by the ratio:

$$\left[\frac{\int \mu [f(r)]^2 \, dv}{\mu_s v_s} \right]^{\frac{1}{2}} \tag{7.34}$$

Thus the energy tunability which we consider is given by:

$$T_{Eh} = \frac{1}{\omega_o} \sqrt{\frac{2}{\mu_s v_s}} \frac{d\omega_o}{dh} \tag{7.35}$$

But the maximum energy tunability for saturated ferrites is given by:

$$T_{Eh\ max} = \frac{\gamma}{\omega_o} \sqrt{\frac{2}{\mu_s v_s}} \tag{7.36}$$

A similar calculation is now made for the varactor. The stored signal energy for a varactor is given by:

$$W_e = \frac{1}{2} C v^2 \tag{7.37}$$

where C is the varactor capacitance at the signal frequency and v is the signal voltage amplitude of the varactor. Using this quantity yields the varactor energy tunability given by:

$$T_{Ee} = \frac{1}{\omega_o} \sqrt{\frac{2}{C}} \frac{d\omega_o}{d\nu} \tag{7.38}$$

It is most meaningful to compare the ferrites and varactor energy tunability for the same pump frequency. It is then sufficient to compare the product $\omega_o T_E$. For the 0. 100" sphere of YIG described in Section 6. 4 this quantity is:

$$\omega_o T_{Eh} = 4.6 \times 10^5 \text{ Mc}/\sqrt{\text{Joule}} \tag{7.39}$$

For an ordinary MA450 series varactor measurements show that $\frac{\Delta\omega_o}{\Delta v} \cong 700$ Mc/volt. A conservative estimate for C, which includes the varactor mount and other stray capacitance,

is approximately 10 pf. Thus:

$$\omega_o T_{Ee} = 3 \times 10^8 \text{ Mc}/\sqrt{\text{Joule}} \tag{7.40}$$

This computation shows that the energy tunability for a currently available varactor is about three orders of magnitude larger than the upper bound for the 0.100" sphere of YIG. The two energy tunabilities would be equal for a sample of 0.010" diameter. Unfortunately, this comparison is somewhat misleading since the maximum energy tunability for the ferromagnetic resonance configuration cannot be successfully approached at this dimension. The principal reason is, of course, the difficulty of coupling the signal energy tightly into such a small sample.

Though a similar comparison could be made for the two unsaturated configurations, it can be seen from Table 7-1 that both of these are several orders of magnitude smaller than the ferromagnetic resonance configuration. However the thin film tends to be comparable with the varactor by virtue of its small volume. The energy tunability for the experimental circuit described earlier can be computed from the signal-frequency coil inductance and the tunability. The stored signal energy is given by:

$$\frac{1}{2} L_s (i - i_o)^2$$

where $L_s \cong 5\,\mu h$. From the curve of Fig. 5-15, the energy tunability can be shown to be:

$$T_E = \frac{2 \times 10^3}{\sqrt{\text{Joule}}} \tag{7.41}$$

which is only about an order of magnitude smaller than the varactor. Thus, when thin films can be utilized at microwave frequencies they will be competitive with varactors for the construction of phase-shift amplifiers.

7.5 Noise Phenomena in Ferrite Phase-Shift Amplifiers

Although an ideal, lossless reactive mixer contributes no excess noise in a phase-shift amplifier, an actual reactive mixer deviates from this ideal. In addition to the noise contributed by the reactive mixer, Adams has shown that the second stage or down conversion is inherently noisy (Ref. 48). In fact, in many cases this is the dominant noise

source in a phase-shift amplifier. In this section, the sources of excess noise in ferrite phase-shift amplifiers, and their relative importance, are studied. First, the sources of noise associated with using ferrite as a reactive mixer are considered. Next, the noise contributed in the second stage is discussed, and a minimum noise figure is computed.

7. 5. 1 Survey of Noise Phenomena in Ferrites. There are a number of basic noise sources associated with the ferrite phase-shift amplifier. Perhaps the most obvious of these is the thermal noise which results from the equivalent resistance in the signal-frequency circuit. Not so obvious, however, is the noise which results directly from the presence of the material. Since ferrites tend to be electrical insulators this noise is not shot noise, but it may be thermal noise. It has been observed to be somewhat dependent upon pump power and independent of sample temperature for a wide range of temperatures. It tends to occur for conditions under which the sample is lossy, and so can presumably be explained by the phenomena responsible for ferrite loss.

The thermal noise due to stray loss in the signal-frequency circuit, even though small, is important because it is amplified. It might be expected that stray losses could be made negligible by suitable design of the signal circuit to minimize stray loss. However, physical constraints limit the design of this circuit. For example, losses can be minimized by winding the signal coil with wire of large cross-section but the wire size is restricted by the necessity for minimizing signal-coil disturbance of the r-f field. The signal circuit can be designed for optimum noise figure with respect to these constraints, but the optimum is typically the design for minimum loss. The excess available noise at the load due to the stray losses in the input-circuit coil, assuming the circuit is input-bandwidth limited, is given by:

$$N_i = k T_s \beta_i \frac{R}{R_s} G_t \tag{7.42}$$

where R_s is the source resistance, R the equivalent series resistance, T_s is the source temperature, β_i is the input bandwidth and G_t is the transducer gain.

The explanation of the noise which is induced in the sample depends upon the configuration, because the loss mechanisms tend to differ for different configurations. For

magnetically saturated ferrites near ferromagnetic resonance, the losses have been successfully explained by Suhl (Ref. 47) as resulting from the excitation of spin waves which were discussed in a previous section. Spin waves carry energy and contribute noise in a manner analogous to lattice vibrations in a conductor. However, there is considerable theoretical and experimental evidence that their excitation is nearly independent of the temperature of the crystal, which tends to explain the observed temperature independence of noise power generated in a ferromagnetic sample. The tendency of spin waves to be excited above a certain threshold level of r-f field intensity implies that the power loss and hence the noise of a ferromagnetic sample is negligible up to a certain r-f power level. Denton (Ref. 23) found this to be the case in his ferromagnetic parametric amplifier. Thus the excess noise due to spin waves will tend to be unimportant for pump powers far below this threshold.

A different loss mechanism explains the losses in samples far below magnetic saturation. The losses in this case are believed to be the result of the motion of domain walls although the exact energy conversion mechanism from domain wall motion to the actual energy dissipation phenomenon is not well known. The noise associated with this motion has been explained by the so-called Barkhausen effect (Ref. 49) which is a result of the fact that the permeability curve for a material is not a smooth continuous curve but is made up of small discontinuous jumps. These discontinuities can be explained from the domain theory and the observation that the domains tend to reverse individually in a random manner. For this reason, the random domain wall motion in a pumped sample contributes excess noise which is not thermal in nature but depends strongly upon the pump power. In addition, it is known that the individual domains are magnetically saturated, so spin waves can propagate in them and presumably can contribute to excess noise. As would then be expected, unsaturated or multidomain samples tend to contribute more excess noise than the saturated samples due to the Barkhausen effect. Thus, it is expected that configurations employing magnetically saturated samples are optimum with respect to noise figure.

The excess noise in the thin film consists of both Barkhausen and spin-wave noise unless the sample is sufficiently small that it is a single magnetic domain. A sample such as the one described in Chapter 6 is sufficiently small that it is essentially a single domain and hence can contribute no Barkhausen noise (Ref. 50). In addition the normal operating conditions include biasing the sample far from ferromagnetic resonance where little spin-wave

noise tends to be produced. However more information than is currently available is required about thin film noise mechanisms before comparison of their excess noise to that contributed in bulk samples.

7.5.2 Second-Stage Noise. The second-stage noise is fundamental to phase-shift amplifiers, because up-conversion must always be followed by down-conversion in a resistive mixer which is fundamentally noisy. On the other hand, the contribution of second-stage noise to the overall noise figure of the amplifier tends to be small if the up-conversion gain is large. Adams has discussed the second-stage noise and shown that the excess available noise power it can deliver to a matched load is given by (Ref. 48):

$$N_m = (F_{md} - 1)\, 2kT\, \beta_m\, \zeta \tag{7.43}$$

where F_{md} is the noise figure for a double-sideband mixer with zero correlation between the sidebands, ζ is the detection efficiency, T is the mixer temperature, and β_m is the bandwidth of the entire circuit past the mixer. Adams has also shown that for a matched phase detector $2\zeta(F_{md} - 1) \cong 5$.

7.5.3 Estimate of Minimum Noise Figure. It is of interest to estimate the noise figure of a ferrite phase-shift amplifier assuming that all sources of excess noise in the amplifier have been accounted for in the discussion. The definition for spot noise figure is:

$$F = 1 + \frac{N_{excess}}{kT\beta_s G_t} \tag{7.44}$$

where β_s is the bandwidth of the narrowband filter used to determine spot noise. This filter is normally placed at the mixer output and is sufficiently small that it limits circuit bandwidth (i.e., $\beta = \beta_s$). It is convenient to select $\beta_s = \beta_i$. For the ferrite phase-shift amplifier F is given by:

$$F = 1 + \frac{R}{R_s} + \frac{2\zeta(F_{md} - 1)}{G_t} + \frac{N_{ferrite}}{kT\beta_s G_t} \tag{7.45}$$

where $N_{ferrite}$ is the excess available noise power due to the material at the mixer output.

Examination of the expression for noise figure reveals that it tends to be minimum for some particular pump power. This can be seen most easily by representing $N_{ferrite}(P_p)$ as shown in Fig. 7-4. In addition, it should be recalled that the transducer gain is proportional to pump power up to the Suhl threshold P_{th} and tends to be constant above that power. Assuming the transducer gain is proportional to pump power up to the Suhl threshold and constant for pump powers greater than that value, the idealized noise figure vs. pump power is as shown in Fig. 7-5. The minimum noise figure based upon this idealized model occurs for $P_p = P_{th}$. The actual noise figure is shown in the dashed curve and has a minimum near the Suhl threshold.

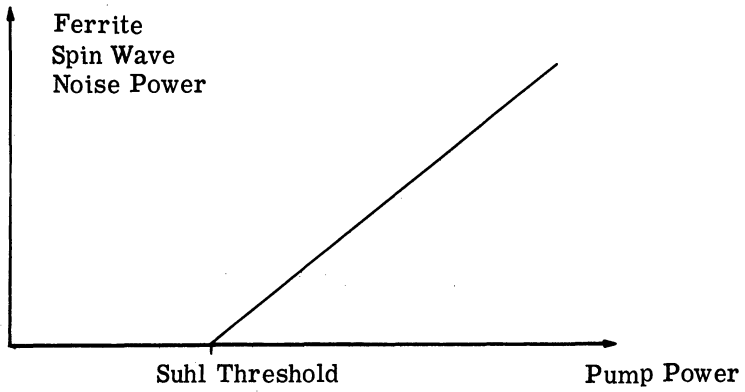

Fig. 7-4. Ideal approximation of dependence of excess material noise on pump power. For saturated samples P_{th} is the Suhl threshold.

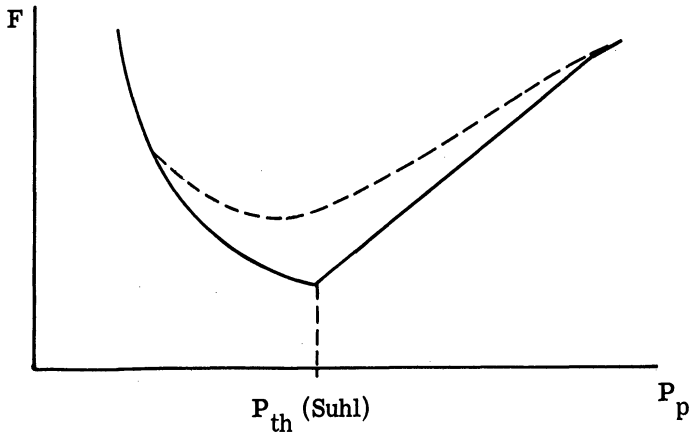

Fig. 7-5. Noise figure vs. pump power assuming $N_{ferrite}(P_p)$ as shown in Fig. 7-4. The solid curve is the ideal and the dashed curve the actual F.

The noise figure is also optimum for some particular source resistance. Assuming the pump power is below the Suhl threshold, we can write noise figure as

$$F = 1 + \frac{R}{R_s} + \frac{5 R_s}{K P_p} \tag{7.46}$$

where we have written $G_t = K P_p / R_s$ which is minimum for:

$$R_s^2 = K P_p R$$

$$R_s^2 = \frac{K P_p R}{5}$$

or:

$$R_s = \frac{G_t R}{5} \tag{7.47}$$

The minimum noise figure is given approximately by:

$$F_{min} = 1 + \frac{10}{G_t}\Big|_{P_p = P_{th}} \tag{7.48}$$

Note that this estimate is under the actual noise figure by an amount due to the actual excess sample noise at P_{th}.

7.6 Summary and Conclusions

This paper has reported the results of an investigation of the ferrite phase-shift amplifier, which is basically a double-sideband reactive-mixer circuit. Reactive mixing occurs in the material between a reference signal and a local oscillator of much higher frequency. It was assumed that filters are available to restrict the power flow to the set of frequencies including the signal, the local oscillator and the upper and lower sidebands. Although the phase-shift amplifier is a double-sideband circuit, the two single-sideband circuits were discussed briefly as an interesting contrast to the phase-shift amplifier circuit.

A rather complete study of the phase-shift amplifier circuit properties was conducted by Adams. For this reason the circuit properties of ferrite phase-shift amplifiers

were not emphasized. The principal interest in this paper has been the study of those physical properties which tend to make ferrites useful in phase-shift amplifiers, and those properties which tend to limit them in this application. Using these properties the theoretical optimum ferrite phase-shift amplifier performance was computed and then compared with the performance of experimental configurations. In each case, explanations were offered for the disparity between theoretical optimum and the practical circuits. The noise properties of the ferrite phase-shift amplifier were studied and used to compute the minimum theoretical noise figure. The ferrite properties which tend to limit the applied local oscillator power were studied and used to compute the maximum useful local oscillator power. The results of this study led to an estimate of the maximum theoretical gain-bandwidth product.

In this study the following original contributions were made:

1. The boundary value problem for ferrite samples in an r-f magnetic field which are small compared to a wavelength was solved, correct to second order in $(a\lambda)$, which a is the sample size and λ the wavelength. This problem is an extension of the lowest-order approximation, which was termed the magnetostatic modes. This portion of the thesis was published in the Journal of Applied Physics (Ref. 17).

2. It was shown that the properties of ferrite reactive mixers can be specified by the so-called pumped susceptibility tensor which is the matrix form of the steady-state solution to the equation of motion, including the fields at all frequencies where real power flows.

3. Using the pumped susceptibility tensor appropriate to the lower-sideband circuit or parametric amplifier, the unity-gain pump-power threshold was found. It was learned that this power is minimized if the signal and lower sideband field distributions are complex conjugates, and if the pump field is uniform throughout the sample and directed along the field which biases the sample.

4. The pumped susceptibility for the upper-sideband converter was found and used to predict the power flow at the upper-sideband and signal frequencies. The ratio of these powers was shown to deviate from the value predicted by the Manley-Rowe relations due to losses in the sample. The effect of these losses on the conversion gain, which was demonstrated by Adams (Ref. 1) for varactors, was similarly reported in this section.

5. The pumped susceptibility tensor for the double-sideband circuit was found assuming the fields were circularly polarized. The optimum field orientations for maximixing the power converted to the sidebands was shown to consist of a signal field directed parallel to the biasing field and a pump field transverse to that field.

A method of synthesizing the prototype model of the phase-shift amplifier was suggested by the optimum field orientation in which the ferrite is used to tune a filter which is resonant at the pump frequency. This prototype is synthesized if the filter is placed between the pump and a matched phase detector. It was shown that a quantity which we call tunability is useful for measuring the performance of the ferrite in tuning the resonant circuit. Tunability is defined as the percentage change in resonant frequency per unit applied field and tends to be proportional to the percentage change in sample permeability per unit applied field. Because the gain-bandwidth product tends to be proportional to pump frequency and because ferrite tunabilities are large in the microwave spectrum, a microwave pump source was assumed in all calculations and was used for all experimental measurements.

6. The tunability was studied for a variety of configurations and found to have interesting properties depending upon the configuration. It was shown that for bulk ferrite samples, the tunability is largest for two bias conditions: 1) near ferromagnetic resonance, and 2) near zero bias. Near ferromagnetic resonance it was shown that tunability is limited fundamentally to $\frac{\gamma}{f_o}$, where γ is the gyromagnetic ratio and f_o is the pump frequency. Near zero bias, no fundamental limit could be found but it was shown that the best materials are those for which the B-H loop is 'square.' That is, those materials which tend to saturate for small magnetic fields are optimum. Perhaps the best material in this respect which has appeared in the literature was reported by Weiss. Using the published data for the material reported by Weiss, it was shown that the tunability is approximately $\frac{350\ \text{Mc}}{f_o}/\text{Oe} \cong 0.035/\text{Oe}$ at x-band.

The tunability of a thin film variable inductor was measured and found to be about 0.2/Oe at 10 Mc. Unfortunately, the currently available thin films were found to suffer from excessive loss at frequencies above VHF, which limits their applicability in phase-shift amplifiers to frequencies somewhat below this range. However, further research in thin films may lead to the development of low-loss films in much the same way that low-loss

bulk ferrites (e.g., YIG) were developed. The realization of thin-film phase-shift amplifiers which compete with varactors versions must await such a development.

7. It was shown that ferrite phase-shift amplifiers which employ bulk ferrite samples tend to be input-bandwidth limited. There are two important reasons for this limitation: 1) the r-f permeability of ferrites is relatively insensitive to the signal-frequency magnetic field for which the tunability is relatively small; 2) the signal energy does not tend to be coupled strongly into the sample for sample shapes which are convenient to use in phase-shift amplifiers. The optimum sample shape with respect to 2) above is a toroid. However, it was shown that even the phase-shift amplifiers which employ optimum samples tend to be input-bandwidth limited.

It was further shown that the thin-film configuration is not necessarily input-bandwidth limited. This result can be attributed to the relatively small threshold per unit bandwidth, and to the relatively narrow pump bandwidth necessary for gain at low pump frequencies.

8. It was shown that the transducer gain for ferrite phase-shift amplifiers is proportional to pump power for small enough power. However, for large pump powers the gain tends to saturate due to certain ferrite nonlinearities. The limiting nonlinearity in ferrite phase-shift amplifiers is different for the two principal bias conditions. For samples biased near ferromagnetic resonance, the limiting nonlinearity is attributed to spin waves which tend to be excited above a certain power threshold. Any pump power greater than this level tends to be dissipated in the sample and is not useful for increasing the gain of the circuit. For samples biased near zero applied magnetic field, the limiting nonlinearity is magnetic saturation of the material. It was shown for this case that the maximum useful amplitude of the magnetic field is of the order of the coercive force for the material.

This pump saturation effect is significant because it tends to limit the gain-bandwidth product of the bulk ferrite configurations. Other factors which contribute to this limitation are: the linear relation between pump threshold and input bandwidth; and the input bandwidth limitation which is characteristic of these circuits. The configuration which is biased near ferromagnetic resonance is the optimum bulk ferrite configuration in this respect.

The maximum gain-bandwidth product for the thin-film configuration is limited by spin-wave excitation, but this effect tends to be less significant in this case because these configurations do not tend to be input-bandwidth limited.

9. It was shown that the excess noise in ferrite phase-shift amplifiers comes primarily from the stray loss in the signal circuit, the material itself and from the detector. The two principal sources of noise in the bulk ferrite material were shown to be spin-wave noise which is produced near ferromagnetic resonance, and Barkhausen noise which is produced near ferromagnetic resonance, and Barkhausen noise which is produced in all unsaturated samples. In single-domain thin films, at frequencies away from ferromagnetic resonance, neither of these noise contributions will be present. It was shown that the noise figure of a ferrite phase-shift amplifier is a function of pump power and is minimized for some particular power. For the ferromagnetic resonance configuration, the minimum occurs for a pump power near the Suhl threshold. However, the detector excess noise tends to be the most significant noise in ferrite phase-shift amplifiers. Assuming that sample noise can be neglected, a minimum noise figure was computed and shown to be:

$$F_{min} = 1 + \frac{10}{G_t}$$

10. A comparison was made between varactors and ferrite reactive mixers on the basis of energy tunability, which was defined as the tunability per unit square root of active signal energy. In the case of ferrites the active signal energy is that which is stored inside the sample and for varactors it is the energy stored in the junction capacitance. This tunability is a measure of the maximum tunability per unit input bandwidth and is a good quantity to use for comparing varactors and ferrites because the latter tend to be input-bandwidth limited. On the basis of energy tunability it was found that only the configurations which are biased near ferromagnetic resonance are comparable with varactors, and these are comparable only for physically unreal conditions. However, it was shown that the thin films are comparable with varactors in their optimum configurations.

The general conclusion which can be drawn from this study is that ferrite phase-shift amplifiers which use bulk ferrite samples will probably find application only if a narrow bandwidth is unimportant. However, it appears that the thin-film variable inductor

might ultimately be useful in these amplifiers particularly after the development of films whose losses at UHF are small. It is believed that this paper has shown from fundamental grounds that further attempts to synthesize wideband ferrite phase-shift amplifiers using bulk samples should not be considered, but that the thin-film phase-shift amplifiers show definite promise and should be explored.

APPENDIX A

MAGNETOSTATIC APPROXIMATION FOR SPHERICAL SAMPLE

We wish to solve the following magnetostatic boundary value problem:

$$\nabla_t^2 \phi + \frac{1}{1+K} \frac{\partial^2 \phi}{\partial z^2} = 0 \qquad \text{inside the sample} \qquad \text{(A-1)}$$

$$\nabla^2 \phi = 0 \qquad \text{outside the sample} \qquad \text{(A-2)}$$

where the boundary conditions are continuity of the potential and the normal component of magnetic flux density. Because the solution for a sphere is sought, a spherical coordinate system will be considered whose center lies at the center of the sample and whose z-axis lies along the field which biases the sample.

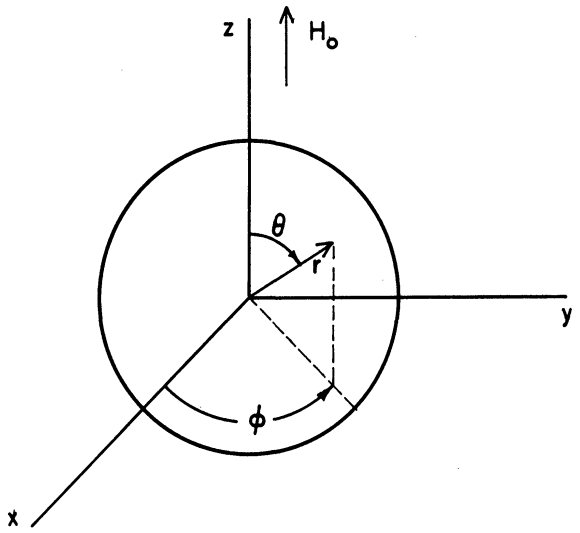

Fig. A-1. Coordinate system convenient for solution to boundary value problem.

The solution for the potential outside the sample is well known:

$$\phi = A \frac{P_n^m(\cos\theta)}{r^{n+1}} e^{im\psi} \qquad \text{(A-3)}$$

However, the solution for the potential inside requires further thought. Notice that if the following definitions are made:

$$\begin{aligned} x' &= x \\ y' &= y \\ z' &= (1+K)^{\frac{1}{2}} z \end{aligned} \tag{A-4}$$

then the differential equation for the potential inside the sample reduces to

$$\nabla'^2 \phi = 0 \ , \tag{A-5}$$

where the use of the prime indicates that derivatives with respect to the primed coordinates are taken. The equation of the surface in the primed coordinates, i. e. ,

$$x'^2 + y'^2 + \frac{z'^2}{1+K} = r_o^{\ 2} \ , \tag{A-6}$$

is no longer that of a sphere. Rather it is that of an oblate or prolate spheroid according to whether K is greater than or less than zero, respectively. The advantage of making the definition of the primed variables is that the solution to Eq. A. 1 is known in these variables. Further, their relation to the actual coordinates can easily be computed. Let the spheroidal variables be η', θ', ϕ' for which $\eta' = \eta_o$ is the equation of the sample surface. The solution to Eq. A. 1 in these variables is:

$$\phi = B\, P_n^m(\cos\theta')\, P_n^m(i \sinh \eta)\, e^{im\phi'} \tag{A-7}$$

where it has been assumed that $K < 0$ for which the surface will be an oblate spheroid in the artificial coordinates.

These artificial coordinates are related to the actual coordinates by the relations:

$$\begin{aligned} x &= x' = a \cosh\eta \sin\theta \cos\phi \\ y &= y' = a \cosh\eta \sin\theta \sin\phi \\ z &= \frac{z'}{\sqrt{1+K}} = \frac{a}{\sqrt{1+K}} \sinh\eta \cos\theta \end{aligned} \tag{A-8}$$

From these relations the sample surface can be found in terms of known quantities.

$$r_o = \frac{z'}{\sqrt{1+K}} = \frac{a \sinh \eta_o}{\sqrt{1+K}} \cos \theta' \Big|_{\theta'=0}$$

$$r_o = x_o' = a \cosh \eta_o \sin \theta' \Big|_{\theta'=\frac{\pi}{2}} \tag{A-9}$$

Thus

$$\tanh \eta_o = \sqrt{1+K}$$

Substituting this quantity in the equation of the surface it can be shown that:

$$a = \frac{r_o}{\cosh \eta_o}$$

$$= -K r_o \tag{A-10}$$

But for oblate spheroids $K < 0$ so this quantity is positive. Notice also that on the sample surface that

$$x = r_o \sin \theta \cos \phi = a \cosh \eta_o \sin \theta' \cos \phi'$$

and

$$y = r_o \sin \theta \sin \phi = a \cosh \eta_o \sin \theta' \sin \phi'$$

for which it is clear that $\phi = \phi'$ and $\theta = \theta'$.

For matching of the boundary conditions it will be necessary to find the derivatives of the potential in terms of the real coordinates. These can easily be evaluated by the chain rule once the derivatives of the artificial coordinates with respect to the real coordinates are known. For this purpose we make the following computations. Let the coordinates x, y, z be given by

$$x = f(\eta', \theta', \phi'), \quad y = g(\eta', \theta', \phi'), \quad z = k(\eta', \theta', \phi')$$

For convenience the primes will be dropped in these calculations. The desired derivatives,

$\frac{\partial \eta}{\partial x}$ etc., can be found:

$$\frac{\partial \eta}{\partial x} = \frac{1}{J} \frac{\partial(y,z)}{\partial(\theta,\phi)} \quad , \quad \text{etc.}$$

where

$$J = \begin{vmatrix} x_\eta & x_\theta & x_\phi \\ y_\eta & y_\theta & y_\phi \\ z_\eta & z_\theta & z_\phi \end{vmatrix}$$

and where:

$$x_\eta = a \sinh \eta \sin \theta \cos \phi \qquad x_\theta = a \cosh \eta \cos \theta \cos \phi$$

$$x_\phi = -a \cosh \eta \sin \theta \sin \phi \qquad y_\eta = a \sinh \eta \sin \theta \sin \phi$$

$$y_\theta = a \cosh \eta \cos \theta \sin \phi \qquad y_\phi = a \cosh \eta \sin \theta \cos \phi$$

$$z_\eta = \frac{a \cosh \eta \cos \theta}{\sqrt{1+K}} \qquad z_\theta = \frac{-a \sinh \eta \sin \theta}{\sqrt{1+K}} \qquad z_\phi = 0 \qquad \text{(A-11)}$$

$$\frac{\partial \eta}{\partial y} = \frac{1}{J} \frac{\partial(z,x)}{\partial(\theta,\phi)} \qquad \frac{\partial \eta}{\partial z} = \frac{1}{J} \frac{\partial(x,y)}{\partial(\theta,\phi)}$$

$$\frac{\partial \theta}{\partial x} = \frac{1}{J} \frac{\partial(y,z)}{\partial(\phi,\eta)} \qquad \frac{\partial \theta}{\partial y} = \frac{1}{J} \frac{\partial(z,x)}{\partial(\phi,\eta)} \qquad \frac{\partial \theta}{\partial z} = \frac{1}{J} \frac{\partial(x,y)}{\partial(\phi,\eta)}$$

$$\frac{\partial \phi}{\partial x} = \frac{1}{J} \frac{\partial(y,z)}{\partial(\eta,\theta)} \qquad \frac{\partial \phi}{\partial y} = \frac{1}{J} \frac{\partial(z,x)}{\partial(\eta,\theta)} \qquad \frac{\partial \phi}{\partial z} = \frac{1}{J} \frac{\partial(x,y)}{\partial(\eta,\theta)}$$

$$J = \begin{vmatrix} \sinh \eta \sin \theta \cos \phi & \cosh \eta \cos \theta \cos \phi & -\cosh \eta \sin \theta \sin \phi \\ \sinh \eta \sin \theta \sin \phi & \cosh \eta \cos \theta \sin \phi & \cosh \eta \sin \theta \cos \phi \\ \frac{\cosh \eta \cos \theta}{\sqrt{1+K}} & \frac{-\sinh \eta \sin \theta}{\sqrt{1+K}} & 0 \end{vmatrix}$$

$$\frac{1}{\sqrt{1+K}} (\cosh^3 \eta \cos^2 \theta \sin \theta \cos^2 \phi + \cosh \eta \sinh^2 \eta \sin^3 \theta \sin^2 \phi$$

$$+ \cosh^3 \eta \cos^2 \theta \sin \theta \sin^2 \phi + \sinh^2 \cosh \eta \sin^3 \theta \cos^2 \phi)$$

$$= \frac{\cosh^3 \eta \cos^2 \theta \sin \theta + \sinh^2 \cosh \eta \sin^3 \theta}{\sqrt{1+K}}$$

$$= \frac{\cosh \eta \sin \theta (\cosh^2 \eta \cos^2 \theta + \sinh^2 \eta \sin^2 \theta)}{\sqrt{1+K}} \qquad \text{(A-12)}$$

$$\frac{\partial \eta}{\partial x} = \frac{\begin{vmatrix} \frac{\partial y}{\partial \theta} & \frac{\partial y}{\partial \phi} \\ \frac{\partial z}{\partial \theta} & \frac{\partial z}{\partial \phi} \end{vmatrix}}{J} = \frac{\cosh \eta \sinh \eta \sin^2 \theta \cos \phi}{(1+K) J} \qquad \text{(A-13)}$$

$$J = \begin{vmatrix} \sinh \eta \sin \theta \cos \phi & \cosh \eta \cos \theta \cos \phi & -\cosh \eta \sin \theta \sin \phi \\ \sinh \eta \sin \theta \sin \phi & \cosh \eta \cos \theta \sin \phi & \cosh \eta \sin \theta \cos \phi \\ \frac{\cosh \eta \cos \theta}{\sqrt{1+K}} & \frac{-\sinh \eta \sin \theta}{\sqrt{1+K}} & 0 \end{vmatrix}$$

$$= \frac{\cosh^3 \eta \cos^2 \theta \sin \theta \cos^2 \phi}{\sqrt{1+K}} + \cosh \eta \sinh^2 \eta \sin^3 \theta \sin^2 \phi$$

$$+ \frac{\cosh^3 \eta \cos^2 \theta \sin \phi \sin^2 \phi}{\sqrt{1+K}} + \frac{\cosh \eta \sinh^2 \eta \sin^3 \theta \cos^2 \phi}{\sqrt{1+K}}$$

$$= \frac{\cosh \eta \sin \theta}{\sqrt{1+K}} (\cosh^2 \eta \cos^2 \theta + \sinh^2 \eta \sin^2 \theta)$$

$$J\big|_{\eta_o} = \frac{\cosh^3 \eta_o \sin \theta}{\sqrt{1+K}} [\cos^2 \theta + (1+K) \sin^2 \theta] \qquad \text{(A-14)}$$

$$\frac{\partial \theta}{\partial x} = \frac{1}{J} \begin{vmatrix} \frac{\partial y}{\partial \phi} & \frac{\partial y}{\partial \eta} \\ \frac{\partial z}{\partial \phi} & \frac{\partial z}{\partial \eta} \end{vmatrix}$$

$$= \frac{1}{J} \begin{vmatrix} \cosh \eta \sin \theta \cos \phi & \sinh \eta \sin \theta \sin \phi \\ 0 & \frac{\cosh \eta \cos \theta}{\sqrt{1+K}} \end{vmatrix}$$

$$= \frac{\cosh^2 \eta \sin \theta \cos \theta \cos \phi}{\sqrt{1+K}\ J} = \frac{\cosh \eta \cos \theta \cos \phi}{\cosh^2 \eta \cos^2 \theta + \sin^2 \eta \sin^2 \theta} \qquad \text{(A-15)}$$

$$\frac{\partial \theta}{\partial y} = \frac{1}{J} \begin{vmatrix} \frac{\partial z}{\partial \phi} & \frac{\partial z}{\partial \eta} \\ \frac{\partial x}{\partial \phi} & \frac{\partial x}{\partial \eta} \end{vmatrix}$$

$$= \frac{1}{J} \begin{vmatrix} 0 & \frac{\cosh \eta \cos \theta}{\sqrt{1+K}} \\ -\cosh \eta \sin \theta \sin \phi & \sinh \eta \sin \theta \cos \phi \end{vmatrix}$$

$$= \frac{\cosh^2 \eta \sin \theta \cos \theta \sin \phi}{\sqrt{1+K}\ J}$$

$$\frac{\partial \phi}{\partial x} = \frac{1}{J} \begin{vmatrix} \frac{\partial y}{\partial \eta} & \frac{\partial y}{\partial \theta} \\ \frac{\partial z}{\partial \eta} & \frac{\partial z}{\partial \theta} \end{vmatrix}$$

$$= \frac{1}{J} \begin{vmatrix} \sinh \eta \sin \theta \sin \phi & \cosh \eta \cos \theta \sin \phi \\ \frac{\cosh \eta \cos \theta}{\sqrt{1+K}} & \frac{-\sinh \eta \sin \theta}{\sqrt{1+K}} \end{vmatrix}$$

$$= -\frac{(\cosh^2 \eta \cos^2 \theta + \sinh^2 \eta \sin^2 \theta) \sin \phi}{\sqrt{1+K}\ J} = -\frac{\sin \phi}{\cosh \eta \sin \theta} \qquad \text{(A-17)}$$

$$\frac{\partial \phi}{\partial y} = \frac{1}{J} \begin{vmatrix} \frac{\partial z}{\partial \eta} & \frac{\partial z}{\partial \theta} \\ \frac{\partial x}{\partial \eta} & \frac{\partial x}{\partial \theta} \end{vmatrix}$$

$$= \frac{1}{J} \begin{vmatrix} \frac{\cosh \eta \cos \theta}{\sqrt{1+K}} & \frac{-\sinh \eta \sin \theta}{\sqrt{1+K}} \\ \sinh \eta \sin \theta \cos \phi & \cosh \eta \cos \theta \cos \phi \end{vmatrix}$$

$$= \frac{(\cosh^2 \eta \cos^2 \theta + \sinh^2 \eta \sin^2 \theta) \cos \phi}{\sqrt{1+K}\ J} = \frac{\cos \phi}{\cosh \eta \sin \theta} \qquad \text{(A-18)}$$

$$\frac{\partial \phi}{\partial z} = \frac{1}{J}\begin{vmatrix} \sinh \eta \sin \theta \cos \phi & \cosh \eta \cos \theta \cos \phi \\ \sinh \eta \sin \theta \sin \phi & \cosh \eta \cos \theta \sin \phi \end{vmatrix} = 0 \qquad \text{(A-19)}$$

$$\frac{\partial \eta}{\partial y} = \frac{1}{J}\begin{vmatrix} \frac{\partial z}{\partial \theta} & \frac{\partial z}{\partial \phi} \\ \frac{\partial x}{\partial \theta} & \frac{\partial x}{\partial \phi} \end{vmatrix}$$

$$= \frac{1}{J}\begin{vmatrix} \frac{-\sinh \eta \sin \theta}{\sqrt{1+K}} & 0 \\ \cosh \eta \cos \theta \cos \phi & -\cosh \eta \sin \theta \sin \phi \end{vmatrix}$$

$$= \frac{\sinh \eta \cosh \eta \sin^2 \theta \sin \phi}{\sqrt{1+K}\ J} \qquad \text{(A-20)}$$

$$\frac{\partial \eta}{\partial z} = \frac{1}{J}\begin{vmatrix} \frac{\partial x}{\partial \theta} & \frac{\partial x}{\partial \phi} \\ \frac{\partial y}{\partial \theta} & \frac{\partial y}{\partial \phi} \end{vmatrix}$$

$$= \frac{1}{J}\begin{vmatrix} \cosh \eta \cos \theta \cos \phi & -\cosh \eta \sin \theta \sin \phi \\ \cosh \eta \cos \theta \sin \phi & \cosh \eta \sin \theta \cos \phi \end{vmatrix}$$

$$= \frac{1}{J}\left(\cosh^2 \eta \cos \theta \sin \theta\right) \qquad \text{(A-21)}$$

$$\frac{\partial \theta}{\partial z} \quad \frac{1}{J}\begin{vmatrix} \frac{\partial x}{\partial \phi} & \frac{\partial x}{\partial \eta} \\ \frac{\partial y}{\partial \phi} & \frac{\partial y}{\partial \eta} \end{vmatrix}$$

$$= \frac{1}{J}\begin{vmatrix} -\cosh \eta \sin \theta \sin \phi & \sinh \eta \sin \theta \cos \phi \\ \cosh \eta \sin \theta \cos \phi & \sinh \eta \sin \theta \sin \phi \end{vmatrix}$$

$$= -\frac{\cosh \eta \sinh \eta \sin^2 \theta}{J} \qquad \text{(A-22)}$$

These quantities can be used to find the components of flux density

$$\frac{b_x}{\mu_o} = (1+K)\frac{\partial \phi}{\partial x} - i\nu \frac{\partial \phi}{\partial y} \qquad \frac{b_y}{\mu_o} = i\nu \frac{\partial \phi}{\partial x} + (1+K)\frac{\partial \phi}{\partial y}$$

$$\frac{b_z}{\mu_o} = \frac{\partial \phi}{\partial z}$$

$$\frac{\partial \phi}{\partial x} = \frac{\partial \eta}{\partial x}\frac{\partial \phi}{\partial \eta} + \frac{\partial \theta}{\partial x}\frac{\partial \phi}{\partial \theta} + \frac{\partial \phi}{\partial x}\frac{\partial \phi}{\partial \phi}$$

$$= \frac{\sinh \eta \sin \theta \cos \phi}{\cosh^2 \eta \cos^2 \theta + \sinh^2 \eta \sin^2 \theta}\frac{\partial \phi}{\partial \eta} + \frac{\cosh \eta \cos \theta \cos \phi}{\cosh^2 \eta \cos^2 \theta + \mathrm{sh}^2 \eta \sin^2 \theta}\frac{\partial \phi}{\partial \theta}$$

$$- \frac{\sin \phi}{\cosh \eta \sin \theta}\frac{\partial \phi}{\partial \phi} \qquad \text{(A-23)}$$

$$\frac{\partial \phi}{\partial y} = \frac{\partial \eta}{\partial y}\frac{\partial \phi}{\partial \eta} + \frac{\partial \theta}{\partial y}\frac{\partial \phi}{\partial \theta} + \frac{\partial \phi}{\partial y}\frac{\partial \phi}{\partial \phi}$$

$$= \frac{\sinh \eta \sin \theta \sin \phi}{\mathrm{ch}^2 \eta \cos^2 \theta + \mathrm{sh}^2 \eta \sin^2 \theta}\frac{\partial \phi}{\partial \eta} + \frac{\cosh \eta \cos \theta \sin \phi}{\cosh^2 \eta \cos^2 \theta + \sinh^2 \eta \sin^2 \theta}\frac{\partial \phi}{\partial \theta}$$

$$\frac{\cos \phi}{\cosh \eta \sin \theta}\frac{\partial \phi}{\partial \phi} \qquad \text{(A-24)}$$

$$\frac{\partial \phi}{\partial z} = \frac{\partial \eta}{\partial z}\frac{\partial \phi}{\partial \eta} + \frac{\partial \theta}{\partial z}\frac{\partial \phi}{\partial \theta} + \frac{\partial \phi}{\partial z}\frac{\partial \phi}{\partial \phi}$$

$$= \frac{\sqrt{1+K}\cosh \eta \cos \theta}{\mathrm{ch}^2 \eta \cos^2 \theta + \mathrm{sh}^2 \eta \sin^2 \theta}\frac{\partial \phi}{\partial \eta} - \frac{\sqrt{1+K}\sinh \eta \sin \theta}{\mathrm{ch}^2 \eta \cos^2 \theta + \mathrm{sh}^2 \eta \sin^2 \theta}\frac{\partial \phi}{\partial \theta} \qquad \text{(A-25)}$$

The normal (i. e., radial) component of flux density is given by:

$$\frac{b_r^{(0)}}{\mu_o} = \frac{1}{\mu_o}\left(b_x \sin \theta \cos \phi + b_y \sin \theta \sin \phi + b_z \cos \theta\right)$$

$$h_r^{(0)} = \frac{(1+K)}{D}\left\{\sinh\eta \sin^2\theta\cos^2\phi\ \frac{\partial\phi}{\partial\eta} + \cosh\eta\cos\theta\sin\theta\cos^2\phi\ \frac{\partial\phi}{\partial\theta}\right\}$$

$$- (1+K)\ \frac{\sin\theta\cos\phi\sin\phi}{\cosh\eta\sin\theta}\ \frac{\partial\phi}{\partial\phi} - \frac{i\nu}{D}\left\{\text{sh}\,\eta\sin^2\theta\sin\phi\cos\phi\ \frac{\partial\phi}{\partial\eta}\right.$$

$$\left. + \cosh\eta\sin\theta\cos\theta\cos\phi\sin\phi\ \frac{\partial\phi}{\partial\theta}\right\} - \frac{i\nu\cos^2\phi}{\cosh\eta}\ \frac{\partial\phi}{\partial\phi}$$

$$+ \frac{i\nu}{D}\left\{\sinh\sin^2\theta\sin\phi\cos\phi\ \frac{\partial\phi}{\partial\eta} + \text{ch}\,\eta\cos\theta\sin\theta\cos\phi\sin\phi\ \frac{\partial\phi}{\partial\theta}\right\}$$

$$- i\nu\ \frac{\sin^2\phi}{\text{ch}\,\eta}\ \frac{\partial\phi}{\partial\phi} + \frac{1+K}{D}\left\{\text{sh}\,\eta\sin^2\theta\sin^2\phi\ \frac{\partial\phi}{\partial\eta}\right.$$

$$\left. + \text{ch}\,\eta\cos\theta\sin\theta\sin^2\phi\ \frac{\partial\phi}{\partial\theta}\right\} + \frac{(1+K)}{\cosh\eta}\sin\phi\cos\phi\ \frac{\partial\phi}{\partial\phi} + \frac{\sqrt{1+K}\,\text{ch}\,\eta\cos^2\theta}{D}\ \frac{\partial\phi}{\partial\eta}$$

$$- \quad 1+K\ \frac{\text{sh}\,\eta\sin\theta\cos\theta}{D}\ \frac{\partial\phi}{\partial\theta} \qquad \text{(A-26)}$$

$$(h+m)_r = \frac{1+K}{D}\left[\text{sh}\,\eta\sin^2\theta\ \frac{\partial\phi}{\partial\eta} + \text{ch}\,\eta\cos\theta\sin\theta\ \frac{\partial\phi}{\partial\theta}\right]$$

$$\frac{i\nu}{\text{ch}\,\eta}\ \frac{\partial\phi}{\partial\phi} + \frac{\sqrt{1+K}\,\text{ch}\,\eta\cos^2\theta}{D}\ \frac{\partial\phi}{\partial\eta} - \frac{\sqrt{1+K}\,\text{sh}\,\eta\sin\theta\cos\theta}{D}\ \frac{\partial\phi}{\partial\theta}$$

but at the surface

$$\frac{\text{sh}\,\eta}{\text{ch}\,\eta} = \sqrt{1+K} \qquad \text{(A-27)}$$

and

$$D = \cosh^2\eta_o\,(\cos^2\theta + (1+K)\sin^2\theta)$$

$$(h+m)_{r\ \text{surface}} = \left(\frac{(1+K)}{D}\ \text{ch}\,\eta\sin^2\theta + \frac{\sin\eta}{D}\cos^2\theta\right)\frac{\partial\phi}{\partial\eta} - \frac{i\nu}{\text{ch}\,\eta}\ \frac{\partial\phi}{\partial\phi}$$

$$(h+m)_{r\ \text{surface}} = \frac{\text{sh}\,\eta_o}{\text{ch}^2\eta_o}\ \frac{\partial\phi}{\partial\eta} - \frac{i\nu}{\text{ch}\,\eta_o}\ \frac{\partial\phi}{\partial\phi}$$

$$(h+m)_{r\ \text{surface}} = \frac{(1+K)}{\text{sh}\,\eta_o}\ \frac{\partial\phi}{\partial\eta} - \frac{i\nu}{\text{ch}\,\eta_o}\ \frac{\partial\phi}{\partial\phi} \qquad \text{(A-28)}$$

From this equation and from the condition of continuity of potential the constants A and B can be eliminated and the characteristic equation of the magnetostatic modes results:

$$-\frac{1}{a} = i\sqrt{1+K}\,\frac{P_n^{m'}(i\sinh\eta_o)}{P_n^{m}(i\sinh\eta_o)} \pm \frac{m\nu}{\cosh\eta_o} \tag{A-29}$$

It will be convenient to define $\xi_o = \sinh\eta_o$ The Legendre polynomials can be written in the product form:

$$P_n^m(i\,\xi_o) = A(1+\xi_o^{\,2})^{\frac{1}{2}|m|}\, i\,\xi_o \prod_{r=1}^{\frac{1}{2}(n-|m|)} (\xi_o^{\,2} - \xi_{or}^{\,2})$$

where ξ_{or} are the zeros of P_n^m

$$\frac{i\,P_n^{m'}(i\,\xi_o)}{P_n^m(i\,\xi_o)} = \frac{|m|\,\xi_o^{\,2}}{1+\xi_o^{\,2}} + 2\prod_{r=1}^{\frac{1}{2}(n-|m|)} \frac{\xi_o^{\,2}}{(-\xi_o^{\,2} - \xi_{or}^{\,2})} \tag{A-30}$$

If this relation is substituted in the characteristic equation, then it can be used to find the characteristic roots $\xi_{on,m,r}$. A graphical solution is perhaps the best. To that purpose note that $\xi_o^{\,2} = \frac{1+K}{K}$ and note that for $\xi_o^{\,2} < 0$ the ratio of Legendre polynomials has poles at ξ_{or}^2 and hence a set of roots ξ_{onmr} is guaranteed. However, for $\xi_o^{\,2} > 0$ no such guarantee is possible and no more than one root is possible. The characteristic equation is written in for form:

$$i\sqrt{1+K}\,\frac{P_n^{m'}(i\,\xi_o)}{P_n^{m}(i\,\xi_o)} = F(\xi_o) \tag{A-31}$$

$$\mp\frac{m\nu}{(1+\xi_o^{\,2})^{\frac{1}{2}}} - \frac{1}{a} = H(\xi_o)$$

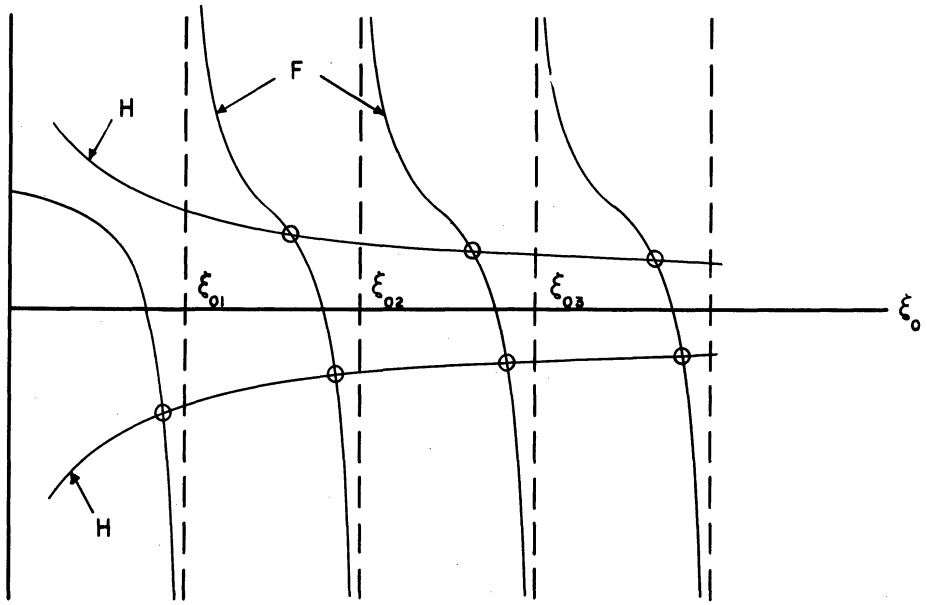

Fig. A-2. Graphical solution of characteristic equation [i.e., $H(\xi_0) = F(\xi_0)$] for the set of roots $\xi_0 = \xi_{onmr}$.

Certain features of these roots can be noted from the graph. Observe that for increasing ξ_0 the roots approach the zeros of the Legendre polynomials. Notice also that they alternate along the ξ_0 axis and in particular do not tend to be degenerate for m and -m. This fact will be used in the chapter concerning the lower sideband circuit.

It has been shown that $\xi_0^2 = \frac{1+K}{K}$ which must be negative for solutions to the characteristic equation. The implications of these facts are that each root corresponds to a resonant frequency which of course depends upon the biasing field. In addition it is true that the frequency range for which these roots exist is defined by that for which $\frac{1+K}{K} < 0$. That frequency range is $\gamma H_0 \leq \omega \leq \gamma\sqrt{H_0(H_0 + m)}$ and is of course the same as that observed by Walker in his more general paper.

APPENDIX B

SUSCEPTIBILITY COMPONENTS INDEPENDENT OF POSITION IN SAMPLE

The requirement that the susceptibility tensor components be independent of position in the sample effectively demands that the internal dc magnetic field be uniform. Clearly this cannot be the case if the sample is placed in the uniform field of a magnet since the demagnetizing field will be highly nonuniform for such an arrangement. However it is possible to maintain a uniform internal field in the following physical arrangement (see Fig. B-1) from a long cylinder of the material desired and of the diameter of interest cut a right section of the length desired; place this section in a strip line of spacing equal to the section length; obtain two more cuts from the original cylinder which are each long compared with the spacing of the strip line and place them, one on either side of the strip line coaxial with the section included in it; magnetize to saturation along the common axis. The dc field in the section between the strip line plates will be uniform since it is in the middle portion of a long ferromagnetic cylinder. The microwave energy will be contained in the strip line and so the section so included will be the equivalent of that pictured in Fig. B-1 in which the internal dc field is uniform.

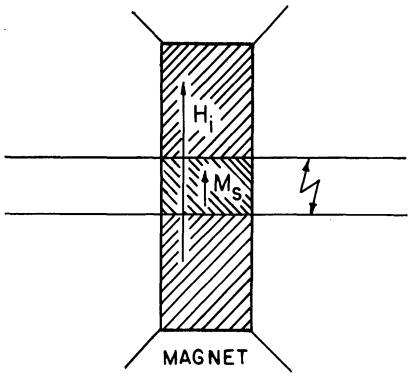

Fig. B-1. Configuration for which bias magnetic field is uniform. The field H_i is uniform in the section labelled M_s between the conducting plates.

APPENDIX C

CHARACTERISTIC EQUATION FOR SECOND-ORDER-CORRECT BOUNDARY VALUE PROBLEM

The characteristic equation for the example boundary value problem can be found from substituting the scalar and vector potentials in Eq. 3.45. However, computation of the components of these potentials requires knowledge of the magnetostatic approximation to the magnetization. The components of the magnetostatic approximation to the magnetization are:

$$\begin{aligned} M_{ox} &= K\left[\cos\theta\,\frac{\partial\phi}{\partial r} - \frac{\sin\theta}{r}\,\frac{\partial\phi}{\partial\theta}\right] - i\nu\left[\sin\theta\,\frac{\partial\phi}{\partial r} + \frac{\cos\theta}{r}\,\frac{\partial\phi}{\partial\theta}\right] \\ M_{oy} &= i\nu\left[\cos\theta\,\frac{\partial\phi}{\partial r} - \frac{\sin\theta}{r}\,\frac{\partial\phi}{\partial\theta}\right] + K\left[\sin\theta\,\frac{\partial\phi}{\partial r} + \frac{\cos\theta}{r}\,\frac{\partial\phi}{\partial\theta}\right] \end{aligned} \tag{C-1}$$

Let the magnetostatic potential for the mode in question be:

$$\phi = I_{n_o}\left(\frac{\beta_{m_o} r}{\sqrt{1+K}}\right) e^{i n_o \theta} \cos \beta_{m_o} z \tag{C-2}$$

Then

$$\begin{aligned} \frac{\partial\phi}{\partial r} &= \frac{\beta_{m_o}}{\sqrt{1+K}}\, I'_{n_o}\left(\frac{\beta_{m_o} r}{\sqrt{1+K}}\right) e^{i n_o \theta} \cos\beta_{m_o} z \\ \frac{\partial\phi}{\partial\theta} &= i\, n_o\, I_{n_o}\left(\frac{\beta_{m_o} r}{\sqrt{1+K}}\right) e^{i n_o \theta} \cos \beta_{m_o} z \end{aligned} \tag{C-3}$$

These quantities can be used to compute the lowest order approximation to the vector potential in which the following observation is made:

$$\begin{aligned} \int_0^{2\pi} e^{-in\theta'} \cos\theta' e^{i n_o \theta} d\theta' &= \pi \quad \text{if } n = n_o \pm 1 \\ &= 0 \quad \text{otherwise} \end{aligned} \tag{C-4}$$

and

$$\begin{aligned} \int_0^{2\pi} e^{-in\theta} \sin\theta\, e^{i n_o \theta} d\theta &= \frac{\pi}{i} \qquad n = n_o \pm 1 \\ &= 0 \quad \text{otherwise .} \end{aligned}$$

Using these relations and the orthogonality relations of the z components, the components of the vector potential A_{ox} and A_{oy} are given by the relations on pages 201 and 202. The denominator of Green's function has been written as $f(m_o \pi \alpha)$ in these equations. These lengthy expressions can be summarized by making the definitions A_{n_o+1} and B_{n_o-1} (see page 203). Then using these definitions the components of the vector potential can be written:

$$A_{ox} = \frac{\pi \cos \beta_{m_o} z}{f(m_o \pi \alpha)} \left[(K-\nu) A_{n_o+1}(r) e^{i(n_o+1)\theta} + (K+\nu) B_{n_o-1}(r) e^{i(n_o-1)\theta} \right] \quad \text{(C-9)}$$

$$A_{oy} = \frac{i\pi \cos \beta_{m_o} z}{f(m_o \pi \alpha)} \left[(\nu-K) A_{n_o+1}(r) e^{i(n_o+1)\theta} + (K+\nu) B_{n_o-1}(r) e^{i(n_o-1)\theta} \right] \quad \text{(C-10)}$$

Matching boundary conditions will require knowledge of the normal component of the vector potential. For this reason it is computed here.

Outside the sample:

$$A_n\Big|_{surf} = k_o^2 (\cos\theta A_{ox} + \sin\theta A_{oy})\Big|_{r=a}$$

$$= \frac{\pi k_o^2 \cos \beta_{m_o} z}{f(m_o \pi \alpha)} \left[(K-\nu) A_{n_o+1}(r) e^{in_o\theta} + (K+\nu) B_{n_o-1}(r) e^{in_o\theta} \right] \quad \text{(C-11)}$$

Inside the sample:

$$A_n\Big|_{surf} = k_i^2 \left[\left((1+K) A_{ox} - i\nu A_{oy} \right) \cos\theta + (i\nu A_{ox} + K A_{oy}) \sin\theta \right] \quad \text{(C-12)}$$

$$= \frac{k_i^2 \pi \cos \beta_{m_o} z}{f(m_o \pi \alpha)} \left[\left\{ (1+K) \left((K-\nu) A_{n_o+1}(r) e^{i(n_o+1)\theta} + (K+\nu) B_{n_o-1}(r) e^{i(n_o-1)\theta} \right) + \nu \left(\nu-K) A_{n_o+1}(r) e^{i(n_o+1)\theta} + (K+\nu) B_{n_o-1}(r) e^{i(n_o-1)\theta} \right) \cos\theta \right\} \right.$$

$$\left. + \left\{ i\nu \left((K-\nu) A_{n_o+1}(r) e^{i(n_o+1)\theta} + (K+\nu) B_{n_o-1}(r) e^{i(n_o-1)\theta} \right) + \right. \right.$$

$$+ i(1+K)\left((\nu - K)\, A_{n_o+1}(r)\, e^{i(n_o+1)\theta} + (K+\nu)\, B_{n_o-1}(r)\, e^{i(n_o-1)\theta} \right)\Big\} \sin\theta \Big] \qquad \text{(C-13)}$$

Thus the normal component of the vector potential inside the sample at the sample surface is given by:

$$A_n\Big|_{\text{surf.}} = \frac{k_i^2\, \pi \cos \beta_{m_o} z}{f(m_o \pi \alpha)} \left[(1+K-\nu)(K-\nu)\, A_{n_o+1}(r) + (1+K+\nu)(K+\nu)\, B_{n_o-1}(r) \right] e^{i n_o \theta}$$

In addition to the normal components of the vector potential the normal derivative of the scalar potential must be found inside the sample at the surface in order to apply the boundary condition of the continuity of the normal components of flux density. In terms of the quantities previously defined A_{n_o+1} and B_{n_o-1} it is possible to write this normal derivative:

$$\frac{\partial \phi^{(2)}}{\partial r}\Big|_{r=a} = \frac{k_i^2 \cos(\beta_{m_o} z)\, e^{i n_o \theta}}{(1+K)\, f(m_o \pi \alpha) a\, J_{n_o}(\alpha_2 a)} \int_o^a J_{n_o}(\alpha_2 r) r\, dr \Big[(K-\nu)^2 \left(A'_{n_o+1}(r) + \frac{n_o+1}{r} A_{n_o+1}(r) \right) + (K+\nu)^2 \left(B'_{n_o-1}(r) - \frac{n_o-1}{r} B_{n_o-1}(r) \right) \Big] \qquad \text{(C-14)}$$

This expression can be written in a more useful form by substituting the functional form for A'_{n_o+1} and B'_{n_o-1} However, it is convenient to reduce these quantities by manipulation of the appropriate recursion formulas for the Bessel functions

$$z\, J'_n(z) = -z\, J_{n+1}(z) + n\, J_n(z)$$

$$z\, J'_n(z) = -z\, J_{n+1}(z) + n\, J_n(z)$$

and

$$z\, J'_n(z) = z\, J_{n-1}(z) - n\, J_n(z)$$

Using these relations and the well-known integral

$$\int J_\nu(kz)\, J_\nu(\ell z)\, z\, dz = \frac{z}{k^2 - \ell^2}\left[\ell\, J_\nu(kz)\, J'_\nu(\ell z) - k\, J_\nu(\ell z)\, J'_\nu(kz)\right]$$

it can be shown that the expression for the normal derivative of the scalar potential can be written:

$$\left.\frac{\partial \phi^2}{\partial r}\right|_{r=a} = \frac{k_i^{\,2} \cos(\beta_{m_o} z)\, e^{i n_o \theta}}{K\sqrt{1+K}\, f(m_o \pi \alpha)\, a\, J_{n_o}(\alpha_2 a)} \int_{o^*}^{a} J_{n_o}(\alpha_2 r)\, r\, dr \left[\frac{4 n_o K^2 \nu}{\sqrt{1+K}} I_{n_o}\left(\frac{\beta_{m_o} a}{\sqrt{1+K}}\right) K_{n_o}(\beta_{m_o} a)\right.$$

$$+ (K+\nu)^2 \left\{\left(I_{n_o}\left(\frac{\beta_{m_o} a}{\sqrt{1+K}}\right) K_{n_o+1}(\beta_{m_o} a) - K_{n_o-1}(\beta_{m_o} a)\right)\right.$$

$$\left. - K_{n_o}(\beta_{m_o} a)\left[I_{n_o+1}\left(\frac{\beta_{m_o} a}{\sqrt{1+K}}\right) - I_{n_o-1}\left(\frac{\beta_{m_o} a}{\sqrt{1+K}}\right)\right] I_{n_o}(\beta_{m_o} r)\right\} \qquad \text{(C-15)}$$

$$\left. + \frac{2(K^2+\nu^2)}{\sqrt{1+K}} I_{n_o}\left(\frac{\beta_{m_o} r}{\sqrt{1+K}}\right)\left[I_{n_o}(\beta_{m_o} r)\, K_{n_o+1}(\beta_{m_o} r) + I_{n_o+1}(\beta_{m_o} r)\, K_{n_o}(\beta_{m_o} r)\right]\right]$$

It will be convenient to define:

$$h_{n_o m_o}(K,\nu) = \frac{4 n_o K^2 \nu}{\sqrt{1+K}} I_{n_o}\left(\frac{\beta_{m_o} a}{\sqrt{1+K}}\right) K_{n_o}(\beta_{m_o} a)$$

$$+ (K^2+\nu^2)\left\{I_{n_o}\left(\frac{\beta_{m_o} a}{\sqrt{1+K}}\right)\left(K_{n_o+1}(\beta_{m_o} a) - K_{n_o-1}(\beta_{m_o} a)\right)\right. \qquad \text{(C-16)}$$

$$\left. - K_{n_o}(\beta_{m_o} a)\left[I_{n_o+1}\left(\frac{\beta_m a}{\sqrt{1+K}}\right) - I_{n_o-1}\left(\frac{\beta_m a}{\sqrt{1+K}}\right)\right]\right\}$$

Then from the integral relation:

$$\int_0^a J_{n_o}(\alpha_2 r')\, I_{n_o}(\beta_m r')\, r'\, dr' = \frac{a}{\alpha_2^2 - \beta_m^2}\left[\beta_m J_{n_o}(\alpha_2 a)\, I'_{n_o}(\beta_{m_o} a) - \alpha_2 J'_{n_o}(\alpha_2 a)\, I_{n_o}(\beta_{m_o} a)\right]$$

but

$$\beta_{m_o} a\, I'_{n_o}(\beta_{m_o} a) = -\beta_{m_o} a\, I'_{n_o+1}(\beta_{m_o} a) + n_o\, I_{n_o}(\beta_{m_o} a)$$

and

$$\alpha_2 a\, J'_{n_o}(\alpha, a) = -\alpha_2 a\, J_{n_o+1}(\alpha_2 a) + n_o\, J_{n_o}(\alpha_2 a)$$

Thus:

$$\int_0^a J_{n_o}(\alpha_2 r')\, I_{n_o}(\beta_m r')\, r'\, dr' = \frac{a}{(\alpha_2^2 - \beta_{m_o}^2)}\left[\alpha_2 J_{n_o+1}(\alpha_2 a)\, I_{n_o}(\beta_{m_o} a) - \beta_m I_{n_o}(\beta_{m_o} a)\, J_{n_o}(\alpha_2 a)\right] \qquad \text{(C-17)}$$

The coefficient of this integral in the expression for $\frac{\partial \phi^{(2)}}{\partial r}$ is proportional to k^2 and since this development is only correct to second order in k this integral need only be computed to zero order in k. The following observations should be made:

$$J_{n_o}(\alpha_2 a) \underset{k \to 0}{\longrightarrow} i^{n_o} I_{n_o}(\beta_m a)$$

$$\alpha_2 \underset{k \to 0}{\longrightarrow} i\beta_m$$

Thus

$$\frac{1}{J_n(\alpha_2 a)} \int_0^a J_{n_o}(\alpha_2 r')\, I_{n_o}(\beta_{m_o} r')\, r'\, dr' \underset{k \to 0}{\longrightarrow} \frac{a}{\beta_m} I_{n_o+1}(\beta_m a)$$

A further reduction is possible using the following observations:

$$\beta_{m_o} r\, I_{n_o-1}(\beta_m r) = 2(n_o-1)\, I_{n_o}(\beta_{m_o} r) - \beta_{m_o} r\, I_{n_o+1}(\beta_{m_o} r)$$

$$\beta_{m_o} r\, K_{n_o-1}(\beta_{m_o} r) = 2(n_o-1)\, K_{n_o}(\beta_{m_o} r) - \beta_{m_o} r\, K_{n_o+1}(\beta_{m_o} r)$$

so that:

$$\begin{aligned}
\beta_{m_o} r\Big[I_{n_o-1}(\beta_{m_o} r)\, K_{n_o}(\beta_{m_o} r) - I_{n_o}(\beta_{m_o} r)\, K_{n_o-1}(\beta_{m_o} r)\Big] &= K_{n_o}(\beta_{m_o} r)\Big[2(n_o-1)\, I_{n_o}(\beta_{m_o} r) \\
&- \beta_{m_o} r\, I_{n_o+1}(\beta_{m_o} r)\Big] - I_{n_o}(\beta_{m_o} r)\Big[2(n_o-1)\, K_{n_o}(\beta_{m_o} r) - \beta_{m_o} r\, K_{n_o+1}(\beta_{m_o} r)\Big] \\
&= -\beta_{m_o} r\Big[I_{n_o+1}(\beta_{m_o} r)\, K_{n_o}(\beta_{m_o} r) - I_{n_o}(\beta_{m_o} r)\, K_{n_o+1}(\beta_{m_o} r)\Big] \qquad \text{(C-18)}
\end{aligned}$$

and also

$$\begin{aligned}
&- \beta_{m_o} r\, I_{n_o}\left(\frac{\beta_{m_o} r}{\sqrt{1+K}}\right)\Big[(K-\nu)^2\Big(I_{n_o}(\beta_{m_o} r)\, K_{n_o+1}(\beta_{m_o} r) - I_{n_o+1}(\beta_{m_o} r)\, K_{n_o}(\beta_{m_o} r)\Big) \\
&- (K+\nu)^2\Big(I_{n_o+1}(\beta_{m_o} r)\, K_{n_o}(\beta_{m_o} r) - I_{n_o}(\beta_{m_o} r)\, K_{n_o+1}(\beta_{m_o} r)\Big)\Big] \\
&= - \beta_{m_o} r\, I_{n_o}\left(\frac{\beta_{m_o} r}{\sqrt{1+K}}\right)(K^2+\nu^2)\Big(I_{n_o}(\beta_{m_o} r)\Big[K_{n_o+1}(\beta_{m_o} r) - K_{n_o-1}(\beta_{m_o} r)\Big] \\
&- K_{n_o}(\beta_{m_o} r)\Big[I_{n_o+1}(\beta_{m_o} r) - I_{n_o-1}(\beta_{m_o} r)\Big]\Big) \\
&= (\beta_m r)(K^2+\nu^2)\, I_{n_o}\left(\frac{\beta_{m_o} r}{\sqrt{1+K}}\right)\Big(I_{n_o}(\beta_{m_o} r)\Big[K_{n_o+1}(\beta_{m_o} r) + K_{n_o-1}(\beta_{m_o} r)\Big] \\
&- K_{n_o}(\beta_{m_o} r)\Big[I_{n_o+1}(\beta_{m_o} r) + I_{n_o-1}(\beta_{m_o} r)\Big] \\
&- 2\, I_{n_o}(\beta_{m_o} r)\, K_{n_o+1}(\beta_{m_o} r) - K_{n_o}(\beta_{m_o} r)\, I_{n_o+1}(\beta_{m_o} r)\Big) \qquad \text{(C-19)} \\
&= - 2\beta_{m_o} r(K^2+\nu^2)\, I_{n_o}\left(\frac{\beta_{m_o} r}{\sqrt{1+K}}\right)\Big[I_{n_o}(\beta_{m_o} r)\, K_{n_o+1}(\beta_{m_o} r) - K_{n_o}(\beta_{m_o} r)\, I_{n_o+1}(\beta_{m_o} r)\Big]
\end{aligned}$$

Substituting these observations in $\frac{\partial \phi^{(2)}}{\partial r}$ we obtain:

$$\left.\frac{\partial \phi^{(2)}}{\partial r}\right|_{r=a} = \frac{k_i^2 \, e^{i n_o \theta} \cos \beta_{m_o} z}{K \sqrt{1+K}\, f(m_o \pi \alpha)\, a\, I_{n_o}(\beta_{m_o} a)} \int_o^a I_{n_o}(\beta_{m_o} r)\, r\, dr \Bigg[h_{n_o m_o} I_{n_o}(\beta_{m_o} r)$$

$$- 2 \beta_{m_o} r (K^2 + \nu^2) I_{n_o}\left(\frac{\beta_{m_o} r}{\sqrt{1+K}}\right)\Big(I_{n_o}(\beta_{m_o} r)\, K_{n_o+1}(\beta_{m_o} r)$$

$$- K_{n_o}(\beta_{m_o} r)\, I_{n_o+1}(\beta_{m_o} r)\Big) \Bigg] \qquad \text{(C-20)}$$

$$= \frac{k_i^2 \, e^{i n_o \theta} \cos \beta_{m_o} z}{K \sqrt{1+K}\, f(m_o \pi \alpha)\, a\, I_{n_o}(\beta_{m_o} a)} \Bigg[\Big(a\, I_{n_o}^2(\beta_{m_o} a)$$

$$- I_{n_o - 1}(\beta_m a)\, I_{n_o+1}(\beta_{m_o} a)\Big)\, h_{n_o m_o}$$

$$- 2(K^2 + \nu^2) \int_o^a \beta_{m_o} I_{n_o}\left(\frac{\beta_{m_o} r}{\sqrt{1+K}}\right) I_{n_o}(\beta_{m_o} r)\Big(I_{n_o}(\beta_{m_o} r)\, K_{n_o+1}(\beta_{m_o} r)$$

$$- K_{n_o}(\beta_{m_o} r)\, I_{n_o+1}(\beta_{m_o} r)\Big) r^2\, dr \Bigg] \qquad \text{(C-21)}$$

Although the integral cannot be evaluated directly, a digital computer is useful for approximating it once K and ν are known. But since this expression need be correct to only second order in k then K and ν need be correct to only zero order. The values $K_{n_o m_o \ell_o}$ $\gamma_{n_o m_o \ell_o}$ are known from the magnetostatic approximation. For convenience let us introduce the notation $H_{n_o m_o}(K, \nu)$ so that

$$\left.\frac{\partial \phi^{(2)}}{\partial r}\right|_{r=a} = k_i^2 \, H_{n_o m_o}(K, \nu)\, e^{i n_o \theta} \cos \beta_{m_o} z \, , \qquad \text{(C-22)}$$

where $H_{n_o m_o}(K, \nu)$ is given by

$$H_{n_o m_o}(K,\nu) = \frac{1}{K\sqrt{1+K}\, f(m_o\pi\alpha)\, a\, I_{n_o}(\beta_{m_o} a)} \left[\left(a\, I^2_{n_o}(\beta_{m_o} a) - I_{n_o-1}(\beta_{m_o} a)\, I_{n_o+1}(\beta_{m_o} a) \right) h_{n_o m_o} \right.$$

$$- 2(K^2+\nu^2) \int_o^a \beta_{m_o} I_{n_o}\left(\frac{\beta_{m_o} r}{\sqrt{1+K}} \right) \left[I_{n_o}(\beta_{m_o} r)\, I_{n_o}(\beta_{m_o} r)\, K_{n_o+1}(\beta_{m_o} r) \right.$$

$$\left. \left. - K_{n_o}(\beta_{m_o} r)\, I_{n_o+1}(\beta_{m_o} r) \right] r^2\, dr \right] \qquad \text{(C-23)}$$

From the solution to Green's function the potential Φ^2 has been shown to be

$$\Phi^{(2)} = \phi^{(2)} + \frac{B\, K_{n_o}(\alpha_1 a)\, J_{n_o}(\alpha_2 r)}{J_{n_o}(\alpha_2 a)} \cos \beta_{m_o} z\, e^{i n_o \theta} \qquad \text{(C-24)}$$

Using this definition and the values found for the normal component of flux density due to the vector potential, we can write the characteristic equation.

$$\alpha B K'_n(\alpha_1 a) + k_o^2 \left[\frac{\pi}{f(m_o\pi\alpha)} \left((K-\nu) A_{n_o+1}(a) + (K+\nu) B_{n_o-1}(a) \right) \right] = B \left[K_{n_o}(\alpha_1 a) \frac{\alpha_2 J'_{n_o}(\alpha_2 a)}{J_n(\alpha_2 a)} (1+K) \right.$$

$$\left. + n_o \nu K_n(\alpha_1 a) \right] + B(1+K) H_{n_o m_o}(\nu, K)\, k_i^2$$

$$+ k_i^2 \left(\frac{\pi}{f(m_o\pi\alpha)} \left[(1+K-\nu)(K-\nu) A_{n_o+1}(a) + (1+K+\nu)(K+\nu) B_{n_o-1}(a) \right] \right) \qquad \text{(C-25)}$$

Then neglecting common factors in the equation this expression can be rewritten as:

$$\alpha_1 \frac{K'_{n_o}(\alpha_1 a)}{K_{n_o}(\alpha_1 a)} - (1+K)\, \alpha_2 \frac{J'_{n_o}(\alpha_2 a)}{J_{n_o}(\alpha_2 a)} - \frac{n_o \nu}{a} =$$

$$\frac{1}{B} \left(\frac{k_i^2 \pi}{f(m_o\pi\alpha)} \left[(1+K-\nu)(K-\nu) A_{n_o+1}(a) + (1+K+\nu)(K+\nu) B_{n_o-1}(a) \right] \right.$$

$$\left. - \frac{k_o^2 \pi}{f(m_o\pi\alpha)} \left[(K-\nu) A_{n_o+1}(a) + (K+\nu) B_{n_o-1}(a) \right] \right) + (1+K) k_o^2 H_{n_o m_o}(\nu, K) \qquad \text{(C-26)}$$

The parameter B need be known only to zero order if the above equation is to be correct to second order. Equation 3.46 is useful for determining $B(k \to 0)$:

$$B \underset{k \to 0}{\longrightarrow} \frac{I_{n_o}\left(\frac{\beta_{m_o} a}{\sqrt{1+K}}\right)}{K_{n_o}(\beta_{m_o} a)} \tag{C-27}$$

Use of this definition yields the characteristic equation of the sample modes.

$$\alpha_1 \frac{K'_{n_o}(\alpha_1 a)}{K_{n_o}(\alpha_1 a)} - (1+K)\,\alpha_2 \frac{J'_{n_o}(\alpha_2 a)}{J_{n_o}(\alpha_2 a)} \pm \frac{n_o \nu}{a} = \frac{H(K, \nu, k_i^2, k_o^2)}{I_{n_o}\left(\frac{\beta_{m_o} a}{\sqrt{1+K}}\right)} \tag{C-28}$$

This expression appears in the text as Eq. 3.64 where $H(K_1 \gamma k_i^2 k_o^2)$ is given by:

$$H = \frac{K_{n_o}(\beta_{m_o} a)\,\pi}{f(m_o \pi \alpha)} \left(k_i^2 \left[(1+K-\nu)(K-\nu) A_{n_o+1}(a) + (1+K+\nu)(K+\nu) B_{n_o-1}(a) \right.\right.$$
$$\left.\left. - k_o^2 \left[(K-\nu) A_{n_o+1}(a) + (K+\nu) B_{n_o-1}(a) \right] \right) + (1+K) k_o^2 H_{n_o m_o} \right. \tag{C-29}$$

Thus the characteristic equation for the example problem has been determined correct to second order in k.

$$A_{x_o} = \frac{\pi \cos \beta_{m_o} z}{f(m_o \pi \alpha)} \left\{ K \left(e^{i(n_o+1)\theta} \left[K_{n_o+1}(\beta_{m_o} r) \int_o^r \frac{\beta_{m_o}}{\sqrt{1+K}} I'_{n_o}\left(\frac{\beta_{m_o} r'}{\sqrt{1+K}} \right) I_{n_o+1}(\beta_{m_o} r') r' \, dr' \right.\right.\right.$$

$$\left. + I_{n_o}(\beta_{m_o} r) \int_r^a \frac{\beta_{m_o}}{\sqrt{1+K}} I'_{n_o}\left(\frac{\beta_{m_o} r'}{\sqrt{1+K}} \right) K_{n_o+1}(\beta_m r') \, d' \, dr' \right] + e^{i(n_o-1)\theta} \left[K_{n_o-1}(\beta_{m_o} r) \int_o^r \frac{\beta_{m_o}}{\sqrt{1+K}} I'_{n_o}\left(\frac{\beta_{m_o} r'}{\sqrt{1+K}} \right) I_{n_o-1}(\beta_{m_o} r') \, r' \, dr' \right.$$

$$\left. + I_{n_o-1}(\beta_{m_o} r) \int_r^a \frac{\beta_{m_o}}{\sqrt{1+K}} I'_{n_o}\left(\frac{\beta_{m_o} r'}{\sqrt{1+K}} \right) K_{n_o-1}(\beta_{m_o} r') \, r' \, dr' \right] - e^{i(n_o+1)\theta} \left[n_o K_{n_o+1}(\beta_{m_o} r) \int_o^r I_{n_o}\left(\frac{\beta_{m_o} r'}{\sqrt{1+K}} \right) I_{n_o+1}(\beta_{m_o} r') \, r' \, dr' \right.$$

$$\left. + n_o I_{n_o+1}(\beta_{m_o} r) \int_r^a I_{n_o}\left(\frac{\beta_{m_o} r'}{\sqrt{1+K}} \right) K_{n_o+1}(\beta_{m_o} r') \, dr' \right] + e^{i(n_o-1)\theta} n_o \left[K_{n_o-1}(\beta_m r) \int_o^r I_{n_o}\left(\frac{\beta_{m_o} r'}{\sqrt{1+K}} \right) I_{n_o-1}(\beta_{m_o} r') \, dr' \right.$$

$$\left. \left. + K_{n_o-1}(\beta_{m_o} r) \int_r^a I_{n_o}\left(\frac{\beta_{m_o} r'}{\sqrt{1+K}} \right) K_{n_o-1}(\beta_{m_o} r') \, dr' \right] \right) - i\nu \left(-i e^{i(n_o+1)\theta} \left[K_{n_o+1}(\beta_{m_o} r) \int_o^r \frac{\beta_{m_o}}{\sqrt{1+K}} I'_{n_o}\left(\frac{\beta_{m_o} r'}{\sqrt{1+K}} \right) I_{n_o+1}(\beta_{m_o} r') \, r' \, dr' \right.\right.$$

$$\left. + I_{n_o+1}(\beta_{m_o} r) \int_r^a \frac{\beta_{m_o}}{\sqrt{1+K}} I'_{n_o}\left(\frac{\beta_{m_o} r'}{\sqrt{1+K}} \right) K_{n_o+1}(\beta_{m_o} r') \, r' \, dr' \right] + i e^{i(n_o-1)\theta} \left[K_{n_o-1}(\beta_{m_o} r) \int_o^r \frac{\beta_{m_o}}{\sqrt{1+K}} I'_{n_o}\left(\frac{\beta_{m_o} r'}{\sqrt{1+K}} \right) I_{n_o-1}(\beta_{m_o} r') \, r' \, dr' \right.$$

$$\left. + I_{n_o-1}(\beta_{m_o} r) \int_r^a \frac{\beta_{m_o}}{\sqrt{1+K}} I'_{n_o}\left(\frac{\beta_{m_o} r'}{\sqrt{1+K}} \right) K_{n_o-1}(\beta_{m_o} r') \, r' \, dr' \right] + i e^{i(n_o+1)\theta} n_o \left[K_{n_o+1}(\beta_{m_o} r) \int_o^r I_{n_o}\left(\frac{\beta_{m_o} r'}{\sqrt{1+K}} \right) I_{n_o+1}(\beta_m r') \, dr' \right.$$

$$\left. + I_{n_o+1}(\beta_{m_o} r) \int_r^a I_n\left(\frac{\beta_{m_o} r'}{\sqrt{1+K}} \right) K_{n_o+1}(\beta_{m_o} r') \, dr' \right] + i e^{i(n_o-1)\theta} n_o \left[K_{n_o-1}(\beta_{m_o} r) \int_o^r I_{n_o}\left(\frac{\beta_{m_o} r'}{\sqrt{1+K}} \right) I_{n_o-1}(\beta_{m_o} r') \, dr' \right.$$

$$\left. \left. + I_{n_o-1}(\beta_{m_o} r) \int_r^a I_{n_o}\left(\frac{\beta_{m_o} r'}{\sqrt{1+K}} \right) K_{n_o-1}(\beta_{m_o} r') \, dr' \right] \right) \right\} \qquad \text{(C-5)}$$

$$A_{oy} = \frac{\pi \cos \beta_{m_o} z}{f(m_o \pi \alpha)} \left\{ i\nu \left(e^{i(n_o+1)\theta} \left[K_{n_o+1}(\beta_{m_o} r) \int_o^r \frac{\beta_{m_o}}{\sqrt{1+K}} I'_{n_o}\left(\frac{\beta_{m_o} r'}{\sqrt{1+K}}\right) I_{n_o+1}(\beta_{m_o} r')\, r'\, dr' \right.\right.\right.$$

$$\left. + I_{n_o+1}(\beta_{m_o} r) \int_r^a \frac{\beta_{m_o}}{\sqrt{1+K}} I'_{n_o}\left(\frac{\beta_{m_o} r'}{\sqrt{1+K}}\right) K_{n_o+1}(\beta_{m_o} r')\, r'\, dr' \right] + e^{i(n_o-1)\theta} \left[K_{n_o-1}(\beta_{m_o} r) \int_o^r \frac{\beta_{m_o}}{\sqrt{1+K}} I'_{n_o}\left(\frac{\beta_{m_o} r'}{\sqrt{1+K}}\right) I_{n_o-1}(\beta_{m_o} r')\, r'\, dr' \right.$$

$$\left. + I_{n_o-1}(\beta_{m_o} r) \int_r^a \frac{\beta_{m_o}}{\sqrt{1+K}} I'_{n_o}\left(\frac{\beta_{m_o} r'}{\sqrt{1+K}}\right) K_{n_o-1}(\beta_{m_o} r')\, r'\, dr' \right] - e^{i(n_o+1)\theta} n_o \left[K_{n_o+1}(\beta_{m_o} r) \int_o^r I_{n_o}\left(\frac{\beta_{m_o} r'}{\sqrt{1+K}}\right) I_{n_o+1}(\beta_{m_o} r')\, dr' \right.$$

$$\left. + I_{n_o+1}(\beta_{m_o} r) \int_r^a I_{n_o}\left(\frac{\beta_{m_o} r'}{\sqrt{1+K}}\right) K_{n_o+1}(\beta_{m_o} r')\, dr' \right] + e^{i(n_o-1)\theta} n_o \left[K_{n_o-1}(\beta_{m_o} r) \int_o^r I_{n_o}\left(\frac{\beta_{m_o} r'}{\sqrt{1+K}}\right) I_{n_o-1}(\beta_{m_o} r')\, dr' \right.$$

$$\left. \left. + I_{n_o-1}(\beta_{m_o} r) \int_r^a I_{n_o}\left(\frac{\beta_{m_o} r'}{\sqrt{1+K}}\right) K_{n_o-1}(\beta_{m_o} r')\, dr' \right] \right) + i K \left(-e^{i(n_o+1)\theta} \frac{\beta_{m_o}}{\sqrt{1+K}} \left[K_{n_o+1}(\beta_{m_o} r) \int_o^r I_{n_o}\left(\frac{\beta_{m_o} r'}{\sqrt{1+K}}\right) I_{n_o+1}(\beta_{m_o} r')\, r'\, dr' \right.\right.$$

$$\left. + I_{n_o+1}(\beta_{m_o} r) \int_r^a I'_{n_o}\left(\frac{\beta_{m_o} r'}{\sqrt{1+K}}\right) K_{n_o+1}(\beta_{m_o} r')\, r'\, dr' \right] + e^{i(n_o-1)\theta} \frac{\beta_{m_o}}{\sqrt{1+K}} \left[K_{n_o-1}(\beta_{m_o} r) \int_o^r I_{n_o}\left(\frac{\beta_{m_o} r'}{\sqrt{1+K}}\right) I_{n_o-1}(\beta_{m_o} r')\, r'\, dr' \right.$$

$$\left. + I_{n_o-1}(\beta_{m_o} r) \int_r^a I'_{n_o}\left(\frac{\beta_{m_o} r'}{\sqrt{1+K}}\right) K_{n_o-1}(\beta_{m_o} r')\, r'\, dr' \right] + e^{i(n_o+1)\theta} n_o \left[K_{n_o+1}(\beta_{m_o} r) \int_o^r I_{n_o}\left(\frac{\beta_{m_o} r'}{\sqrt{1+K}}\right) I_{n_o+1}(\beta_{m_o} r')\, dr' \right.$$

$$\left. + I_{n_o+1}(\beta_{m_o} r) \int_r^a I_{n_o}\left(\frac{\beta_{m_o} r'}{\sqrt{1+K}}\right) K_{n_o+1}(\beta_{m_o} r')\, dr' \right] + e^{i(n_o-1)\theta} n_o \left[K_{n_o-1}(\beta_{m_o} r) \int_o^r I_{n_o}\left(\frac{\beta_{m_o} r'}{\sqrt{1+K}}\right) I_{n_o-1}(\beta_{m_o} r')\, dr' \right.$$

$$\left. \left. + I_{n_o-1}(\beta_{m_o} r) \int_r^a I_{n_o}\left(\frac{\beta_{m_o} r'}{\sqrt{1+K}}\right) K_{n_o-1}(\beta_{m_o} r')\, dr' \right] \right\} \qquad \text{(C-6)}$$

$$A_{n_o+1}(r) = K_{n_o+1}(\beta_{m_o} r) \frac{\beta_{m_o}}{\sqrt{1+K}} \int_o^r I'_{n_o}\left(\frac{\beta_{m_o} r'}{\sqrt{1+K}}\right) I_{n_o+1}(\beta_{m_o} r')\, r'\, dr' + I_{n_o+1}(\beta_{m_o} r) \frac{\beta_{m_o}}{\sqrt{1+K}} \int_r^a I'_{n_o}\left(\frac{\beta_{m_o} r'}{\sqrt{1+K}}\right) K_{n_o+1}(\beta_{m_o} r')\, r'\, dr'$$

$$- n_o \left[K_{n_o+1}(\beta_{m_o} r) \int_o^r I_{n_o}\left(\frac{\beta_{m_o} r'}{\sqrt{1+K}}\right) I_{n_o+1}(\beta_{m_o} r')\, dr' + I_{n_o+1}(\beta_{m_o} r) \int_r^a I_{n_o}\left(\frac{\beta_{m_o} r'}{\sqrt{1+K}}\right) K_{n_o+1}(\beta_{m_o} r')\, dr' \right] \qquad \text{(C-7)}$$

$$B_{n_o-1}(r) = \frac{\beta_{m_o}}{\sqrt{1+K}} K_{n_o-1}(\beta_{m_o} r) \int_o^r I'_{n_o}\left(\frac{\beta_{m_o} r'}{\sqrt{1+K}}\right) I_{n_o-1}(\beta_{m_o} r')\, r'\, dr' + I_{n_o-1}(\beta_{m_o} r) \int_r^a I'_{n_o}\left(\frac{\beta_{m_o} r'}{\sqrt{1+K}}\right) K_{n_o-1}(\beta_{m_o} r')\, r'\, dr$$

$$+ n_o \left[K_{n_o-1}(\beta_{m_o} r) \int_o^r I_{n_o}\left(\frac{\beta_{m_o} r'}{\sqrt{1+K}}\right) I_{n_o-1}(\beta_{m_o} r')\, dr' + I_{n_o-1}(\beta_{m_o} r) \int_r^a I_{n_o}\left(\frac{\beta_{m_o} r'}{\sqrt{1+K}}\right) K_{n_o-1}(\beta_{m_o} r')\, dr' \right] \qquad \text{(C-8)}$$

APPENDIX D

LOWER SIDEBAND PUMPED SUSCEPTIBILITY TENSOR

The steady-state solution to the equation of motion for the lower sideband case $\overline{M} = \overline{\overline{x}} \cdot \overline{H}$ can be found by inverting the following matrix equation:

$$\gamma M_o \begin{bmatrix} H_{x_1} \\ H_{y_1} \\ H_{x_\ell}^* \\ H_{y_\ell}^* \end{bmatrix} = \begin{bmatrix} \omega_o + i\alpha\omega_1 & -i\omega_1 & \gamma H_{z_2} & 0 \\ i\omega_1 & \omega_o + i\alpha\omega_1 & 0 & \gamma H_{z_2} \\ \gamma H_{z_2}^* & 0 & \omega_o - i\alpha\omega_\ell & i\omega_\ell \\ 0 & \gamma H_{z_2}^* & -i\omega_\ell & \omega_o - i\alpha\omega_\ell \end{bmatrix} \begin{bmatrix} M_{x_1} \\ M_{y_1} \\ M_{x_\ell}^* \\ M_{y_\ell}^* \end{bmatrix} \quad \text{(D-1)}$$

The pumped susceptibility tensor $\overline{\overline{x}}$ is the inverse of the four by four matrix in the above equation. The determinant of this matrix to first order in H_{z_2} is:

$$D = \left[(\omega_o + i\alpha\omega_1)^2 - \omega_1^2\right]\left[(\omega_o - i\alpha\omega_\ell)^2 - \omega_\ell^2\right]$$

The tensor elements of $\overline{\overline{x}}$ can be found from the system of minors.

$$x_{11} = \frac{\gamma M_o}{D} \begin{vmatrix} \omega_o + i\alpha\omega_1 & 0 & \gamma H_{z_2} \\ 0 & \omega_o - i\alpha\omega_\ell & i\omega_\ell \\ \gamma H_{z_2}^* & -i\omega_\ell & \omega_o - i\alpha\omega_\ell \end{vmatrix} \quad \text{(D-2)}$$

$$= \frac{\gamma M_o\left[(\omega_o + i\alpha\omega_1)\left((\omega_o - i\alpha\omega_\ell)^2 - \omega_\ell^2\right)\right]}{D}$$

$$x_{11} = \frac{\gamma M_o(\omega_o + i\alpha\omega_1)}{(\omega_o + i\alpha\omega_1)^2 - \omega_1^2}$$

In this paper we will be concerned primarily with low-loss ferrites for which $\alpha << 1$. Thus, to first approximation in α the above tensor element can be written:

$$x_{11} \cong \frac{\gamma M_o(\omega_o + i\alpha\omega_1)}{\omega_o^2 - \omega_1^2 + 2i\alpha\omega_1\omega_o} \tag{D-3}$$

Similarly, for the remaining tensor elements:

$$x_{12} = -\frac{\gamma M_o}{D}\begin{vmatrix} -i\omega_1 & \gamma H_{z_2} & 0 \\ 0 & \omega_o - i\alpha\omega_\ell & i\omega_\ell \\ \gamma H_{z_2}^* & -i\omega_\ell & \omega_o - i\alpha\omega_\ell \end{vmatrix}$$

$$= \gamma M_o \frac{i\omega_1\left[(\omega_o - i\alpha\omega_\ell)^2 - \omega_\ell^2\right]}{D}$$

$$\cong i\frac{\gamma M_o \omega_1}{\omega_o^2 - \omega_1^2 + 2i\alpha\omega_1\omega_\ell} \tag{D-4}$$

$$x_{13} = \frac{\gamma M_o}{D}\begin{vmatrix} -i\omega_1 & \gamma H_{z_2} & 0 \\ \omega_o + i\alpha\omega_1 & 0 & \gamma H_{z_2} \\ \gamma H_{z_2}^* & -i\omega_\ell & \omega_o - i\alpha\omega_\ell \end{vmatrix}$$

$$= \frac{\gamma M_o}{D}\gamma H_{z_2}\left[\omega_1\omega_\ell - \omega_o^2 - 2i\alpha\omega_o(\omega_1 - \omega_\ell)\right]$$

$$x_{13} = \frac{\gamma^2 M_o H_{z_2}\left[\omega_1\omega_\ell - \omega_o^2 - 2i\alpha(\omega_1 - \omega_\ell)\right]}{(\omega_o^2 - \omega_1^2 + 2i\alpha\omega_1\omega_o)(\omega_o^2 - \omega_\ell^2 - 2i\alpha\omega_o\omega_\ell)} \tag{D-5}$$

$$x_{14} = -\frac{\gamma M_o}{D}\begin{vmatrix} -i\omega_1 & \gamma H_{z_2} & 0 \\ \omega_o + i\alpha\omega_1 & 0 & \gamma H_{z_2} \\ 0 & \omega_o - i\alpha\omega_\ell & i\omega_\ell \end{vmatrix}$$

$$= -i\,\frac{\gamma^2 M_o H_{z_2}\left[(\omega_o - i\alpha\omega_\ell)\,\omega_1 - \omega_\ell(\omega_o + i\alpha\omega_1)\right]}{(\omega_o^2 - \omega_1^2 + 2i\alpha\omega_1)(\omega_o^2 - \omega_\ell^2) - 2i\alpha\omega_o\omega_\ell} \qquad \text{(D-6)}$$

$$x_{21} = -\frac{\gamma M_o}{D}\begin{vmatrix} i\omega_1 & 0 & \gamma H_{z_2} \\ \gamma H_{z_2}^* & \omega_o - i\alpha\omega_\ell & i\omega_\ell \\ 0 & -i\omega_\ell & \omega_o - i\alpha\omega_\ell \end{vmatrix}$$

$$= -i\,\frac{\gamma M_o}{D}\,\omega_1\left[(\omega_o - i\alpha\omega_\ell)^2 - \omega_\ell^2\right]$$

$$\cong i\,\frac{\gamma M_o \omega_1}{\omega_o^2 - \omega_1^2 + 2i\alpha\omega_1\omega_o} \qquad \text{(D-7)}$$

$$x_{22} = -\frac{\gamma M}{D}\begin{vmatrix} \omega_o + i\alpha\omega_1 & \gamma H_{z_2} & 0 \\ \gamma H_{z_2}^* & \omega_o - i\alpha\omega_\ell & i\omega_\ell \\ 0 & -i\omega_\ell & \omega_o - i\alpha\omega_\ell \end{vmatrix}$$

$$x_{22} = \frac{\gamma M_o(\omega_o + i\alpha\omega_1)}{\omega_o^2 - \omega_1^2 + 2i\alpha\omega_o\omega_1} \qquad \text{(D-8)}$$

$$x_{23} = -\frac{\gamma M_o}{D}\begin{vmatrix} \omega_o + i\alpha\omega_1 & \gamma H_{z_2} & 0 \\ i\omega_1 & 0 & \gamma H_{z_2} \\ 0 & -i\omega_\ell & \omega_o - i\alpha\omega_\ell \end{vmatrix}$$

$$= -i\,\frac{\gamma^2 H_{z_2} M_o\left[(\omega_o + i\alpha\omega_1)\omega_\ell - \omega_1(\omega_o - i\alpha\omega_\ell)\right]}{(\omega_o^2 - \omega_1^2 + 2i\alpha\omega_o\omega_1)(\omega_o^2 - \omega_\ell^2 - 2i\alpha\omega_o\omega_\ell)} \qquad \text{(D-9)}$$

$$x_{24} = \frac{\gamma M_o}{D}\begin{vmatrix} \omega_o + i\alpha\omega_1 & \gamma H_{z_2} & 0 \\ i\omega_1 & 0 & \gamma H_{z_2} \\ \gamma H_{z_2}^* & \omega_o - i\alpha\omega_\ell & i\omega_\ell \end{vmatrix}$$

$$= -\frac{\gamma^2 M_o H_{z_2}\left[\omega_o^2 + i\alpha\omega_o(\omega_1 - \omega_\ell) - \omega_1\omega_\ell\right]}{(\omega_o^2 - \omega_1^2 + 2i\alpha\omega_o\omega_1)(\omega_o^2 - \omega_\ell^2 - 2i\alpha\omega_o\omega_\ell)} \qquad \text{(D-10)}$$

$$x_{31} = \frac{\gamma M_o}{D}\begin{vmatrix} i\omega_1 & \omega_o + i\alpha\omega_1 & \gamma H_{z_2} \\ \gamma H_{z_2}^* & 0 & i\omega_\ell \\ 0 & \gamma H_{z_2}^* & \omega_o - i\alpha\omega_\ell \end{vmatrix}$$

$$x_{31} = \frac{\gamma^2 M_o H_{z_2}^*\left[\omega_1\omega_2 - \omega_o^2 - 2i\alpha\omega_o(\omega_1 - \omega_\ell)\right]}{(\omega_o^2 - \omega_1^2 + 2i\alpha\omega_o\omega_1)(\omega_o^2 - \omega_\ell^2 - 2i\alpha\omega_o\omega_\ell)} \qquad \text{(D-11)}$$

$$x_{32} = -\frac{\gamma M_o}{D}\begin{vmatrix} \omega_o + i\alpha\omega_1 & -i\omega_1 & 0 \\ \gamma H_{z_2}{}^* & 0 & i\omega_\ell \\ 0 & \gamma H_{z_2}{}^* & \omega_o - i\alpha\omega_\ell \end{vmatrix}$$

$$= -i\,\frac{\gamma^2 M_o H_{z_2}{}^*\left[-\omega_\ell(\omega_o + i\alpha\omega_1) + \omega_1(\omega_o - i\alpha\omega_\ell)\right]}{(\omega_o{}^2 - \omega_1{}^2 + 2i\alpha\omega_o\omega_1)(\omega_o{}^2 - \omega_\ell{}^2 - 2i\alpha\omega_o\omega_\ell)} \qquad \text{(D-12)}$$

$$x_{33} = \frac{\gamma M_o}{D}\begin{vmatrix} \omega_o + i\alpha\omega_1 & -i\omega_1 & 0 \\ i\omega_1 & \omega_o + i\alpha\omega_1 & \gamma H_{z_2} \\ 0 & \gamma H_{z_2}{}^* & \omega_o - i\alpha\omega_\ell \end{vmatrix}$$

$$= \frac{\gamma M_o(\omega_o - i\alpha\omega_\ell)}{\omega_o{}^2 - \omega_\ell{}^2 - 2i\alpha\omega_o\omega_\ell} \qquad \text{(D-13)}$$

$$x_{34} = -\frac{\gamma M_o}{D}\begin{vmatrix} \omega_o + i\alpha\omega_1 & -i\omega_1 & 0 \\ i\omega_1 & \omega_o\ \ i\alpha\omega_1 & \gamma H_{z_2} \\ \gamma H_{z_2}{}^* & 0 & i\omega_\ell \end{vmatrix}$$

$$x_{34} = -i\,\frac{\gamma M_o \omega_\ell}{\omega_o{}^2 - \omega_\ell{}^2 - 2i\alpha\omega_o\omega_n} \qquad \text{(D-14)}$$

$$x_{41} = -\frac{\gamma M_o}{D}\begin{vmatrix} i\omega_1 & \omega_o + i\alpha\omega_1 & 0 \\ \gamma H_{z_2}{}^* & 0 & \omega_o - i\alpha\omega_\ell \\ 0 & \gamma H_{z_2}{}^* & -i\omega_\ell \end{vmatrix}$$

$$= i\frac{\gamma^2 M_o H_{z_2}{}^*\left[\omega_1(\omega_o - i\alpha\omega_\ell) - \omega_\ell(\omega_o + i\alpha\omega_1)\right]}{(\omega_o{}^2 - \omega_1{}^2 + 2i\alpha\omega_o\omega_1)(\omega_o{}^2 - \omega_\ell{}^2 - 2i\alpha\omega_o\omega_\ell)} \qquad \text{(D-15)}$$

$$x_{42} = \frac{\gamma M_o}{D}\begin{vmatrix} \omega_o + i\alpha\omega_1 & -i\omega_1 & \gamma H_{z_2} \\ \gamma H_{z_2}{}^* & 0 & \omega_o - i\alpha\omega_\ell \\ 0 & \gamma H_{z_2}{}^* & -i\omega_\ell \end{vmatrix}$$

$$= -\frac{\gamma^2 M_o H_{z_2}{}^*\left[(\omega_o{}^2 + 2i\alpha\omega_o(\omega_1 - \omega_\ell) - \omega_\ell\omega_1)\right]}{(\omega_o{}^2 - \omega_1{}^2 + 2i\alpha\omega_o\omega_1)(\omega_o{}^2 - \omega_\ell{}^2 - 2i\alpha\omega_o\omega_\ell)} \qquad \text{(D-16)}$$

$$x_{43} = -\frac{\gamma M_o}{D}\begin{vmatrix} \omega_o + i\alpha\omega_1 & -i\omega_1 & \gamma H_{z_2} \\ i\omega_1 & \omega_o + i\alpha\omega_1 & 0 \\ 0 & \gamma H_{z_2}{}^* & -i\omega_\ell \end{vmatrix}$$

$$x_{43} = i\frac{\gamma M_o \omega_\ell}{\omega_o{}^2 - \omega_\ell{}^2 - 2i\alpha\omega_o\omega_\ell} \qquad \text{(D-17)}$$

$$x_{44} = \frac{\gamma M_o}{D} \begin{vmatrix} \omega_o + i\alpha\omega_1 & -i\omega_1 & \gamma H_{z_2} \\ i\omega_1 & \omega_o + i\alpha\omega_1 & 0 \\ \gamma H_{z_2}^* & 0 & \omega_o - i\alpha\omega_\ell \end{vmatrix}$$

$$\cong \frac{\gamma M_o(\omega_o - i\alpha\omega_\ell)}{\omega_o^2 - \omega_\ell^2 - 2i\alpha\omega_o\omega_\ell} \qquad \text{(D-18)}$$

The following symmetries can be noted:

$$\begin{aligned} x_{11} &= x_{22} \\ x_{12} &= -x_{21} \\ x_{13} &= x_{24} \\ x_{14} &= -x_{23} \\ x_{33} &= x_{44} \\ x_{34} &= -x_{43} \\ x_{31} &= x_{42} \\ x_{32} &= -x_{41} \end{aligned} \qquad \text{(D-19)}$$

In the calculations of the power at the signal and lower sideband the term Im x_{11} and Im x_{33} appear. These functions are:

$$\text{Im } x_{11} = -\frac{\alpha\omega_1(\omega_o^2 + \omega_1^2)}{(\omega_o^2 - \omega_1^2)^2 + 4\alpha^2\omega_1^2\omega_o^2} \leq 0 \qquad \text{(D-20)}$$

for all ω_o and ω_1. Similarly:

$$\text{Im } x_{33} = \frac{\alpha\omega_\ell(\omega_o^2 + \omega_\ell^2)}{(\omega_o^2 - \omega_\ell^2)^2 + 4\alpha^2\omega_o^2\omega_1^2} \geq 0 \qquad \text{(D-21)}$$

for all ω_o and ω_ℓ.

APPENDIX E

UPPER SIDEBAND PUMPED SUSCEPTIBILITY TENSOR

The pumped susceptibility tensor for the upper sideband converter can be found by inverting the following matrix:

$$(\gamma M_o)^{-1} \begin{bmatrix} \gamma H_o + i\alpha\omega_1 & -i\omega_1 & \gamma H_{z_2}{}^* & 0 \\ i\omega_1 & \gamma H_o + i\alpha\omega_1 & 0 & \gamma H_{z_2}{}^* \\ \gamma H_{z_2} & 0 & \gamma H_o + i\alpha\omega_u & -i\omega_u \\ 0 & \gamma H_{z_2} & i\omega_u & \gamma H_o + i\alpha\omega_u \end{bmatrix} \tag{E-1}$$

The determinant of this matrix to first order in H_{z_2} is:

$$D = \left[(\gamma H_o + i\alpha\omega_1)^2 - \omega_1{}^2\right]\left[(\gamma H_o + i\alpha\omega_u)^2 - \omega_u{}^2\right]$$

This determinant can be used to find the tensor elements to first order in H_{z_2}

$$x_{11} = \frac{\gamma M_o}{D} \begin{vmatrix} \gamma H_o + i\alpha\omega_1 & 0 & \gamma H_{z_2}{}^* \\ 0 & \gamma H_o + i\alpha\omega_u & -i\omega_u \\ \gamma H_{z_2} & i\omega_u & \gamma H_o + i\alpha\omega_u \end{vmatrix}$$

$$= \frac{\gamma M_o(\gamma H_o + i\alpha\omega_1)}{(\gamma H_o + i\alpha\omega_1)^2 - \omega_1{}^2} \tag{E-2}$$

$$x_{12} = -\frac{\gamma M_o}{D} \begin{vmatrix} -i\omega_1 & \gamma H_{z_2}{}^* & 0 \\ 0 & \gamma H_o + i\alpha\omega_u & -i\omega_u \\ \gamma H_{z_2} & i\omega_u & \gamma H_o + i\alpha\omega_u \end{vmatrix}$$

$$= i \frac{\gamma M_o \omega_1}{(\gamma H_o + i\alpha\omega_1)^2 - \omega_1^2} \qquad \text{(E-3)}$$

$$x_{13} = \frac{\gamma M_o}{D} \begin{vmatrix} -i\omega_1 & \gamma H_{z_2}{}^* & 0 \\ \gamma H_o + i\alpha\omega_1 & 0 & \gamma H_{z_2}{}^* \\ \gamma H_{z_2} & \omega_u & \gamma H_o + i\alpha\omega_u \end{vmatrix}$$

$$= - \frac{\gamma^2 H_{z_2}{}^* M_o \left[\omega_1\omega_u + (\gamma H_o + i\alpha\omega_u)(\gamma H_o + i\alpha\omega_1)\right]}{\left[(\gamma H_o + i\alpha\omega_1)^2 - \omega_1^2\right]\left[(\gamma H_o + i\alpha\omega_u)^2 - \omega_u^2\right]}$$

$$= - \frac{\gamma^2 H_{z_2} M_o \left[\omega_1\omega_u + (\gamma H_o)^2 + 2i\alpha\gamma H_o(\omega_u + \omega_1)\right]}{\left[(\gamma H_o + i\alpha\omega_1)^2 - \omega_1^2\right]\left[(\gamma H_o + i\alpha\omega_u)^2 - \omega_u^2\right]} \qquad \text{(E-4)}$$

$$x_{14} = - \frac{\gamma M_o}{D} \begin{vmatrix} -i\omega_1 & \gamma H_{z_2}{}^* & 0 \\ \gamma H_o + i\alpha\omega_1 & 0 & \gamma H_{z_2}{}^* \\ 0 & \gamma H_o + i\alpha\omega_u & -i\omega_u \end{vmatrix}$$

$$= -i \frac{\gamma^2 M_o H_{z_2}{}^* \left[\omega_1(\gamma H_o + i\alpha\omega_u) + \omega_u(\gamma H_o + i\alpha\omega_1)\right]}{\left[(\gamma H_o + i\alpha\omega_1)^2 - \omega_1^2\right]\left[(\gamma H_o + i\alpha\omega_u)^2 - \omega_u^2\right]} \qquad \text{(E-5)}$$

$$x_{21} = -\frac{\gamma M_o}{D}\begin{vmatrix} i\omega_1 & 0 & \gamma H_{z_2}{}^* \\ \gamma H_{z_2} & \gamma H_o + i\alpha\omega_u & -i\omega_u \\ 0 & i\omega_u & \gamma H_o + i\alpha\omega_u \end{vmatrix}$$

$$= -i\frac{\gamma M_o \omega_1}{(\gamma H_o + i\alpha\omega_1)^2 - \omega_1{}^2} \qquad \text{(E-6)}$$

$$x_{22} = \frac{\gamma M_o}{D}\begin{vmatrix} \gamma H_o + i\alpha\omega_1 & \gamma H_{z_2}{}^* & 0 \\ \gamma H_{z_2} & \gamma H_o + i\alpha\omega_u & -i\omega_u \\ 0 & i\omega_u & \gamma H_o + i\alpha\omega_u \end{vmatrix}$$

$$= \frac{\gamma M_o(\gamma H_o + i\alpha\omega_u)}{(\gamma H_o + i\alpha\omega_u)^2 - \omega_u{}^2} \qquad \text{(E-7)}$$

$$x_{23} = -\frac{\gamma M_o}{D}\begin{vmatrix} \gamma H_o + i\alpha\omega_1 & \gamma H_{z_2}{}^* & 0 \\ i\omega_1 & 0 & \gamma H_{z_2}{}^* \\ 0 & i\omega_u & \gamma H_o + i\alpha\omega_u \end{vmatrix}$$

$$= i\frac{\gamma^2 M_o H_{z_2}{}^*\left[\omega_u(\gamma H_o + i\alpha\omega_1) + \omega_1(\gamma H_o + i\alpha\omega_u)\right]}{\left[(\gamma H_o + i\alpha\omega_1)^2 - \omega_1{}^2\right]\left[(\gamma H_o + i\alpha\omega_u)^2 - \omega_u{}^2\right]} \qquad \text{(E-8)}$$

$$x_{24} = \frac{\gamma M_o}{D} \begin{vmatrix} \gamma H_o + i\alpha\omega_1 & \gamma H_{z_2}{}^* & 0 \\ i\omega_1 & 0 & \gamma H_{z_2}{}^* \\ \gamma H_{z_2} & \gamma H_o + i\alpha\omega_u & -i\omega_u \end{vmatrix}$$

$$= - \frac{\gamma^2 M_o H_{z_2}{}^* \left[(\gamma H_o + i\alpha\omega_u)(\gamma H_o + i\alpha\omega_1) + \omega_1\omega_u \right]}{\left[(\gamma H_o + i\alpha\omega_1)^2 - \omega_1{}^2 \right] \left[(\gamma H_o + i\alpha\omega_u)^2 - \omega_u{}^2 \right]} \qquad \text{(E-9)}$$

$$x_{31} = \frac{\gamma M_o}{D} \begin{vmatrix} i\omega_1 & \gamma H_o + i\alpha\omega_1 & \gamma H_{z_2}{}^* \\ \gamma H_{z_2} & 0 & -i\omega_u \\ 0 & \gamma H_{z_2} & \gamma H_o + i\alpha\omega_u \end{vmatrix}$$

$$= - \frac{\gamma^2 M_o H_{z_2} \left[\omega_1\omega_u + (\gamma H_o + i\alpha\omega_1)(\gamma H_o + i\alpha\omega_u) \right]}{\left[(\gamma H_o + i\alpha\omega_1)^2 - \omega_1{}^2 \right] \left[(\gamma H_o + i\alpha\omega_u)^2 - \omega_u{}^2 \right]} \qquad \text{(E-10)}$$

$$x_{32} = - \frac{\gamma M_o}{D} \begin{vmatrix} \gamma H_o + i\alpha\omega_1 & -i\omega_1 & 0 \\ \gamma H_{z_2} & 0 & -i\omega_u \\ 0 & \gamma H_{z_2} & \gamma H_o + i\alpha\omega_u \end{vmatrix}$$

$$= -i \frac{\gamma^2 M_o H_{z_2} \left[\omega_u(\gamma H_o + i\alpha\omega_1) + \omega_1(\gamma H_o + i\alpha\omega_u) \right]}{\left[(\gamma H_o + i\alpha\omega_1)^2 - \omega_1{}^2 \right] \left[(\gamma H_o + i\alpha\omega_u)^2 - \omega_u{}^2 \right]} \qquad \text{(E-11)}$$

$$x_{33} = \frac{\gamma M_o}{D} \begin{vmatrix} \gamma H_o + i\alpha\omega_1 & -i\omega_1 & 0 \\ i\omega_1 & \gamma H_o + i\alpha\omega_1 & \gamma H_{z_2}{}^* \\ 0 & \gamma H_{z_2} & \gamma H_o + i\alpha\omega_u \end{vmatrix}$$

$$= \frac{\gamma M_o(\gamma H_o + i\alpha\omega_u)}{(\gamma H_o + i\alpha\omega_u)^2 - \omega_u{}^2} \qquad \text{(E-12)}$$

$$x_{34} = -\frac{\gamma M_o}{D} \begin{vmatrix} \gamma H_o + i\alpha\omega_1 & -i\omega_1 & 0 \\ i\omega_1 & \gamma H_o + i\alpha\omega_1 & \gamma H_{z_2}{}^* \\ \gamma H_{z_2} & 0 & -i\omega_u \end{vmatrix}$$

$$= i\frac{\gamma M_o \omega_u}{(\gamma H_o + i\alpha\omega_u)^2 - \omega_u{}^2} \qquad \text{(E-13)}$$

$$x_{41} = -\frac{\gamma M_o}{D} \begin{vmatrix} i\omega_1 & \gamma H_o + i\alpha\omega_1 & 0 \\ \gamma H_{z_2} & 0 & \gamma H_o + i\alpha\omega_u \\ 0 & \gamma H_{z_2} & i\omega_u \end{vmatrix}$$

$$= i\frac{\gamma^2 M_o H_{z_2}\left[\omega_1(\gamma H_o + i\alpha\omega_u) + \omega_u(\gamma H_o + i\alpha\omega_1)\right]}{\left[(\gamma H_o + i\alpha\omega_1)^2 - \omega_1{}^2\right]\left[(\gamma H_o + i\alpha\omega_u)^2 - \omega_u{}^2\right]} \qquad \text{(E-14)}$$

$$x_{42} = \frac{\gamma M_o}{D} \begin{vmatrix} \gamma H_o + i\alpha\omega_1 & -i\omega_1 & \gamma H_{z_2}{}^* \\ \gamma H_{z_2} & 0 & \gamma H_o + i\alpha\omega_u \\ 0 & \gamma H_{z_2} & i\omega_u \end{vmatrix}$$

$$= - \frac{\gamma^2 M_o H_{z_2} \left[(\gamma H_o + i\alpha\omega_1)(\gamma H_o + i\alpha\omega_u) + \omega_1\omega_u \right]}{\left[(\gamma H_o + i\alpha\omega_1)^2 - \omega_1{}^2 \right] \left[(\gamma H_o + i\alpha\omega_u)^2 - \omega_u{}^2 \right]} \qquad \text{(E-15)}$$

$$x_{43} = - \frac{\gamma M_o}{D} \begin{vmatrix} \gamma H_o + i\alpha\omega_1 & -i\omega_1 & \gamma H_{z_2}{}^* \\ i\omega_1 & \gamma H_o + i\alpha\omega_1 & 0 \\ 0 & \gamma H_{z_2} & i\omega_u \end{vmatrix}$$

$$= -i \frac{\gamma M_o \omega_u}{(\gamma H_o + i\alpha\omega_u)^2 - \omega_u{}^2} \qquad \text{(E-16)}$$

$$x_{44} = \frac{\gamma M_o}{D} \begin{vmatrix} \gamma H_o + i\alpha\omega_1 & -i\omega_1 & \gamma H_{z_2} \\ i\omega_1 & \gamma H_o + i\alpha\omega_1 & 0 \\ \gamma H_{z_2} & 0 & \gamma H_o + i\alpha\omega_u \end{vmatrix}$$

$$= \frac{\gamma M_o (\gamma H_o + i\alpha\omega_u)}{(\gamma H_o + i\alpha\omega_u)^2 - \omega_u{}^2} \qquad \text{(E-17)}$$

The following symmetries can be observed:

$$\begin{aligned} x_{11} &= x_{12} \\ x_{12} &= -x_{21} \\ x_{13} &= x_{24} \\ x_{14} &= -x_{23} \\ x_{31} &= x_{42} \\ x_{32} &= -x_{41} \\ x_{33} &= x_{44} \\ x_{34} &= -x_{43} \end{aligned} \tag{E-18}$$

Observe also that:

$$\text{Im } x_{11} = - \frac{\alpha \omega_1 (\gamma H_o)^2 + \omega_1^2 \gamma M_o}{\left((\gamma H_o)^2 - \omega_1^2\right)^2 + 4 \alpha^2 \gamma^2 H_o^2 \omega_1^2} \leq 0 \tag{E-19}$$

and that:

$$\text{Im } x_{33} = - \frac{\gamma M_o \alpha \omega_u (\gamma^2 H_o^2 + \omega_u^2)}{(\gamma^2 H_o^2 - \omega_u^2)^2 + 4 \alpha^2 \gamma^2 H_o^2 \omega_u^2} \leq 0 \tag{E-20}$$

for all H_o and ω_u.

APPENDIX F

SIGNAL FIELD DISTRIBUTION FOR FERROMAGNETIC RESONANCE CONFIGURATION

The field distribution of the actual flat coil can be approximated very closely by that of an infinitesimally thin current loop as shown in Fig. F-1.

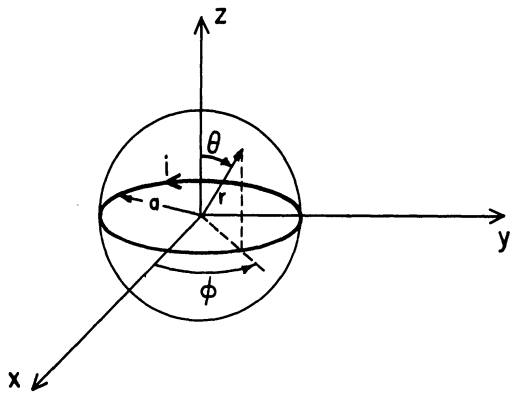

Fig. F-1. Coordinate system appropriate for calculation of magnetic field produced by current loop i.

If the space surrounding this loop can be divided conveniently into two regions by a spherical shell of which the loop forms a great circle, the magnetic field in the two regions exclusive of the shell can be found from the scalar potential ϕ where

$$\nabla^2 \phi = 0 \tag{F-1}$$

The boundary conditions are that the potential vanishes at infinite distance from the shell, that it be regular at the origin and that the magnetic field derived from ϕ (i.e., $\nabla\phi$) must be given by the field distribution known for the current loop on its axis:

$$\begin{aligned} &\lim_{r\to\infty} \phi = 0 \\ &\lim_{r\to 0} \phi < \infty \\ &\nabla\phi\big|_{\text{axis}} = \overline{H}\ (\text{loop}) \end{aligned} \tag{F-2}$$

In the region outside of the spherical shell the potential is given by:

$$\phi = \sum_{n=0}^{\infty} \frac{a_n}{r^{n+1}} P_n(\cos\theta) \qquad r > a \tag{F-3}$$

and inside by:

$$\phi = \sum_{n=0}^{\infty} b_n r^n P_n(\cos\theta) \qquad r < a \tag{F-4}$$

The magnetic field of a current loop on its axis is given by:

$$H = H_o \frac{y^3}{(1+y^2)^{\frac{3}{2}}} \tag{F-5}$$

where H_o is the field at the center of the coil (i. e., $H_o = \frac{ni}{2a}$). $y = \frac{a}{z}$, a = coil radius and z = coordinate along the coil axis. This expression can be expanded in a power series:

$$H = H_o y^3 \sum_{k=0}^{\infty} \frac{(-1)^k (\frac{3}{2})_k}{k!} (y^2)^k \qquad y < 1 \tag{F-6}$$

The r component of the field outside the shell is given by

$$H_r = \nabla_r \phi = - \sum_{n=0}^{\infty} \frac{(n+1)\, a_n}{r^{n+2}} P_n(\cos\theta) \tag{F-7}$$

which on the axis reduces to:

$$H_r = \nabla_r \phi \Big|_{\substack{r=z \\ \theta=0}} = - \sum_{n=0}^{\infty} \frac{(n+1)\, a_n}{z^{n+2}} \tag{F-8}$$

From the boundary conditions Eq. 6-4 must be the same as Eq. 6-6.

$$\sum_{n=0}^{\infty} \frac{(n+1)\, a_n}{z^{n+2}} = H_o \sum_{k=0}^{\infty} \frac{(-1)^k (\frac{3}{2})_k (\frac{a}{z})^{2k+3}}{k!} \tag{F-9}$$

Then equating coefficients of like powers of z gives:

$$a_n = 0 \qquad n \text{ even}$$

$$= H_o \frac{(-1)^k \left(\frac{3}{2}\right)_k a^{2k+3}}{(n+1)\, k!} \qquad n = 2k+1 \tag{F-10}$$

$$a_{2k+1} = H_o \frac{(-1)^k \left(\frac{3}{2}\right)_k a^{2k+3}}{2(k+1)\, k!} \tag{F-11}$$

Thus

$$\phi = aH_o \sum_{k=0}^{\infty} \frac{(-1)^k \left(\frac{3}{2}\right)_k \left(\frac{a}{r}\right)^{2(k+1)}}{k!\, 2(k+1)} P_{2k+1}(\cos\theta) \qquad r > a \tag{F-12}$$

and by a similar procedure it may be found that:

$$\phi = H_o \sum_{k=0} \frac{(-1)^k \left(\frac{3}{2}\right)_k \left(\frac{r}{a}\right)^{2k+1}}{(2k+1)\, k!} P_{2k+1}(\cos\theta) \qquad r < a \tag{F-13}$$

It is possible to use these potentials to find the field distribution for all space surrounding the current loop from which the stored energy can be found. However, it is slightly easier to find the stored energy by making use of the following identity:

$$\int_{\text{space}} |\nabla\phi|^2 \, d\upsilon = \int \nabla \cdot \phi\nabla\phi \, d\upsilon - \int \phi\nabla^2\phi \, d\upsilon$$

$$= \int_{\text{surf}} \phi\nabla\phi \cdot n \, ds \tag{F-14}$$

The space which we will consider consists of two regions namely those inside and outside the sphere. The surface for the region outside is doubly connected and consists of the outside of the spherical shell and the surface at infinity. Since $\phi \to 0$ at infinity it is only the integral on the outside of the spherical shell which need be evaluated. The volume inside of the spherical shell is bounded by the inside surface of that shell. This identity can now be used to evaluate the stored energy:

$$W = \frac{1}{2}\mu_o \int |H|^2 \, dv = \mu_o \int_{\substack{\text{inside} \\ \text{and outside surf.}}} \phi \nabla\phi \cdot n \, ds \tag{F-15}$$

$$\int_{\text{outside}} \phi \nabla\phi \cdot n \, ds = \int \phi \frac{\partial \phi}{\partial r} r^2 \Big|_{r=a} d\cos\theta \, d\phi \tag{F-16}$$

$$= a H_o^2 \sum_{k,\ell=0}^{\infty} \frac{(-1)^k (-1)^\ell \left(\frac{3}{2}\right)_k \left(\frac{3}{2}\right)_\ell}{2k!\,\ell!\,(k+1)} \int_{-1}^{1} \int_{o}^{2\pi} a^2 P_{2k+1}(\cos\theta) P_{2\ell+1}(\cos\theta) \, d\cos\theta \, d\phi \tag{F-17}$$

The orthogonality relations can be used to reduce the double sum to a single sum:

$$= \pi a^3 H_o^3 \sum_{k=0}^{\infty} \frac{\left(\frac{3}{2}\right)_k^2}{(k!)^2} \frac{2}{4k+3} \tag{F-18}$$

$$= H_o^2 v \sum_{k=0}^{\infty} \frac{\left(\frac{3}{2}\right)_k}{(k!)^2} \frac{3}{2(2k+3)} \tag{F-19}$$

where $v = \frac{4}{3}\pi a^3$.

Similarly the surface integral for the inside surface can be evaluated:

$$\int \phi \frac{\partial \phi}{\partial r} ds = \int \phi \frac{\partial \phi}{\partial r}\Big|_{r=a} a^2 \, d(\cos\theta) \, d\phi \tag{F-20}$$

$$= H_o^2 \sum_{k,\ell=0}^{\infty} \frac{(-1)^{k+\ell} \left(\frac{3}{2}\right)_k \left(\frac{3}{2}\right)_\ell}{(k!)\,\ell!\,(2k+1)} a \int_{-1}^{1} \int_{o}^{2\pi} a^2 P_{2k+1}(\cos\theta) P_{2\ell+1}(\cos\theta) \, d(\cos\theta) \, d\phi \tag{F-21}$$

$$= 2\pi a^3 H_o^2 \sum_{k=0}^{\infty} \frac{\left(\frac{3}{2}\right)_k^2}{(k!)^2 (2k+1)} \frac{2}{4k+3} \tag{F-22}$$

$$= v H_o^2 \sum_{k=0}^{\infty} \frac{\left(\frac{3}{2}\right)_k^2}{(k!)^2 \left(k+\frac{1}{2}\right)} \frac{3}{2(4k+3)} \cong \sim H_o^2 \tag{F-23}$$

Then substituting the surface integrals in (6-13) yields

$$W = \frac{1}{2}\mu_o \int |H|^2 \, dv$$

$$\cong \frac{1}{2}\mu_o (2v) H_o^2$$

$$= \frac{v}{v_s} (\mu_o v_s H_o^2) \qquad \text{(F-24)}$$

The radius of the 30-turn coil was approximately 1 cm; the radius of the sample is approximately 0. 175 cm. Using these values then

$$\frac{v}{v_s} \cong 9 \times 10^3 \qquad \text{(F-25)}$$

This is the quantity called A in Eq. 6. 67 in the text and which was sought in this calculation.

REFERENCES

1. D. K. Adams, A Study of Double Sideband Reactive Mixers, Cooley Electronics Laboratory Technical Report No. 134, The University of Michigan, Ann Arbor, Michigan, December 1962.

2. J. M. Manley and H. E. Rowe, "General Energy Relations in Nonlinear Reactances, Proc. IRE, Vol. 44, July 1959, pp. 904-913.

3. H. Heffner and G. Wade, "Noise, Gain and Bandwidth Characteristics of Variable Amplifiers," J. Appl. Phys., Vol. 29, 1958, p. 1321.

4. D. K. Adams, A Study of Phase-Shift Amplifier Techniques, Cooley Electronics Laboratory, Final Report, Contract No. DA-36-039 AMC-00059(E), The University of Michigan, Ann Arbor, Michigan, March 1964.

5. J. Smit and H. P. J. Wijn, Ferrites, John Wiley and Sons, New York, New York, 1960, p. 6.

6. C. Kittel, Introduction to Solid State Physics, John Wiley and Sons, New York, New York, 1960, pp. 402-451.

7. R. F. Soohoo, Theory and Applications of Ferrites, Prentice Hall, Inc., Englewood Cliffs, New Jersey, 1960, p. 60.

8. B. Lax and K. J. Button, Microwave Ferrites and Ferrimagnetics, McGraw-Hill Book Company, Inc., New York, New York, 1962, pp. 152-153.

9. N. Bloembergen, "On the Ferromagnetic Resonance in Ni and Supermalloy," Phys. Rev., Vol. 78, June 1950, pp. 572-580.

10. A. G. Gurevich, Ferrites at Microwave Frequencies, Consultants Bureau Enterprises Inc., New York, New York, 1963.

11. Ibid., p. 32.

12. C. Kittel, "On the Theory of Ferromagnetic Resonances Absorption," Phys. Rev., Vol. 73, 1948, p. 155.

13. J. O. Artman, "Microwave Resonance Relations in Anisotropic Single Crystal Ferrites," Proc. IRE, Vol. 44, 1956, p. 1284.

14. B. Lax and K. J. Button, op. cit., p. 192.

15. A. G. Gurevich, op. cit., pp. 101-106.

16. R. L. White and I. H. Solt, Jr., "Multiple Ferromagnetic Resonance in Ferrite Spheres," Phys. Rev., Vol. 104, 1956, p. 56.

17. W. B. Ribbens, "Effect of Electromagnetic Propagation on the Magnetostatic Modes," J. Appl. Phys., Vol. 34, No. 9, September 1963, pp. 2639-2645.

18. L. R. Walker, "Magnetostatic Modes in Ferromagnetic Resonance," Phys. Rev., Vol. 105, 1957, p. 390.

19. W. B. Ribbens, "The Size Independence of Magnetostatic Modes," Proc. IEEE, Vol. 51, No. 2, February 1963.

20. R. I. Joseph and E. Schlölman, "Theory of Magnetostatic Modes in Long Axially Magnetized Cylinders, J. Appl. Phys., Vol. 32, June 1961, p. 1001.

REFERENCES (Cont.)

21. W. A. Yager, et al., "Ferromagnetic Resonances in Nickel Ferrite," Phys. Rev., Vol. 80, 1950, p. 744.

22. H. Suhl, "Theory of the Ferromagnetic Microwave Amplifier," J. Appl. Phys., Vol. 28, 1957, p. 1225.

23. R. T. Denton, "Theoretical and Experimental Characteristics of a Ferromagnetic Amplifier Using Longitudinal Pumping," J. Appl. Phys., Vol. 32, 1960, 300s.

24. D. K. Adams, op. cit., "A Study of Double Sideband Reactive Mixers," p. 31.

25. D. B. Anderson and J. C. Aukland, "Transmission Phase Relations of Four-Frequency Parametric Devices," Proc. PGMTT National Symposium, 1961.

26. J. S. Schwinger, "The Mathematical Analysis of Waveguide Discontinuities," Lecture Notes, Department of Electrical Engineering, Massachusetts Institute of Technology, Cambridge, Massachusetts, January 1959.

27. D. K. Adams, op. cit., "A Study of Double Sideband Reactive Mixers," p. 30.

28. Ibid., "A Study of Double Sideband Reactive Mixers," p. 45.

29. M. T. Weiss, "The Behavior of Ferroxdure at Microwave Frequencies," IRE National Convention Record, Vol. 3, Pt. 8, 1955, p. 95.

30. D. K. Adams, op. cit., "A Study of Double Sideband Reactive Mixers," p. 147.

31. A. G. Gurevich, op. cit., pp. 135-141.

32. R. C. Lecraw and E. G. Spencer, "Tensor Permeabilities of Ferrites Below Magnetic Saturation," IRE National Convention Record, 1956, pp. 66-74.

33. A. G. Gurevich, op. cit., p. 35.

34. J. Nemarich and J. Caceris, "Temperature Dependence of Microwave Permeabilities for Polycrystalline Ferrite and Garnet Materials," Diamond Ordnance Fuze Laboratories, Technical Report 647, Ordnance Corps, Washington, D. C., October 1958.

35. M. T. Weiss, "A Phenomenological Theory of the Reggia Spencer Phase Shifter," Proc. IRE, Vol. 47, No. 6, June 1959.

36. D. O. Smith, "Magnetization Reversal in Thin Films," J. Appl. Phys., Vol. 29, No. 3, March 1958, pp. 264-273.

37. A. A. Read and A. V. Pohm, "Magnetic Film Parametric Amplifiers," Proc. NEC, 1959, pp. 65-79.

38. A. V. Pohm, et al., "High Frequency Magnetic Film Parametrons for Computer Logic," Proc. NEC, 1959, pp. 202-214.

39. F. Reggia, "Magnetically Tunable Microwave Bandpass Filter," Microwave J., Vol. 6, No. 1, January 1963, pp. 72-74.

40. G. R. Jones, "Calculated Magnetic Fields in Ferrite Rods, Discs, and Slabs," Technical Report No. 574, Diamond Ordnance Fuze Laboratories, U. S. Department of Commerce, Office of Technical Services, Washington, D. C.

REFERENCES (Cont.)

41. F. Reggia and E. G. Spencer, "A New Technique in Ferrite Phase Shifting for Beam Scanning of Microwave Antennas," Proc. IRE, Vol. 45, 1957, p. 1510.

42. S. J. Mason, "Feedback Theory - Some Properties of Signal Flowgraphs," Proc. IRE, Vol. 41, September 1953, pp. 1144-1156.

43. C. S. Lorens, "A Proof of the Non-Interesting Loop Rule for the Solution of Linear Flowgraphs," Research Laboratory of Electronics, MIT, Cambridge, Massachusetts, Quarterly Progress Report, January 1956, pp. 97-102.

44. A. Brandli, "Parametric Circuits at Low Frequencies Using Ferrites and Thin Magnetic Films, Bull. ASE., Vol. 51, No. 20, October 1960, pp. 1047-1053.

45. D. K. Adams, op. cit., "A Study of Phase-Shift Amplifier Techniques," p. 24.

46. J. Smit and H. P. J. Wign, op. cit., pp. 301-317.

47. H. Suhl, "The Nonlinear Behavior of Ferrites at High Microwave Signal Levels," Proc. IRE, Vol. 44, 1956, p. 1270.

48. D. K. Adams, op. cit., "A Study of Phase-Shift Amplifier Techniques," p. 30.

49. R. M. Bozorth, Ferromagnetism, Van Nostrand, Inc., Princeton, New Jersey, 1951, p. 524.

50. G. E. Fanslow, "A Magnetic Film Low Frequency Parametric Amplifier," Proc. NEC, 1963, pp. 433-451.

51. E. J. Angelo, Electronic Circuits, McGraw-Hill Book Company, Inc., New York, New York, 1958, p. 370.

52. A. V. Pohm, et al., "Electronic Thin Film Technology," Seminar Notes presented at the 20th National Electronics Conference, Chicago, Illinois, October 1964.

53. R. T. Denton and W. B. Snow, "Origin of Noise in Ferromagnetic Parametric Amplifier," Proc. IRE, Vol. 50, No. 2, February 1962, p. 208.

54. R. W. Roberts, "Investigation of Microwave Non-linear Effects Utilizing Ferromagnetic Materials," Quarterly Progress Report No. 5, Contract No. DA 36-039 sc-73278, Melabs, Palo Alto, California, March 1962.

55. M. Weiss, "Solid State Microwave Amplifier and Oscillator Using Ferrites," J. Appl. Phys., Vol. 29, 1958, p. 421.

56. W. Whirry and F. Wang, "Experimental Study of the Modified Semistatic Ferrite Amplifier," J. Appl. Phys., Vol. 30, 1959, p. 1505.

57. P. Fletcher and R. Bell, "Ferrimagnetic Resonance Modes in Spheres," J. Appl. Phys., Vol. 30, 1959, p. 687.

58. E. Peressini, T. Hartwich, and M. Weiss, "An Experimental Study of Parallel Pumped Ferromagnetic Amplifier," Aerospace Corporation, Contract No. AF 04(647)-930, Air Force Systems Command, USAF, Brighton, Mass., 1962.

DISTRIBUTION LIST

No. of Copies	
2	Commanding Officer, U. S. Army Electronics Command, U. S. Army Electronics Laboratories, Fort Monmouth, New Jersey, Attn: Senior Scientist, Electronic Warfare Division
1	Commanding General, U. S. Army Electronic Proving Ground, Fort Huachuca, Arizona, Attn: Director, Electronic Warfare Department
1	Commanding General, U. S. Army Materiel Command, Bldg. T-7, Washington 25, D. C., Attn: AMCRD-DE-E-R
1	Commanding Officer, Signal Corps Electronics Research Unit, 9560th USASRU, P. O. Box 205, Mountain View, California
1	U. S. Atomic Energy Commission, 1901 Constitution Avenue, N.W., Washington 25, D. C., Attn: Chief Librarian
1	Director, Central Intelligence Agency, 2430 E Street, N.W., Washington 25, D. C., Attn: OCD
1	U. S. Army Research Liaison Officer, MIT-Lincoln Laboratory, Lexington 73, Massachusetts
1	Commander, Air Force Systems Command, Andrews Air Force Base, Washington 25, D. C., Attn: SCSE
1	Headquarters, USAF, Washington 25, D. C., Attn: AFRDR
1	Commander, Aeronautical Systems Division, Wright-Patterson Air Force Base, Ohio, Attn: ASRNCC-1
1	Commander, Aeronautical Systems Division, Wright-Patterson Air Force Base, Ohio, Attn: ASAPRD
1	Commander, Aeronautical Systems Division, Wright-Patterson Air Force Base, Ohio, Attn: ASRN-CS
1	Commander, Aeronautical Systems Division, Wright-Patterson Air Force Base, Ohio, Attn: ASNP
1	Commander, Electronic Systems Division, L. G. Hanscom Field, Bedford, Massachusetts
1	Commander, Rome Air Development Center, Griffiss Air Force Base, New York, Attn: RAYLD
1	Commander, Air Proving Ground Center, Eglin Air Force Base, Florida, Attn: ADJ/Technical Report Branch

DISTRIBUTION LIST (Cont.)

No. of Copies	
1	Chief of Naval Operations, EW Systems Branch, OP-35, Department of the Navy, Washington 25, D. C.
1	Chief, Bureau of Ships, Code 691C, Department of the Navy, Washington 25, D. C.
1	Commander, Bu Naval Weapons, Code RRRE-20, Department of the Navy, Washington 25, D. C.
1	Commander, Naval Ordnance Test Station, Inyokern, China Lake, California, Attn: Test Director - Code 30
1	Commander, Naval Air Missile Test Center, Point Mugu, California
1	Director, Naval Research Laboratory, Countermeasures Branch, Code 5430, Washington 25, D. C.
1	Director, Naval Research Laboratory, Washington 25, D. C., Attn: Code 2021
1	Director, Air University Library, Maxwell Air Force Base, Alabama, Attn: CR-4987
1	Commanding Officer-Director, U. S. Navy Electronic Laboratory San Diego 52, California
1	Commanding Officer, U. S. Naval Ordnance Laboratory, Silver Spring 19, Maryland
3	Chief, U. S. Army Security Agency, Arlington Hall Station, Arlington 12, Virginia, 22212 Attn: 2 Cpys - IADEV 1 Copy - EW Div. IATOP
1	President, U. S. Army Defense Board, Headquarters, Fort Bliss, Texas
1	President, U. S. Army Airborne and Electronics Board, Fort Bragg, North Carolina
1	U. S. Army Anti-Aircraft Artillery and Guided Missile School, Fort Bliss, Texas, Attn: ORL
1	Commander, USAF Security Service, San Antonio, Texas, Attn: CLR
1	Chief of Naval Research, Department of the Navy, Washington 25, D. C., Attn: Code 427
1	Commanding Officer, 52d U. S. Army Security Agency, Special Operations Command, Fort Huachuca, Arizona
1	President, U. S. Army Security Agency Board, Arlington Hall Station, Arlington 12, Virginia
1	The Research Analysis Corporation, McLean, Virginia, 22101 Attn: Document Control Officer

DISTRIBUTION LIST (Cont.)

No. of Copies	
10	Headquarters, Defense Documentation Center, Cameron Station, Alexandria, Virginia
1	Commanding Officer, U. S. Army Electronics Research and Development Laboratory, Fort Monmouth, New Jersey, Attn: U. S. Marine Corps Liaison Office, Code: SIGRA/SL-LNR
1	Director, Fort Monmouth Office, Communications-Electronics Combat Developments Agency, Building 410, Fort Monmouth, New Jersey
7	Commanding Officer, U. S. Army Electronics Command, U. S. Army Electronics Laboratories, Fort Monmouth, New Jersey, Attn: 1 Copy - Director of Research 1 Copy - Technical Documents Center - ADT/E 1 Copy - Chief, Special Devices Branch, Electronic Warfare Division 1 Copy - Chief, Advanced Techniques Branch, Electronic Warfare Division 1 Copy - Chief, Jamming and Deception Branch, Electronic Warfare Division 1 Copy - File Unit No. 2, Mail and Records, Electronic Warfare Division 1 Copy - Chief, Vulnerability Br., Electromagnetic Environment Division
1	Commanding Officer, U. S. Army Signal Missile Support Agency, White Sands Missile Range, New Mexico, Attn: SIGWS-MEW
1	Commanding Officer, U. S. Naval Air Development Center, Johnsville, Pennsylvania, Attn: Naval Air Development Center Library
1	Headquarters, Aeronautical Systems Division, Wright-Patterson Air Force Base, Ohio, Attn: ASRNCC-10
1	U.S.A.F. Project Rand, The Rand Corporation, 1700 Main Street, Santa Monica, California
1	Stanford Electronic Laboratories, Stanford University, Stanford, California
1	Director, National Security Agency, Fort George G. Meade, Maryland, Attn: RADE-1
1	Bureau of Naval Weapons Representative, Lockheed Missiles and Space Company, P. O. Box 504, Sunnyvale, California
1	Dr. B. F. Barton, Director, Cooley Electronics Laboratory, The University of Michigan, Ann Arbor, Michigan
35	Cooley Electronics Laboratory, The University of Michigan, Ann Arbor, Michigan

Above distribution is effected by Electronic Warfare Division, Surveillance Department, USAEL, Evans Area, Belmar, New Jersey. For further information contact Mr. I. O. Myers, Senior Scientist, Telephone 59-61252.

Unclassified
Security Classification

DOCUMENT CONTROL DATA - R&D

(Security classification of title, body of abstract and indexing annotation must be entered when the overall report is classified)

1. ORIGINATING ACTIVITY *(Corporate author)*
Cooley Electronics Laboratory
Dept. of Electrical Engineering
University of Michigan, Ann Arbor, Mich.

2a. REPORT SECURITY CLASSIFICATION
Unclassified

2b. GROUP

3. REPORT TITLE

A Study of the Ferrite Phase-Shift Amplifier

4. DESCRIPTIVE NOTES *(Type of report and inclusive dates)*

Technical Report

5. AUTHOR(S) *(Last name, first name, initial)*

W. B. Ribbens

6. REPORT DATE	7a. TOTAL NO. OF PAGES	7b. NO. OF REFS
January 1965	229	--

8a. CONTRACT OR GRANT NO.
DA36-039 AMC 03733(E)

b. PROJECT NO.
IP021102A04201

c. Task No. -01

d. Subtask No. -02

9a. ORIGINATOR'S REPORT NUMBER(S)
6137-6T

9b. OTHER REPORT NO(S) *(Any other numbers that may be assigned this report)*
Technical Report No. 159

10. AVAILABILITY/LIMITATION NOTICES

Qualified requesters may obtain copies of this report from DDC

11. SUPPLEMENTARY NOTES

12. SPONSORING MILITARY ACTIVITY
USAECOM, Ft. Mon., N. J.
(AMSEL-RD-SE)

13. ABSTRACT

Report describes the use of ferrites as the non-linear reactive element in phase-shift amplifiers.

DD FORM 1 JAN 64 1473 0101-807-6800

UNCLASSIFIED
Security Classification

14. KEY WORDS	LINK A		LINK B		LINK C	
	ROLE	WT	ROLE	WT	ROLE	WT
Phase-shift amplifiers Non-linear elements Ferrites						

INSTRUCTIONS

1. ORIGINATING ACTIVITY: Enter the name and address of the contractor, subcontractor, grantee, Department of Defense activity or other organization *(corporate author)* issuing the report.

2*a*. REPORT SECURITY CLASSIFICATION: Enter the overall security classification of the report. Indicate whether "Restricted Data" is included. Marking is to be in accordance with appropriate security regulations.

2*b*. GROUP: Automatic downgrading is specified in DoD Directive 5200.10 and Armed Forces Industrial Manual. Enter the group number. Also, when applicable, show that optional markings have been used for Group 3 and Group 4 as authorized.

3. REPORT TITLE: Enter the complete report title in all capital letters. Titles in all cases should be unclassified. If a meaningful title cannot be selected without classification, show title classification in all capitals in parenthesis immediately following the title.

4. DESCRIPTIVE NOTES: If appropriate, enter the type of report, e.g., interim, progress, summary, annual, or final. Give the inclusive dates when a specific reporting period is covered.

5. AUTHOR(S): Enter the name(s) of author(s) as shown on or in the report. Enter last name, first name, middle initial. If military, show rank and branch of service. The name of the principal author is an absolute minimum requirement.

6. REPORT DATE: Enter the date of the report as day, month, year; or month, year. If more than one date appears on the report, use date of publication.

7*a*. TOTAL NUMBER OF PAGES: The total page count should follow normal pagination procedures, i.e., enter the number of pages containing information.

7*b*. NUMBER OF REFERENCES: Enter the total number of references cited in the report.

8*a*. CONTRACT OR GRANT NUMBER: If appropriate, enter the applicable number of the contract or grant under which the report was written.

8*b*, 8*c*, & 8*d*. PROJECT NUMBER: Enter the appropriate military department identification, such as project number, subproject number, system numbers, task number, etc.

9*a*. ORIGINATOR'S REPORT NUMBER(S): Enter the official report number by which the document will be identified and controlled by the originating activity. This number must be unique to this report.

9*b*. OTHER REPORT NUMBER(S): If the report has been assigned any other report numbers *(either by the originator or by the sponsor)*, also enter this number(s).

10. AVAILABILITY/LIMITATION NOTICES: Enter any limitations on further dissemination of the report, other than those imposed by security classification, using standard statements such as:

(1) "Qualified requesters may obtain copies of this report from DDC."

(2) "Foreign announcement and dissemination of this report by DDC is not authorized."

(3) "U. S. Government agencies may obtain copies of this report directly from DDC. Other qualified DDC users shall request through _____."

(4) "U. S. military agencies may obtain copies of this report directly from DDC. Other qualified users shall request through _____."

(5) "All distribution of this report is controlled. Qualified DDC users shall request through _____."

If the report has been furnished to the Office of Technical Services, Department of Commerce, for sale to the public, indicate this fact and enter the price, if known.

11. SUPPLEMENTARY NOTES: Use for additional explanatory notes.

12. SPONSORING MILITARY ACTIVITY: Enter the name of the departmental project office or laboratory sponsoring *(paying for)* the research and development. Include address.

13. ABSTRACT: Enter an abstract giving a brief and factual summary of the document indicative of the report, even though it may also appear elsewhere in the body of the technical report. If additional space is required, a continuation sheet shall be attached.

It is highly desirable that the abstract of classified reports be unclassified. Each paragraph of the abstract shall end with an indication of the military security classification of the information in the paragraph, represented as *(TS)*, *(S)*, *(C)*, or *(U)*.

There is no limitation on the length of the abstract. However, the suggested length is from 150 to 225 words.

14. KEY WORDS: Key words are technically meaningful terms or short phrases that characterize a report and may be used as index entries for cataloging the report. Key words must be selected so that no security classification is required. Identifiers, such as equipment model designation, trade name, military project code name, geographic location, may be used as key words but will be followed by an indication of technical context. The assignment of links, roles, and weights is optional.